RANGE DEPENDENT SIGNALS AND MAXIMUM ENTROPY METHODS FOR UNDERWATER ACOUSTIC TOMOGRAPHY

Thesis by

Elizabeth Ann Kendall

In Partial Fulfillment of the Requirements

for the Degree of

Doctor of Philosophy

California Institute of Technology

Pasadena, California

1985

(Submitted January 24, 1985)

To my husband, Timothy M. Casey

and my parents,

Anna A. and Walter W. Kendall

Acknowledgements

The assistance and cooperation of many individuals led to the completion of this thesis. I want to thank my patient advisor, Prof. T. K. Caughey, and the members of my committee. Dr. C. H. Chapman and Dr. M. Brown provided computer programs and notes essential to my work, and Dr. B. Cornuelle was consulted on several issues. Interstate Electronics Corporation of Anaheim, California, provided generous support and a VAX 11/750, and many past and present employees of IEC contributed, including Dr. L. R. Roberts, Mr. R. A. Robinson, Mr. J. M. Turner, and Ms. S. G. Schultz.

Abstract

A new method for simulating underwater acoustic signals in range dependent environments is presented, and the approach utilizes Maslov asymptotic theory as developed by C. H. Chapman for synthetic seismograms. The simulated range dependent signals are then used in active underwater acoustic tomography exercises, where changes in observed acoustic transmissions are inverted to obtain information about ocean sound velocity structure. The inversions are performed with both the generalized inverse and the maximum entropy inverse, and a new numerical method for finding the maximum entropy inverse with noisy data is presented. The numerical technique follows the $\mathcal{C}$ statistic approach proposed by Bryan and Skilling.

TABLE OF CONTENTS

LIST OF ILLUSTRATIONS

LIST OF TABLES

NOMENCLATURE

1.0 INTRODUCTION

There are three purposes or goals of this work. First, a new method of simulating underwater acoustic signals is presented, and it is based on Maslov asymptotic theory (10) and techniques from seismology. Second, range dependent acoustic amplitude inversions for active underwater acoustic tomography are performed. The tomography seeks information about ocean sound velocity structure by comparing observed acoustic signals with nominal ones, and aspects of resolution and linearity are discussed. The last goal of this work is to compare maximum entropy inversions with the most common method used in underwater tomography, the generalized inverse. A new numerical technique, based upon the $\mathcal{E}$ statistic approach of Bryan and Skilling (6), for maximum entropy inversions of noisy data is presented.

The Maslov asymptotic theory signal simulation is the major contribution of this work, and it does appear to be a useful, informative alternative to the standard parabolic approximation. The method should be faster for some applications, and it should lend insight into range dependent effects.

The maximum entropy inverse is an interesting concept based on sounder principles than the generalized inverse, minimum norm, approach. It

looks for the most probable solution, adding no new constraints, and it has been used effectively in image processing. Results given here show it can resolve structure better than the generalized inverse for some cases. In a high noise environment, however, it allows too many degrees of freedom and errant inversions to occur. The numerical method for the maximum entropy inverse that is described in this thesis is more stable and converges better than other ones.

The linearity and resolution of the simulated underwater acoustic tomography exercises did not permit accurate inversions. Higher order derivatives and more source and receiver pairs are required, but some sample inversions have been performed with limited success.

This paper is divided into seven chapters. Chapter 2 gives the uses, issues, and types of underwater acoustic tomography. Chapter 3 provides a derivation of the Maslov asymptotic theory technique for simulating range dependent acoustic signals, and numerical methods are presented. Chapter 4 discusses inverse theory, and the generalized and maximum entropy inverses are explained and compared. Chapter 5 presents results for simulated underwater acoustic amplitude inversions, and Chapter 6 summarizes the conclusions of this thesis. Chapter 7 provides listings of some of the key computer programs.

2.0 UNDERWATER ACOUSTIC TOMOGRAPHY

2.1 USES AND ISSUES

Ocean structure or weather is important to physical oceanography, global weather patterns, ocean shipping and mining, and submarine warfare, and ocean remote sensing has recently received a considerable amount of attention. Infrared sensors, altimeters, synthetic aperture radars and other sensors on satellites such as SEASAT in 1978 give oceanographers the opportunity to remotely measure temperature, velocity currents, ocean circulation and sea surface structure. These remote sensors are a considerable improvement over a system of point-by-point shipborne measurements because they provide a complete, nearly instantaneous ocean image. However, only the very top layer of the ocean can be penetrated by these satellite sensors, and they therefore do not provide information about the ocean structure below the surface. Active underwater acoustic tomography, proposed by W. Munk and C. Wunsch in 1979 (30), is a remote sensing technique that probes the part of the ocean that is opaque to satellite instruments.

Active ocean acoustic tomography combines medical tomography, conventional seismology, and underwater acoustics. In medical tomography, from the Greek word for "slice," X-rays are passed directly through a patient, and transforms of the X-ray data produce a three-dimentional image of the inside of the patient's body. In seismology, perturbations in signals between pairs of sources and receivers are used to infer the structure of the earth.

Active ocean acoustic tomography utilizes perturbations in acoustic signals sent between transmitters and receivers to identify ocean structure below the surface. Acoustic travel time or signal perturbations are used to infer ocean sound velocities or velocity currents, and sound velocity information leads to temperature, salinity, and density measurements. As in medical tomography, a three-dimensional image of the ocean structure is produced. However, due to the complicated geometry and incomplete sampling, transform techniques cannot be used in active ocean acoustic tomography.

Due to the conflicting effects of temperature and pressure, ocean sound velocity profiles typically reach a minimum value about one kilometer below the surface. This configuration leads to multipaths, and acoustic signals emitted at various launch angles from a single source travel over many different paths to reach one receiver. The paths travel at distinct depths, as shown in Figure 2-1, and they therefore sample or probe different portions of the water column. This phenomenon is put to use in active acoustic tomography, where a single source and receiver pair can provide p pieces of information if the signal travels over p paths. Thus, m sources and n receivers on n+m moorings give mxnxp pieces of information as compared to m+n pieces for conventional shipborne instruments, and p is approximately ten.

Figures 2-2a and 2-2b depict sample results from the 1981 travel time acoustic tomography experiment described in B. Cornuelle's thesis of 1983 (15). Figure 2-2a is the true sound velocity disturbance at a depth of 800 m and over a range of 300 km by 300 km, and Figure 2-2b is the comparable inverse solution. Four sources and five receivers were used in the experiment, and the transmissions were at a carrier frequency of 224 Hz with a 20 Hz bandwidth. Munk and Wunsch proposed ocean tomography to monitor ocean mesoscale weather that has scales on the order of five days, 500 km in range and 5 km in depth. It is this mesoscale structure that appears in Figure 2-2, and the 1981 experiment yielded a map every three days for seventy consecutive days. Entire ocean basins can eventually be watched in this way, or regions of high currents, where conventional measurements cannot be taken, can be surveyed.

Problems in analysis, instrumentation and logistics must be solved before an active underwater acoustic tomography system can be developed. As with any sensing problem, ocean tomography consists of a forward problem and an inverse problem. For the forward problem, underwater acoustic signals in all kinds of ocean conditions must be analyzed and predicted and this is the topic of Sections 2.2, 2.3, and Chapter 3. Acoustic wave travel times and amplitudes for various source and receiver geometries and ocean profiles must be simulated

so that observations can be compared to them. The difference between the observed and the predicted data is then used in the inverse problem, where the solution is a three-dimensional image of the sound velocity in the region between the transmitters and receivers. The inverse problem consists of deriving $\delta C(x)$, the perturbed sound velocity that is a function of position $\underline{x}$, from observed data, $\underline{d}$. Typically, an underdetermined matrix equation

$$\underline{d} = E \ \underline{\delta C} \tag{2-1}$$

is solved for $\underline{\delta C}$, a vector of discrete sound velocity values. E is the matrix of derivatives relating a data point, d_i, to a sound velocity value, δC_j. Since the problem is underdetermined, additional constraints are assumed to give a unique solution, and methods are discussed in Section 2.2 and Chapter 4.

Other key aspects of the tomography problem are ray identification, mooring localization and timekeeping. The p different pieces of information from a single source and receiver pair can only be unraveled if each arrival over a different ray path can be identified. If the receiver is an array, angle of arrival can be used, but otherwise only the nominal travel time will be available. Mooring motion must be minimized,

and a simulation of tidal motion is of use. Precise timekeeping is required for travel time data and ray identification.

In their initial paper, Munk and Wunsch stated several design requirements. To identify arrivals, signals should be coded and distinguished by matched filters at the receivers. Multipath arrivals can be separated only if the time resolution is less than 50 msec, and a precision of 25 msec is required for travel time inversions. Mooring motion should be less than 35 meters, and timekeeping must be precise to 25 msec over one year. Cornuelle's thesis in 1983 (15) describes the results of a 1981 travel time inversion experiment where the expected signal was only 40 msec, and he simulated mooring motion to get reasonable results.

The logistics of an active tomography system are complicated. Shore based receivers may be attractive, although they complicate the modeling problem. Satellite data should be used in consort with the acoustic data, but a transmission link would be required. Certain transmitter and receiver configurations would be theoretically optimum but too difficult to implement.

The methods discussed here can be applied to other inverse problems, such as ultrasonic imaging or passive acoustic tomography. Passive ocean acoustic tomography was proposed by A. Rockmore in 1982 (33), and it produces a three-dimensional image of the acoustic structure beneath the sea surface. An array of receivers and a detailed analysis of the ocean sound velocity structure are required, and this technique should be of interest to the antisubmarine warfare community.

2.2 TRAVEL TIME INVERSIONS

A schematic of a travel time tomography exercise is shown in Figure 2-3, where four transmitters send acoustic signals to five receivers. Only four paths per source are available, so there are only twenty-four pieces of information, but thirty-six δC_j values are sought, one for each block of water indicated. The travel time for each signal i is

$$T_i = \int_{\Gamma_i} \frac{d\ell}{C(\underline{x})} \quad , \tag{2-2}$$

where $C(\underline{x})$ is the sound velocity, Γ_i is the path for ray i and $d\ell$ is incremental path length. If T_{io} is the nominal travel time, C_o is the constant nominal sound velocity and $\delta C(\underline{x})$ is the perturbation sound velocity, then

$$T_i - T_{oi} = \int_{\Gamma_i} \frac{d\ell}{C_o + \delta C(\underline{x})} - \int_{\Gamma_{io}} \frac{d\ell}{C_o} \quad , \tag{2-3}$$

By Fermat's principle, the change in the ray path due to $\delta C(\underline{x})$ is secondary to the change in arrival time, so after linearization equation 2-3 becomes

$$\delta T_i = - \int_{\Gamma_{io}} \frac{d\ell}{C_o^2} \, \delta C(\underline{x}) \quad , \tag{2-4}$$

and after discretization

$$\delta T_i = - \sum_{j=1}^{J} \frac{R_{ij}}{C_o^2} \delta C_j \quad . \tag{2-5}$$

Here R_{ij} is the distance that ray i travels in block j, the sum is over all thirty-six blocks, and equation 2-5 fits the form given in equation 2-1.

Real ocean travel time inversions are similar to the one shown in the schematic except the ray paths are three-dimensional and difficult to predict. The ocean inverse problem is usually divided into separate horizontal slice and vertical slice problems, and no direct three-dimensional inversions have been performed to date. In the schematic, thirty-six unknowns are sought from twenty-four relations, and this sort of underdetermined problem usually occurs in the ocean as well.

Munk and Wunsch state that the underdetermined nature of the tomography system, which defines its spatial resolution, is the single greatest problem facing system development. Munk, Wunsch and Cornuelle suggest several ways to improve this situation, and any available piece of valid information about $\delta C(\underline{x})$ can be used. Satellite data about ocean eddies or circulation can be used, and measurements taken over periods of time can be averaged together if tidal or other predictable effects are accounted for by numerical codes and Kalman

filtering. Cornuelle added hydrodynamic constraints, requiring that vertical structure in $\delta C(\underline{x})$ satisfy certain modal relations that had been observed in mesoscale fluctuations. He also had the horizontal structure fit a Gaussian covariance form with a 100 km correlation length, and he used the stochastic inverse described in Chapter 4.

As with any measurement system, good resolution and good noise performance are conflicting requirements, and a tradeoff must be made. Noise factors for underwater travel time inversions are mooring motion, timekeeping errors, ray identification, peak resolution, and nonlinearities. The ocean is a severe noise environment but fortunately the mesoscale structure evolves slowly and simple averaging can be applied. Cornuelle averaged for an entire day, correcting for mooring motion. Cornuelle's inverse estimator was the minimum variance biased estimator because he desired maps of the evolution of mesoscale dynamics and was not primarily interested in the magnitude of the disturbance.

2.3 AMPLITUDE INVERSIONS

The resolution and noise performance of a tomography system can also be improved if signal waveform information is used with the travel time data. An ocean experiment on amplitude inversions has not yet been attempted, but some analysis and simulation has appeared in the literature. J. Cohen and N. Bleistein have done synthetic amplitude inversions with a method described in a text edited by J. DeSanto in 1979 (13). Their analysis yields the following relation between $P_o(\underline{x},t)$, the nominal pressure waveform, and $\delta P(\underline{x},t)$ the observed difference

$$\int_0^\infty dz' \int_{-\infty}^{\infty}\int_{-\infty}^{\infty} dx'\, dy' \, \frac{-2\,\delta C(\underline{x}')}{C_o^3(\underline{x}')} \int_0^t dt' \; P_o(\underline{x}',t')\, P_o(t-t',\, \underline{x}')$$

$$= \int_0^t dt' \; (t-t') \;\; \delta P(\underline{x},t') \quad . \qquad (2\text{-}6)$$

This integral over time t and space $\underline{x}'$ is derived with Green's theorem, and it has been successfully inverted for very simple nominal sound velocity profiles, $C_o(\underline{x})$. It is obviously too cumbersome to be used on realistic profiles, and it does not address noisy measurements.

M. Brown's thesis of 1982 (5) approached acoustic amplitude inversions in a way that is more compatible with active ocean acoustic tomography,

and his technique is extended to range dependent environments in this thesis. Brown derives linear, discrete relations for acoustic amplitude and intensity perturbations as functions of sound velocity fluctuations, and they fit the form given in equation 2-1. He neglects ray path geometry changes, as is standardly done in travel time inversions, and he justifies this simplification by the following analysis.

Brown's amplitude function is determined by a time function $\theta(p)$ that is defined in Chapter 3, with p the horizontal wave slowness. θ can be expressed in terms of a Taylor series around $T(p_j)$, the geometric arrival time for a given ray j with horizontal slowness p_j

$$\theta(p) = T(p_j) + \left.\frac{\partial\theta}{\partial p}\right|_j (p - p_j) + \left.\frac{\partial^2\theta}{\partial p^2}\right|_j (p - p_j)^2/2 \quad . \quad (2\text{-}7)$$

Geometric arrivals, which will produce the largest observable amplitudes, have

$$\left.\frac{\partial\theta}{\partial p}\right|_j = 0 \quad , \quad (2\text{-}8)$$

so the variation of $\theta(p)$ from $T(p)$ is second order in $p - p_j$. Therefore path changes are negligible for the dominant amplitude signals.

Brown's simulation added Gaussian white noise at a five percent level to waveform measurements, and he used amplitude and intensity inversions

in consort with travel time inversions. He performed travel time inversions first and used those results as the nominal cases for the waveform inversions. The travel time data included noise with standard deviation

$$\sigma_i \cong \frac{1}{2\pi\Delta f_{rms}} \sqrt{\frac{1}{\frac{S}{N}}} , \qquad (2\text{-}9)$$

where S/N is the signal to noise ratio and Δf_{rms} is the root mean square frequency resolution, approximately equal to one-third of the bandwidth.

Brown drew the following comparison between travel time, amplitude and intensity inversions:

1. If individual ray arrivals are clearly resolvable, amplitude and intensity inversions do not add much information.

2. If the ray arrivals are confused and low frequency energy is present, waveform inversions can significantly improve the quality of the inversion.

Brown's simulation and analysis are expanded upon in this thesis, but real-world problems complicate amplitude inversions. Random ocean fluctuations cause a large degree of randomness in ocean acoustic

amplitude signatures. This effect is evident in Figure 2-4, where single realizations, an hourly average and a daily average of an acoustic signal are portrayed, and Section 2.4 provides further insight. Mooring localization and the fact that absolute amplitudes are not available in the ocean will also degrade amplitude inversions.

2.4 RANDOM FLUCTUATIONS IN ACOUSTIC SIGNALS

Random effects in the ocean can cause large random fluctuations in acoustic signals. Ocean internal waves and turbulence cause random microstructure in the sound velocity profile, and acoustic multipaths are split into random micro-multipaths. Signals traveling over the random paths interfere with one another, and large scale variations can occur. This randomness can obviously impact ocean acoustic tomography, and it is discussed in S. M. Flatte's text of 1979 (16) and in M. Brown's 1982 thesis (5).

Random effects become more important as range or frequency is increased and Figure 2-5 from Flatte predicts when stochastic modeling must be considered. Flatte's analysis only considered ocean internal waves according to the Garrett and Munk spectrum, and it predicts that deterministic geometric ray tracing is valid for frequencies below 200 Hz and ranges less than 100 km. For low frequencies at ranges beyond 100 km the Rytov extension is required, and this solution gives a first order perturbation term for mean square phase and intensity fluctuations. Nominal ray paths and waveforms still follow the geometric optics model, however, so mean or average received signals are unaffected.

By Flatte's analysis, therefore, low frequency long range active acoustic tomography can be carried out with deterministic models applied to

averaged signals. As demonstrated in Figure 2-4, and by the 1981 tomography experiment described by Cornuelle, 1982 (14), acoustic signals stablize over a period of about a day, and a viable tomography system could monitor mesoscale structure on a daily basis.

M. Brown attempted to invert averaged acoustic signals in his 1982 thesis, but his efforts failed. His present opinion, revealed in personal communication, is that nonlinear effects caused his difficulty and that his examples did not fit the small angle approximation

$$\omega \, \delta T_i << 1 \quad . \tag{2-10}$$

Here ω is the frequency and δT_i is the travel time perturbation.

Higher order moments of the sound velocity disturbance will also complicate inversions of averaged data. The relationships between travel time or acoustic pressure and the sound velocity are nonlinear, but a linearized relation such as equation 2-4 can be iterated in the inversion process to yield the nonlinear solution. If the sound velocity is stochastic, however, higher order moments appear, and the iterations cannot solve directly for the mean value.

For example, the nonlinear travel time relation is

$$T = \int \frac{d\ell}{C_o + \delta C(\underline{x})} \quad , \tag{2-11}$$

or for the mean value with a deterministic path

$$\langle T \rangle = \int \left\langle \frac{1}{C_o + \delta C(\underline{x})} \right\rangle \, d\ell \quad . \tag{2-12}$$

In series form, equation 2-11 is

$$T = \int d\ell / C_o \left[1 - \frac{\delta C(\underline{x})}{C_o} + \left(\frac{\delta C(\underline{x})}{C_o} \right)^2 \cdots \right], \tag{2-13}$$

while equation 2-12 is

$$\langle T \rangle = \int \frac{d\ell}{C_o} \left[1 - \frac{\langle \delta C(\underline{x}) \rangle}{C_o} + \frac{\langle \delta C(\underline{x})^2 \rangle}{C_o^2} \cdots \right] . \tag{2-14}$$

Since the mean square value is not the same as the mean value squared, equation 2-14 cannot be linearized and then iterated to find $\langle \delta C(\underline{x}) \rangle$ without introducing errors due to higher order terms.

Despite the complications stated above and M. Brown's failed attempt, it is anticipated that signal inversions for ocean acoustic tomography can be performed even in a random medium. Further work is required in this area before experiments can be carried out.

2.5 FUTURE APPLICATIONS

The ultimate role for active underwater acoustic tomography should be as a key component of a comprehensive remote ocean sensing network. Satellite ocean measurements of surface conditions should be combined with tomographic observations made at depth. This procedure will decrease the number of unknowns required from the tomographic inversion, and it will probe the subsurface ocean structure that is not observable with spaceborne instruments alone.

The computer codes, inversion techniques, and instrumentation required for active acoustic tomography should speed the development of passive ocean acoustic tomography. This concept, introduced by A. Rockmore (33) in 1982, aims to provide three-dimensional maps of the acoustic structure in the ocean. Data from passive receivers will be inverted to locate acoustic sources, and this approach should offer improved signal processing for some acoustic array configurations.

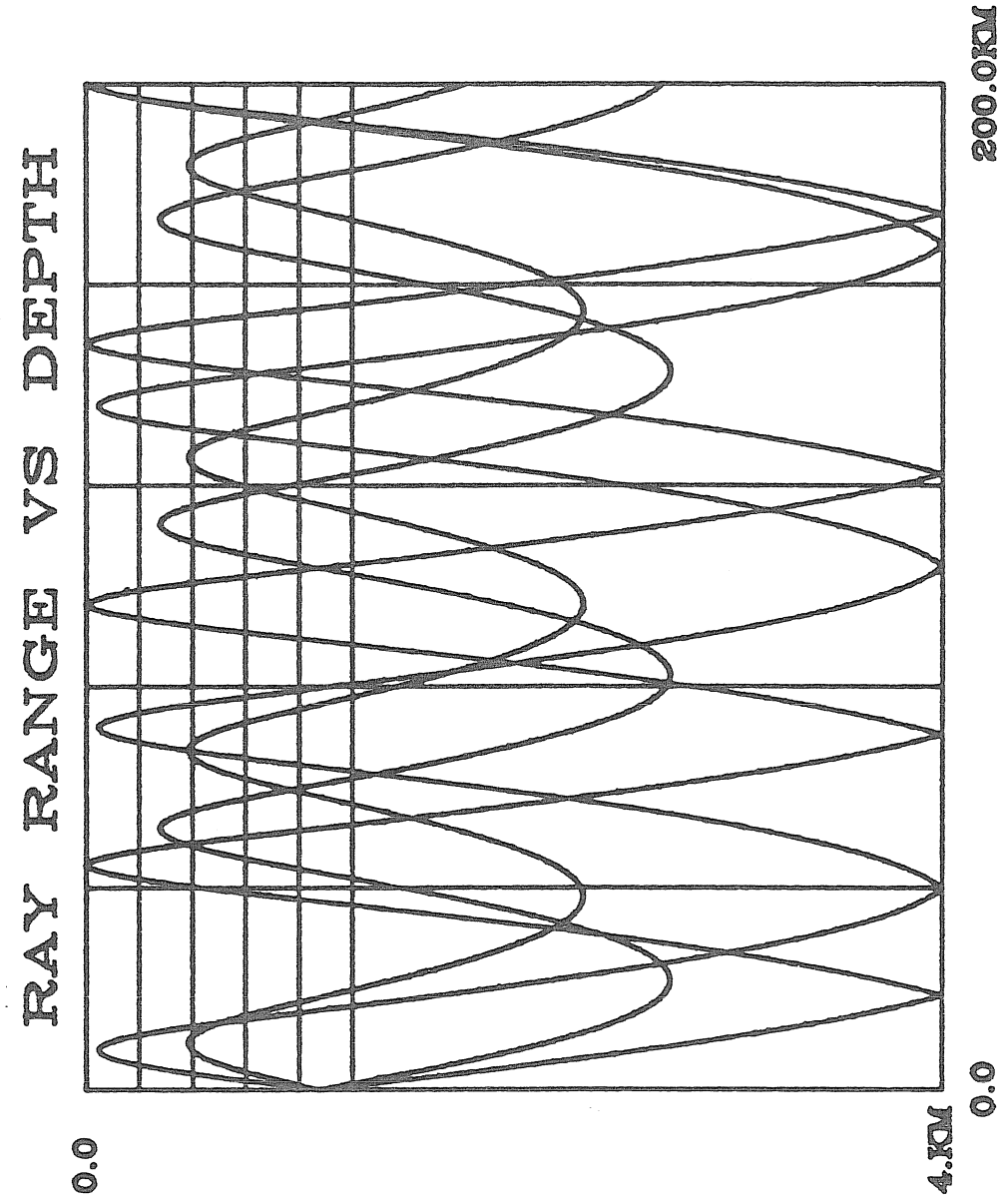

FIGURE 2-1: ACOUSTIC MULTIPATHS

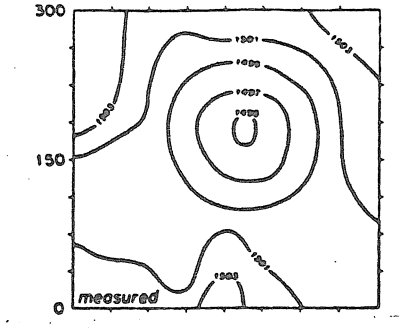

FIGURE 2-2a: CONTOURS OF MEASURED SOUND SPEED AT 800 m DEPTH

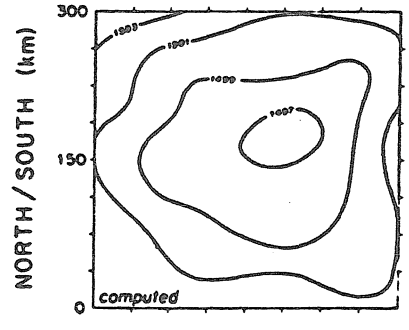

FIGURE 2-2b: CONTOURS COMPUTED FROM TRAVEL TIME INVERSION

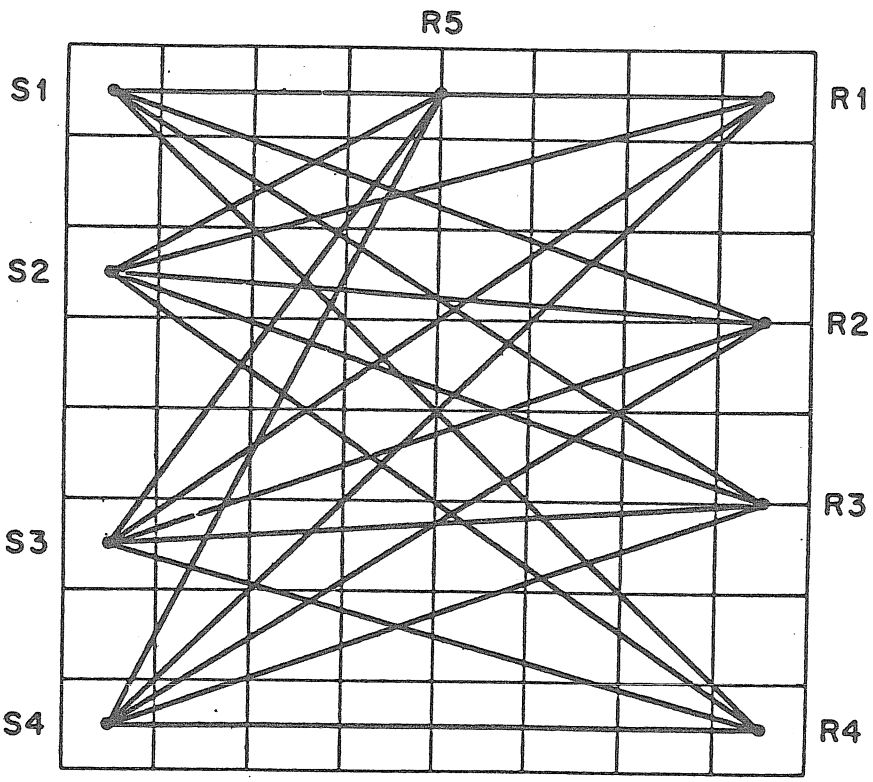

FIGURE 2-3: SAMPLE TRAVEL TIME TOMOGRAPHY EXERCISE

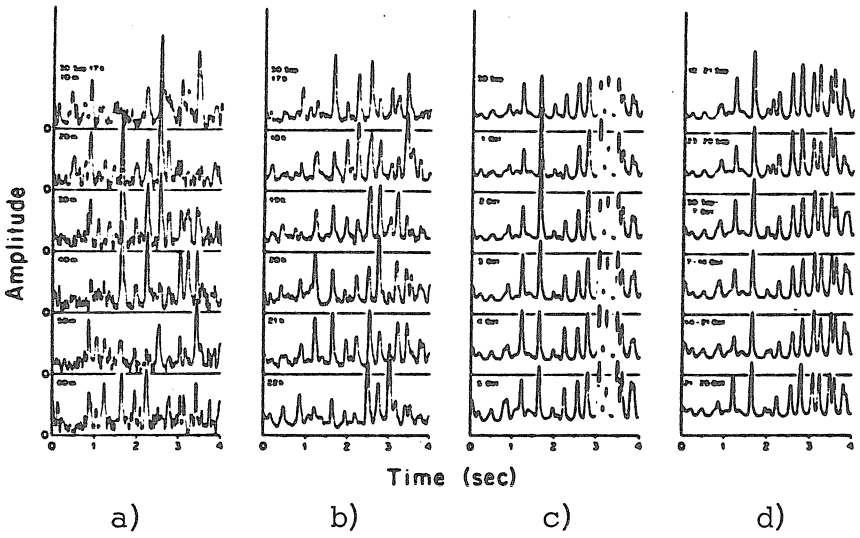

FIGURE 2-4: ACOUSTIC AMPLITUDE RECORDS WITH a) NO AVERAGING, b) ONE HOUR AVERAGING, c) ONE DAY, AND d) ONE WEEK AVERAGING

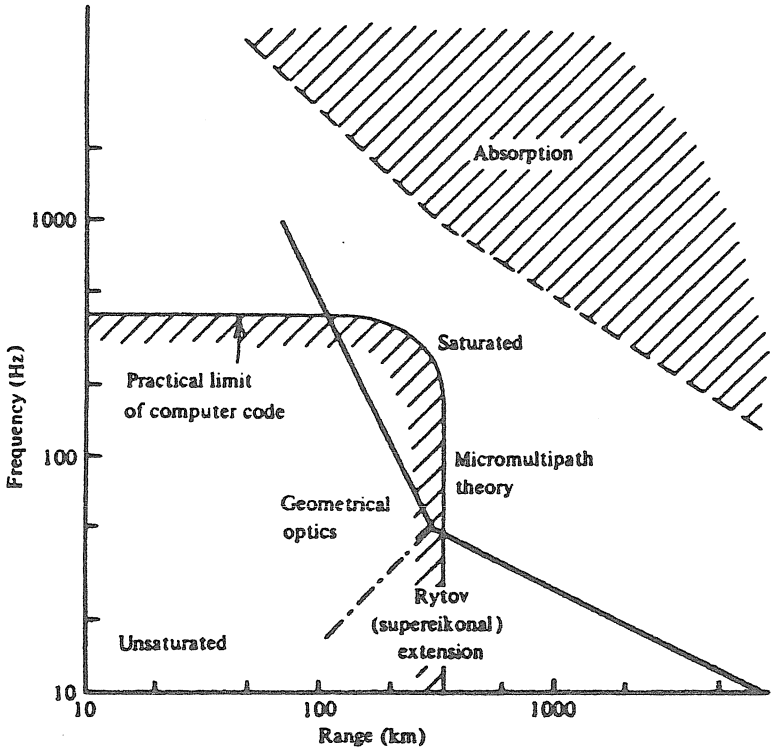

FIGURE 2-5: LIMITS OF GEOMETRICAL OPTICS

CHAPTER 2 NOTATION

$C(\underline{x})$	sound velocity
C_o	nominal sound velocity
$\underline{d}$	observed measurement differences
$d\ell$	incremental path length
E	derivative matrix
N	noise
P	pressure
P_o	nominal pressure
p	horizontal wave slowness
R_{ij}	distance ray i travels in block j
S	signal
T	geometric arrival time
Γ_i	path for ray i
$\underline{\delta C}$	vector of sound velocity values
δP	observed pressure perturbation
$\underline{\delta T}$	observed travel time differences
Δf_{rms}	approximately equal to 1/3 bandwidth
Θ	time function
σ_i	travel time noise standard deviation
ω	frequency

3.0 SYNTHETIC UNDERWATER ACOUSTIC SIGNALS

3.1 INTRODUCTION

Underwater acoustic tomography requires solutions to two distinct problems: the forward problem of predicting ocean acoustic signals under various conditions and the inverse problem of obtaining ocean structure from signal data. This chapter describes methods used here to simulate range dependent underwater acoustic signals, and therefore it presents a solution to the forward problem.

Historically, ocean acoustics has been concerned with predicting the steady state, single frequency propagation loss versus range for a given signal. Seismology and underwater acoustic amplitude tomography, however, require detailed analyses of the signal waveform versus time. Due to these distinctions, the methods used here are taken from seismology rather than conventional underwater acoustics. In addition, these methods are faster and simpler than the parabolic approximation, finite difference or finite element techniques, and it is this speed, with acceptable sacrifices in accuracy, that makes the lengthy inversion process feasible.

Synthetic waveforms for seismology, also called synthetic seismograms, have often been generated using either asymptotic ray theory or transform methods. Asymptotic ray theory is valid in laterally inhomogeneous media, but caustics, shadows and critical points must

be treated as special cases. Transform methods have been utilized in laterally homogeneous media where the independent variables in the wave equation separate. One transform solution derived by C. H. Chapman (8) was successfully used for range independent acoustic tomography by M. G. Brown (5).

The approach used here to produce synthetic underwater acoustic signals uses Maslov asymptotic theory that combines asymptotic ray theory and transform techniques to yield one simple, general method applicable in laterally inhomogeneous media. Maslov asymptotic theory extends transform solutions to inhomogeneous media by a canonical transformation, and it utilizes asymptotic ray theory when the transform solution breaks down.

The approach used here was developed primarily by C. H. Chapman, and the range independent version or the WKBJ solution was first used by M. Brown to simulate ocean acoustic signals. The range dependent solution utilizes Maslov asymptotic theory presented by Maslov (27, 28) and in English by Kravtsov (24). This derivation closely follows Chapman and Drummond's 1982 article (10) and Kravtsov's review, and asymptotic ray theory and the WKBJ range independent solution are discussed separately first.

3.2 ASYMPTOTIC RAY THEORY

Asymptotic ray theory or ART is the mathematical basis for geometrical ray theory, and it is widely used for synthetic seismograms and to compute underwater acoustic travel times. It is used here under Maslov asymptotic theory when the transform solution breaks down and to compute geometric arrival times for travel time inversions.

The wave equation for excess acoustic pressure P is

$$\nabla^2 P(\underline{x}, t) - \frac{1}{C^2(\underline{x})} \frac{\partial^2}{\partial t^2} P(\underline{x}, t) = 0 \quad , \tag{3-1}$$

or in the frequency domain

$$\nabla^2 \hat{P}(\underline{x}, \omega) + \omega^2 / C^2(\underline{x}) \hat{P}(\underline{x}, \omega) = 0 \quad , \tag{3-2}$$

where $\hat{P}(\underline{x}, \omega)$ is the Fourier transform of $P(\underline{x}, t)$. Under asymptotic ray theory, an asymptotic series solution to equation 3-2 is sought, so the relation

$$\hat{P}(\underline{x}, \omega) = \sum_{n=0}^{\infty} \frac{A^{(n)}(\underline{x})}{(-i\omega)^n} e^{i\omega T(\underline{x})} \tag{3-3}$$

is substituted. Coefficients of like powers of ω must be zero, and the eikonal equation

$$(\nabla T)^2 - \frac{1}{C^2(\underline{x})} = 0 \tag{3-4}$$

and the transport equation

$$2\,\nabla A^{o} \cdot \nabla T + A^{o}\,\nabla^2 T = 0 \tag{3-5}$$

result.

The Maslov asymptotic theory result to follow requires the Hamiltonian form of the eikonal equation, and the Hamiltonian $\mathcal{H}$ is

$$\mathcal{H}(\underline{x}, \underline{p}) = \frac{1}{2}\left(\underline{p}^2 - u^2(\underline{x})\right) , \tag{3-6}$$

where $\underline{p}$ is the wave slowness vector,

$$\underline{p} = \nabla T , \tag{3-7}$$

and u is the magnitude of $\underline{p}$ or $1/C(\underline{x})$. The eikonal equation then is reduced to $\mathcal{H} = 0$, and the solution is obtained by the method of characteristics with the characteristic lines defined by

$$\frac{dx_i}{\partial\mathcal{H}/\partial p_i} = \frac{dT}{p_i\,\partial\mathcal{H}/\partial p_i} = \frac{-dp_i}{\partial\mathcal{H}/\partial x_i} = d\nu , \tag{3-8}$$

or

$$\frac{dx_i}{d\nu} = \dot{x}_i = p_i \tag{3-9a}$$

$$d p_i / d\nu = \frac{1}{2} \frac{\partial}{\partial x_i} u^2 \tag{3-9b}$$

and

$$\frac{dT}{d\nu} = u^2(\underline{x}) \quad . \tag{3-9c}$$

Here $d\nu = u\, d\ell$, with $d\ell$ representing incremental ray arc length.

The travel time derivative (3-9c) can also be expressed in terms of the Lagrangian that can be found by the Legendre transformation. The variables $(\underline{x}, \underline{p}, t)$ are transformed to $(\underline{x}, \dot{\underline{x}}, t)$, and the Lagrangian is related to the Hamiltonian by (Goldstein (18))

$$\mathcal{L}(\underline{x}, \dot{\underline{x}}) = \underline{p} \cdot \dot{\underline{x}} - \mathcal{H}(\underline{x}, \underline{p}) \quad . \tag{3-10}$$

The travel time for geometric arrivals is then related to the Lagrangian by

$$T(\underline{x}, \underline{x}_o) = \int_{\nu_o}^{\nu} \mathcal{L}(\underline{x}, \dot{\underline{x}})\, d\nu$$

$$= \int_{\ell_o}^{\ell} u\, d\ell = \int_{\underline{x}_o}^{\underline{x}} \underline{p} \cdot d\underline{x} \quad . \tag{3-11}$$

Equation 3-11 gives the solution to the eikonal equation expressed in terms of use to Maslov asymptotic theory. The transport equation 3-5 must now be solved, and the first result is

$$A^{o2}(\underline{x}) = A^{o2}(\underline{x}_o) \frac{u^2(\underline{x}_o)}{u^2(\underline{x})} \frac{\partial(x_o, y_o, z_o)}{\partial(x, y, z)} \tag{3-12}$$

The amplitude term is infinite at caustics, but solutions can be obtained at either side of a caustic. The general result is

$$A^{o}(\underline{x}) = A^{o}(\underline{x}_o) \frac{u(\underline{x}_o)}{u(\underline{x})} \left| \frac{\partial \underline{x}_o}{\partial \underline{x}} \right|^{\frac{1}{2}} e^{-i\pi\sigma(\underline{x}, \underline{x}_o)/2} , \tag{3-13}$$

where $\sigma(\underline{x}, \underline{x}_o)$ is an integer representing the KMAH index (Ziolkowski and Deschamps, 1980 (34)). $\sigma(\underline{x}_o, \underline{x}_o)$ is zero, and σ is constant between caustics. The index is incremented when a ray crosses a caustic, and the increment agrees with the number of dimensions a ray tube loses at the caustic.

The final result for the ART acoustic pressure waveform is then

$$P(\underline{x}, t) = \sum_{\text{rays}} \text{Real}\left[A^{o}(\underline{x}) \; \delta\left(t - T(\underline{x}, \underline{x}_o)\right) \right]$$

$$= \sum_{\text{rays}} \frac{u(\underline{x}_o)}{u(\underline{x})} \left| \frac{\partial \underline{x}_o}{\partial(\underline{x})} \right|^{\frac{1}{2}} \text{Re}\left[A^{o}(\underline{x}_o) \; \delta\left(t - T(\underline{x}, \underline{x}_o)\right) e^{\frac{-i\pi\sigma(\underline{x}, \underline{x}_o)}{2}} \right]. \tag{3-14}$$

The summation is over all rays, and the solution is invalid if the Jacobian is zero. Higher order terms from the series in equation 3-3 do not rectify the problem at caustics, but the methods given in the next two sections are valid alternatives.

3.3 WKBJ TRANSFORM SOLUTION

The integral transform solution given here is valid when the sound velocity C is only a function of depth. The transform coordinates are ω, p, and z, where p is the horizontal wave slowness, and the WKBJ solution to the ordinary differential equation in z is used. The key to the solution, introduced by C. H. Chapman in 1978 (8) , is evaluating the frequency transform first and keeping the wave number real. The derivation here follows M. G. Brown (5).

The wave equation for excess acoustic pressure due to an impulsive point source in a laterally homogeneous medium with r as cylindrical range is

$$\nabla^2 P(r,z,t) - \frac{1}{C^2(z)} \frac{\partial^2}{\partial t^2} P(r,z,t)$$

$$= - \frac{\delta(r)}{2\pi} \delta(z-z_o) \delta(t) \quad , \qquad (3\text{-}15)$$

with boundary conditions

$$P(t,r,0) = 0$$

$$\frac{\partial P}{\partial z} (t,r,h) = 0 \qquad (3\text{-}16)$$

Taking the Fourier transform, denoted $\hat{P}$, and the Hankel transform, denoted by $\bar{P}$, equation 3-15 becomes

$$\frac{d^2}{dz^2} \hat{\bar{P}}(\omega,p,z) + \omega^2(u^2(z) - p^2) \hat{\bar{P}}(\omega,p,z)$$

$$= - \delta(z-z_o) \quad . \tag{3-17}$$

Here p, the horizontal wave slowness, is

$$p = \frac{1}{C(z)} \cos \phi(z) \quad , \tag{3-18}$$

where ϕ is the angle of the ray to the horizontal.

The WKBJ solution to equation 3-17 is found from substituting the asymptotic series (Ahluwalia and Keller (2))

$$\hat{\bar{P}}(z) = \sum_{n=0}^{\infty} \frac{1}{(iK)^n} \bar{A}^n(z) \; e^{i\omega\tau(p,z)} \tag{3-19}$$

into equation 3-17. Here wave number K is ω/C_o , with C_o an arbitrary reference value of C, and the WKBJ solution retains the lowest power terms of K to give

$$\left(\frac{d\tau}{dz} \right)^2 = u^2(z) - p^2(z) \qquad (3\text{-}20)$$

and

$$2 \frac{d\tau}{dz} \frac{d\bar{A}^o}{dz} + \frac{d^2\tau}{dz^2} \bar{A}^o = 0 \quad . \qquad (3\text{-}21)$$

The condition on equation 3-20 is that τ is zero at z_o.

The general transformed result for an omnidirectional source is

$$\hat{\bar{P}}(\omega,p,z) = -\sum_{\text{rays}} \frac{e^{-i\pi\sigma(\underline{x},\underline{x}_o)/2} \; e^{i\omega\tau(p,z)}}{2i\omega\left(u(\underline{x})^2 - p^2\right)^{\frac{1}{4}} \left(u(\underline{x}_o)^2 - p^2\right)^{\frac{1}{4}}} \quad , \qquad (3\text{-}22)$$

with $\sigma(\underline{x},\underline{x}_o)$ as the KMAH index, u as wave slowness and p as horizontal wave slowness. $\tau(p,z)$ is the delay time function

$$\tau(p,z) = \int_{z_o}^{z} \left(u^2(z') - p^2\right)^{\frac{1}{2}} dz' \qquad (3\text{-}23a)$$

$$= T(p,z) - p\,R(p,z) \quad . \qquad (3\text{-}23b)$$

T is the travel time given by equation 3-11, and R is the range where the ray last crosses the receiver depth,

$$R(p,z) = \int_{z_o}^{z} \frac{p\ dz'}{(u(z')^2 - p^2)^{1/2}} \quad dz' \quad . \tag{3-24}$$

The integrals in equations 3-23 and 3-24 are evaluated for the entire ray path, and the KMAH index in equation 3-22 counts the number of refractions or reflections.

The amplitude is proportional to

$$\beta(p, z; z_o) = 1.0 \Big/ \left((u^2(z_o) - p^2)^{\frac{1}{4}} \quad (u^2(z) - p^2)^{\frac{1}{4}}\right)$$

$$= 1.0 \Big/ (q_o\ q)^{\frac{1}{2}} \quad , \tag{3-25}$$

where q is the vertical wave slowness, $^{1}/_{C(z)} \sin \phi(z)$. This amplitude term is singular at ray turning points where q is zero.

The integral transforms now must be inverted in

$$P(r,z,t) = \frac{i}{8\pi^2 C_o} \sum_{\text{rays}} \int dp\ p\ b_\ell\ \beta(p,z;z_o)$$

$$\int_{-\infty}^{\infty} d\omega\ \omega J_o(\omega pr)\ e^{-i\omega\left(t - \tau_\ell\ (p,z)\right)} \quad , \tag{3-26}$$

where J_o is the Bessel function with the asymptotic form for $\omega pr >> 1$ of

$$J_o(\omega pr) \sim \left(\frac{2}{\pi\omega pr}\right)^{\frac{1}{2}} \left[e^{i\omega pr - i\pi/4} + e^{-i\omega pr + i\pi/4} \right] . \quad (3\text{-}27)$$

In equation 3-26 b_ℓ has been used for the KMAH index term, and τ_ℓ denotes τ for a ray type ℓ. Using equation 3-27, the Fourier transform identity

$$\mathcal{F}\left[\frac{H(t)}{t^{1/2}}\right] = \left(\frac{\pi}{\omega}\right)^{\frac{1}{2}} e^{i\pi/4} , \quad (3\text{-}28)$$

and retaining only terms for outgoing waves gives

$$P(r,z,t) = -\frac{1}{4\pi^2 C_o} \left(\frac{2}{r}\right)^{\frac{1}{2}} \mathcal{I}m \frac{d}{dt} \left\{ \Lambda(t) * \sum_{\text{rays}} \int dp\, p^{\frac{1}{2}} b_\ell \beta(p,z;z_o) \delta\left(t - \theta(p,r,z)\right) \right\} . \quad (3\text{-}29)$$

Here

$$\Lambda(t) = H(t)/t^{1/2} + iH(-t)/(-t)^{1/2} , \quad (3\text{-}30)$$

and θ is given by

$$\theta(p,r,z) = \tau(p,z) + pr$$

$$= T(p,z) + p\left(r - R(p,z)\right) \quad . \tag{3-31}$$

The function θ is the time for the plane wavefront for a given ray to hit the receiver since $(r - R)$ is the distance from the range where the ray last crosses the receiver depth to the actual receiver location. Stationary points of θ with respect to p correspond to geometric arrivals where R equals r.

The delta function in equation 3-29 can be evaluated to yield

$$P(r,z,t) = -\frac{1}{4\pi^2 C_o}\left(\frac{2}{r}\right)^{\frac{1}{2}} \mathcal{I}_m \frac{d}{dt}\left[\Lambda(t) * \sum_{\ell \text{ rays}} b_\ell \sum_{t=\theta_\ell} \frac{p^{1/2}\,\beta(p,z;z_o)}{\left|{}^{d\theta}/_{dp}\right|}\right] , \tag{3-32}$$

and the summation is over all ray types and all rays with θ values equal to the desired time values t. Equation 3-32 is singular for geometric arrivals, however, so an alternative smoothed solution is sought (Chapman, 1978 (8) and Chapman and Dey-Sarkar, 1978 (9)). For the smoothing, P(r,z,t) from equation 3-29 is convolved with the boxcar function

$$B(t) = \frac{1}{2\Delta t}\left[H(t+1) - H(t-1)\right] \tag{3-33}$$

to give

$$P(r,z,t) * \frac{1}{\Delta t} B(t/\Delta t) = -\frac{1}{8\pi^2 \Delta t C_o}\left(\frac{2}{r}\right)^{1/2} \mathcal{I}m \frac{d}{dt}\left[\Lambda(t) * \sum_{\ell \text{ rays}} b_\ell \sum_{\theta = t \pm \Delta t} \int p^{1/2}\, \beta(p,z)\, dp\right] \tag{3-34}$$

The summation in equation 3-34 is over all rays with θ falling within the interval $t \pm \Delta t$. If $\beta(p,z)$ and p vary smoothly and slowly, the integrals in equation 3-34 can be approximated to give the following final WKBJ transform solution

$$P(r,z,t) = -\frac{1}{8\pi^2 \Delta t C_o}\left(\frac{2}{r}\right)^{1/2} \mathcal{I}m \frac{d}{dt}\left[\Lambda(t) * \sum_{\ell \text{ rays}} b_\ell \sum_{\theta(p,z) = t \pm \Delta t} \left(\frac{p}{qq_o}\right)^{1/2} \Delta p\right] . \tag{3-35}$$

Now Δp is the interval defined by $t \pm \Delta t = \theta(p,z)$, and equation 3-35 is valid at caustics and geometric arrivals. This solution is invalid, however, at turning points where q is zero.

Equation 3-14, the ART result, is invalid at caustics but valid at turning points, and equation 3-35, the WKBJ transform solution, is acceptable at caustics but singular at turning points. Maslov asymptotic theory, described in the next section, provides a method to utilize each of these solutions in their respective regions of validity, and to extend the WKBJ result to laterally nonhomogeneous media.

3.4 MASLOV ASYMPTOTIC THEORY

Ray paths involve nine variables: $\underline{x}$, $\underline{p}$, and $\underline{x}_o$. If $\underline{x}_o$, the source position, is specified, then any three other variables will completely define the ray. Standard ray solutions trace the ray in coordinate space $\underline{x}$, but Maslov asymptotic theory (Kravtsov, 1968 (24), Maslov, 1965 (27) and 1972 (28) and Chapman, 1982 (10)) seeks a solution in a mixed $\underline{x}$ and $\underline{p}$ frame that is applicable in laterally inhomogeneous media. For a wave velocity C that varies in x and z but not in y, the solution basis is designated

$$\underline{y} = (p,y,z) \quad . \tag{3-36}$$

If the wave velocity C is a function of x, y, and z, the optimal solution basis is

$$\underline{z} = (p,r,z) \quad . \tag{3-37}$$

Note that q is used as the z or vertical component of wave slowness while r corresponds to the y or out of plane slowness.

The modified wave equation in space will now be solved. The equations are initially much more complicated than the $\underline{x}$ frame equations, but, due to a Legendre transformation, the end result is simple and totally analogous to equations 3-14 and 3-35.

The pressure in the $(\underline{y},\omega)$ frame, $\hat{\tilde{P}}(\underline{y},\omega)$, is related to the pressure in the $(\underline{x},\omega)$ frame, $\hat{P}(\underline{x},\omega)$, by the Fourier transform

$$\hat{\tilde{P}}(\underline{y},\omega) = \left(-\frac{i\omega}{2\pi}\right)^{\frac{1}{2}} \int_{-\infty}^{\infty} \hat{P}(\underline{x},\omega)\ e^{-i\omega px}\ dx\ ,\quad \omega > 0. \tag{3-38}$$

The inverse transform is

$$\hat{P}(\underline{x},\omega) = \left(\frac{i\omega}{2\pi}\right)^{\frac{1}{2}} \int_{-\infty}^{\infty} \hat{\tilde{P}}(\underline{y},\omega)\ e^{i\omega px}\ dx, \tag{3-39}$$

and the following three results are useful

$$i\omega p\ \hat{\tilde{P}}(\underline{y},\omega) = \left(-\frac{i\omega}{2\pi}\right)^{\frac{1}{2}} \int_{-\infty}^{\infty} \frac{\partial}{\partial x}\ \hat{P}(\underline{x},\omega)\ e^{-i\omega px}\ dx \tag{3-40}$$

$$\frac{\partial}{\partial p}\ \hat{\tilde{P}}(\underline{y},\omega) = \left(-\frac{i\omega}{2\pi}\right)^{\frac{1}{2}} \int_{-\infty}^{\infty} -i\omega x\ \hat{P}(\underline{x},\omega)\ e^{-i\omega px}\ dx \tag{3-41}$$

$$f\left(-\frac{1}{i\omega}\frac{\partial}{\partial p}\right)\hat{\tilde{P}}(\underline{y},\omega) = \left(-\frac{i\omega}{2\pi}\right)^{\frac{1}{2}} \int_{-\infty}^{\infty} f(x)\ \hat{P}(\underline{x},\omega)\ e^{-i\omega px}\ dx\ . \tag{3-42}$$

The function f is arbitrary, and on the left hand side of equation 3-42 it is a function of the differential operator.

The new wave equation from equations 3-1 and 3-38 to 3-42 becomes

$$(-\omega^2 p^2 + \nabla_{\perp}^2) \hat{\tilde{P}}(\underline{y},\omega)$$

$$+ \omega^2 u^2(-\frac{1}{i\omega}\frac{\partial}{\partial p}, z) \hat{\tilde{P}}(\underline{y},\omega) = 0 \quad , \tag{3-43}$$

with $\nabla_{\perp}^2 = \frac{\partial^2}{\partial y^2} + \frac{\partial^2}{\partial z^2}$. Equation 3-43 can be solved by an asymptotic series method, letting

$$\hat{\tilde{P}}(\underline{y},\omega) = \sum_{n=o}^{\infty} \frac{\tilde{A}^n(\underline{y})}{(-i\omega)^n} e^{i\omega\tilde{T}(\underline{y})} \quad , \tag{3-44}$$

with ~ used to distinguish the P, A, and T values from those in equation 3-3 for the $\underline{x}$ frame solution or in equation 3-19 for the Hilbert transform solution.

Modified eikonal (equation 3-4) and transport (equation 3-5) equations can be derived, but these involve the term $u(-\frac{\partial\tilde{T}}{\partial p}, y, z)$ and are too complicated to solve. Instead, $\tilde{T}(\underline{y})$ and $\tilde{A}^o(\underline{y})$ can be found by the properties of Legendre transformations. The travel time or $\underline{x}$ frame phase function $T(\underline{x})$ was found from equation 3-11

$$\frac{dT(\underline{x})}{d\nu} = \mathcal{L}(\underline{x}, \dot{\underline{x}}) = \underline{p} \cdot \dot{\underline{x}} - \mathcal{H} \ .$$

The new phase function $\tilde{T}(\underline{y})$ in mixed $\underline{y}$ space can be found from a partial Legendre transformation

$$\frac{d\,\tilde{T}(\underline{y})}{d\nu} = \tilde{\mathcal{L}}(\underline{y}, \dot{\underline{y}}) \tag{3-45a}$$

$$= r\dot{y} + q\dot{z} - \mathcal{H} \tag{3-45b}$$

$$= \frac{dT}{d\nu} - p\frac{dx}{d\nu} \quad . \tag{3-45c}$$

Equation 3-45c can be integrated to give the valuable result

$$\tilde{T}(\underline{y}) = T(x(\underline{y}), y, z) - px(\underline{y}) \quad . \tag{3-46}$$

The $x(\underline{y})$ represents the range as a function of the (p,y,z) coordinates of the ray. If the source and receiver are in the (x,z) plane, and out of plane or y variations are not considered, equation 3-46 becomes equation 3-23b. Therefore $x(p,z)$ is the same as $R(p,z)$ in equation 3-23b, and

$$\tilde{T}(p,z) = \tau(p,z)$$

$$= T(x(p,z), z) - px(p,z) \quad . \tag{3-47}$$

The new phase function $\tilde{T}(p,z)$ for laterally inhomogeneous media is functionally the same as the intercept or delay time $\tau(p,z)$ used in the WKBJ transform result. The only distinction is that the range $x(p,z)$ and

the travel time $T(x(p,z), z)$ must now be calculated along the entire range dependent ray path. Equivalent to $R(p,z)$ for an (x,z) plane problem, $x(p,z)$ in equation 3-47 again represents the range where the ray last crosses the receiver depth, and p is the horizontal slowness at that point.

The amplitude term $\tilde{A}^{o}(\underline{y})$ in equation 3-44 can now be solved by looking at the transformed result $P(\underline{x},t)$. Using equation 3-39,

$$P(\underline{x},t) = -\frac{1}{2^{1/2}\pi} \frac{d}{dt} \mathcal{I}m \left\{ \Lambda(t) * \sum_{t=\tilde{\theta}(p,\underline{x})} \tilde{A}^{o}(\underline{y}) \Big/ \left| \frac{\partial \tilde{\theta}}{\partial p} (p,\underline{x}) \right| \right\} , \tag{3-48}$$

with $\Lambda(t)$ the function given in equation 3-30 and

$$\tilde{\theta}(p,x,z) = \tilde{T}(\underline{y}) + \bar{p}x$$

$$= T(x(p,z), z) + p(x - x(p, z)) . \tag{3-49}$$

In equation 3-49, x is the receiver x coordinate while $x(p,z)$ is the x coordinate at the point where the ray last crosses the receiver depth. $\tilde{\theta}(p,x,z)$ is analogous to $\theta(p,r,z)$ in equation 3-31, but their physical interpretations differ. $\theta(p,r,z)$ is the time for the plane wavefront for a given ray to hit the receiver, but $\tilde{\theta}(p,x,z)$ differs from that time since

p may change before the wavefront reaches the receiver. $\tilde{\theta}(p,x,z)$ is a product of the Legendre transformation and does not have the intuitive physical significance that $\theta(p,r,z)$ does.

Geometric arrivals occur when $\tilde{\theta}(p,x,z)$ equals $T(x(p,z),z)$ and $x(p,z)$ equals x, the receiver range. In the neighborhood of these arrivals, equation 3-48 can be replaced with the first motion approximation

$$P(\underline{x},t) = \sum_{x=x(p,z)} \mathrm{Re} \left\{ \frac{\tilde{A}^{o}(\underline{y})}{\left| \frac{\partial x(p,z)}{\partial p} \right|^{1/2}} \delta(t - T(\underline{x})) \right.$$

$$\left. e^{i\pi(1-\gamma)/4} \right\} \qquad (3\text{-}50)$$

with

$$\gamma = \mathrm{sign}\left(\frac{\partial x(p,z)}{\partial p}\right) \quad . \qquad (3\text{-}51)$$

If the wave velocity C is a general function of x,y and z, a solution in the $\underline{z}$ domain, equation 3-37, must be developed (Chapman, 1982 (10)). For a C(x,z) problem, however, caustics for the $\underline{x}$ frame solution, equation 3-14, and for the $\underline{y}$ frame solution, equation 3-50, will not coincide and the two solutions can be blended together to form one generally applicable solution for laterally (x) inhomogeneous media. The next step in this derivation identifies the two conditions for caustics and specifies a way to merge the two solutions.

Equations 3-50 and 3-14 are both applicable in laterally inhomogeneous media away from their respective caustics, so

$$\tilde{A}^{o}(\underline{y}) = A^{o}(\underline{x}) \left| \frac{\partial x}{\partial p}(p,z) \right|^{1/2} e^{-i\pi(1-\gamma)/4} \tag{3-52a}$$

$$= A^{o}(\underline{x}_{o}) \frac{u(\underline{x}_{o})}{u(\underline{x})} \left| \frac{\partial \underline{x}_{o}}{\partial \underline{x}} \right|^{\frac{1}{2}} \left| \frac{\partial x(y)}{\partial p} \right|^{\frac{1}{2}}$$

$$e^{-i\pi\sigma(\underline{x},\underline{x}_{o})/2} e^{-i\pi(1-\gamma)/4} \tag{3-52b}$$

Equation 3-52b can then be substituted back into equation 3-50 to give the desired solution to the transformed wave equation 3-43.

The ART $\underline{x}$ frame solution, equation 3-14, has caustics where the Jacobian $\partial(x,z)/\partial(x_{o},z_{o})$ is zero, and this occurs when the rays cross in $\underline{x}$ space. At these locations dx is zero for z fixed and dp_{o} nonzero, and these $\underline{x}$ caustics are identified by

$$q \frac{\partial x}{\partial p_{o}} = 0 \quad . \tag{3-53}$$

This condition is not satisfied at turning points where q is zero since in general $\partial x/\partial p_{o}$ is infinite there.

The $\underline{y}$ frame transform solution, equations 3-50 and 3-52b, is singular if

$$\frac{\partial(x,z)}{\partial(x_o,z_o)} \quad \frac{\partial p}{\partial x(\underline{y})} \quad = \quad 0 \quad , \tag{3-54}$$

and this means that

$$q \frac{\partial p}{\partial p_o} \quad = \quad 0 \quad . \tag{3-55}$$

In laterally homogeneous media, $\partial p / \partial p_o$ is one, and condition 3-55 is satisfied at turning points where q is zero. In laterally inhomogeneous media, $\partial p / \partial p_o$ is zero when the rays are parallel in $\underline{x}$ space or cross in the $\underline{y}$ frame.

Conditions 3-53 and 3-55 can be used in an acoustic signal simulation to determine which solution is valid for a given ray arriving at a certain (x,z) receiver location. A smooth weighing function, $w(\phi_o)$, can be used so that only the valid or most accurate solution is used for a given ray. Let $w_a(\phi_o)$ weight the ART result, and $w_t(\phi_o)$ weight the transform result. Their sum must equal one, and $w_a(\phi_o)$ will be zero unless condition 3-55 is met and the transform result is invalid. The transform solution will be used wherever it is valid because it is more accurate than the ART result.

The final form of the Maslov asymptotic theory solution is (Chapman, 1982)

$$P(\underline{x},t) = \frac{M(t)}{4\pi C_o^2} * \Bigg[\sum_{x=x(\underline{y})} w_a(\phi_o) \; \mathrm{Re}\left\{ \delta(t - T(\underline{x})) \frac{|p_o|^{\frac{1}{2}} \; e^{-i\pi\sigma(\underline{x},\underline{x}_o)/2}}{\left| x \; q \; q_o \; \partial x(\underline{y})/\partial p_o \right|^{1/2}} \right\}$$

$$- \frac{1}{2^{1/2}\pi} \frac{d}{dt} \; \mathrm{Im} \left\{ \Lambda(t) * \sum_{t=\tilde{\theta}(\underline{x},p)} \frac{w_t(\phi_o) \left| p_o \frac{\partial p}{\partial p_o} \right|^{1/2}}{\left| x \; q \; q_o \right|^{1/2} \left| \frac{\partial \tilde{\theta}}{\partial p_o} \right|} \right.$$

$$\left. e^{-i\pi\sigma(\underline{x},\underline{x}_o)/2 - i\pi(1-\gamma)/4} \right\} \Bigg] \quad , \qquad (3\text{-}56)$$

where the Jacobian has been replaced by the appropriate function

$$\frac{\partial(x_o, z_o)}{\partial(x,z)} = \frac{|p_o^x|}{\left| q \; q_o \; \frac{\partial x}{\partial p_o} \right|} \qquad (3\text{-}57)$$

and M(t) represents the source time function. The terms in equation 3-56 are summed over all ray types.

Similar to equation 3-32 for the WKBJ result, the transform term in equation 3-56 is singular at geometric arrivals and must be convolved with a boxcar function. The end result is totally analogous to equation 3-35 with Δp_o replacing Δp.

3.5 NUMERICAL METHODS

3.5.1 RAY PATHS IN TRIANGLES

Some key issues must be addressed before equation 3-56 can be implemented in a computer simulation of underwater acoustic signals. First of all, a discrete representation of the sound velocity profile must be selected. Cubic spline fits to sound velocity points are frequently used, but in a range dependent ocean the ray paths could only be found by lengthy numerical integrations. For this study of tomography, this process is too time consuming, so instead the profile is approximated by linear functions in triangles. This procedure was used by Chapman, 1982 (10) and for underwater acoustics by Roberts, 1974 (32), and the ray paths for this case are circular. Intersection points, range, travel time, and even the derivative of travel time with respect to C have analytical solutions, and the rays can be quickly calculated.

Some of the mathematics essential to this procedure will be summarized here and was originally done by C. H. Chapman, 1983 (12). The sound velocity within any given triangle j is linearized to

$$C(x,z) = a_j x + b_j z + C_{o_j} \quad , \tag{3-58}$$

and local horizontal and vertical vectors $\underline{i}_j$ and $\underline{k}_j$ can be defined by

$$\underline{i}_j = \frac{1}{|\nabla C|_j} (-b_j, a_j) \tag{3-59a}$$

$$\underline{k}_j = -\frac{1}{|\nabla C|_j} (a_j, b_j) \tag{3-59b}$$

If the ray tangential and perpendicular vectors are $\underline{n}$ and $\underline{m}$, respectively, defined by

$$\underline{n} = (\cos\phi, \sin\phi) \tag{3-60a}$$

$$\underline{m} = (\sin\phi, -\cos\phi) \quad , \tag{3-60b}$$

then the local horizontal slowness p'_j is conserved, so

$$p'_j = \frac{\underline{n} \cdot \underline{i}}{C(x, z)} = \frac{1}{|\nabla C_j| C} (-b_j \cos\phi + a_j \sin\phi) \tag{3-61}$$

is a constant throughout a triangle.

The circular ray path has radius and center defined by

$$\xi_j = \frac{C}{-b_j \cos\phi + a_j \sin\phi} \tag{3-62a}$$

$$x_{C_j} = x + \mathscr{e}_j \xi_j \sin\phi \tag{3-62b}$$

$$z_{C_j} = z - \mathscr{e}_j \xi_j \cos\phi \quad , \tag{3-62c}$$

with

$$\ell_j = \text{sign}\,(-a_j \sin\phi + b_j \cos\phi) \tag{3-63}$$

and ϕ defined positive clockwise. Equations 3-62 can easily be used to find the points where the ray paths enter or leave a triangle.

Unless a certain block of ocean has a discrete δC_j that alters C_{o_j} in a triangle, the velocity $C(x,z)$ is continuous across triangles. If δC_j is nonzero, either p or q is changed across a boundary. Travel time can be found from

$$T(x,z) = \int_\Gamma \frac{d\ell}{C} = \int_\Gamma \frac{\xi\, d\phi}{a_j x + b_j z + C_{o_j}} \tag{3-64a}$$

$$= \frac{1}{|\nabla C|_j} \left\{ \tanh^{-1} (\underline{n}^{out} \cdot \underline{k}_j) - \tanh^{-1} (\underline{n}^{in} \cdot \underline{k}_j) \right\} , \tag{3-64b}$$

with $\underline{n}^{in}$ and $\underline{n}^{out}$ denoting the entrance and exit values of $\underline{n}$ in triangle j, respectively. The travel time derivative when a_j and b_j are nonzero is

$$\left(\frac{\partial T(x,z)}{\partial C}\right)_j = -\int_\Gamma \frac{d\ell}{C^2} \qquad (3\text{-}65a)$$

$$= \frac{1}{\xi_j}\left[-\frac{b_j \tan\phi/_2 + a_j}{2\,|\nabla C|^2\,\mathcal{J}}\right.$$

$$\left. + \frac{(2a_j^2 + b_j^2)\tan\phi/_2 - a_j b_j}{2\,b_j\,|\nabla C|^2\,\mathcal{J}}\right]\Bigg|_{\phi^{in}}^{\phi^{out}}, \qquad (3\text{-}65b)$$

with

$$\mathcal{J} = b_j(\tan^2\phi/_2 - 1) + 2a_j\tan\phi/_2 \quad . \qquad (3\text{-}66)$$

When a_j is zero, the derivative is simply

$$-\frac{1}{\xi_j b_j^2}\tan\phi\Bigg|_{\phi^{in}}^{\phi^{out}}, \qquad (3\text{-}67a)$$

and when b_j is zero it is

$$\frac{-1}{\xi_j a_j^2\tan\phi}\Bigg|_{\phi^{in}}^{\phi^{out}} \quad . \qquad (3\text{-}67b)$$

The derivatives $\frac{\partial x}{\partial p_o}$ and $\frac{\partial p}{\partial p_o}$, and the sign of $\frac{\partial x}{\partial p}$ are required for equation 3-56. $\frac{\partial x}{\partial p}$ is positive in a triangle where no turning point occurs, and it is negative otherwise. The other two derivatives can only be found after a lengthy derivation that involves a transmission matrix D such that

$$\begin{bmatrix} d\alpha_j \\ dp'_j \end{bmatrix} = D \begin{bmatrix} d\alpha_1^{in} \\ dp'_1 \end{bmatrix} , \tag{3-68}$$

where $d\alpha$ is the ray tube cross section in the plane of the rays and p'_1 is the local horizontal wave slowness in the first triangle, related to $\underline{p}_o = (p_o, q_o)$ by

$$p'_1 = \underline{i}_1 \cdot \underline{p}_o \quad . \tag{3-69}$$

The important derivative terms are

$$\left(\frac{\partial p}{\partial p_{o_j}}\right) = \frac{\underline{m}_1 \cdot \underline{i}_1}{\underline{m}_1 \cdot \underline{i}} \quad \frac{\underline{m}_j \cdot \underline{i}}{\underline{m}_j \cdot \underline{i}_j} \quad \left[D_{22} + D_{12} \quad \frac{|\nabla C|_j}{C_j^2} \quad \frac{(\underline{k}_j \cdot \underline{i})^2}{(\underline{m}_j \cdot \underline{i})^2} \right] \tag{3-70}$$

and

$$\left(\frac{\partial x}{\partial p_o} \right)_j = \frac{\underline{m}_1 \cdot \underline{i}_1}{\underline{m}_1 \cdot \underline{i}} \quad \frac{D_{12}}{\underline{m}_j \cdot \underline{i}} \quad , \tag{3-71}$$

where $\underline{m}_1$ is the value of $\underline{m}$ at the entrance of the first triangle and $\underline{m}_j$, C_j are at the exit of the j^{th} triangle where the ray last crosses the receiver depth. $\underline{i}$ is the true horizontal vector, (1,0), and q, needed in equation 3-56, is $^1/_{C_j} \quad \underline{m}_j \cdot \underline{i}$.

The matrix D was found by Chapman, 1983 (12), and it is given by

$$D = \kappa_j \; Q_{j-1} \; \ldots \; Q_2 \; \kappa_2 \; Q_1 \; \kappa_1 \tag{3-72}$$

with

$$\kappa_j = \begin{bmatrix} \dfrac{\underline{m}_j^{out} \cdot \underline{i}_j}{\underline{m}_j^{in} \cdot \underline{i}_j} & \dfrac{1}{p_j'^2 \, |\nabla C|_j} \; (\kappa_{11} - 1) \\ 0 & 1 \end{bmatrix} \tag{3-73a}$$

$$Q_j = \begin{bmatrix} Q_{11} & 0 \\ S_2 \, Q_{11} + S_1 \, S_3 & S_1 \dfrac{\underline{\ell}_j \cdot \underline{m}_j^{out}}{\underline{i}_j \cdot \underline{m}_j^{out}} \end{bmatrix} \tag{3-73b}$$

for

$$Q_{11} = \frac{\underline{\ell}_j \cdot \underline{m}_{j+1}^{in}}{\underline{\ell}_j \cdot \underline{m}_j^{out}} \tag{3-74a}$$

$$S_1 = \frac{\underline{i}_{j+1} \cdot \underline{m}_{j+1}^{in}}{\underline{\ell}_j \cdot \underline{m}_{j+1}^{in}} \tag{3-74b}$$

$$S_2 = \frac{-(\underline{\ell}_j \cdot \underline{k}_{j+1})^2 \quad |\nabla C|_{j+1}}{(\underline{\ell}_j \cdot \underline{m}_{j+1}^{in})^2 \quad C_{j+1}^{in\ 2}} \tag{3-74c}$$

and

$$S_3 = \frac{(\underline{\ell}_j \cdot \underline{k}_j)^2 \quad |\nabla C|_j}{(\underline{\ell}_j \cdot \underline{m}_j^{out})\ (\underline{i}_j \cdot \underline{m}_j^{out})\ C_j^2} \tag{3-74d}$$

Here $\underline{\ell}_j$ is the vector for the orientation of the triangle boundary at the exit of the j^{th} triangle.

3.5.2 CONVOLUTION

Chapman's 1982 article (10) describes an extremely efficient algorithm to convolve the function $\Lambda(t)$ with the transform impulse response in equation 3-56. This method has been used here.

The source function M(t) selected agrees with Brown's 1982 work (5), and it is a sinusoid source of specified bandwidth and carrier frequency. The source function is modeled by N cycles of a carrier frequency ω_C, and the bandwidth in all cases is ω_C/N. The source function is differentiable because the transitions at the end points are smooth.

3.5.3 THETA FUNCTION TABLES

Chapman and Buland's 1983 article (11) exploits the Θ and $\tilde{\Theta}$ functions of equations 3-31 and 3-49 to find geometric arrivals under various conditions. Usually a boundary value problem must be solved to find geometric arrival times, $T(\underline{x})$, and a lengthy ray shooting method is required. Θ or $\tilde{\Theta}$, however, are found without solving the boundary value problem, and geometric arrivals can be found from a good Θ table because geometric arrivals occur when $\partial\Theta/\partial p$ or $\partial\tilde{\Theta}/\partial p$ changes sign.

3.6 SAMPLE SYNTHETIC SIGNALS

Equation 3-56 and the numerical methods of section 3.5 represent a new technique for calculating synthetic underwater acoustic signals in a range dependent ocean. In this section, sample signals will be calculated and compared to alternative methods. Other methods to compute synthetic signals are discussed in summary texts on underwater acoustics (2 and 13).

For range independent calculations, transform methods, normal mode expansions and ray theory are commonly used. Emphasis to date has been on computing acoustic propagation loss versus range, but normal mode theory with a stationary phase approximation, asymptotic ray theory and direct numerical integration of the inverse Fourier transforms are three ways to produce synthetic waveforms. The literature contains many comparisons of range independent programs with various levels of accuracy, complexity, and memory requirements.

Range dependent programs are still under development, and not many comparisons with experimental data have been made. This is partially due to the fact that range dependent sampling of the sound velocity profiles is always incomplete. At least five techniques are available: ray

theory, normal mode theory, finite difference, finite element, and the parabolic approximation. Finite difference and finite element methods address the problem of ocean bottom interaction very well, but the parabolic approximation solution is the most popular approach for a range dependent medium. The parabolic approximation converts the elliptic Helmholtz equation to a parabolic equation solvable by marching in range, and the approximation is valid because the acoustic rays make very narrow angles to the horizontal. The parabolic solution is valid in strongly range dependent oceans, and time dependent, bottom topography and stochastic effects can all be incorporated.

Parabolic solution programs require good initial conditions from a normal mode calculation or another method, and small range steps are often required. Jensen and Krol, 1975 (23) use range steps of 100 m and 1.0 km for maximum vertical sound velocity gradients of 0.1 sec^{-1} and 1.0 sec^{-1}, respectively, and smaller steps are required for higher frequency transmissions. The parabolic solution is very efficient for propagation loss versus range computations because of range marching, but it is slower and less efficient than Maslov theory for the waveform synthesis of use to underwater acoustic tomography.

Many sample synthetic signals are presented in this section. All computations are carried out in sound velocity profile environments represented

by Munk's canonical sound velocity profile (30), where the sound velocity

$$C(z) = C_a \left[1 + \epsilon \quad (\eta + e^{-\eta} - 1)\right] \tag{3-75a}$$

$$\eta = 2 \quad (z - z_a)/H_a \quad . \tag{3-75b}$$

Here C_a is the minimum sound velocity at the sound axis, z_a is the depth of the axis, and H_a and ϵ are the scale depth and coefficient, respectively.

This canonical sound velocity profile is a simple analytic way to represent the features of the sound channel without introducing discontinuities.

Figures 3-1 to 3-4 are from a range independent case where C_a is 1495 m/sec, z_a is 1200 m, H_a is 1200 m and ϵ is 0.005, and this sound velocity profile is depicted in Figure 3-1. The ocean depth is 4000 m, the source depth is 1195 m, the receiver is at 1100 m, and the total range is 200 km. Acoustic rays connecting the source and receiver are shown in Figure 3-2 for transmission angles of plus and minus 10 degrees. Figure 3-3 gives the horizontal wave slowness, p, versus depth for eight of the rays plotted in Figure 3-2, and, in this range independent

case, the horizontal wave slowness is a constant for a given ray. Figure 3-4 portrays the received signal versus time, and the time extends from 133.01 seconds to 136 seconds, with a time step of 0.0015 seconds. Figure 3-4 provides the pressure trace and eight peak arrivals can be identified. The source had 10 Hz bandwidth and center frequency for this simulated transmission.

Figures 3-5 to 3-8 are comparable to the first set, but a range dependent sound velocity profile is utilized here, and the source is at 1295. m. The sound velocity profiles at ranges 0 and 200 km are identical to those in Figure 3-1, but the inner profiles have minimum velocities of 1480 m/sec. Profiles are linearly interpolated between the different regions, and the range increment is 1 km. Figure 3-6, the ray plot, is not noticeably different from Figure 3-2, but the range dependence is evident in Figure 3-7. The horizontal wave slowness now varies for a given ray, and the effect is quite pronounced. The pressure record is provided in Figure 3-8.

Additional sample synthetic signals are provided in Figures 3-9 to 3-14. For this case the sound velocity profile was 1500 m/sec from the ocean surface to 1500 m depth and a linear profile to 1575 m/sec at the 3000 m deep ocean bottom. The sound source, of 200 Hz bandwidth centered at

200 Hz, is at 1000 m, and it has a 5 degree downward Gaussian beam with a 5 degree standard deviation. The receiver is 15 km away from the source, at many different depths.

M. Brown's (5) sample signals for this case are provided in Figure 3-9, and his results are from the parabolic approximation and the WKBJ transform approach. Figures 3-10 to 3-14 give the Maslov theory results for receiver depths of 1115.66, 1225.57, 1335.49, 1445.41, and 1500.36 meters, respectively. The time axis extends from 9.94 to 10.1 seconds in 0.25 m/sec intervals, and 600 individual rays between plus and minus 15 degrees to the horizontal were traced. Geometric arrivals are indicated by thick vertical lines on the time axis, and the overall agreement is quite good. The waveforms at 1115.66, 1445.41 and 1500.36 m exhibit the best agreement, while the more complicated waveforms at the other two depths do show some discrepancies.

3.7 SUMMARY

The benefits, drawbacks, and unknown aspects of the Maslov theory acoustic waveform simulation will be summarized here. The benefits are the following:

1. The method is based on an innovative, powerful mathematical theory that proposes an alternative to the parabolic equation (PE) approach for range dependent ocean problems.

2. The method will be faster than the PE approach for some cases where the signal waveform as a function of time is desired.

3. The method provides insight into caustics, mixed parameter space approaches, delay function tables, and the use of smoothing algorithms.

The major potential drawbacks are the following:

1. In range dependent media, many rays must be traced from source to receiver, and the number of rays is

determined by the number of distinct ray types. Ray path computation can be quite time consuming.

2. The method is quite sensitive to sound velocity profile and source and receiver positions, and computational requirements for the number of rays, triangles and time steps must be carefully examined.

Much more work should be done on applying Maslov asymptotic theory to underwater acoustics signal simulation, including:

1. Ray shooting and sound velocity profile computational requirements must be carefully examined for many different types of sound velocity profiles.

2. Transition regions between the ART and WKBJ solutions must be studied.

3. Many cases should be run to compare the accuracy and computation time of the Maslov theory results with that of the parabolic equation solutions.

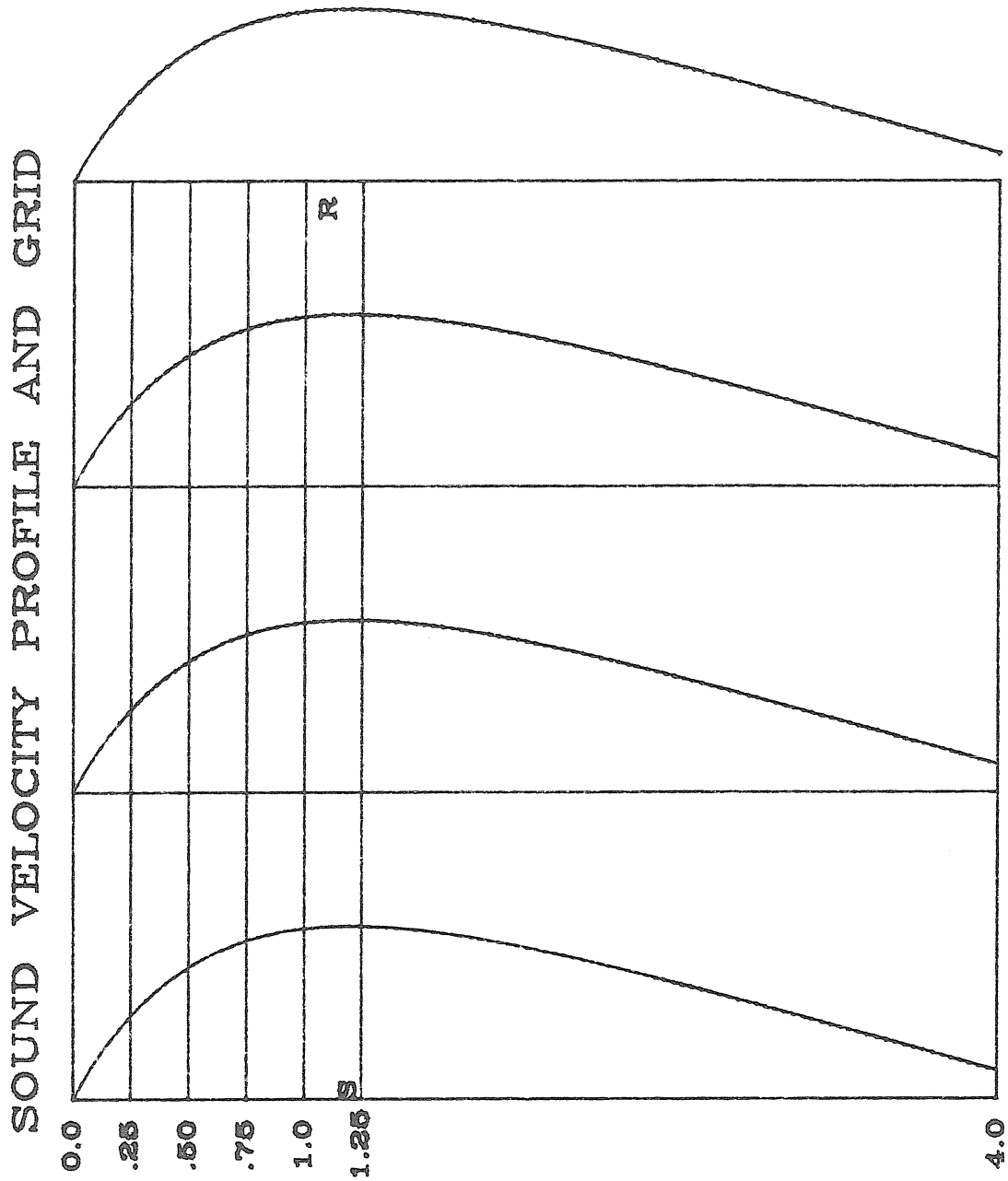

FIGURE 3-1: RANGE INDEPENDENT SOUND VELOCITY PROFILE

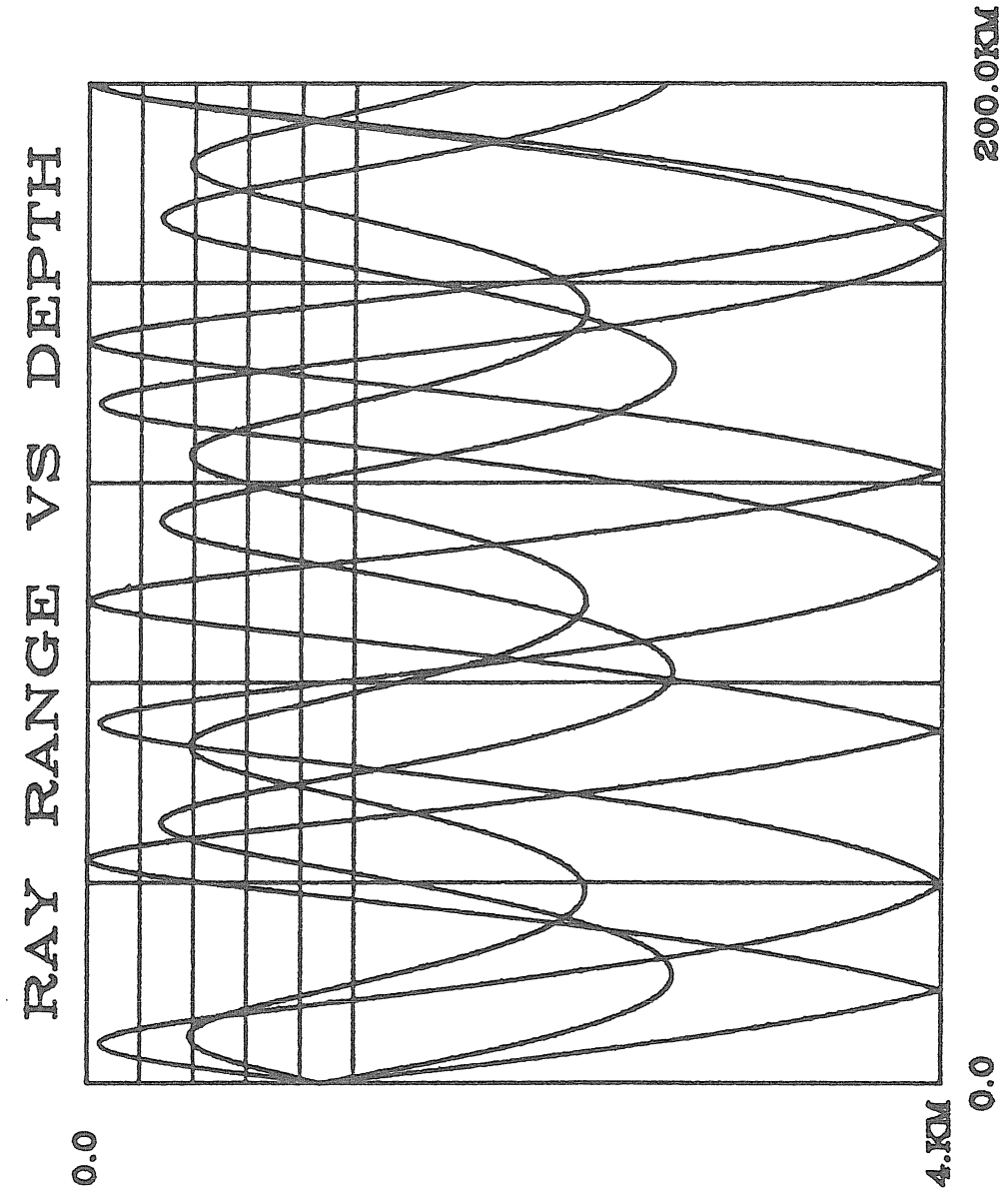

FIGURE 3-2: RANGE INDEPENDENT RAYS

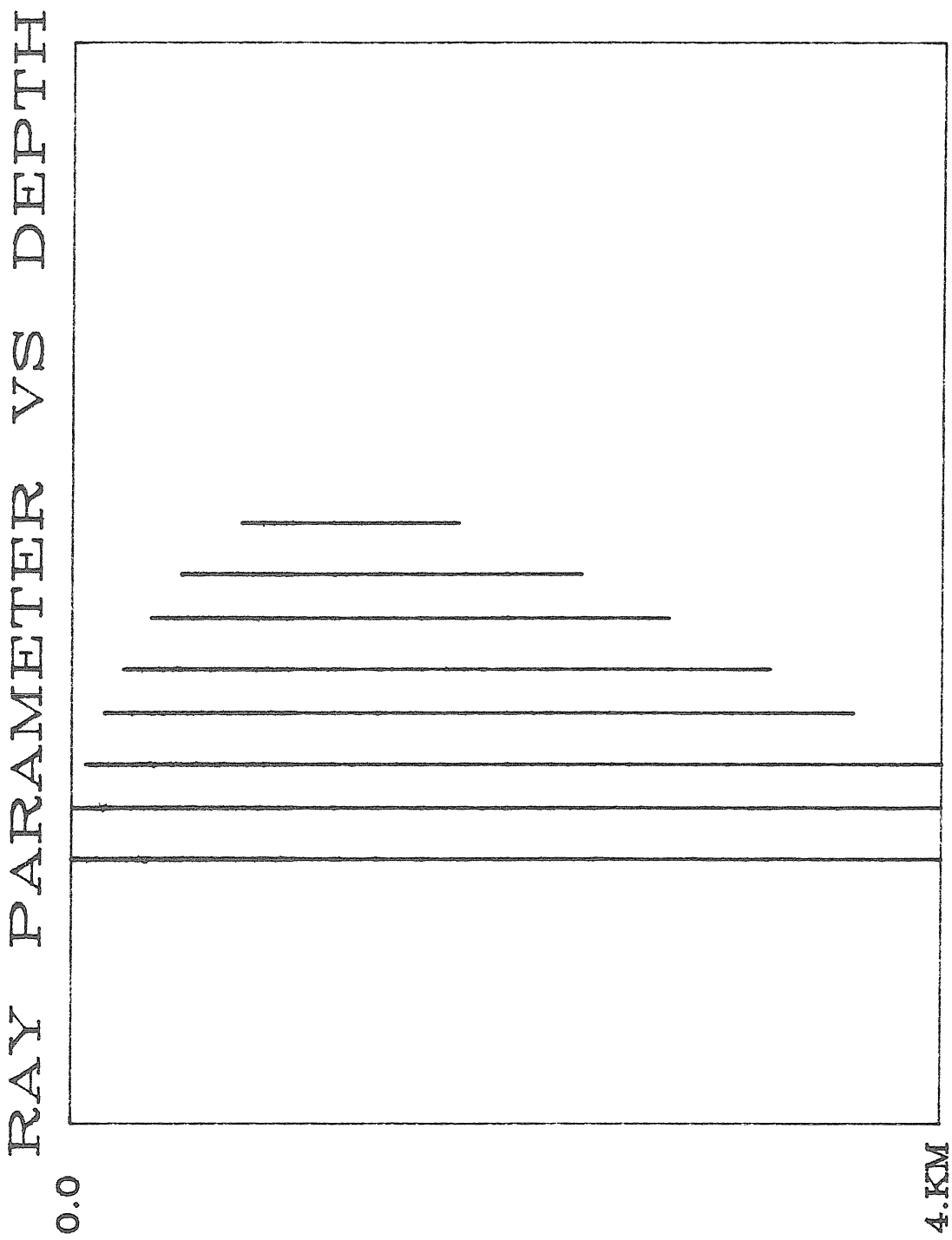

FIGURE 3-3: HORIZONTAL SLOWNESS VERSUS DEPTH

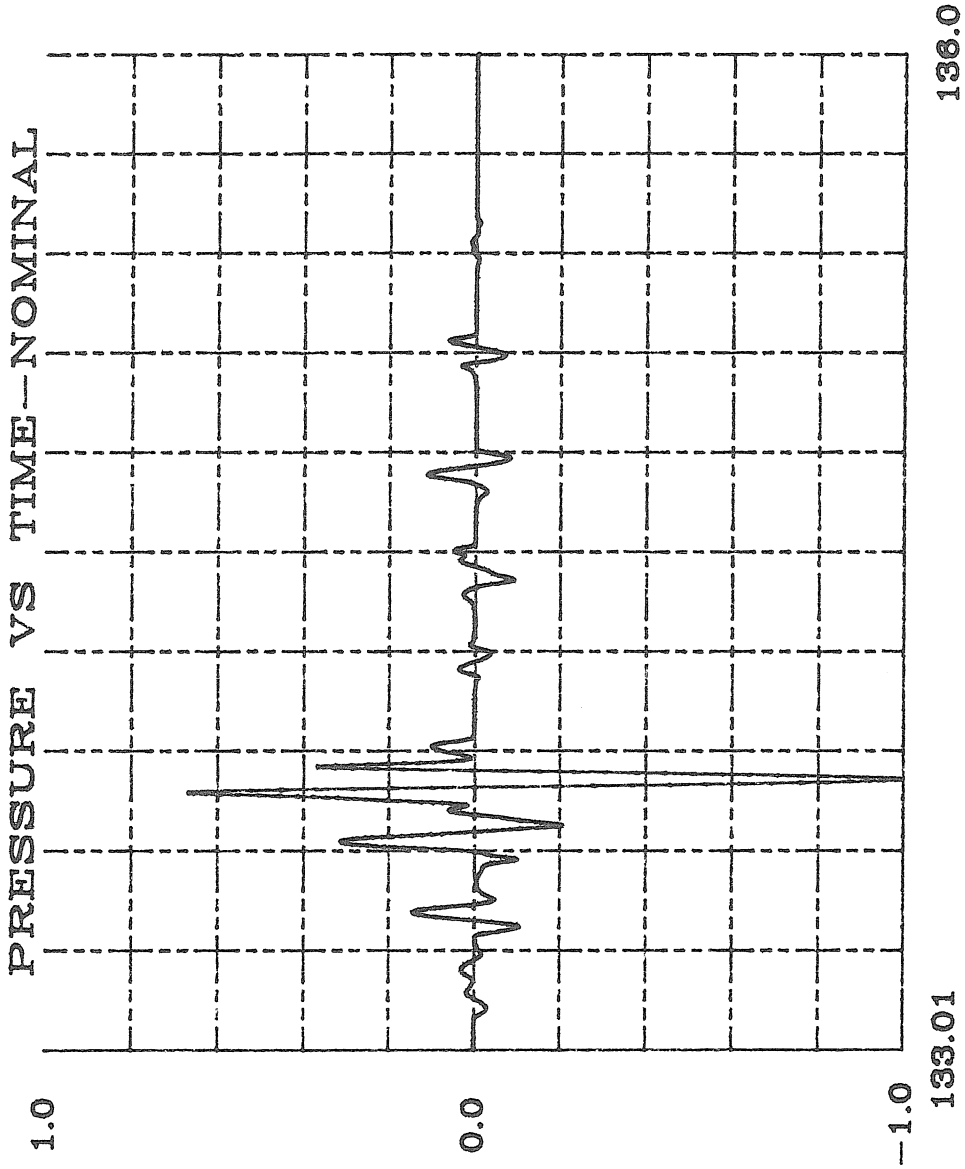

FIGURE 3-4: RANGE INDEPENDENT CASE SIGNAL

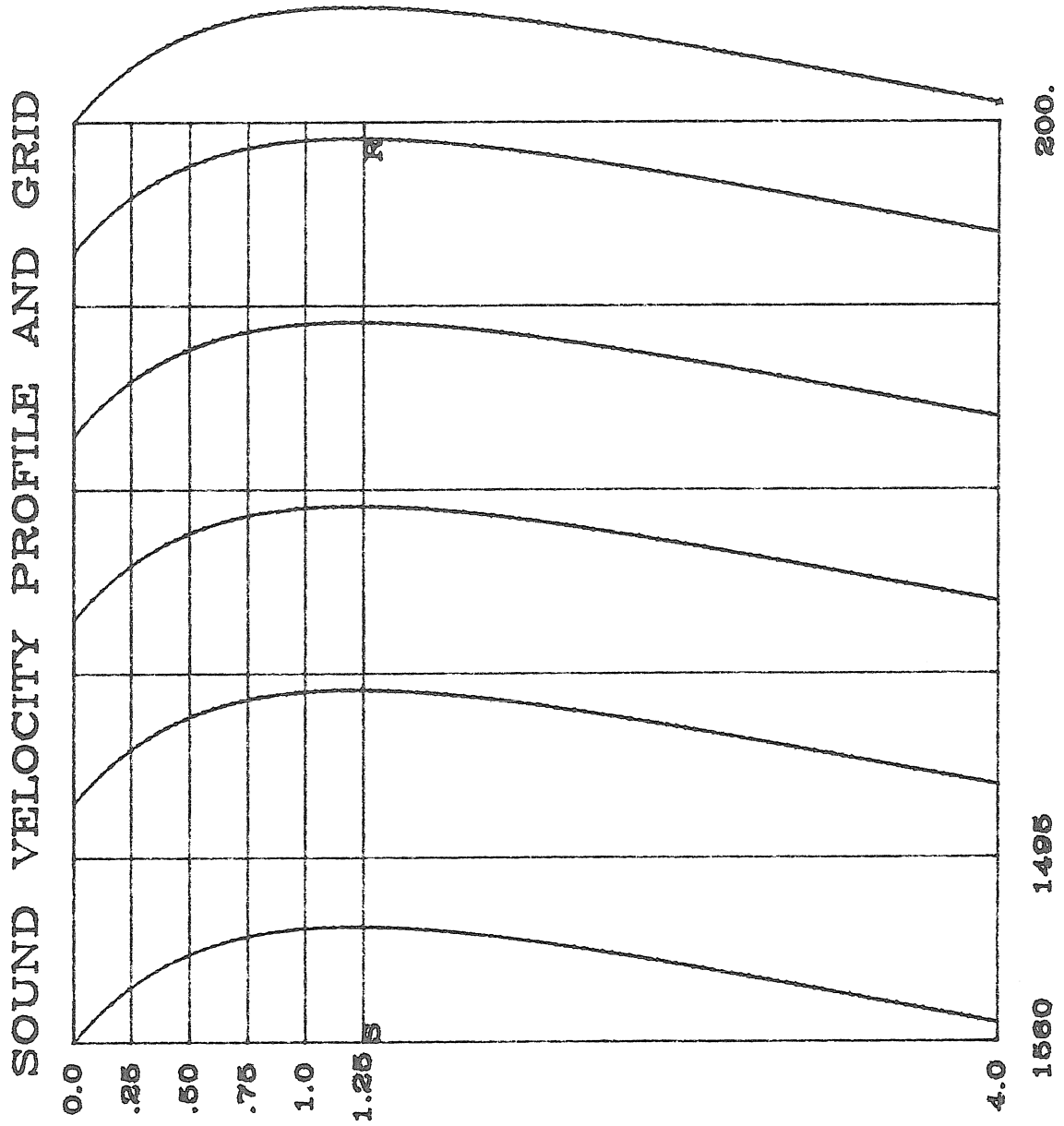

FIGURE 3-5: RANGE DEPENDENT SOUND VELOCITY PROFILE

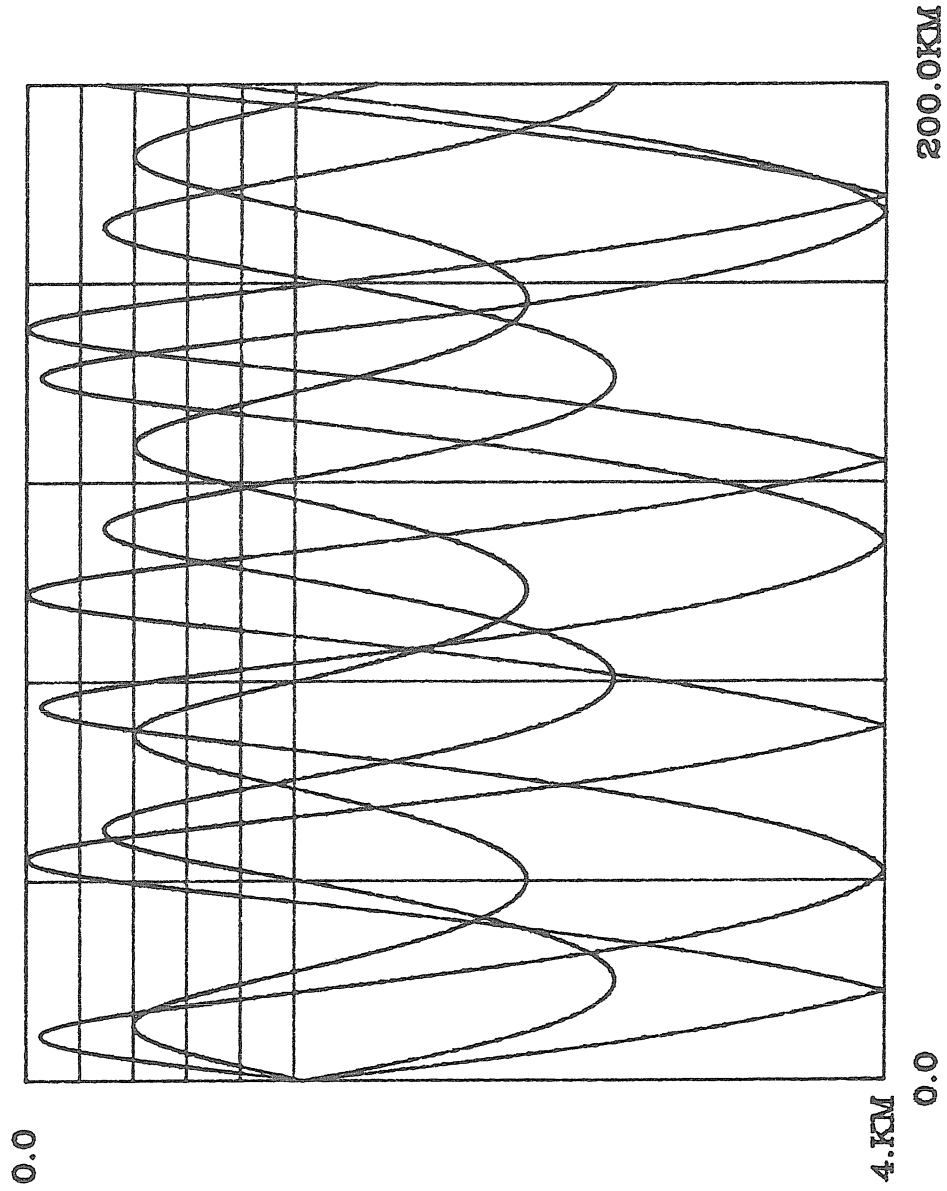

FIGURE 3-6: RANGE DEPENDENT RAYS

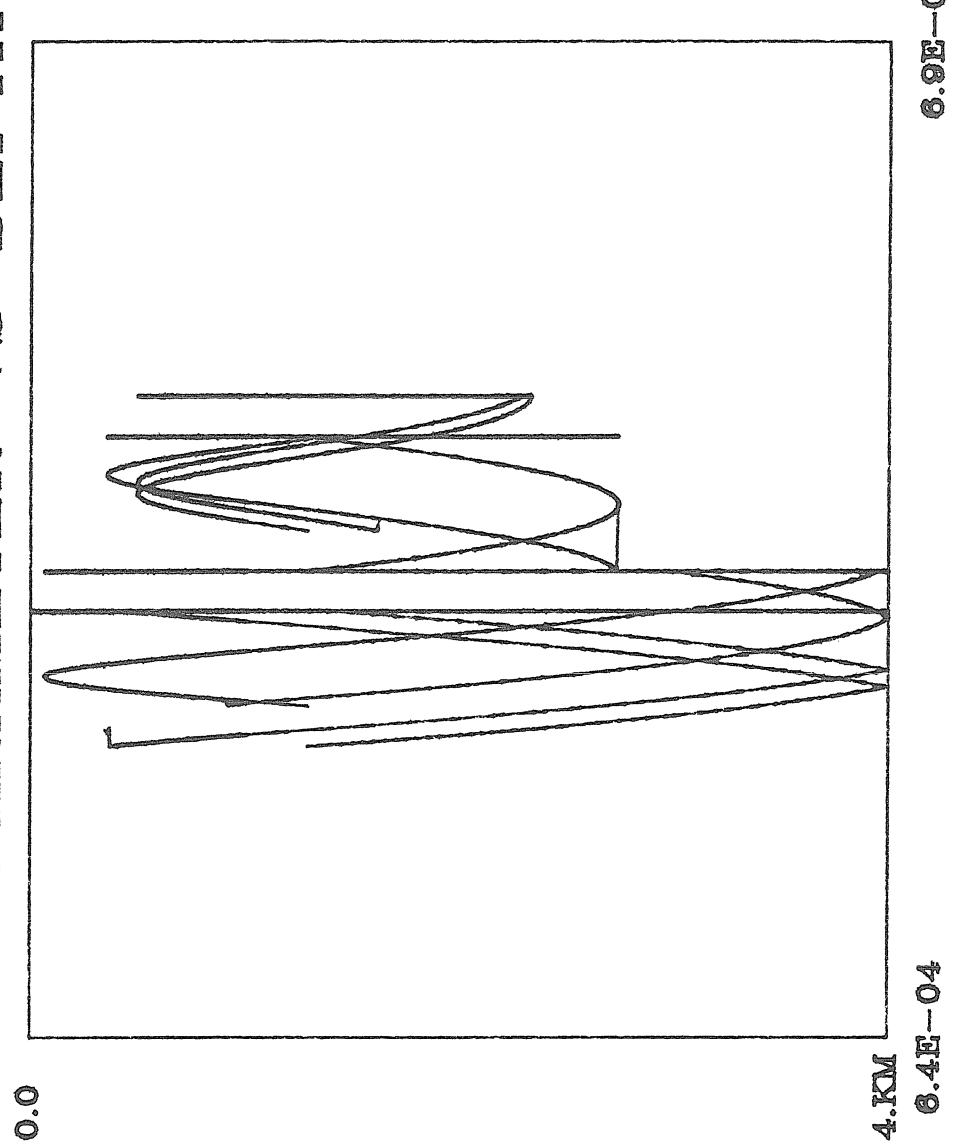

FIGURE 3-7: HORIZONTAL SLOWNESS VERSUS DEPTH

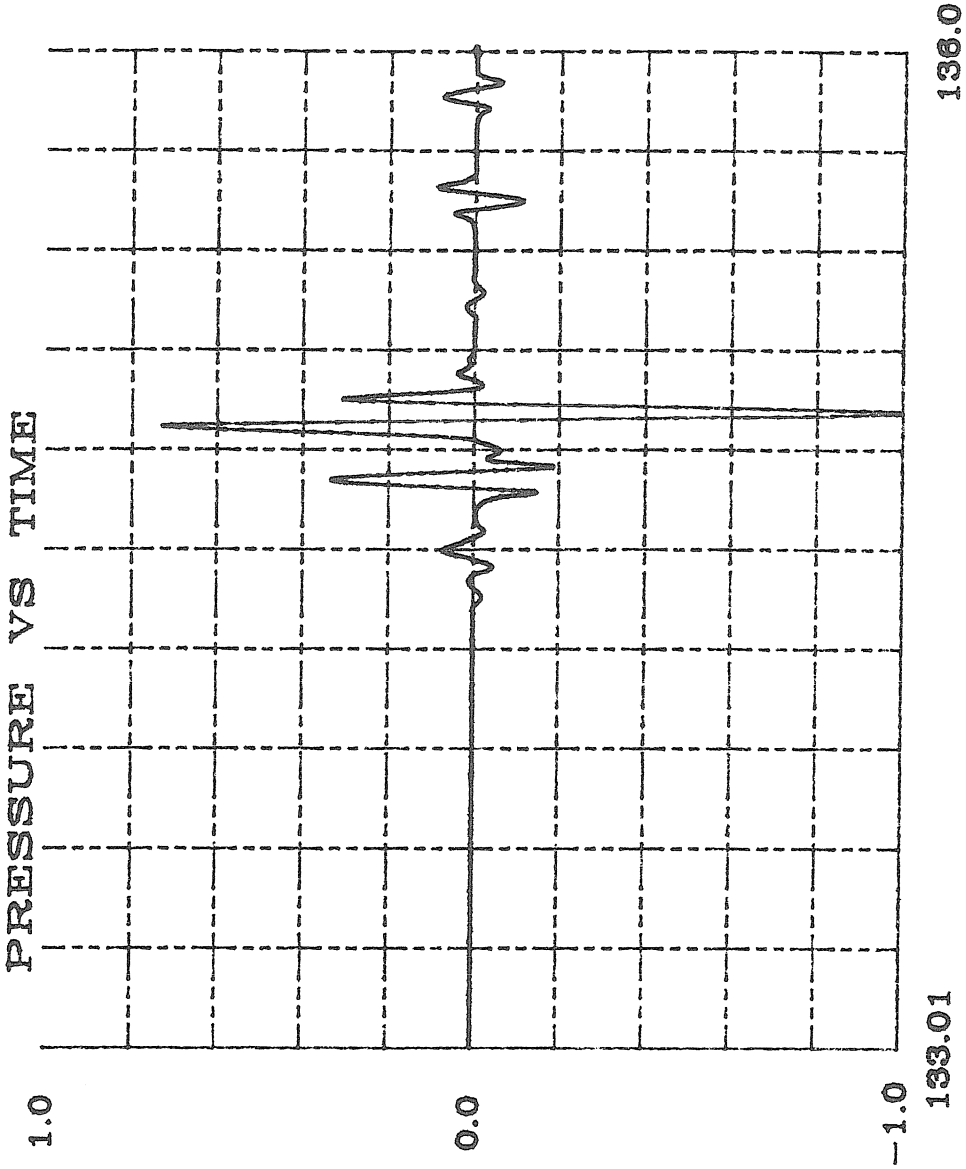

FIGURE 3-8: RANGE DEPENDENT CASE SIGNAL

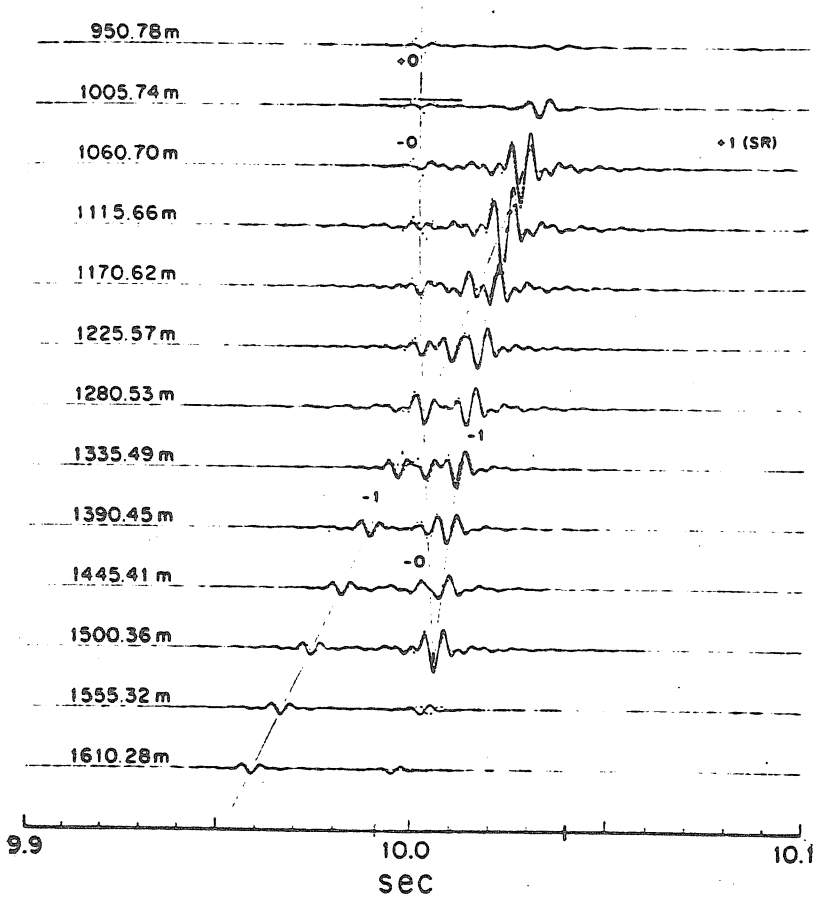

FIGURE 3-9: SAMPLE ACOUSTIC SIGNALS

FOR 1000 m SOURCE

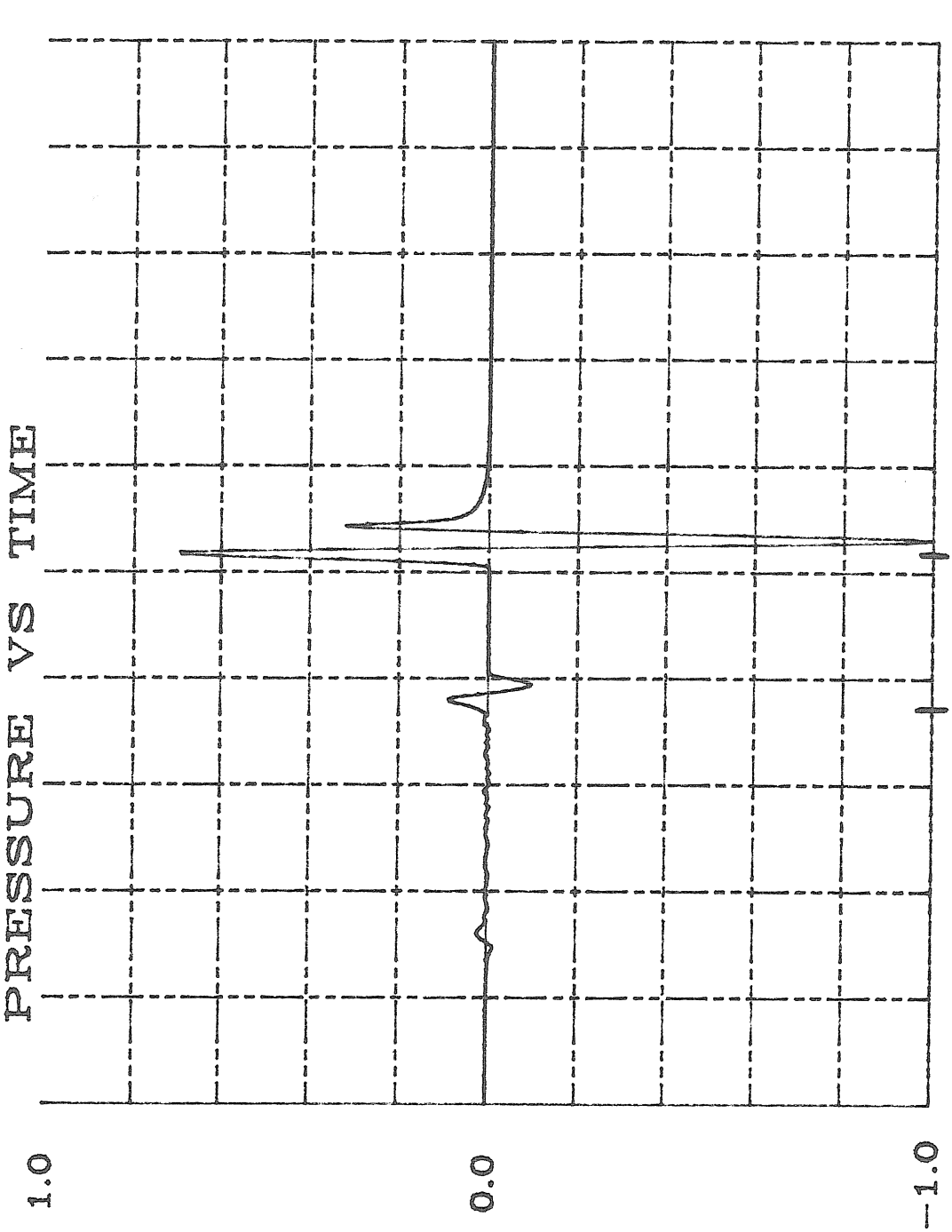

FIGURE 3-10: SIGNAL FOR 1115.66 m DEPTH

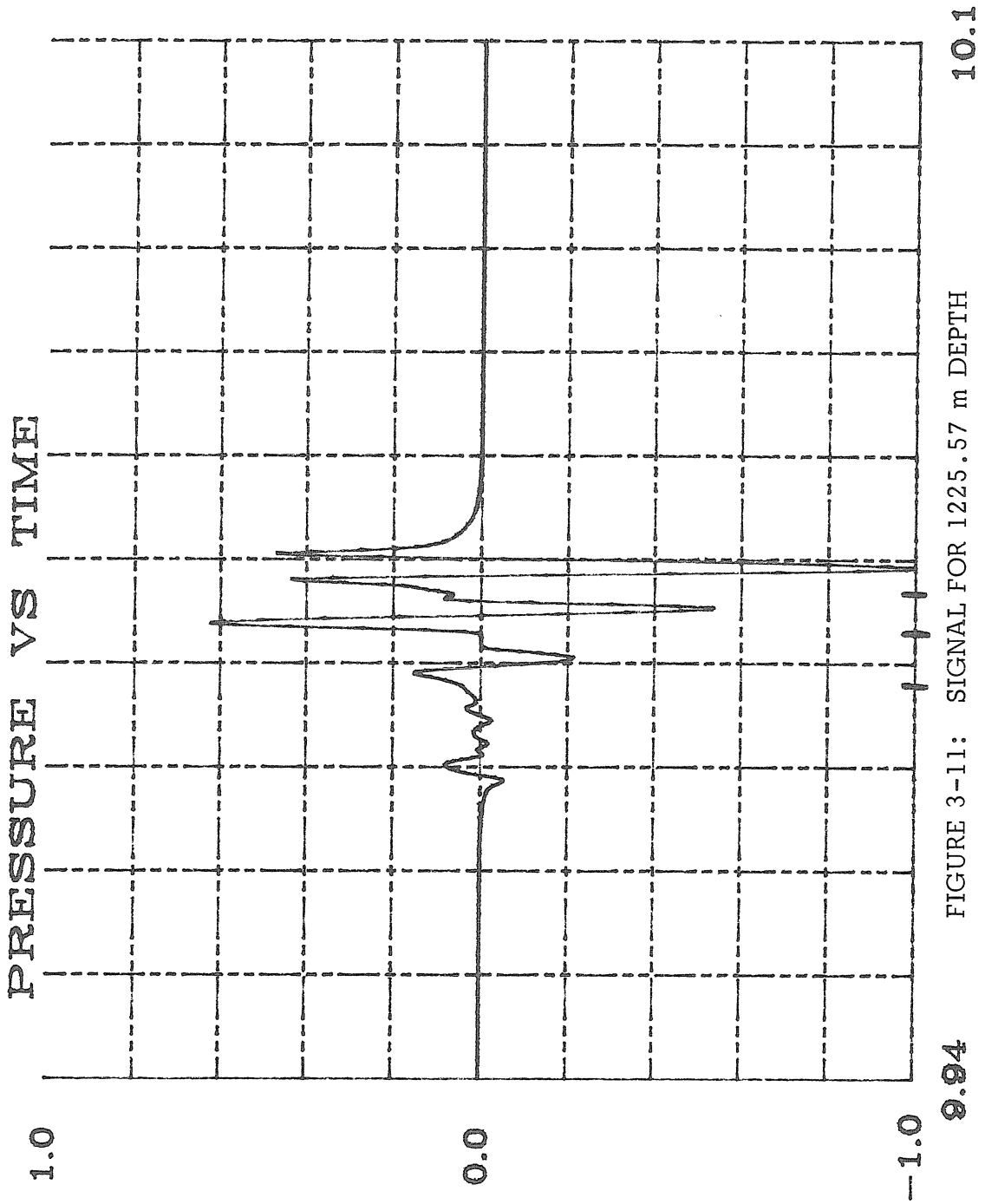

FIGURE 3-11: SIGNAL FOR 1225.57 m DEPTH

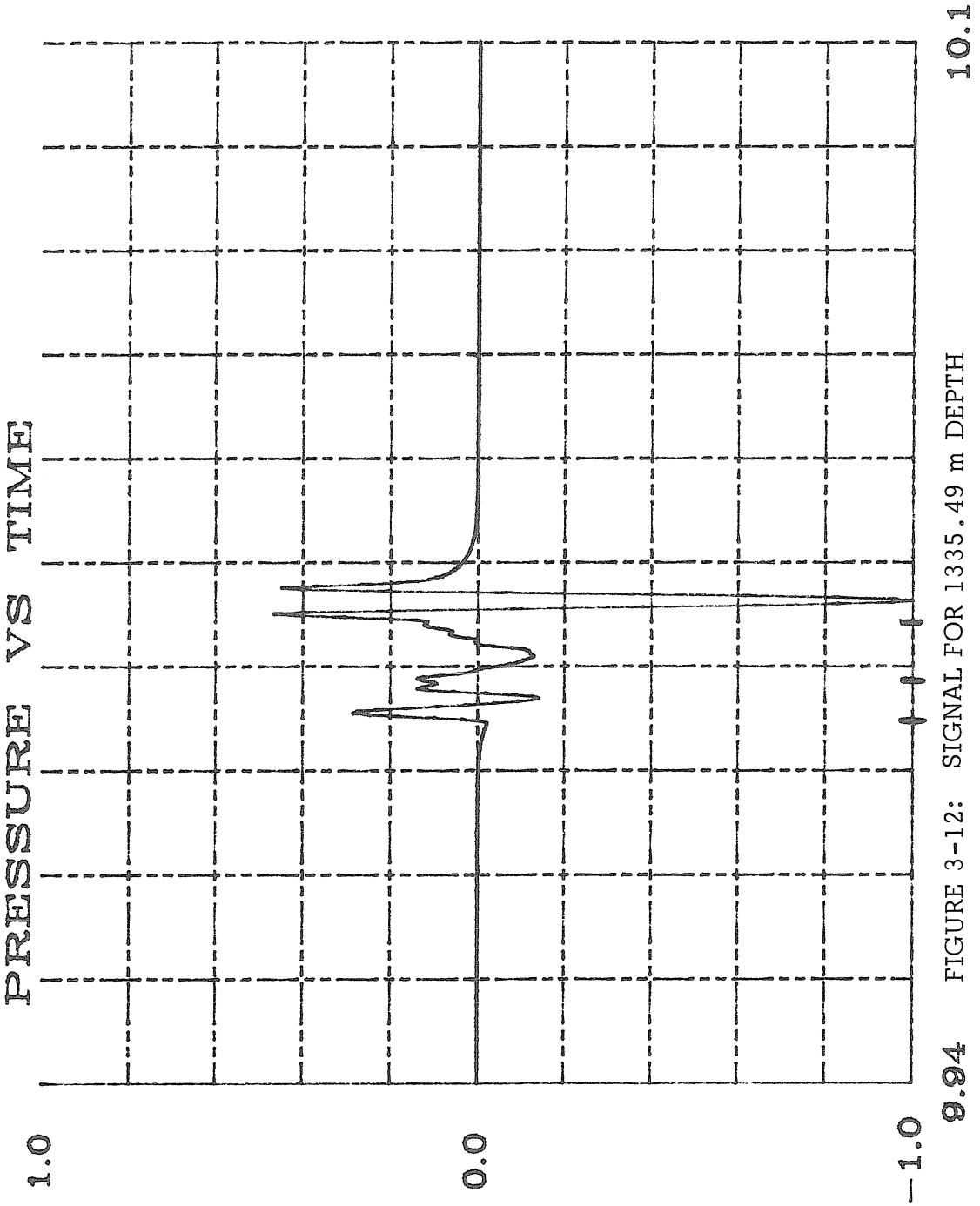

FIGURE 3-12: SIGNAL FOR 1335.49 m DEPTH

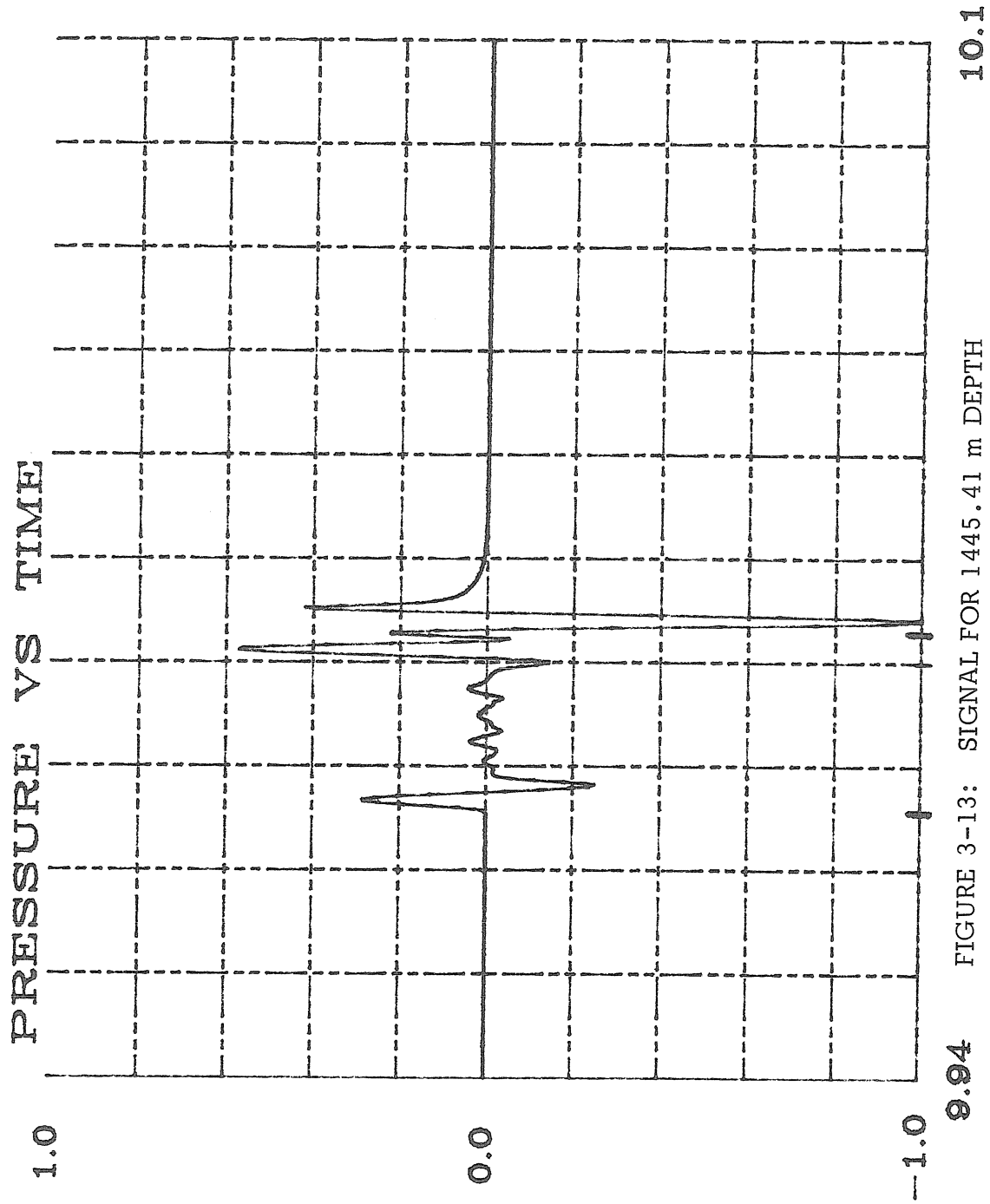

FIGURE 3-13: SIGNAL FOR 1445.41 m DEPTH

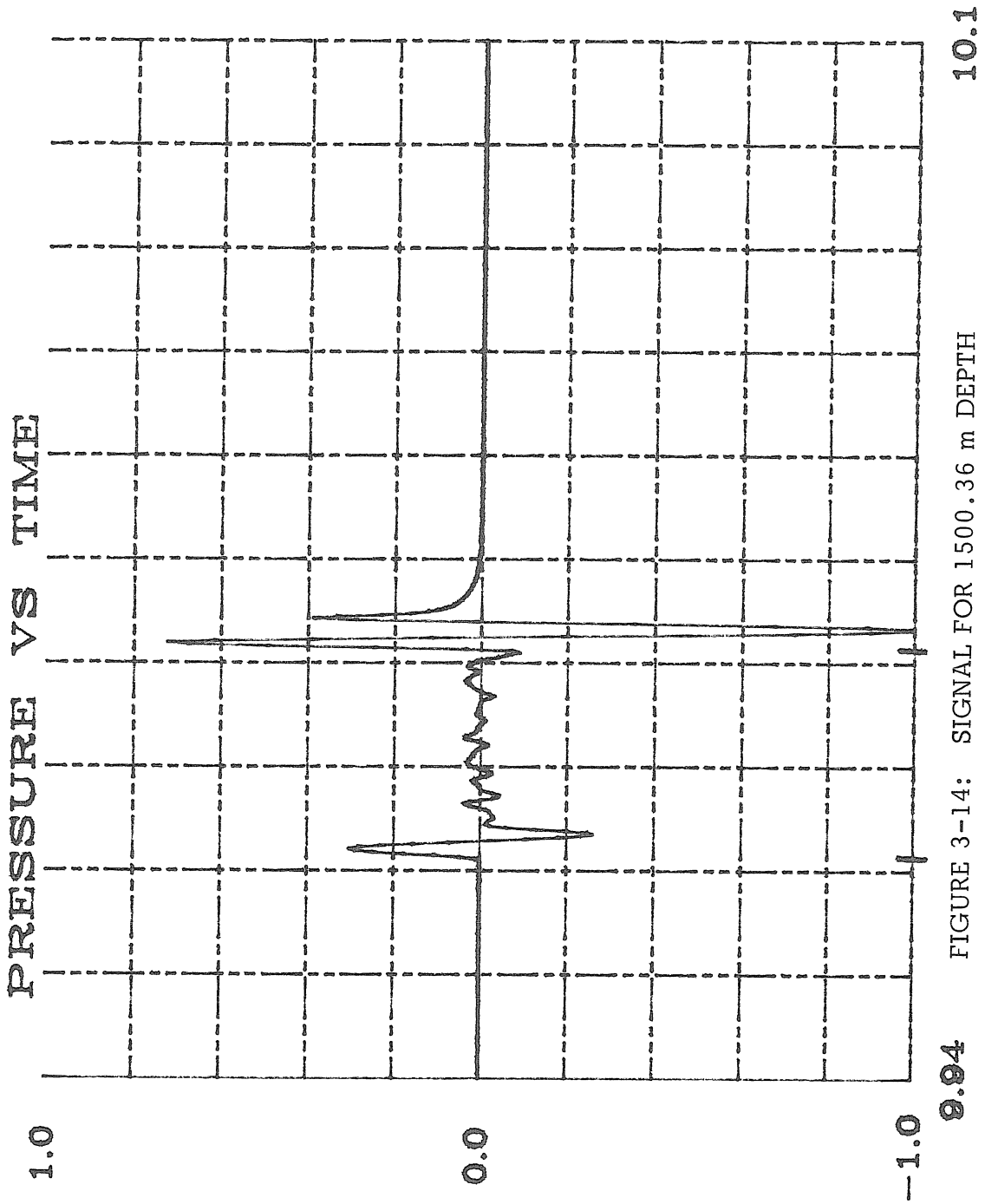

FIGURE 3-14: SIGNAL FOR 1500.36 m DEPTH

CHAPTER 3 NOTATION

a_j, b_j, C_{o_j}	coeffs used in linear $C(x,z)$
$A(\underline{x})$	amp term in $\underline{x}$ frame
$\bar{A}(p,z)$	amp term in Hilbert-Fourier transform
$\tilde{A}(\underline{y})$	amp term in $\underline{y}$ space
b_ℓ	reflection, refraction coefficient for ray type ℓ
$B(t)$	box car function $\frac{1}{2}\left[H(t+1) - H(t-1)\right]$
C_a	sound velocity at axis
C_o	reference value for C
$C(\underline{x})$	sound velocity
D	transmission matrix
$\mathcal{F}$	Fourier transform
h	ocean depth
H	Heaviside step function
H_a	scale depth for sound axis
$\mathcal{H}$	Hamiltonian
$J_o(\omega pr)$	Bessel function
$\underline{i}_j$	local horizontal vector
j	subscript for triangle index
K	wave number, ω/C_o
$\underline{k}_j$	local vertical vector

κ	transmission matrix
$\underline{\ell}_j$	vector for exit boundary in jth triangle
$\mathfrak{L}$	Lagrangian
$\underline{n}$, $\underline{m}$	ray tangential and perpendicular vectors
M(t)	source function
o	subscript denoting initial value, superscript for lowest order
$\underline{p}$	wave slowness vector (p,r,q)
p	horizontal wave slowness
p_o	initial p
p'_j	local horizontal wave slowness in triangle j
$P(\underline{x},t)$	excess acoustic pressure
$\hat{P}(\underline{x},\omega)$	Fourier transform of $P(\underline{x},t)$
$\underline{\hat{P}}(p,z,\omega)$	Hilbert and Fourier transform of $P(\underline{x},t)$
$\hat{P}(\underline{y},\omega)$	$P(\underline{x},\omega)$ transformed to $\underline{y}$ space
q	vertical wave slowness
Q	transmission matrix
r	range $\left((x - x_o)^2 + (y - y_o)^2\right)^{\frac{1}{2}}$ or out-of-plane slowness
R	range where ray last crosses receiver depth
$\mathscr{e}_j$	sign of $(-a_j \sin\phi + b_j \cos\phi)$
$\mathscr{e}$	arc length along ray
t	time
$T(\underline{x})$	geometric arrival time in $\underline{x}$ frame

$\tilde{T}(\underline{y})$	phase function in $\underline{y}$ frame
u	$1/C$, wave slowness
w	weighting function
$\underline{x}$	position of (x, y, z)
$\underline{x}_o$	initial position
$x(\underline{y})$	x coordinate as a function of (p,z)
$\dot{\underline{x}}$	vector $\frac{dx}{d\nu}, \frac{dy}{d\nu}, \frac{dz}{d\nu}$
x_{C_j}	x coordinate for center of circle in triangle j
$\underline{y}$	mixed solution basis (p, y, z)
z_a	depth of sound velocity axis
z_{C_j}	z coordinate for center of circle in triangle j

$\beta(p,z;z_o)$	amplitude function
γ	sign of $\partial x(\underline{y})/\partial p$
Γ	ray path
$\delta(m)$	delta function
∇^2	Laplacian $\frac{\partial^2}{\partial x^2} + \frac{\partial^2}{\partial y^2} + \frac{\partial^2}{\partial z^2}$
$\nabla_\perp^2$	$\partial^2/\partial y^2 + \partial^2/\partial z^2$
∇	gradient
Δt	time step

ϵ	scale coefficient for canonical sound velocity profile
η	scaled depth used in canonical sound velocity profile
Θ	time function $T(\underline{x}) + p(r - R)$
$\tilde{\Theta}$	time function $T(\underline{x}) + p(x - x(\underline{y}))$ for $\underline{y}$ frame
$\Lambda(t)$	function of Heaviside function
ν	ray coordinate such that $d\nu = C d\ell$
ξ_j	radius of circle in triangle j
$\sigma(\underline{x}, \underline{x}_o)$	KMAH index
τ	delay time function
ϕ	angle ray makes to horizontal, positive clockwise
ϕ^{in}, ϕ^{out}	ϕ at exit and entrance of triangle
ω	frequency
*	denotes convolution
$\frac{\partial(x_o, y_o, z_o)}{\partial(x, y, z)} = \frac{\partial \underline{x}_o}{\partial \underline{x}}$	ratio of cross sectional area of ray tube at $\underline{x}_o$ to that at $\underline{x}$, Jacobian

4.0 INVERSE THEORY

4.1 FUNDAMENTALS

As stated earlier, underwater acoustics is comprised of a forward problem and an inverse problem. Chapter 3 gave one solution to the complicated forward problem of predicting underwater acoustic signals under depth and range dependent conditions. The inverse problem seeks information about ocean structure from observed differences between an incoming acoustic signal and a predicted, nominal one, and Chapter 4 discusses techniques to solve this problem. This first section is an introduction to inverse theory, while sections two and three describe two common approaches, the generalized inverse and the maximum entropy inverse. The last section compares these two methods that are both used in the ocean acoustic inversions performed in Chapter 5.

Over the past twenty-five years, inverse theory has been actively used in seismology, medicine, and image processing. Much of the information presented in this section is taken from two review articles by Parker, 1977 (31) and Aki and Richards, 1980 (3) . This chapter discusses inverse theory in detail to motivate and explain the use of the generalized and maximum entropy inverses in Chapter 5.

In underwater acoustic tomography, a set of amplitude or travel time data is inverted to find a function, the sound velocity $C(\underline{x})$. Inverse

theory differs from statistical parameter estimation because a function, not just a group of numbers, is sought from a set of data. This continuous function $C(\underline{x})$ represents an infinite set of values, and the inverse problem is therefore vastly underdetermined. $C(\underline{x})$ can be modeled by discrete layers or blocks of ocean, but the inverse problem almost always remains underdetermined.

The first issue confronting an inverse problem is its restrictions. Computational time, instrumentation, data handling, and the limitations of your forward problem solution all restrict your ability to solve the inverse problem. If the continuous function is beyond your capabilities, a discrete version of $C(\underline{x})$ must be selected.

The issues of existence and uniqueness are essential. The restrictions and assumptions may not admit any solutions, or they may be underestimated, leading to nonuniqueness. The maximum entropy method discussed in Section 4.3 and nonlinearities can lead to problems in uniqueness.

The method and assumptions chosen to solve the underdetermined inverse problem must have good resolution and good statistical behavior. Spatial resolution of the $C(\underline{x})$ function is important, but data resolution is also a problem because some of the data may be contradictory. When the data

set includes noise, a tradeoff between resolution and noise performance must be made since good resolution can mean bad noise behavior. The bias and variance for the inverse estimator should be evaluated.

The observed data set is almost always a nonlinear function of the desired $C(\underline{x})$ model, but the nonlinear problem cannot usually be solved directly. Some iterative procedure is required, and the issues of existence, uniqueness, resolution, and noise performance are further complicated.

The last step toward a data inversion is construction, and this item is discussed in the next three sections. Enough assumptions have been made to reduce the underdetermined problem to a well-defined one, and now an algorithm must be developed to yield a solution. The algorithms for the generalized and stochastic inverses are well-established, but the construction of the maximum entropy inverse is still under development.

4.2 THE GENERALIZED INVERSE AND THE STOCHASTIC INVERSE

The generalized inverse and the stochastic inverse both evolve from a linearized model for the incoming data d that is a function of an unknown $C(\underline{x})$. If d is acoustic travel time data, it is related to $C(\underline{x})$ by

$$d = \int_{\Gamma} \frac{d\ell}{C(\underline{x})} \quad , \tag{4-1}$$

where Γ stands for a ray path and $d\ell$ is incremental arc length. Let d_o be a nominal predicted travel time for a reference $C_o(\underline{x})$ profile, then

$$d_o = \int_{\Gamma} \frac{d\ell}{C_o(\underline{x})} \quad , \tag{4-2a}$$

and

$$d = \int_{\Gamma} \frac{d\ell}{C_o(\underline{x}) + \delta C(\underline{x})} \tag{4-2b}$$

$$= \int_{\Gamma} \frac{d\ell}{C_o(\underline{x})} \left(1 - \frac{\delta C(\underline{x})}{C_o(\underline{x})} + \ldots \right) \quad . \tag{4-2c}$$

If the actual datum used for inversion is d_i, the difference between d and d_o, then

$$d_i = d - d_o \cong -\int_{\Gamma_i} \frac{d\ell}{C_o(\underline{x})^2} \delta C(\underline{x}). \tag{4-3}$$

Equation 4-3 completes the linearization, and the discretization leads to

$$d_i \cong \sum_{j=1}^{J} \frac{\partial d_i}{\partial C_j} \delta C_j \quad , \tag{4-4}$$

for a particular time difference d_i and discrete values of $\delta C(\underline{x})$ named δC_j. The derivative is

$$\frac{\partial d_i}{\partial C_j} = -\int_{\Gamma_j} \frac{ds}{C_o(\underline{x})^2} \quad , \tag{4-5}$$

the travel time derivative given in equations 3-65 and 3-66. Equation 4-4 applies to any linearized data system expressible as

$$\underline{d} = E\ \underline{\delta C} \quad , \tag{4-6}$$

with

$$E_{ij} = \frac{\partial d_i}{\partial C_j} \quad .$$

Equation 4-6 relates I values of d_i to J values of δC_j, and typically J exceeds I, or, at any rate, the inverse of E is singular. Therefore a generalized inverse must be sought, and the procedure here follows Aki and Richards, 1980 (3). The generalized inverse results when the following assumptions are added to the constraints of equation 4-6:

1. The generalized inverse is the minimum $\widehat{\underline{\delta C}}$ solution, so that the magnitude of $\widehat{\underline{\delta C}}$ is minimized. Therefore the new solution $\hat{\underline{C}}$ differs from $\underline{C}_o$ by the minimum amount allowed by the constraints stated in equation 4-6.

2. If the data $\underline{d}$ contain contradictory values, the generalized inverse minimizes $|\underline{d} - E\ \widehat{\underline{\delta C}}|^2$ or $|\hat{\underline{d}} - \underline{d}|^2$,

where

$$\hat{\underline{d}} = E\ \widehat{\underline{\delta C}} \quad . \tag{4-7}$$

These contradictions can arise from the forward solution, the linearization, the discretization, or noise.

Once the above assumptions have been made the solution proceeds directly from work originally done by Lanczos, 1961 (25). The generalized inverse solution is

$$\widehat{\underline{\delta C}} = V_{nz}\ \Lambda_{nz}^{-1}\ U_{nz}^T\ \underline{d} \quad , \tag{4-8}$$

for the eigenvectors and eigenvalues satisfying

$$EE^T = U\ \Lambda^2\ U^T \tag{4-9a}$$

$$E^TE = V\ \Lambda^2\ V^T \quad , \tag{4-9b}$$

and the subscript nz denotes the nonzero eigenvalues and associated eigenvectors. The matrix E has I rows and J columns, EE^T is an I by I square, while E^TE is J by J. If the inverse problem is underdetermined, some of the eigenvalues in Λ^2 will be zero, and these zeroes and their associated eigenvectors are excluded from the generalized inverse.

The model and data resolution properties of the generalized inverse are easily found. Using equation 4-8 and implying the nz subscript,

$$E = U \Lambda V^T \quad , \tag{4-10}$$

leading to

$$\widehat{\underline{\delta C}} = V \Lambda^{-1} U^T U \Lambda V^T \underline{\delta C} \quad , \tag{4-11a}$$

or

$$\widehat{\underline{\delta C}} = V V^T \underline{\delta C} \quad . \tag{4-11b}$$

Therefore, VV^T is the model resolution matrix, and a well-defined inverse problem has the identity matrix as its resolution matrix. A similar analysis for $\underline{d}$ and $\hat{\underline{d}}$ produces UU^T as the data resolution matrix, and the identity matrix results if none of the data is contradictory.

The noise performance of the generalized inverse motivates the development of the stochastic inverse. If the data contain zero mean uncorrelated Gaussian noise with variance σ_d^2, the model covariance matrix becomes

$$< \underline{\widehat{\delta C}}\ \underline{\widehat{\delta C}}^T > = \sigma_d^2 \quad V \quad \Lambda^{-2} \quad V^T \qquad . \tag{4-12}$$

If some of the eigenvalues are small, the variance of the δC_j values can be unreasonably large. Unfortunately, these same small eigenvalues gave good resolution, so a tradeoff is required.

The stochastic inverse was introduced by Franklin, 1970 (17) and treats both $\underline{d}$ and $\underline{\delta C}$ as random variables with covariance matrices R_d, R_C, and R_{Cd}. Franklin's solution is a biased, minimum variance estimator using the inverse linear operator L such that the expected value of

$$\sum_{j=1}^{J} \left(\widehat{\delta C}_j - \sum_{i=1}^{I} L_{ji}\ d_i\right)^2 \tag{4-13}$$

is a minimum. For the correlated case,

$$L = R_{Cd}\ R_d^{-1} \tag{4-14a}$$

and

$$\underline{\widehat{\delta C}} = R_{Cd}\ R_d^{-1}\ \underline{d} \qquad , \tag{4-14b}$$

while the uncorrelated case gives

$$\underline{\widehat{\delta C}} = R_C\ E^T (E\ R_C E^T + R_d)^{-1}\ \underline{d} \qquad . \tag{4-15}$$

If the δC_j values are uncorrelated with variance σ_C^2, and the d_i values are uncorrelated with variance σ_d^2, equation 4-15 reduces to

$$\underline{\widehat{\delta C}} = V \quad \Lambda \, (\Lambda^2 + \epsilon \, \mathcal{I})^{-1} \, U^T \, \underline{d} \quad , \tag{4-16}$$

with the subscript nz implied and

$$\epsilon = \sigma_d^2 / \sigma_C^2 \quad . \tag{4-17}$$

The inversion specified in equation 4-16 has the following model resolution, data resolution, and model covariance properties:

$$\underline{\widehat{\delta C}} = V \, \Lambda^2 \, (\Lambda^2 + \epsilon \, \mathcal{I})^{-1} \, V^T \, \underline{\delta C} \tag{4-18a}$$

$$\underline{\hat{d}} = U \, \Lambda^2 \, (\Lambda^2 + \epsilon \, \mathcal{I})^{-1} \, U^T \, \underline{d} \tag{4-18b}$$

$$\langle \underline{\widehat{\delta C}} \; \underline{\widehat{\delta C}}^T \rangle = \sigma_d^2 \, V \, \Lambda^2 \, (\Lambda^2 + \epsilon \, \mathcal{I})^{-2} \, V^T \quad . \tag{4-18c}$$

Eigenvalues that are smaller than ϵ will be damped, leading to better noise performance but poorer resolution than the generalized inverse.

The generalized and stochastic inverses presented in this form are only valid for the linear relation 4-6 between $\underline{d}$ and $\underline{\delta C}$. The nonlinear

equation 4-2 can be solved by iterating the linear procedure, and the method of Marquardt, 1963 (26) has been used here. This technique iterates with damped inverses similar to equation 4-16, varying the damping coefficient ϵ so that the norm of $\underline{d} - \underline{\hat{d}}$ is reduced in each iteration. For the stochastic inverse, convergence almost always occurs if ϵ is left as σ_d^2/σ_C^2, but for the generalized inverse the damping coefficient can be varied to give the fastest convergence.

4.3 THE MAXIMUM ENTROPY INVERSE

4.3.1 BASIC PRINCIPLES

The maximum entropy filter was introduced by J. P. Burg, a geophysicist, in 1967 (7) and by E. T. Jaynes, 1968 (21). It has been used extensively in spectral analysis, and its use in image processing is increasing. It differs from the generalized and stochastic inverse in several ways. The maximum entropy inverse can be based upon the nonlinear equation 4-2b or the linear equation 4-6, and the additional assumptions are quite different from those described in section 4.2. The resolution and statistical behavior of the maximum entropy inverse cannot be calculated directly due to its highly nonlinear form. In general, however, its resolution exceeds that of the generalized inverse, and its noise performance is comparable.

The basic principles of the maximum entropy inverse have often been forgotten or abused in its application to spectral analysis, according to Jaynes, 1982 (22). To avoid this in the case of underwater acoustic tomography, a review of the approach is presented here. The derivation is from Jaynes, 1982 (22) and Ables, 1974 (1).

The central principles of the maximum entropy inverse can be stated as follows:

1. The result of any transformation imposed on experimental data shall incorporate and be consistent with all relevant data, and it should be maximally noncommital with regard to unavailable data.
2. When inferences based on incomplete information are required to transform a set of experimental data, the inferences should be drawn from the probability distribution that has the maximum entropy permitted by the information that is available. This is justified by the fact that the distributions with higher entropy are the most probable in nature.

The first principle given above means that the assumptions used in Section 4.2 to produce the generalized inverse cannot be used to yield the maximum entropy solution. The requirement that $|\underline{\widehat{\delta C}}|$ be minimized must be discarded, and this makes sense intuitively because that assumption could place too much importance on the arbitrarily chosen $C_o(\underline{x})$. The second assumption, fitting the data $\underline{d}$ in the least squares sense, is discarded for the maximum entropy solution in the noise free case.

The second principle stated above utilizes the following connection between entropy and probability, called the Entropy Concentration theorum by Jaynes. A random experiment has J possible results at each trial,

and N trials are performed. Therefore there are J^N possible outcomes for the entire experiment, and each outcome yields a set of numbers of occurrences, $\{n_j\}$, for the results, giving a set of frequencies $\{f_j = n_j/N \ , \ 1 \leq j \leq J\}$. The entropy S is a function of these frequencies defined as

$$S(f_1, \ldots f_J) = - \sum_{j=1}^{J} f_j \log f_j \ , \tag{4-19}$$

and it appears below in the probability ratio.

Out of the J^N possible outcomes, the number that yield a particular set of frequencies $\{f_j\}$ is the multiplicity factor

$$W(f_1, \ldots f_J) = \frac{N!}{(Nf_1)! \ldots (Nf_J)!} \ , \tag{4-20}$$

and as N goes to infinity, the Stirling approximation gives

$$\frac{1}{N} \log W \sim S(f_1, \ldots f_J) \ , \tag{4-21}$$

the entropy function. Given two outcomes with multiplicity factors W_1 and W_2, the ratio of the probability of event 1 occurring versus that of event 2 occurring is

$$\frac{W_1}{W_2} \sim e^{N(S_1 - S_2)} \quad . \tag{4-22}$$

Therefore, the event with the higher entropy has the greater probability of occurrence, where equations 4-21 and 4-22 strictly apply only as N gets very large.

A certain fraction F of all of the possible outcomes will have an entropy within the range

$$S_{max} - \Delta S \leq S(f_j) \leq S_{max} \quad , \tag{4-23}$$

where S_{max} is the maximum entropy attainable under the constraints of the experiment. Asymptotically, $2N\Delta S$ is distributed as chi-squared with J - I - 1 degrees of freedom, where I is the total number of constraints, and thus ΔS can be found from

$$\Delta S = \frac{1}{2N} \chi^2_{dof}(1 - F) \quad . \tag{4-24}$$

The above equations can be used to check the validity of the maximum entropy assumption, and an example will be presented below. Intuitive notions from statistical mechanics and the second law of thermodynamics must also be kept in mind. Nature appears to have a "strong preference"

for situations of higher entropy. When N reaches the scale of Avogadro's number, the relative preference given by equation 4-23 becomes so overwhelming that exceptions are never seen.

Jaynes presents a simple example to further elucidate his equations. Consider an experiment that consists of tossing a die, J = 6, for N equal to 1000 realizations. On this information alone, what are the six frequencies of occurrence? The uniform distribution with f_i equal to 1/6 is the obvious answer, and it is also the maximum entropy solution. The only constraint for the problem is that

$$\sum_{j=1}^{6} f_j = 1 \quad , \tag{4-25}$$

and the entropy is given by equation 4-19. Using a Lagrangian multiplier λ, the function ξ

$$- \sum_{j=1}^{6} f_j \log f_j + \lambda \left[\sum_{j=1}^{6} f_j - 1 \right] \tag{4-26}$$

must be maximized with respect to f_j, and this yields

$$-1 - \log f_j + \lambda = 0 \quad , \tag{4-27}$$

or $f_j = 1/6$. The maximum entropy, S_{max}, is 1.792, and, by equation 4-23, 95 percent of all possible outcomes have entropy between 1.786 and 1.792.

Now the same experiment is run with a loaded die, and the constraint 4-25 is replaced by the observed

$$\sum_{j=1}^{6} j f_j = 4.5 \quad , \tag{4-28}$$

with j the number of spots up on the die. The maximum entropy solution, found with a Lagrangian multiplier, has probabilities

$$\{0.0543, 0.0788, 0.1142, 0.1654, 0.2398, \text{and } 0.3475\}$$

and entropy, S_{max} of 1.614. 95 percent of all possible outcomes have entropy between 1.609 and 1.614. An alternative solution assumes a binomial distribution with $p = 0.7$, satisfying the observation 4-28. However, this solution has only an entropy of 1.414, an event with a probability of about 10^{-84} according to equation 4-24.

Maximum entropy solutions differ from maximum likelihood methods if the probability density assumed for the maximum likelihood approach is

incorrect. If it is correct, the two solutions are identical, but if the assumed distribution is wrong or unknown, the maximum entropy solution identifies the most probable probability distribution for the solution.

4.3.2 APPLICATIONS AND ALGORITHMS

The principles and equations stated in Section 4.3.1 can be applied to many different data processing or inverse problems, including:

1. I autocovariances are observed for N realizations of a time series $\{ y_1, \ldots y_T \}$. What is the most probable time series, or, of more interest, what is the power spectrum of the most probable time series?
2. The two-dimensional Fourier transform of an image is observed. The transform consists of I discrete constraints, and the scene is comprised of luminance distributed over J pixels with the j^{th} pixel receiving a fraction n_j/N of the total luminance. What is the most probable image?

The first problem is the classical one solved by Burg, 1967 (7) , and his elegant solution is only valid when noise free autocovariances are observed and when $T >> I$. The maximum entropy solution to the second imaging problem can be extended to underwater acoustic tomography. Then, I travel time or amplitude perturbations are the observed constraints, and some total quantity of δC, the sound velocity disturbance, is distributed over J elements of the ocean. The most probable image in this case represents the most probable ocean structure profile that fits the observations.

Noise free geophysical inverse problems were solved by Bevensee, 1981 (4) , and his algorithm will be presented here. The linear system, equation 4-6, expresses the constraints of the problem

$$\underline{d} = E\,\underline{\delta C} \quad ,$$

and the simplest example is the planar, straight path travel time problem depicted in Figure 4-1. There are six sources and six receivers, and twenty-four paths are used. Twenty-four nominal travel times are expected, but other values are observed and $\underline{d}$ represents the differences between prediction and observation.

The maximum entropy inverse seeks the solution $\underline{\widehat{\delta C}}$ that satisfies $\underline{d} = E\,\underline{\widehat{\delta C}}$ and maximizes

$$S = -\sum_{j=1}^{J} \widehat{\delta C}_j \log \widehat{\delta C}_j \quad . \tag{4-29}$$

The function ζ must be maximized, where ζ includes I Lagrangian multipliers

$$-\sum_{j=1}^{J} \widehat{\delta C}_j \log \widehat{\delta C}_j + \sum_{i=1}^{I} \lambda_i \left[\sum_{j=1}^{J} E_{ij} \widehat{\delta C}_j - d_i \right] \quad . \tag{4-30}$$

The extremum of 4-30 with respect to $\widehat{\delta C}_j$ satisfies

$$- 1 - \log \widehat{\delta C}_j + \sum_{i=1}^{I} \lambda_i E_{ij} = 0 \qquad (4\text{-}31a)$$

or

$$\widehat{\delta C}_j = \exp \left[- 1 + \sum_{i=1}^{I} \lambda_i E_{ij} \right] , \qquad (4\text{-}31b)$$

and there are J equations for the J unknowns in $\underline{\widehat{\delta C}}$. The remaining I values, λ_i, are found from equation 4-6 or

$$\sum_{j=1}^{J} E_{ij} \widehat{\delta C}_j = d_i \quad . \qquad (4\text{-}32)$$

Equation 4-31a and 4-32 together give I+J equations for I+J unknowns, expressible as

$$\underline{\Phi} \left(\underline{\widehat{\delta C}} , \underline{\lambda} \right) = \underline{0} \qquad (4\text{-}33a)$$

$$\begin{bmatrix} - 1 - \log \widehat{\delta C}_1 + \sum_{i=1}^{I} \lambda_i E_{i1} \\ \vdots \\ - 1 - \log \widehat{\delta C}_J + \sum_{i=1}^{I} \lambda_i E_{iJ} \\ \sum_{j=1}^{J} E_{1j} \widehat{\delta C}_j - d_1 \\ \vdots \\ \sum_{j=1}^{J} E_{Ij} \widehat{\delta C}_j - d_I \end{bmatrix} = \underline{0} \qquad (4\text{-}33b)$$

Equation 4-33b can be solved by iterations after initial values $\underline{\widehat{\delta C}}_o$ and $\underline{\lambda}_o$ are specified and the equation is linearized to

$$\underline{\Phi}\ (\underline{v}) - \underline{\Phi}\ (\underline{v}_o) \cong G_o\ \underline{\delta v} \quad . \tag{4-34}$$

Here $\underline{v}$ is the vector of variables $\widehat{\delta C}_j$ and λ_i, and G_o is the matrix of derivatives

$$G_{k\ell_o} = \left.\frac{\partial \Phi_k}{\partial v_\ell}\right|_o \quad . \tag{4-35}$$

Terms in G_o include

$$\frac{\partial \Phi_k}{\partial v_\ell}\ , \ k \text{ and } \ell \leq J = \frac{-\delta_{k\ell}}{\widehat{\delta C}_k} \tag{4-36a}$$

$$\frac{\partial \Phi_k}{\partial v_\ell}\ , \ k \leq J, \ell > J = E_{(\ell - J)k} \tag{4-36b}$$

$$\frac{\partial \Phi_k}{\partial v_\ell}\ , \ k > J, \ell \leq J = E_{(k-J)\ell} \tag{4-36c}$$

$$\frac{\partial \Phi_k}{\partial v_\ell}\ , \ k \text{ and } \ell > J = 0 \quad . \tag{4-36d}$$

The iterated solution is found by summing incremental solutions from

$$\underline{\delta v}_m = G_m^{-1} \left(\underline{\Phi}\ (\underline{v}) - \underline{\Phi}\ (\underline{v}_m)\right) \quad , \tag{4-37}$$

for the m^{th} iteration, and the damping method of Marquardt (26) can be used to assure convergence

The algorithm given above works well, and sample solutions will be given in Section 4.4. However, this solution is applicable only for the noise-free constraints of equation 4-32, and the process quickly becomes unwieldly as I + J gets large. An alternative solution, valid with noisy data, was originally proposed by Ables, 1974 (1) and performed by Gull and Daniell, 1978 and 1980 (19 and 20).

The data $\underline{d}$ are assumed to include zero mean uncorrelated Gaussian noise with variance σ_d^2, and therefore the quantities

$$h_i = \frac{1}{\sigma_d} \left(d_i - \sum_{j=1}^{J} E_{ij} \widehat{\delta C}_j \right) \qquad (4\text{-}38)$$

are I samples from a standard normal distribution. The statistic $\sum_{i=1}^{I} h_i^2$ follows a χ^2 distribution and for 50 percent and 95 percent confidence, respectively,

$$\chi^2_{0.50} \cong I \qquad (4\text{-}39a)$$

and

$$\chi^2_{0.95} \cong I + 1.645 (2I)^{1/2} . \qquad (4\text{-}39b)$$

The new constraint for the maximum entropy solution with noisy data is

$$\sum_{i=1}^{I} \frac{1}{\sigma_d^2} \left(d_i - \sum_{j=1}^{J} E_{ij} \widehat{\delta C}_j\right)^2 = \chi_\mu^2 \ , \tag{4-40}$$

for confidence level μ.

This constraint yields a new function ξ to be maximized, and only one Lagrangian multiplier is required. The new ξ is

$$- \sum_{j=1}^{J} \widehat{\delta C}_j \log \widehat{\delta C}_j + \lambda_1 \left[\sum_{i=1}^{I} \frac{1}{\sigma_d^2} \left(d_i - \sum_{j=1}^{J} E_{ij} \widehat{\delta C}_j\right)^2 - \chi_\mu^2 \right] \ , \tag{4-41}$$

and at the extremum $\underline{\widehat{\delta C}}$ and λ_1 satisfy

$$-1 \ -\log \widehat{\delta C}_j - \frac{2\lambda_1}{\sigma_d^2} \sum_{i=1}^{I} E_{ij} \left(d_i - \sum_{j=1}^{J} E_{ij} \widehat{\delta C}_j\right) = 0 \tag{4-42}$$

and equation 4-40. Equations 4-40 and 4-42 can be combined into I+1 equations in a new $\underline{\Phi}(\underline{\widehat{\delta C}}, \lambda_1)$. The form of equation 4-34 can be used again, but the derivatives are more complicated. The new terms are

$$\frac{\partial \Phi_k}{\partial v_\ell} \quad , \; k,\ell \leq J \quad = \quad - \frac{1}{\widehat{\delta C}_k} \quad \delta_{k\ell} \; - \; \frac{2\lambda_1}{\sigma_d^2} \quad \sum_{i=1}^{I} \; E_{ik} \, E_{i\ell} \qquad (4\text{-}43a)$$

$$\frac{\partial \Phi_k}{\partial v_{J+1}} \quad , \; k \leq J \quad = \quad - \frac{2}{\sigma_d^2} \quad \sum_{i=1}^{I} \; E_{ik} \, (d_i \; - \; \sum_{j=1}^{J} \; E_{ij} \, \widehat{\delta C}_j) \qquad (4\text{-}43b)$$

$$\frac{\partial \Phi_{J+1}}{\partial v_\ell} \quad , \; \ell \leq J \quad = \quad - \frac{2}{\sigma_d^2} \quad \sum_{i=1}^{I} \; E_{i\ell} \, (d_i \; - \; \sum_{j=1}^{J} \; E_{ij} \, \widehat{\delta C}_j) \qquad (4\text{-}43c)$$

$$\frac{\partial \Phi_{J+1}}{\partial v_{J+1}} \quad = \quad 0 \quad , \qquad (4\text{-}43d)$$

and iterative solutions with Marquardt's method will be presented in Section 4.4.

Gull and Daniell successfully used this second maximum entropy technique to invert radio and x-ray astronomy and photographic images. They invert Fourier transform data to formulate a map of the sky, and they describe their maximum entropy solution as a single general-purpose map that cannot lead to conclusions for which there is no evidence in the data. They noted that the maximum resolution consistent with the size of the telescope is attained and sidelobes and spurious points are reduced to

very low levels. Their maps are typically 128 x 128 pixels, and spatial resolution can be improved by factors of 2.5 or more for signal to noise ratios of around 10:1.

Another maximum entropy algorithm was used by Bryan and Skilling, 1980 (6) , and they were also processing images from astronomy. They note that constraint 4-40 deals with only the variance of the data, and the resulting inversions can be distorted due to a nonzero mean. One possible approach would be to constrain the mean value of the variables h_i

$$\Sigma \frac{1}{\sigma_d} (d_i - \Sigma E_{ij} \widehat{\delta C}_j) = 0 \quad , \tag{4-44}$$

and this requires a new Lagrangian multiplier, λ_2. However, this method causes computational problems, and convergence is rare.

Alternatively, Bryan and Skilling propose one constraint involving the $\mathcal{E}$ statistic of the data. The variables h_i are first put in ascending order

$$h_i < h_2 < \ldots < h_I \quad , \tag{4-45}$$

with subscript η denoting the rank. If these values fit an exact normal distribution, the η^{th} sorted residual would be

$$\nu_\eta = Q^{-1}\left(\frac{\eta - 1/2}{I}\right) \quad , \quad \eta = 1,2,\ldots I, \tag{4-46}$$

for Q the cumulative normal probability

$$Q(x) = \frac{1}{(2\pi)^{1/2}} \int_{-\infty}^{x} \exp\left(-\frac{1}{2} u^2\right) du \quad . \tag{4-47}$$

The $\mathcal{E}^2$ statistic is

$$\mathcal{E}^2 = \sum_{\eta=1}^{I} (h_\eta - \nu_\eta)^2 \tag{4-48}$$

with h_η the η^{th} ranked value of the I variables $\frac{1}{\sigma_d}(d_i - \Sigma\, E_{ij}\, \widehat{\delta C}_j)$.

The expected value of $\mathcal{E}^2$, with desired confidence level, is stated by Bryan and Skilling. First, the probability distribution of h_η is written as the binomial distribution

$$\text{Prob}\left[q \le Q(h_\eta) \le q + dq\right]$$

$$= \frac{I!}{(\eta-1)!\,(I-\eta)!}\, q^{\eta-1}\,(1-q)^{I-\eta} dq \quad , \tag{4-49}$$

and then this expression is integrated to obtain

$$<(h - \nu_\eta)^2> \cong <\left(Q(h_\eta) - Q(\nu_\eta)\right)^2> \Big/ (Q'(\nu_\eta))^2 \quad , \qquad (4\text{-}50)$$

where prime signifies differentiation. This result is summed over η to give $<\mathcal{E}^2>$, dominated by values away from the center of distribution. The asymptotic form used is

$$\exp(\nu_\eta^2) \sim \frac{1}{4\pi} \left(\frac{I}{\eta - 1/2}\right)^2 \Big/ \log\left(\frac{I}{\eta - 1/2}\right) \quad , \qquad (4\text{-}51)$$

and the desired expected value is

$$<\mathcal{E}^2> \cong \sum_{\eta=1}^{I/2} \frac{1}{(\eta - 1/2)\log\left(I/(\eta - 1/2)\right)} \quad . \qquad (4\text{-}52)$$

For large I, the result is approximately log (log I).

Bryan and Skilling's maximum entropy constraint is

$$\sum_{\eta=1}^{I} \left(\frac{1}{\sigma_d}(d_i - \Sigma E_{ij} \widehat{\delta C}_j)_\eta - \nu_\eta\right)^2 - <\mathcal{E}^2> = 0 \quad , \qquad (4\text{-}53)$$

and only one Lagrangian multiplier is required. An extremum to the new function ζ occurs where

$$-1 - \log \widehat{\delta C}_j - \frac{2\lambda_1}{\sigma_d} \sum_{\eta=1}^{I} E_{\eta j}(h_\eta - \nu_\eta) = 0 \quad , \qquad (4\text{-}54)$$

and the derivatives for the iterative solution are quite similar to those for Gull and Daniell's algorithm, equation 4-43. The actual derivatives are

$$\frac{\partial \Phi_k}{\partial v_\ell} \quad , \ell, k \leq J \quad = \quad -\frac{1}{\delta C_k} \delta_{k\ell} + \frac{2\lambda_1}{\sigma_d} \sum_{\eta=1}^{I} E_{\eta\ell} E_{\eta k} \qquad (4\text{-}55a)$$

$$\frac{\partial \Phi_k}{\partial v_{J+1}} \quad , k \leq J \quad = \quad -\frac{2}{\sigma_d} \sum_{\eta=1}^{I} E_{\eta k} (h_\eta - \nu_\eta) \qquad (4\text{-}55b)$$

$$\frac{\partial \Phi_{J+1}}{\partial v_\ell} \quad , \ell \leq J \quad = \quad -\frac{2}{\sigma_d} \sum_{\eta=1}^{I} (h_\eta - \nu_\eta) E_{\eta\ell} \qquad (4\text{-}55c)$$

$$\frac{\partial \Phi_{J+1}}{\partial v_{J+1}} \quad = \quad 0 \quad , \qquad (4\text{-}55d)$$

and the same iterative procedure can be used. Convergence typically occurs quickly if Marquardt's method is used.

Gull and Daniell's and Bryan and Skilling's algorithms represent the first two attempts to perform maximum entropy inversions on noisy data. Both fit Gaussian white noise of variance σ_d^2, but the maximum entropy

solution can be forced to fit any desired statistic(s), and the algorithms presented here would require only minor modifications to fit other statistics.

These algorithms only address the linearized problem, equation 4-6. The algorithms could be changed to handle the nonlinear relation, or the process outlined above can be iterated, with Marquardt's damping technique, to converge on the nonlinear solution.

4.4 COMPARISONS

Sections 4.2 and 4.3 discussed five ways to invert data to find the function $C(\underline{x})$. For noise free data, the generalized inverse (GI) or Bevensee's maximum entropy inverse (ME-1) could be used. For noisy data, the stochastic inverse (SI), the maximum entropy solution of Gull and Daniell (ME-2) or the maximum entropy inverse of Bryan and Skilling (ME-3) can be used. In this section, four of these methods will be used on synthetic travel time inversions to see how the solutions compare. Particular examples provide the only comparisons because the resolution and statistical behavior of the maximum entropy inverse cannot be calculated in general.

The first set of travel time problems pertains to the configuration depicted in Figure 4-1. Six sources, named S1 to S6, transmit signals to six receivers, R1 to R6. Twenty-four paths are utilized, and each source transmits to only four receivers. The space between the sources and receivers is segmented into thirty-six blocks of unit length and width, and the nominal speed of transmission is a unit velocity. Therefore, each signal has a nominal travel time equal to the length of the path, and travel times will be altered by disturbances in the speed of transmission, δC_j, in the blocks. When disturbances are present, the observed travel time for signal i is

$$T_i = \sum_{j=1}^{36} \frac{E_{ij}}{1 + \delta C_j} \quad , \tag{4-56}$$

where E_{ij} is the path length for signal i in block j. In the simulation, the travel time difference has been linearized to

$$d_i = - \sum_{j=1}^{36} E_{ij} \ \delta C_j \quad , \tag{4-57}$$

so no nonlinear effects complicate the following comparisons.

Equation 4-57 states the solution to the forward problem of configuration 1, and inversions will produce $\underline{\delta C}$ for an observed $\underline{\delta T}$. The twenty-four paths give the matrix E a rank of twenty-four, and the diagonal elements of the generalized inverse model resolution matrix (equation 4-11b) are presented in Figure 4-2. Values close to one signify that those blocks can be resolved well, and the central blocks with values of .75 to .81 have the best result. Disturbances in the exterior .28 block will not be resolvable with this configuration.

The first four comparisons between the inversions will be done with perfect, noise free $\underline{\delta T}$ measurements so the generalized inverse and Bevensee's ME-1 algorithm are applicable. Because it requires fewer Lagrangian multipliers than ME-1, method ME-3 is also used with low values for σ_d.

Figures 4-3 and 4-4 are for Problem 1a, where a disturbance δC equal to 0.25 was placed in blocks 15, 16, 21, and 22. Figure 4-3 is the generalized inverse solution, and the disturbed blocks were resolved to .194 or .187. The norm of $\underline{\widehat{\delta C}}$ minus $\underline{\delta C}$ was 1.33, and the ratio of the disturbed to the undisturbed solutions exceeded 4.45 for positive values or was less than -3.0 for negative. The maximum entropy inversion is in Figure 4-4, and algorithm ME-1 gives the same result as ME-3 with a standard deviation of 1.0×10^{-4} for the measurement noise. The norm of $\underline{\widehat{\delta C}}$ minus $\underline{\delta C}$ is only 0.76, only 57 percent of the norm for the generalized inverse. The disturbed regions, resolved to .219 and .213, were at least 8.2 times greater than the outer positive blocks and less than -5.9 times greater than the negative blocks. The ME-1 and ME-3 solutions are far superior to the GI inversion.

A bias term was used with the maximum entropy algorithms. The maximum entropy solutions cannot give negative values for $\underline{\widehat{\delta C}}$, so a biased $\underline{\widehat{\delta C}}'$ solution is sought, so that

$$\underline{\widehat{\delta C}}' = \underline{\widehat{\delta C}} + \underline{b} \quad , \tag{4-58}$$

where $\underline{b}$ is a vector of biases b. New travel time data are inverted

$$d_i' = d_i + \sum_{j=1}^{36} E_{ij} \; b \quad . \tag{4-59}$$

In the computations, the minimum value of b that would lead to convergence to a positive definite $\underline{\widehat{\delta C}}'$ was used. Larger values produced big $\underline{d}'$ values and affected the ability of the algorithm to find a solution with $\underline{\hat{d}}'$ almost exactly equal to $\underline{d}'$.

Figures 4-5 and 4-6 are for Problem 1b, where the 0.25 disturbance was moved to the shaded blocks 13, 14, 19, and 20. These blocks are poorly resolved by the generalized inverse to values of .094 to .139, and the norm stated in Figure 4-5 is 1.65. The minimum positive ratio is .094 to .083, or 1.13. The maximum entropy solution in Figure 4-6 is better, but the improvement is not as big as that found in Problem 1a. The ME-3 norm, with a σ_d of 1.0×10^{-4}, is 1.36 and the minimum positive ratio is 1.43. These are both about 20 percent improvements.

Figures 4-7 and 4-8 depict solutions to Problem 1c, and a 1.0 disturbance was placed in block 10. The generalized inverse solves to 0.61, a norm of 2.7 and a minimum ratio of 4.5. The maximum entropy solution renders 0.80, a norm of 1.4 and a minimum ratio of 11.1. The maximum entropy solution is nearly a 100 percent improvement for this case.

The final problem for this configuration with perfect data is Problem 1d, depicted in Figures 4-9 and 4-10. Blocks 7, 9 and 11 have δC's of 0.5

while blocks 20 and 22 have values of -0.5, and neither solution is of any use. The norms are both 3.9, and the minimum ratios are less than 1.0.

Problem 1e is based upon configuration 1 in Figure 4-1, but noisy measurements are inverted. The synthetic travel time data include Gaussian white zero mean noise of standard deviation 0.01, and this represents a two percent noise level on the disturbed travel times. The disturbance is the same as Figure 4-3, and a δC of 0.25 has been placed in blocks 15, 16, 21, and 22.

The stochastic inverse solution, with σ_d of 0.01 and σ_C of 0.1 used in equations 4-16 and 4-17, is shown in Figure 4-11, and the mean values and the standard deviations are indicated. The overall norm for $\underline{\widehat{\delta C}} - \underline{\delta C}$ is the same as that in Figure 4-3 for no noise, but the minimum positive ratio has dropped to 3.5. The resolution has decreased, and the disturbed region values have dropped by six percent. The average standard deviation, $\sigma_{\delta C}$, is 0.011.

Figures 4-12 and 4-13 depict maximum entropy inversions for Problem 1e, and twenty-five realizations were performed. In Figure 4-12 the true σ_d of 0.01 has been used in the ME-3 algorithm. The norm is 1.09 but the minimum positive ratio is only 2.16, demonstrating the lack of

resolution. The average $\sigma_{\delta C}$ is only 0.0083, substantially below that for the stochastic inverse. In Figure 4-13, a σ_d of 0.001 has been used in ME-3, and the resolution improves while the error margin worsens. The norm drops to 0.78, and the minimum positive ratio is 5.61. The average $\sigma_{\delta C}$ is 0.0158, however, and the minimum positive ratio decreases to 3.12 if the error margins are included.

Figure 4-14 shows configuration 2 used in the remaining examples, and eight sources transmit to eight receivers over twenty-four rays through sixty-four blocks. Figure 4-15 gives the generalized inverse model resolution matrix, and resolution is considerably worse than for the thirty-six block case.

Figures 4-16 and 4-17 deal with Problem 2a, a no noise twelve block disturbance with exterior δC's of 0.5 and interior values of 1.0. The generalized inverse, Figure 4-16, has a norm for $\underline{\widehat{\delta C}} - \underline{\delta C}$ of 8.04, and the minimum ratio for the inner to outer values is 1.79. The maximum entropy norm is 6.4, and the minimum inner to outer ratio is 1.95. In both cases, column 5 cannot be distinguished from column 6, leading to minimum overall ratios that are less than one.

Problem 2b is also a case with perfect measurements, and it is shown in Figures 4-18 and 4-19. The four block disturbance has δC of 0.5,

and the generalized inverse norm is 3.84 with a minimum positive ratio of 3.41 and a maximum negative ratio of -2.55. The maximum entropy solution norm is 2.24, and the ratios are 3.44 and -7.32, respectively.

Problem 2c has noisy data, with a true σ_d of 0.05, a ten percent noise level. The disturbance is the same as that for Problem 2b, and the results are given in Figures 4-20, 4-21, and 4-22. The stochastic inverse is in Figure 4-20, and it uses a σ_d of 0.05 and a σ_C of 0.06, the true values. The new norm is 3.58, and the ratios are 2.86 and -2.24. The 0.5 disturbance is solved to .274 or .281, as opposed to .314 or .321 in the no noise case. The average $\sigma_{\delta C}$ is 0.0122.

The maximum entropy solution in Figure 4-21 uses the true σ_d of 0.05 in algorithm ME-3. The resulting norm is 2.84, and the ratios are 2.17 and -6.4. The 0.5 disturbance is resolved to .361 or .335, and the average $\sigma_{\delta C}$ is .0168. Figure 4-22 has a σ_d of 0.01 in algorithm ME-3, and it displays increased resolution with worse error performance. The norm is 2.35, the ratios are 2.92 and -7.0, and the average $\sigma_{\delta C}$ is .0331. The 0.5 disturbance is assigned values of $.392 \pm .024$ or $.404 \pm .028$.

Table 4-1 summarizes the resolution and error results for problems solved for configurations 1 and 2. Norm, ratio, and average $\sigma_{\delta C}$

values are given, and two additional cases not yet discussed are included. In all cases, the maximum entropy inversions gave norms for $\underline{\widehat{\delta C}} - \underline{\delta C}$ that were less than or equal to those for the generalized or stochastic inverses. Problems 1a - c, 1e, 2b and 2c had very well defined, structured disturbances, and these norms were reduced by an average of about thirty percent when the maximum entropy solution was used.

The resolution of the maximum entropy solution usually exceeded that of the generalized or stochastic inverses. In Problem 1c, the 4.5, -2.77 ratios were improved over 150 percent to 11.1 and -8.0. When noise was present, however, in Problems 1e, the maximum entropy solution with less variance gave worse resolution. In Problem 2c, the first maximum entropy solution does have a worse value for the minimum positive ratio, but the 0.5 disturbance was resolved twenty percent better by the maximum entropy than by the stochastic inverse.

The following conclusions can be drawn from this comparison of the generalized, stochastic, and maximum entropy inverses and their algorithms:

1. Bryan and Skilling's ME-3 $\mathcal{E}$ statistic algorithm works well and converges even with very low values for σ_d.

2. The maximum entropy inverses give norms $||\underline{\delta C} - \underline{\hat{\delta C}}||$ equal to or less than the generalized or stochastic inverses.

3. The resolving power of the maximum entropy inverse is better than or equal to that of the other inverses, unless the noise compensation drops the variance to below that of the stochastic inverse.

4. Noncoherent averaging reduces the error of all of the inverses, and the high resolution maximum entropy solutions can be used in instances where averaging can be performed. The mean maximum entropy solution will be the same distance from or closer to truth than the other inverses.

5. A bias term can be used with the maximum entropy algorithm to aid convergence. The bias term should be the least value allowed.

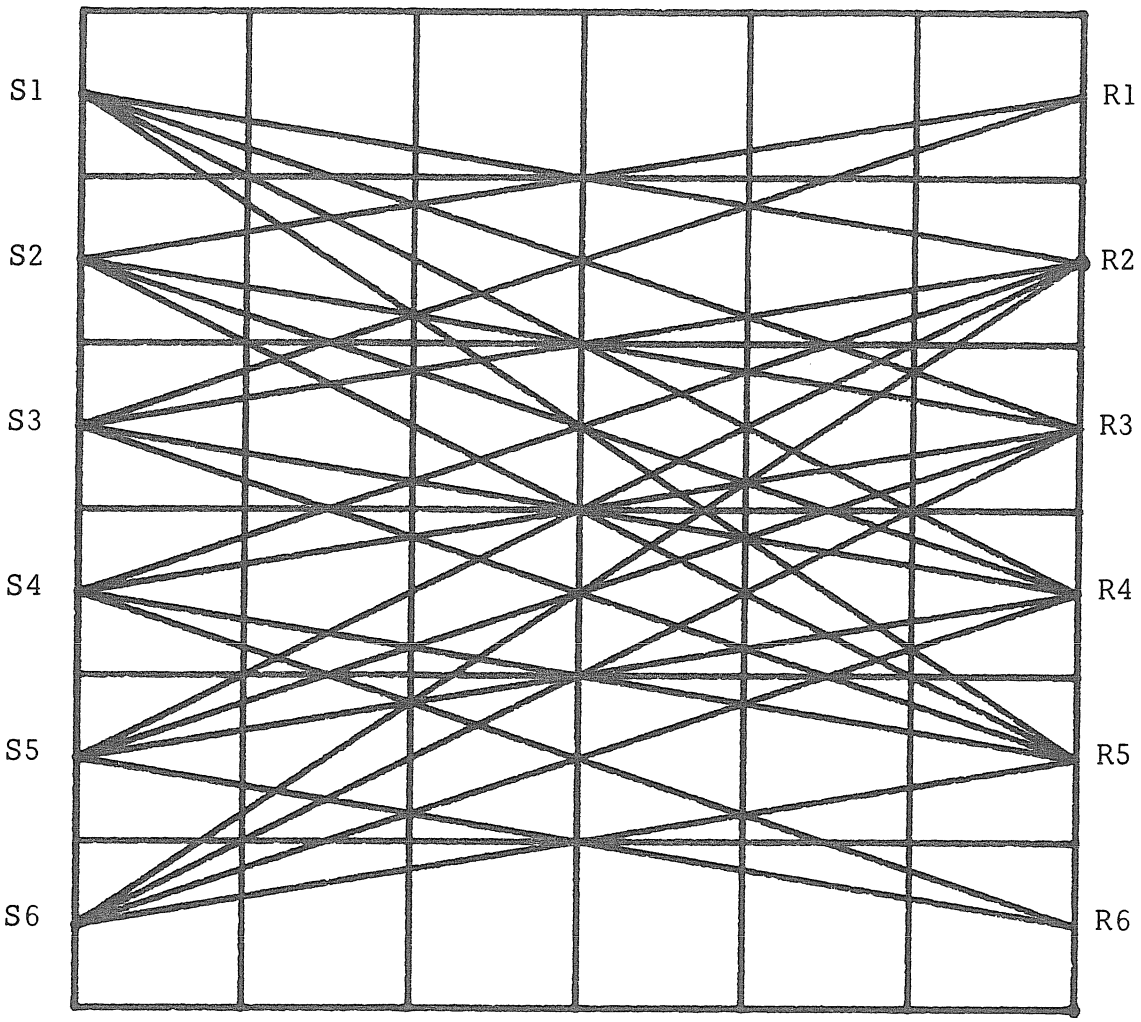

FIGURE 4-1

CONFIGURATION 1 FOR FIRST SET OF SYNTHETIC TRAVEL TIME PROBLEMS

.69	.64	.67	.59	.28	.59
.77	.63	.70	.71	.59	.74
.78	.61	.74	.75	.69	.81
.78	.61	.74	.75	.69	.81
.77	.63	.70	.71	.59	.74
.69	.64	.67	.59	.28	.59

FIGURE 4-2

CONFIGURATION 1
GI RESOLUTION MATRIX DIAGONALS

.028	.028	-.055	-.042	1×10^{-6}	.042
.028	.028	-.055	-.0625	.042	.021
.028	.028	.194	.187	.042	.021
.028	.028	.194	.187	.042	.021
.028	.028	-.055	-.0625	.042	.021
.028	.028	-.055	-.042	1×10^{-6}	.042

FIGURE 4-3: CONFIGURATION 1, PROBLEM a,
SHADED BLOCKS HAVE δC OF 0.25.
GENERALIZED INVERSE SOLUTION,

NORM = 1.33
MINIMUM POSITIVE RATIO = 4.45
MAXIMUM NEGATIVE RATIO = -3.0

.015	.015	-.03	-.022	-.002	.024
.015	.016	-.031	-.036	.025	.011
.016	.016	.219	.213	.026	.011
.016	.016	.219	.213	.026	.011
.015	.016	-.031	-.036	.025	.011
.015	.015	-.03	-.022	-.002	.024

FIGURE 4-4, PROBLEM 1a, MAXIMUM ENTROPY SOLUTIONS ME-1 OR ME-3 WITH σ_d OF .0001.

NORM = .76
MIN. + RATIO = 8.2
MAX. - RATIO = -5.9

.073	.078	.098	.094	.083	.072
.056	.057	.136	.139	.054	.056
.04	.031	-.07	-.074	.034	.040
.017	.024	-.04	-.03	.0077	.023
-.001	-.002	.0029	.0069	-.013	.006
-.018	-.022	.04	.03	1×10^{-6}	-.03

FIGURE 4-5: PROBLEM 1b, SHADED BLOCKS HAVE δC OF 0.25. GENERALIZED INVERSE

NORM = 1.65
MIN. + RATIO = 1.13

.061	.063	.128	.117	.082	.053
.045	.043	.160	.160	.042	.046
.032	.024	-.054	-.055	.024	.033
.01	.018	-.03	-.022	.002	.018
-.0026	-.001	.0056	.010	-.014	.005
-.018	-.019	.036	.027	-.003	-.026

FIGURE 4-6: PROBLEM 1b, MAXIMUM ENTROPY SOLUTION.

NORM = 1.36
MIN. + RATIO = 1.43

.05	-.054	.0038	.078	.055	.032
-.048	-.117	-.0019	.017	-.08	.063
-.034	.11	-.08	.122	-.032	.077
.09	.61	.136	-.067	.088	-.021
.103	-.16	.057	.038	.136	-.0077
.0057	-.22	.052	-.023	1×10^{-6}	.023

FIGURE 4-7: PROBLEM 1c, SHADED BLOCK $\delta C = 1.0$.
GENERALIZED INVERSE.

NORM = 2.7
MIN. + RATIO = 4.5
MAX. - RATIO = -2.77

.027	-.027	.0035	.04	.027	.014
-.025	-.056	4×10^{-4}	.01	-.047	.033
-.021	.069	-.045	.063	-.019	.037
.046	.80	.072	-.038	.05	-.016
.05	-.072	.026	.015	.078	-.011
-.033	-.1	.022	-.012	-.0016	.010

FIGURE 4-8: PROBLEM 1c, MAXIMUM ENTROPY INVERSE.

NORM = 1.4
MIN. + RATIO = 11.1
MAX. - RATIO = -8.0

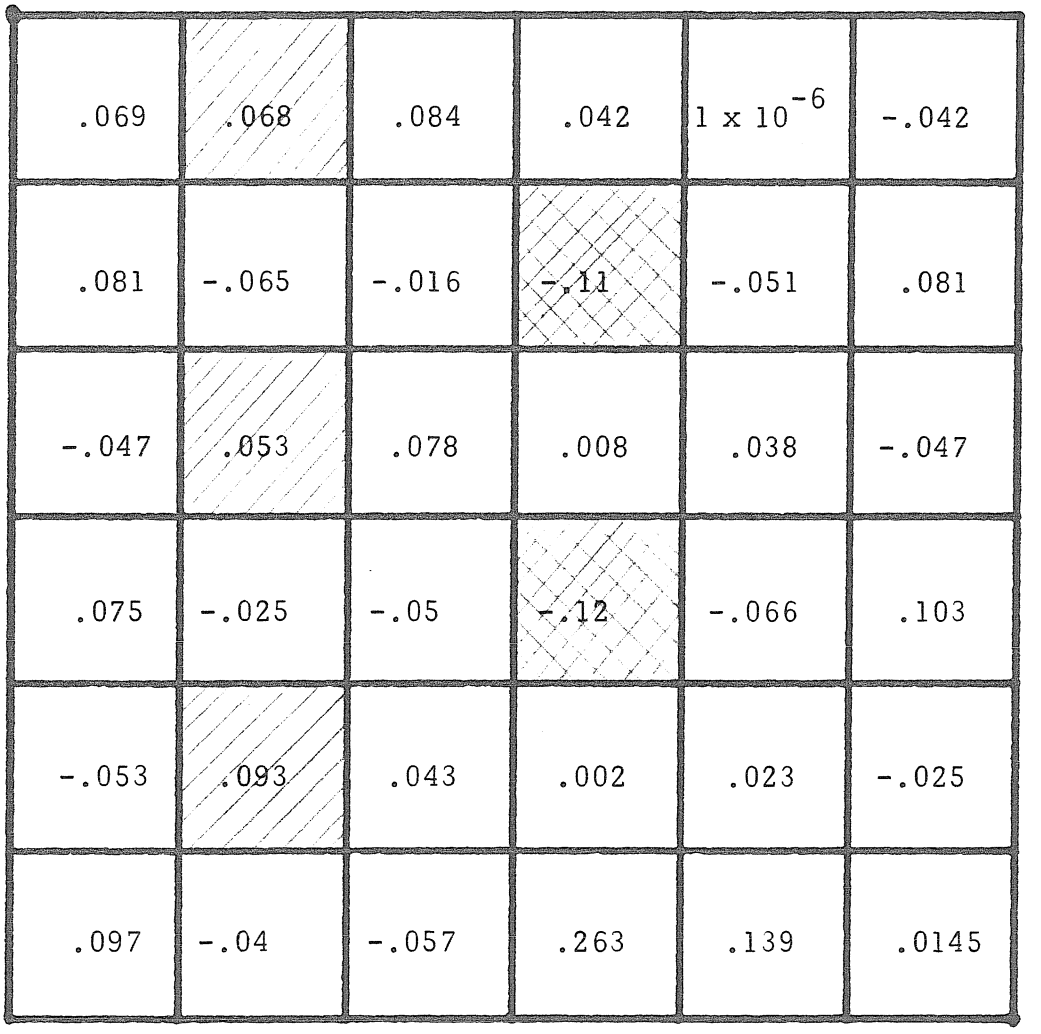

FIGURE 4-9: PROBLEM 1d,
SHADED LEFT BLOCKS HAVE $\delta C = 0.5$,
RIGHT ONES HAVE δC OF -0.5.
GENERALIZED INVERSE

NORM = 3.9
MIN. + RATIO = .68
MAX. - RATIO = -.65

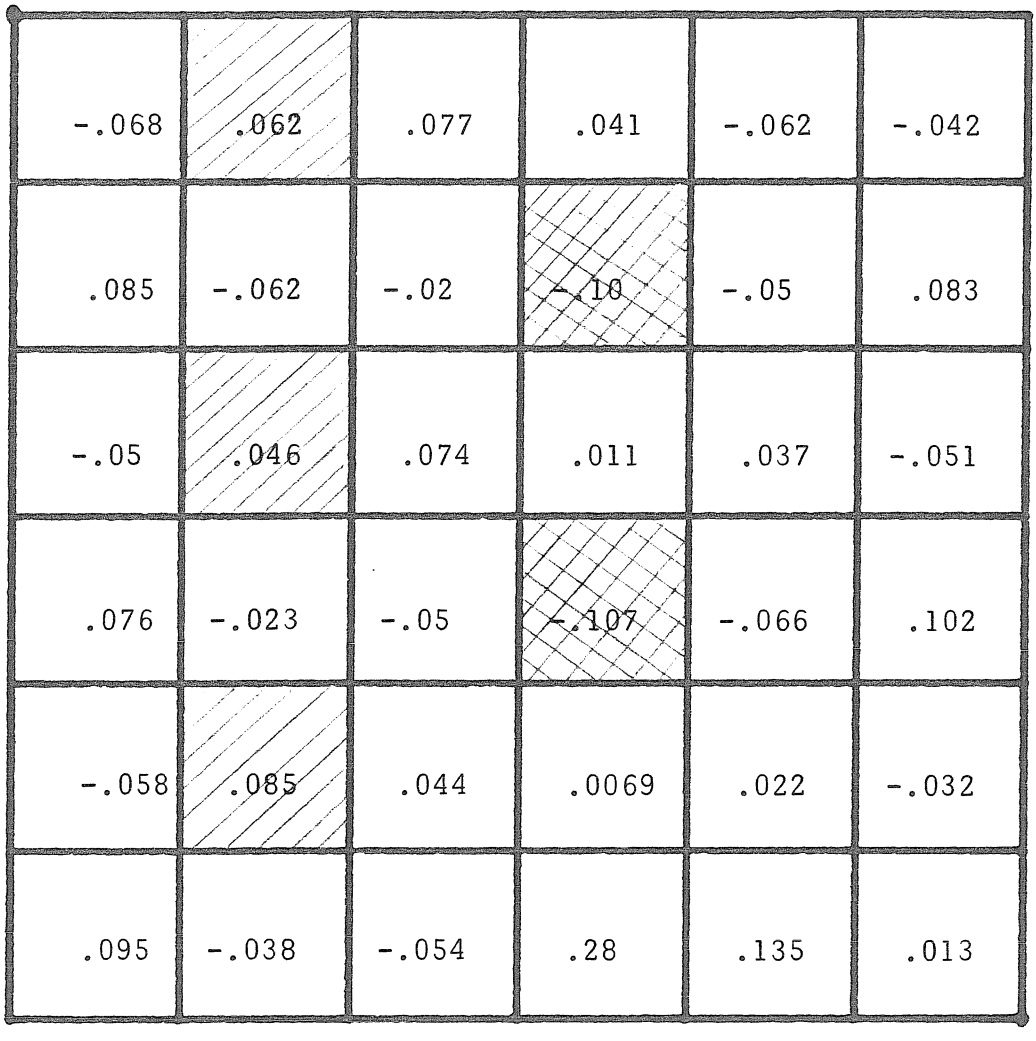

FIGURE 4-10: PROBLEM 1d, MAXIMUM ENTROPY SOLUTION.

NORM = 3.9
MAX. - RATIO =-.56
MIN. + RATIO = .54

.026 (.009)	.018 (.02)	-.044 (.017)	-.036 (.012)	-8×10^{-5} (.004)	.035 (.0098)
.027 (.0061)	.032 (.0094)	-.058 (.01)	-.058 (.011)	.033 (.016)	.026 (.0091)
.031 (.0098)	.033 (.013)	.186 (.01)	.177 (.011)	.051 (.0125)	.022 (.0061)
.031 (.0098)	.033 (.013)	.186 (.01)	.177 (.011)	.051 (.0125)	.022 (.0061)
.027 (.0061)	.032 (.0094	-.058 (.01)	-.058 (.011)	.033 (.016)	.026 (.0091)
.026 (.009)	.018 (.02)	-.044 (.017)	-.036 (.012)	-8×10^{-5} (.004)	.035 (.0098)

FIGURE 4-11: PROBLEM 1e, SHADED BLOCKS HAVE $\delta C = 0.25$, DATA NOISE WITH $\sigma_d = 0.01$. STOCHASTIC INVERSE

NORM = 1.34
MIN. + RATIO = 3.47
MAX - RATIO =-3.05
AVG. σ_{dC} = .011

.01 (.0074)	.0042 (.0087)	.013 (.012)	.0082 (.0098)	.0077 (.0047)	.0079 (.0088)
.015 (.0085)	.022 (.0093)	-.043 (.0058)	-.037 (.009)	-.005 (.008)	.034 (.0074)
.037 (.0085)	.04 (.01)	.181 (.0088)	.16 (.015)	.073 (.0115)	.024 (.0088)
.04 (.0071	.04 (.0093)	.182 (.010)	.16 (.010)	.074 (.0083)	.023 (.0066)
.016 (.0073)	.024 (.01)	-.043 (.0062)	-.037 (.006)	-.0056 (.0083)	.034 (.0065)
.011 (.0056)	.0041 (.012)	.010 (.0126)	.01 (.0091)	.0083 (.0041)	.007 (.0065)

FIGURE 4-12: PROBLEM 1e, MAXIMUM ENTROPY SOLUTION. 25 REALIZATIONS, $\sigma_d = \sigma_d = 0.01$,

ME-3 ALGORITHM
NORM = 1.09
MIN. + RATIO = 2.16
MAX. - RATIO = -3.72
AVG. $\sigma_{\delta C}$ = 0.0083

.0126 (.011)	.016 (.023)	-.022 (.022)	-.021 (.012)	-.002 (.0063)	.024 (.0125)
.013 (.0096)	.017 (.016)	-.031 (.013)	-.037 (.017)	.017 (.02)	.014 (.01)
.018 (.014)	.018 (.0196)	.217 (.014)	.202 (.024)	.036 (.021)	.011 (.01)
.022 (.0135)	.016 (.021)	.218 (.0188)	.203 (.019)	.036 (.017)	.011 (.009)
.015 (.0096)	.017 (.0186)	-.032 (.015)	-.034 (.011)	.015 (.020)	.013 (.01)
.014 (.011)	.018 (.032)	-.027 (.026)	-.016 (.013)	.0003 (.019)	.021 (.01)

FIGURE 4-13: PROBLEM 1e, MAXIMUM ENTROPY SOLUTION, 25 REALIZATIONS. $\sigma_d = 0.01$, $\hat{\sigma}_d = 0.001$

NORM = .78
MIN. + RATIO = 5.61
MAX. - RATIO = -5.97
AVG. $\sigma_{\delta C}$ = .0158

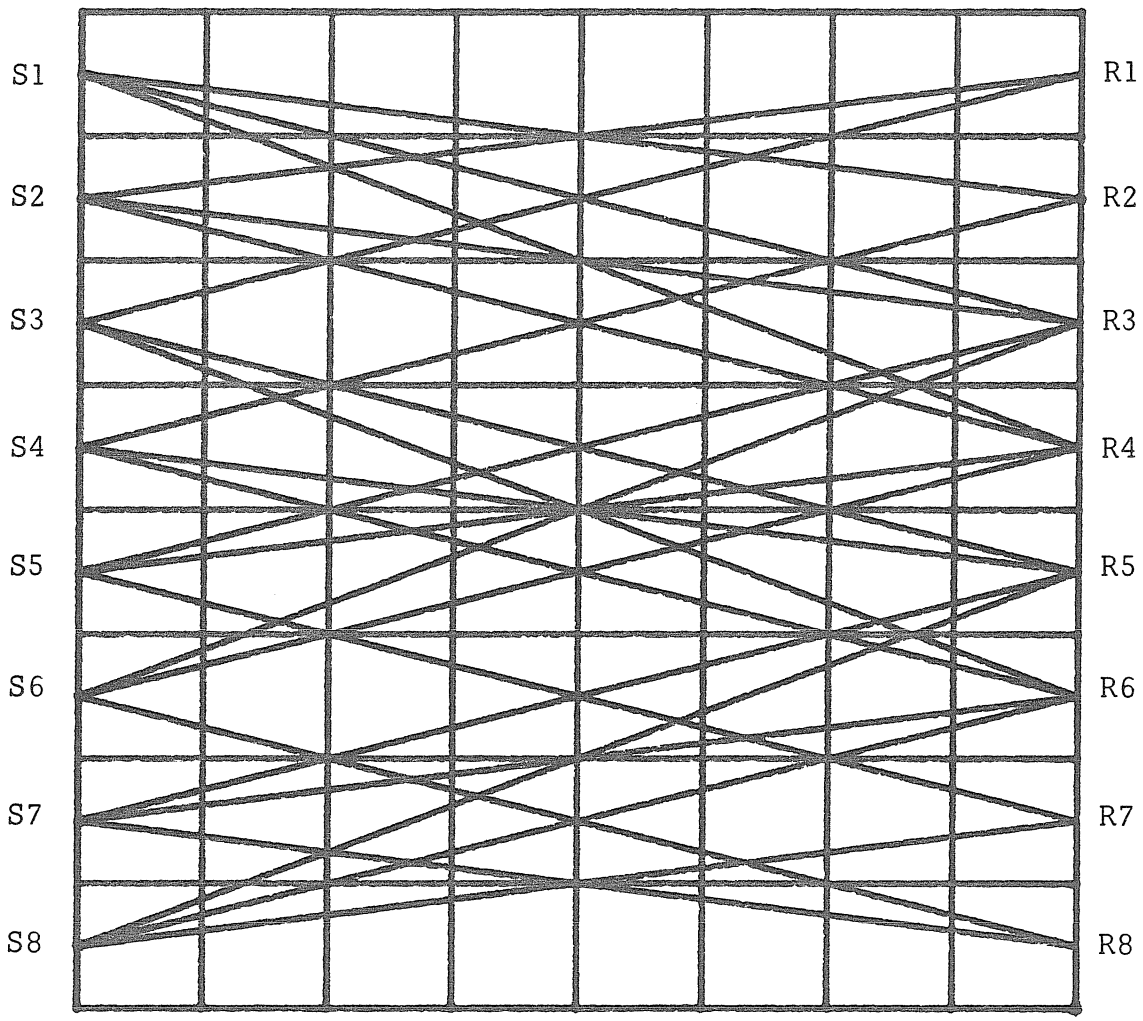

FIGURE 4-14: CONFIGURATION 2.
8 SOURCES, 8 RECEIVERS, 24 RAYS IN 64 BLOCKS.

.52	.29	.266	.266	.277	.277	.31	.31
.53	.36	.34	.34	.34	.34	.38	.41
.56	.40	.35	.35	.35	.35	.32	.51
.59	.38	.37	.37	.36	.36	.34	.49
.59	.38	.37	.37	.36	.36	.34	.49
.56	.40	.35	.35	.35	.35	.32	.51
.53	.36	.34	.34	.34	.34	.38	.41
.52	.29	.27	.27	.28	.277	.31	.31

FIGURE 4-15: CONFIGURATION 2
GENERALIZED INVERSE MODEL RESOLUTION MATRIX
DIAGONAL ELEMENTS

.1	.145	-.21	-.21	.106	.106	.18	.179
.25	.21	.237	.237	.24	.24	.091	.096
.35	.33	.695	.695	.387	.387	.11	.19
.30	.34	.32	.32	.212	.212	.23	.145
-.014	.0095	-.15	-.15	-.018	-.018	.15	.095
.002	-.047	-.042	-.0042	-.033	-.033	.018	.093
-.028	-.068	.025	.0025	-.018	-.018	.087	.067
-.083	-.044	.0042	.0043	.008	.008	.015	.015

FIGURE 4-16: PROBLEM 2a, EXTERIOR SHADED BLOCKS $\delta C = 0.5$, INTERIOR $\delta C = 1.0$. GENERALIZED INVERSE

NORM = 8.04
MIN. + RATIO LESS THAN 1.0.

.14	.093	-.0081	-.0081	.097	.097	.20	.205
.15	.21	.271	.271	.168	.168	-.018	-.034
.26	.45	.88	.88	.357	.36	.21	.18
.29	.28	.365	.365	.19	.19	.056	.11
.095	.016	-.081	-.081	.0096	.0096	.065	.11
-.017	-.0083	-.018	-.018	-.032	-.032	.034	.099
-.031	-.043	.0026	.0026	-.021	-.021	.024	-.035
-.053	-.043	.074	.074	.0039	.0039	.031	.031

FIGURE 4-17: PROBLEM 2a, MAXIMUM ENTROPY

NORM = 6.4
MIN. + RATIO LESS THAN 1.0

.044	-.093	.038	.038	-.074	-.074	-.029	-.029
-.024	.113	.058	.058	-.11	-.12	.112	.095
.062	.11	.051	.051	.314	.314	.073	.093
.027	.035	.048	.048	.321	.321	.092	.088
.032	.12	.014	.014	-.123	-.123	.028	.059
.089	-.052	-.021	-.021	-.047	-.047	-.026	.016
.034	.0158	.027	.027	-.011	-.011	.031	-.043
-.02	-.0023	.028	.028	-.017	-.017	-.035	-.035

FIGURE 4-18: PROBLEM 2b, SHADED BLOCKS δC OF 0.5, GENERALIZED INVERSE

NORM = 3.84
MIN. + RATIO = 3.41
MAX. - RATIO = -2.55

.018	.05	.07	.070	-.0013	-.0013	.0042	.0042
-.038	.048	.0078	-.0078	-.066	-.066	.021	.0026
.024	.11	.04	.04	.413	.413	.12	.062
.052	.018	-.0017	-.0017	.41	.41	.0094	.074
.054	.07	-.013	-.013	-.056	-.56	-.01	.056
.053	.0022	.0027	.0027	-.021	-.021	.045	.033
-.005	-.0045	-.014	-.014	-.017	-.017	-.031	-.056
-.008	-.0085	.069	.069	+.015	.015	.0036	.0036

FIGURE 4-19: PROBLEM 2b, MAXIMUM ENTROPY

NORM = 2.24
MIN. + RATIO = 3.41
MAX. - RATIO = -7.32

.028 (.016)	.056 (.012)	.0068 (.012)	.0068 (.012)	-.046 (.013)	-.046 (.013)	-.04 (.011)	-.04 (.011)
.012 (.017)	.097 (.012)	.048 (.01)	.048 (.01)	-.093 (.012)	-.093 (.012)	.094 (.014)	.102 (.013)
.071 (.017)	.097 (.014)	.074 (.013)	.074 (.013)	.281 (.010)	.281 (.010)	.097 (.011)	.09 (.015)
.0083 (.017)	.03 (.013)	.062 (.012)	.062 (.012)	.274 (.011)	.274 (.011)	.093 (.011)	.093 (.013)
.057 (.017)	.095 (.013)	.043 (.012)	.043 (.013)	-.122 (.011)	-.122 (.011)	.038 (.011)	.055 (.013)
.052 (.017)	-.034 (.014)	-.018 (.013)	-.18 (.012)	-.039 (.010)	-.039 (.010)	-.019 (.011)	.003 (.015)
.021 (.017)	.013 (.012)	.012 (.01)	.0123 (.01)	-.00105 (.012)	-.00105 (.012)	-.0004 (.014)	-.04 (.013)
-.0047 (.016)	.0035 (.012)	.016 (.012)	.016 (.012)	-.009 (.013)	-.009 (.013)	-.017 (.011)	-.017 (.011)

FIGURE 4-20: PROBLEM 2c, $\sigma_d = 0.05$,
STOCHASTIC INVERSE

NORM = 3.58
MIN. + RATIO = 2.86
MAX. - RATIO = -2.24
AVG. $\sigma_{\delta C}$ = .0122

.025 (.023)	-.029 (.0081)	.065 (.016)	.065 (.016)	.039 (.014)	.039 (.0145)	-.0009 (.011)	-.0009 (.011)
-.0034 (.024)	-.058 (.017)	-.014 (.012)	-.014 (.012)	-.059 (.0057)	-.059 (.0057)	.0386 (.015)	.035 (.016)
.03 (.025)	.11 (.034)	.095 (.019)	.095 (.019)	.335 (.017)	.335 (.017)	.154 (.021)	.081 (.018)
.035 (.027)	.011 (.018)	.02 (.0135)	.020 (.0135)	.361 (.021)	.361 (.021)	.026 (.014)	.083 (.02)
.08 (.0195)	.053 (.016)	.0083 (.018)	.0083 (.018)	-.052 (.0083)	-.052 (.0083)	-.0055 (.014)	.048 (.021)
.034 (.017)	.017 (.015)	.017 (.015)	.017 (.015)	-.028 (.0086)	-.028 (.0086)	.045 (.019)	.03 (.019)
-.011 (.014)	-.005 (.016)	-.025 (.010)	-.025 (.010)	-.013 (.0156)	-.013 (.0156)	-.024 (.015)	-.046 (.011)
.053 (.019)	.011 (.014)	.070 (.017)	.070 (.017)	.05 (.019)	.05 (.019)	.013 (.013)	.013 (.013)

FIGURE 4-21: PROBLEM 2c, $\hat{\sigma}_d = \sigma_d = 0.05$,
MAXIMUM ENTROPY
NORM = 2.84
MIN. + RATIO = 2.17
MAX. - RATIO = -6.4
AVG. σ_{dC} = .0168

.019 (.04)	-.045 (.010)	.066 (.027)	.066 (.027)	.0067 (.022)	.0667 (.022)	.0001 (.022)	.0001 (.022)
-.024 (.034)	.048 (.024)	-.012 (.02)	-.012 (.02)	-.065 (.008)	-.065 (.008)	.023 (.025)	.01 (.024)
.02 (.047)	.12 (.062)	.05 (.027)	.05 (.024)	.392 (.024)	.392 (.024)	.134 (.038)	.067 (.023)
.049 (.047)	.012 (.035)	.0044 (.024)	.0044 (.024)	.404 (.028)	.404 (.028)	.015 (.022)	.078 (.026)
.07 (.032)	.06 (.033)	-.01 (.030)	-.01 (.030)	-.056 (.015)	-.056 (.015)	-.011 (.024)	.054 (.027)
.049 (.035)	.01 (.025)	.0054 (.021)	.0054 (.021)	-.025 (.014)	-.025 (.014)	.05 (.032)	.036 (.028)
.0047 (.023)	-.002 (.025)	-.013 (.016)	-.013 (.016)	-.015 (.023)	-.015 (.023)	-.028 (.026)	-.055 (.017)
-.0086 (.032)	-.005 (.022)	.065 (.027)	.065 (.027)	.02 (.028)	.02 (.028)	.0024 (.021)	.0024 (.021)

FIGURE 4-22: PROBLEM 2c, $\sigma_d = .05$, $\hat{\sigma}_d = .01$

USED IN ME-3, MAXIMUM ENTROPY

NORM = 2.35
MIN. + RATIO = 2.92
MAX. - RATIO = -7.0
AVG. $\sigma_{\delta C}$ = .0331

TABLE 4-1 - SUMMARY OF INVERSIONS

PROBLEM	ERROR NORM GI or SI	ERROR NORM ME-1 or ME-3	MIN +, MAX - RATIOS GI or SI	MIN +, MAX - RATIOS ME-1 or ME-3	AVERAGE $\sigma_{\delta C}$ SI	AVERAGE $\sigma_{\delta C}$ ME-3
1a	1.33	.76	4.45, -3.0	8.2, -5.9		
1b	1.65	1.36	1.13, -1.87	1.43, -2.13		
1c	2.7	1.4	4.5, -2.77	11.1, -8.0		
1d	3.9	3.9	.68, -.65	.54, -.56		
1e - noise	1.34	1.09 .78	3.47, - 3.05	2.16, -3.72 5.61, -5.97	.011	.0083 .0158
2a	8.04	6.4	1.79 *	1.95 *		
2b	3.84	2.24	3.41, -2.55	3.41, -7.32		
2c - noise	3.58	2.84 2.35	2.86, -2.24	2.17, -6.4 2.92, -7.0	.0122	.0168 .0331
2d	4.0	3.62	1.0 *	1.0 *		
2e	3.51	2.94	1.0 *	1.0 *		

* Ratio taken within disturbed region

CHAPTER 4 NOTATION

$\underline{b}$	bias vector
$C(\underline{x})$	sound velocity
$C_o(\underline{x})$	reference or nominal sound velocity
$\delta C(\underline{x})$, δC_j	continuous or discrete difference between $C(\underline{x})$ and $C_o(\underline{x})$
$\underline{\widehat{\delta C}}$	estimate of δC vector
$\underline{\widehat{\delta C}}'$	biased estimate of δC vector
d	observed data
d_o	nominal data
d_i	difference between d and d_o
$\underline{\hat{d}}$	estimated data vector
$\underline{d}'$	biased data vector
E	matrix of $\frac{\partial d_i}{\partial C_j}$
E^T	transpose of E
$\mathcal{E}$	E statistic
f_j	frequency of occurrence of result j
F	fraction of outcomes with entropy greater than or equal to $S_{max} - \Delta S$
G	matrix of derivatives
h_i	standard normal variable
$\mathcal{I}$	identity matrix
I	total number of d_i values
J	total number of δC_j values

L	linear operator used in stochastic inverse
n_j	number of times result j occurs
nz	subscript denoting nonzero eigenvalues and associated eigenvectors
N	number of trials in given experiment
R_C	model covariance matrix
R_d	data covariance matrix
R_{Cd}	cross variance matrix for $\underline{\delta C}$ and $\underline{d}$
S	entropy
S_{max}	maximum entropy
T_i	travel time for signal i
U	matrix of eigenvectors of EE^T
$\underline{v}$	vector of unknowns $\underline{\delta C}$, $\underline{\lambda}$
V	matrix of eigenvectors of E^TE
W	multiplicity factor
Q	normal distribution, cumulative normal probability
$\delta_{k\ell}$	Kronecker delta function
Γ_j	ray path
ϵ	σ_d^2/σ_C^2
ξ	function to be maximized to find S_{max} solution
η	order subscript
λ	Lagrangian multiplier

Λ^2	matrix of eigenvalues of EE^T and E^TE
Λ^{-1}	inverse of the matrix of the square root of the eigenvalues of EE^T and E^TE
μ	confidence level
ν_η	ordered statistic
σ_d^2	data variance
σ_C^2	model $\underline{\delta}C$ variance
$\sigma_{\delta C}$	δC estimate standard deviation
Φ	function of $\underline{\delta C}$, $\underline{\lambda}$
χ^2	Chi-Square distribution
$< >$	expected value

5.0 UNDERWATER ACOUSTIC AMPLITUDE INVERSIONS

5.1 DERIVATIVES

The inversion methods discussed in Chapter 4 require linear relations between the measured data $\underline{d}$ and the desired sound velocity function or vector $\underline{\delta C}$. For underwater acoustic tomography, linear relations must be derived for travel time, acoustic amplitude and acoustic intensity as functions of sound velocity. In this section, first order derivatives are presented, and all the equations needed to set up and solve a tomography problem will be derived.

Travel time data are the arrival times of peaks in the received acoustic signal, and geometric arrival times are used. Geometric arrival time for ray i, T_i, was defined in equation 3-11, and the derivative $\partial T_i / \partial C_j$ was stated in equations 3-65a and 3-65b for the linearized sound velocity profile model. The key results are

$$T_i = \int_{\Gamma_i} \frac{d\ell}{C(\underline{x})} \tag{5-1a}$$

and

$$\frac{\partial T_i}{\partial C_j} = - \int_{\Gamma_{ij}} \frac{d\ell}{C^2(\underline{x})} \quad , \tag{5-1b}$$

where $d\ell$ is incremental ray arc length, $C(\underline{x})$ is the sound velocity and Γ_i denotes the path for ray i. Γ_{ij} signifies the portion of ray path i that passes through block j, and the integral in equation 5-16 has a closed form solution for the linearized sound velocity profile model. Equation 5-16 and its analytical representation in equation 3-65b are essential results used throughout the inversion procedure.

It is assumed for all the travel time inversions that follow that the ray path Γ_{ij} remains unchanged despite perturbations in $C(\underline{x})$. This frozen path assumption has been invoked by other workers in underwater acoustic tomography, including W. Munk and C. Wunsch (30) and M. G. Brown (5) , and it was recently investigated by J. A. Mercer and J. R. Booker (29).

Mercer and Booker found that ray paths could in fact be significantly altered by mesoscale structure in the ocean but that differences in travel time could often be accurately predicted by a frozen path model. Apparently, the displacement of rays away from a disturbed region can cause travel time changes that compensate for displacement-related but opposite travel time changes within the disturbed region. The inverse

problem, however, is complicated by any changes in ray path because ocean sampling is affected and no longer agrees with the model. These effects introduce error into ocean acoustic tomography, but they will not be addressed in the following analysis.

Equation 3-56 is the Maslov asymptotic theory solution for acoustic pressure, $P(\underline{x},t)$, and acoustic intensity is given by

$$\mathcal{I}(\underline{x},t) = P^2(\underline{x},t) + \overline{P(\underline{x},t)}^2 \quad , \tag{5-2}$$

where $\overline{P(\underline{x},t)}$ is the Hilbert transform of $P(\underline{x},t)$. Equation 3-56 and the subsequent expression for $\mathcal{I}(\underline{x},t)$ contain several terms that are functions of $C(\underline{x})$. For one ray i, the geometric amplitude term from equation 3-56 that depends on $C(\underline{x})$ is

$$G = M(t) * \delta(t - T_i(\underline{x})) \quad A_g \quad , \tag{5-3}$$

where $M(t)$ is the source function and

$$A_g = \frac{|p_o|^{1/2}}{\left| q\, q_o \quad \frac{\partial x(y)}{\partial p_o} \right|^{1/2}} \quad . \tag{5-4}$$

The derivative of G with respect to $C(\underline{x})$ in block j is

$$\frac{\partial G}{\partial C_j} = - M'(t) \quad A_g \frac{\partial T_i}{\partial C_j}$$

$$+ M(t) * \quad \delta(t - T_i(\underline{x})) \frac{\partial A_g}{\partial C_j} \quad , \qquad (5\text{-}5)$$

and the time derivative is given in equation 5-1. Under the frozen path assumption, the second term $\partial A_g / \partial C_j$ can be neglected, but changes in p_o, q_o, q or $\partial x(\underline{y}) / \partial p_o$ caused by variations in $C(\underline{x})$ can occur. Perturbations in $C(\underline{x})$ at the source or receiver would cause large changes in A_g, but these can be easily accounted for in an underwater tomography exercise.

The transform amplitude term that is dependent on $C(\underline{x})$ in equation 3-56 is similar

$$W = - M(t) * \frac{d}{dt} \quad \mathcal{I}m \left\{ \Lambda(t) * \delta\left(t - \tilde{\Theta}(\underline{x}, p)\right) A_w \right\} \quad , \qquad (5\text{-}6)$$

where

$$A_w = \frac{\left| p_o \frac{\partial p}{\partial p_o} \right|^{1/2}}{\left| qq_o \right|^{1/2} \left| \partial \tilde{\Theta} / \partial p_o \right|} \quad , \qquad (5\text{-}7)$$

$\Lambda(t)$ is in equation 3-30 and

$$\tilde{\Theta}(\underline{x}, p) = T(\underline{x}) + p\left(x - x(p,z)\right) \tag{5-8}$$

as in equation 3-49. The derivative $\frac{\partial W}{\partial C_j}$ is

$$\frac{\partial W}{\partial C_j} = M'(t) * \frac{d}{dt} \mathcal{I}m\left\{\Lambda(t)\, A_w \frac{\partial \tilde{\Theta}_i}{\partial C_j}\right\}$$

$$- M(t) * \frac{d}{dt} \mathcal{I}m\left\{\Lambda(t) * \delta\left(t - \tilde{\Theta}(\underline{x}, p)\right) \frac{\partial A_w}{\partial C_j}\right\} \tag{5-9}$$

for

$$\frac{\partial \tilde{\Theta}_i}{\partial C_j} = \frac{\partial T_i}{\partial C_j} + \frac{\partial}{\partial C_j}\left[p\left(x - x(p,z)\right)\right] \quad . \tag{5-10}$$

The derivative $\frac{\partial A_w}{\partial C_j}$ is comparable to $\frac{\partial A_g}{\partial C_j}$ and will be neglected under the frozen path assumption, but any changes in $C(\underline{x})$ that affect $\frac{\partial p}{\partial p_o}$ will alter A_w. For geometric arrivals, $x(p,z)$ is equal to x, the range to the receiver, and $\frac{\partial \tilde{\Theta}_i}{\partial C_j}$ equals $\frac{\partial T_i}{\partial C_j}$. Geometric arrivals will dominate the received acoustic signal, so in the following examples the travel time derivative is substituted for $\frac{\partial \tilde{\Theta}_i}{\partial C_j}$ in the amplitude derivative of equation 5-9.

Along with the additional terms given in equation 3-56, equations 5-1 to 5-10 define the acoustic amplitude and intensity derivatives used in the following examples. The frozen path assumption has limitations and can be inaccurate, and the properties of these derivatives will be studied in the next section.

5.2 LINEARITY

The derivatives given above provide linear relations between the data vector, $\underline{d}$, and the desired model vector, $\underline{\delta C}$, and the derivatives are stored in the matrix E such that

$$\underline{d} = E \quad \underline{\delta C} \tag{5-11}$$

to a first approximation. The quality and feasibility of the inverse solution depend upon the validity of the linear approximation. In this section, the linearity of the signal waveform derivatives of equations 5-5 and 5-9 is investigated, and the linearity of the travel time derivative itself has been discussed elsewhere.

In the preceding section, the geometric and transform amplitude derivatives with respect to $C(\underline{x})$ in block j were derived, and they are combined to yield a composite pressure derivative

$$\frac{\partial P_i}{\partial C_j} = - M'(t) * \left[\sum_{x=x(\underline{y})} w_a(\phi_o) \; \mathrm{Re}\left(\delta\left(t - T(\underline{x}) \right) \right) \right.$$

$$\left. A_g \; \frac{\partial T_i}{\partial C_j} - \frac{d}{dt} \; \mathfrak{Im}\left(\Lambda(t) \right) \sum_{t=\tilde{\Theta}(\underline{x},p)} w_t(\phi_o) \right.$$

(Equation continued)

$$A_w \frac{\partial T_i}{\partial C_j} \Bigg] \quad . \qquad (5\text{-}12)$$

Here geometric amplitude terms are summed over geometric arrivals and transform amplitudes are summed over all arrivals with $\tilde{\Theta}(\underline{x},p)$ between $t \pm \Delta t$. The travel time derivative is given in equation 5-16, and the weighting factors are those from equation 3-56.

This derivative is used in the model equation for inverting the data

$$P_i - P_{o_i} = \sum_{j=1}^{J} \left(\frac{\partial P_i}{\partial C_j} \right)_o \delta C_j \quad , \qquad (5\text{-}13)$$

where P_i and P_{o_i} are the new and nominal waveform amplitudes observed at times t_i, δC_j is the sound velocity perturbation in block j and $\left({}^{\partial P_i}/_{\partial C_j} \right)_o$ is the nominal derivative of P_i with respect to δC_j.

Many key assumptions were made to arrive at the linear model given in equations 5-12 and 5-13. First, the derivative of the amplitude term, A_w, has been omitted, and this term will be nonzero if p, q, p_o, or ${}^{\partial p}/_{\partial p_o}$ are changed by perturbations in $C(\underline{x})$. p, q, and q_o will be altered if $C(\underline{x})$ at the source or the receiver is perturbed, and ${}^{\partial p}/_{\partial p_o}$ will be affected by any range dependent perturbations. The derivative in equation 5-12 is in phase with the time derivative of the source function, m'(t), while the

$\partial A_w/\partial C_j$ term dropped from equation 5-9 is in phase with the source function, m(t). Omitting $\partial A_w/\partial C_j$ will therefore cause the largest error near the zeros of m'(t), when m(t) would dominate for harmonic sources.

The pressure data in the following examples have been filtered to lessen the impact of this source of error. The data point at a zero crossing of m'(t) and one or two points to either side have been filtered out of the inversion data set.

The second key assumption is the use of the nominal derivative, $\left(\frac{\partial P_i}{\partial C_j}\right)_o$, in the model equation 5-13. If the derivative changes with the sound velocity perturbation, an average derivative

$$\left(\frac{\partial P_i}{\partial C_j}\right)_* = \left(\left(\frac{\partial P_i}{\partial C_j}\right)_o + \frac{\partial P_i}{\partial C_j}\right) \Big/ 2 \qquad (5\text{-}14)$$

would give better linear estimates. For an inverse problem, however, the new derivative $\partial P_i/\partial C_j$ is unknown, but it can be estimated to be

$$\frac{\partial P_i}{\partial C_j} \cong \frac{P'_i(t)}{P'_{i_o}(t)} \left(\frac{\partial P_i}{\partial C_j} \right)_o , \qquad (5\text{-}15)$$

with the required derivatives, denoted by primes, calculated numerically.

If P'_i and $P'_{i_o}(t)$ differ by a large amount, the signals probably have violated the linear model. In the results that follow, points where these two derivative estimates vary by a factor of 2.0 to 10.0 are discarded.

In equation 5-12, the derivative $\partial T_i / \partial C_j$ has been substituted for $\partial \tilde{\theta}_i / \partial C_j$, and this approximation is valid if $x(p,z)$ is nearly equal to x, the receiver range. In the results cited below, only transmission angles with rays close to geometric arrivals are utilized. These nearly geometric arrivals will dominate the signal, so only data points within one to five percent of the observed maximum are used for the inversion.

The following steps, therefore, have been taken to produce the best possible linearity performance:

1. Zero crossing filtering - filter out the point where the signal crosses zero and one or two points to either side.

2. Derivative estimating and averaging - the perturbed derivative, $\partial P_i / \partial C_j$, is estimated by equation 5-15 with derivatives calculated numerically and used in equation 5-14.

3. Derivative matching - if the estimated derivatives $P'_i(t)$ and $P'_{i_o}(t)$ differ by a large amount, the point is discarded.

4. Signal thresholding - only signals greater than or equal to one percent of the maximum observed signal are used.

A sample inverse problem, referred to as linearity test case 1, is proposed in Figures 5-1 to 5-4. A range independent sound velocity field is given, and it is a canonical sound velocity profile, per equation 3-75, with a minimum sound velocity of 1495 m/sec at the sound axis, 1200 m. The scale depth and coefficient are 1200 m and 0.005, respectively. The source and receiver are separated by 200 km, and the ocean is divided into 18 blocks of equal range at depths 0, 250, 500, 750, 1000, 1250, and 4000 m. Sample ray paths from the source at depth 1295 m to the receiver at 1190 m are depicted in Figure 5-2, and the nominal received pressure wave versus time is given in Figure 5-3. The signal is recorded from 133.01 to 136.0 seconds in 0.0015 increments, and the source has a bandwidth of 10.0 Hz

centered at 10.0 Hz. The perturbation is -0.5 m/sec placed in the upper four layers across all ranges, and the perturbed pressure signal, normalized to the nominal wave, appears in Figure 5-4. The perturbed signal does differ slightly from the nominal, both in peak values and in time.

Table 5-1 displays the extent of the linearity found for this first case, and there are three columns of the ratio of the linear estimate to the observed difference,

$$\text{ratio} = \frac{P_{o_i} - P_i}{\sum_{j=1}^{J} \left(\frac{\partial P_i}{\partial C_j} \right)_{*,\ o \text{ or combined}} \delta C_j} \quad . \tag{5-16}$$

The three columns are

1. Perfect Derivatives - an average of the nominal derivative and the simulated perturbed derivative.

2. Estimated Derivatives - an average of the nominal derivative and an estimate of the perturbed derivative, per equation 5-15.

3. Nominal Only - the nominal derivative is used alone.

All three representations track fairly well except in the neighborhood of zero crossings. There, column 1 exhibits the best linearity with extreme values of 1.45, 1.87, .87, 1.97, and 0.52, while column 2 does go negative, -.72, once and has extremes of 1.46, 2.22, .48, 1.7, and 0.58. Column 3 goes negative frequently, and values of 5.35, 17.2, -49.2, and -12.93 occur.

Table 5-1 gives the results without zero crossing filtering, and the average fractional discrepancies between the ratios calculated according to equation 5-16 and the value 1.0 were 0.51, 0.60, and 2.7 for the three columns. A total of 778 data points exceeded the one percent threshold, and after zero crossing filtering the second column method, with an estimated perturbed derivative, gave an average discrepancy of 0.21.

The perturbed signal for linearity test case 2 is provided in Figure 5-5, and a perturbation of 2.0 m/sec has been placed in the upper four layers. The discrepancies for case 2 were much bigger than for case 1, and the three derivative representations, perfect, estimated and nominal only gave average discrepancies between the ratios and the value 1.0 of 2.5, 2.3, and 4.1, respectively. After filtering, the combined nominal and estimated perturbed approach gave an average discrepancy of 1.2

with many bad points showing sign errors. The lack of linearity is surprising for this case where Figure 5-5 does not really significantly differ from Figure 5-3.

The nominal sound velocity profile for linearity test cases 3, 4, and 5 is given in Figure 5-6, and it is range dependent. Canonical sound velocity profiles were used, with axis depths of 1200 m, scale depths of 1200m, and coefficients of 0.005, but the inner four ranges have minimum values of 1480 m/sec while the outer two have 1495 m/sec as their minima. Linear interpolations are used between different profiles, and the signal time and source bandwidth and center frequency are identical to those in case 1. The source depth is 1295 m, just below the receiver at 1290 m. The nominal acoustic pressure signal received under these conditions is depicted in Figure 5-7.

For linearity test case 3, a 0.5 m/sec disturbance was placed throughout the first four layers at all ranges, and the perturbed signal is in Figure 5-8. The linearity results for case 3 are worse than those for case 1, and the three derivative representations, perfect, estimated, and nominal only, yield average discrepancies of 1.0, 1.05, and 2.1, respectively. After filtering, the estimated method gives an average value of 0.39, almost twice that of case 1.

The perturbation for linearity test case 4 is range dependent. A perturbation of 0.25 m/sec was placed in the top four layers for the first and last ranges, but 0.5 m/sec was utilized in the middle region. The three average discrepancies were 0.62, 0.78, and 1.3, and after filtering the estimated derivative approach yielded 0.32 as its average error. The perturbed signal for this case is in Figure 5-9.

The perturbed signal for linearity test case 5 is in Figure 5-10, and a range dependent perturbation of 1.0, 2.0, and 1.0 m/sec, respectively, was placed in the upper four layers of the three ranges. Before filtering, the average discrepancies from linearity were 1.58, 1.58, and 3.19 for the three derivative methods. After zero crossing filtering, the estimated derivative approach had an average of 0.70 but there were not many bad points and an inversion will be attempted on this case in the next section.

Table 5-2 summarizes the results from the five linearity test cases. The average discrepancies between the value 1.0 and the ratio of the observed perturbation to the linear prediction are tabulated for the three derivative models. The approach that combines the estimated perturbed derivative with the nominal derivative clearly performs much better than

the approach that uses the nominal derivative alone. Zero crossing filtering is also beneficial, and the resulting average discrepancy is as little as one-tenth of the original one.

Cases 1, 3, and 4 exhibit good agreement with the linear model, and small range dependent effects do not seem to adversely affect linearity. Case 2 is definitely unacceptable, so a disturbance of 2.0 m/sec causes nonlinear changes. Case 5 is borderline, and an inversion will be attempted for this case.

In conclusion, this study of the linearity of acoustic amplitude has led to the following results:

1. The zero crossing filtering and the combined derivative approach stated in equations 5-14 and 5-15 do improve the linearity of a signal to be inverted.

2. The signals are very sensitive to small sound velocity perturbations, and a disturbance of 1.0 m/sec over 200 km seems to be a threshold level.

3. Small range dependent effects do not adversely affect linearity.

5. Time step effects and additional amplitude derivatives, that is the terms dropped from equations 5-5, 5-9, and 5-10, need to be investigated.

5.3 AMPLITUDE INVERSIONS

Due to the problem with linearity presented in the previous section, accurate amplitude inversions cannot be obtained. However, some sample inversions are presented in this section. The examples are summarized in Tables 5-3 to 5-9 and depicted in Figures 5-11 to 5-35. They vary in nominal sound velocity profile, number of sound velocity perturbation unknowns, the type of perturbation, source and receiver depths, and number of sources. In all cases, a 10 Hz bandwidth source with a center frequency of 10 Hz was used, and the receiver was 200 km from the source. The ocean depth was 4000 m, and the ocean was divided into five equal blocks from the ocean surface to a depth of 1250 m.

The signals from 133.01 to 136. seconds were used in the inversions, with 0.0015 sec time steps. Zero crossing filtering and signal thresholding at 0.01 or 0.05 of the maximum observed signal were carried out, and a combination of the nominal derivative and an estimate of the perturbed derivative was used. In this way, the best possible linearity was achieved.

Tables 5-3 and 5-4 give details pertaining to the eleven major cases used in the inversions, and letter names are assigned to each run. These same configurations are then applied in oceans divided into different numbers of ranges or with different perturbations. The source and

receiver depths and the sound velocity profiles are specified. Sound velocity profiles I and IV are range dependent while II and III are not, and they all are canonical sound velocity profiles.

Figure 5-11 portrays a sample tomography exercise with one source, and a few of the rays are shown. The resolution is determined by the number of rays passing through a given block of the ocean, and in the following examples the ocean is divided into one, three, or five equal ranges.

The first examples are five block inversions attempted on the true disturbance given in Figure 5-12, and the perturbations in the five blocks are 0.75, 0.75, 0.5, 0.25, and 0.25 m/sec, respectively. Runs G and H are executed in this environment, and they are designated G1 and H1 due to the one range configuration. The results are summarized in Figures 5-13 and 5-14, and Table 5-5, and stochastic inverses are used. For the stochastic inverse, signal noise with standard deviations that are 10, 20, 30, or even 40 percent of the maximum observed signal are assumed.

The H1 results in Figure 5-13 and Table 5-5 are good inversions, and 10, 20, or 30 percent noise factors are assumed. As stated in Table 5-5, the fractional average discrepancy between the H1 signal perturbations and the linear model is 0.32, and the minimum and maximum values on the diagonals of the resolution matrices are near 0.90 for all three noise

cases. The inversions in Figure 5-13 give 2.16, 2.14, and 2.07 as estimates for the total dC perturbation, and these are 0.86, 0.86, and 0.83 of the true total, 2.5. The average differences between the inversion and truth are 0.12, 0.1, and 0.08 for the three cases, and the 30 percent noise inversion is quite accurate.

The G1 results in Figure 5-14 and Table 5-5 are not as good as those for H1, and this is due to the large average discrepancy for this data set, 1.2, and poorer resolution. (There is one bad point in the G1 data, and without this point the average discrepancy is 0.68.) The inversion with an assumed 40 percent noise factor does estimate the total dC perturbation to be 2.97, or 1.19 of the true value, and the average difference between this inversion and truth is 0,15, an acceptable value.

Runs K3, H3, N3, P3, Q3, and R3 are executed in the 15 block disturbance depicted in Figure 5-15, and a 0.5 m/sec perturbation is placed in the upper four layers at all ranges. K3 is used for the single source case, and the results are provided in Figure 5-16 and Table 5-6. 0.01 and 0.05 signal thresholds are used in runs K3-1 and K3-5, respectively, and although K3-1 has a larger average discrepancy from linearity, it does yield a better inversion. The diagonals from the K3-1 resolution matrix with 15 percent assumed noise have minimum and maximum values of

0.19 and 0.47. The total dC estimate for this best case is 0.88 of truth, and the inversion differs by 0.14 from truth on average. Neither vertical nor horizontal resolution is really achieved, however.

Runs I3, L3, and O3 are executed in the field depicted in Figure 5-17, a range dependent perturbation. I3 is the single source case, and again the 0.01 signal threshold result is slightly better than the 0.05 one. The inversion is in Figure 5-18. Vertical structure is resolved, but there is no horizontal definition. The total dC estimates for all the I3 and K3 single source runs are good.

Results for run P3 are also in Table 5-6, and a 0.01 signal threshold was used. Although some of the resolution for this run is very low, a good estimate for the total dC is found and the inversion in Figure 5-19 only differs from truth by an average of 0.17.

The 0.5 m/sec disturbance in Figure 5-15 is increased to 2.0 m/sec for run U3, and the results are given in Table 5-6. For this inversion, the dC standard deviation was assumed to be 2.0 rather than the 0.5 m/sec used for all other cases. This inversion fails due to the high discrepancy from the linear model. The discrepancy here is across many points, unlike other runs where just a few bad points cause a high average discrepancy.

Some maximum entropy inversions were performed using the $\mathcal{E}$ statistic algorithm of Bryan and Skilling (6) given in equation 4-55. The I3, L3, and O3 runs were inverted with the maximum entropy inverse because the perturbation in Figure 5-17 has structure that could be distinguished better with the maximum entropy inverse than with the stochastic inverse.

Unlike the stochastic inverse, the maximum entropy inverse performs best when a low noise factor, 2.5 to 5 percent, is assumed. If a noise factor of 20 percent is used, the maximum entropy inverse is apt to bear little resemblance to the true disturbance. The inversions are of reasonably good quality, however, with the low noise factors.

Results for the combined I3 + L3 + O3 run are depicted in Figures 5-26 and 5-27, and this inversion used 824 signal points. To get the generalized inverse for this case, an 800 by 800 matrix was inverted while the maximum entropy inverse computation by the $\mathcal{E}$ statistic approach involved a 16 by 16 matrix and one sum with over 800 terms in it. Therefore, the generalized inverse computation for this case took over 25 times longer than the maximum entropy inverse.

Figure 5-26 gives the maximum entropy result when a 2.5 percent noise factor is assumed, and it should be compared to Figure 5-24, the stochastic inverse. The average difference from truth is 0.19, and

the total dC estimate is 1.15 of truth. The stochastic inverse for a 25 percent noise yielded an average difference of 0.18 and a total dC estimate ratio of 0.91. The two inversions are comparable.

Figure 5-27 provides the result for the 5 percent noise factor, and the average difference here is 0.21 and the total dC estimate is 1.2 of truth. Except for the last block, the vertical resolution is good, and the horizontal resolution is adequate except in blocks 2, 13, and 14.

Due to the lack of linearity, simulated inversions cannot be used to really compare the maximum entropy and generalized inverses. Compensated data are used in the next section to test the two methods.

In conclusion, amplitude inversions with the time derivative alone are not linear enough to provide range dependent information. More derivative terms are required before accurate inversions can be made.

5.4 INVERSIONS WITH COMPENSATED DATA - MAXIMUM ENTROPY INVERSE

In Sections 5.2 and 5.3, it was shown that the travel time derivative defined in equations 5-1 to 5-10 is not enough to produce linear inverse problems for amplitude tomography. Because that approach was not able to provide much insight into amplitude inversions, compensated amplitude signals are used in this section to compare generalized and maximum entropy inverses for sample amplitude tomography exercises.

The compensated signals are formed by taking the derivatives calculated by the Maslov simulation for the nominal and perturbed signals, combining them according to equations 5-14 and 5-15 and multiplying them by the true sound velocity perturbation. The compensated pressure amplitude data are then

$$\delta P_i = \sum_{j=1}^{J} \left(\frac{\partial P_i}{\partial C_j} \right)_* \delta C_j + n_i \qquad (5\text{-}17)$$

where the derivatives are formed per equations 5-14 and 5-15. n_i is a noise term selected by a Gaussian random number generator, and without it the compensated data would be perfectly linear.

The compensated data represent best possible cases to compare the generalized and maximum entropy inverses described in Chapter 4. Improved

amplitude derivatives may lead to simulated or even real ocean tomography exercises that achieve this accuracy.

Figure 5-28 depicts the sample tomography exercise discussed in this section. Sources at 1095, 1195, and 1295 m are used to transmit a 10 Hz bandwidth signal centered at 10 Hz to a receiver 200 km away at a depth of 1190 m. The ocean between the sources and the receiver has been divided into five 40. km long blocks in range and five 250 m deep blocks in depth. The signal from 133 to 136 seconds with 1.5 msec time steps was recorded.

Figures 5-29, 5-30, and 5-31 provide the diagonals from the generalized inverse resolution matrix for the one source (1195 m), two sources (1195 m and 1295 m), and three sources cases, respectively. A value of 1.0 represents perfect resolution, and blocks with less than 0.5 values are not well resolved at all. Gaussian noise with standard deviations of 2.5 percent of the maximum signal are considered.

Figure 5-32 gives the Case 1 perturbation, and 0.5 m/sec values have been placed in each of the upper four layers. The generalized inverse is given in Figure 5-33 for the one source case and the stochastic inverse based on noise with a standard deviation of 2.5 percent of the maximum has been used. The average difference between the estimate and the

true perturbation is 0.11, and columns 1 and 4 are resolved quite well. The comparable maximum entropy inverse, based upon Bryan and Skilling's $\mathcal{E}$ statistic approach (6) given in equation 4-55, is in Figure 5-34, and it has an average difference of 0.15 from truth. The maximum entropy inverse is not as good as the generalized inverse for Case 1 with a single source.

The two source inverses for Case 1 are in Figures 5-35 and 5-36, and the maximum entropy inverse performs worse in this case. The average difference for the maximum entropy inverse drops, but the result is far worse than the generalized inverse. In the three source case, presented in Figures 5-37 and 5-38, the generalized inverse result is adversely affected by numerical roundoff errors caused by the 800 row matrix, and the average difference is .13. Again, the maximum entropy inverse in Figure 5-38 is inferior to the generalized inverse.

Figure 5-39 shows the perturbation for Case 2, and the top four layers are structured to have 0.1, 0.4, or 0.8 perturbations in this case. The results are in Figures 5-40 to 5-45, and the maximum entropy inverses are all more accurate than their generalized inverse counterparts. The two source results are the best, but the maximum entropy inverse in Figure 5-43 gives better depth, range, and average resolution than the generalized inverse in Figure 5-42.

The results for Case 3, with the 0.1, 0.2, or 0.8 perturbations shown in Figure 5-46, are similar to those for Case 2, and they are given in Figures 5-47 to 5-52. The maximum entropy inverse again performs better for the one, two, and three source instances.

The comparisons are summarized in Table 5-10, and the dimension of the square matrices inverted to determine the solutions are given. For the one, two, and three source generalized inverses, square matrices of about 400, 600, and 800 rows, respectively, were inverted. These computations are very time consuming compared to the maximum entropy inversions, where 26 row square matrices were inverted and iterated. Therefore, the maximum entropy calculations took only one to ten percent as long as the generalized inverse, and the results for Cases 2 and 3 are superior. In Case 1, where the perturbation is distributed in a minimum norm, uniform fashion, the maximum entropy result is not as good as the generalized inverse.

Table 5-10 depicts the following facts:

1. For signal data sets with many (>300) points, the maximum entropy inverse can be found in less than one-tenth the time required to yield the generalized inverse.

2. If the perturbation is distributed in a structured, nonuniform way, the maximum entropy inverse provides better depth, range, and average resolution.

3. If the perturbation is uniform, the generalized inverse gives a better average solution.

These results are for low resolution, low noise cases. Higher noise cases led to poor numerical results for the generalized inverse due to small eigenvalues, and the differences between the maximum entropy and generalized inverses were more pronounced. Higher noise cases should be investigated in the future, however, and the maximum entropy inverse can also give erroneous results for high noise cases, as noted in Section 5.3.

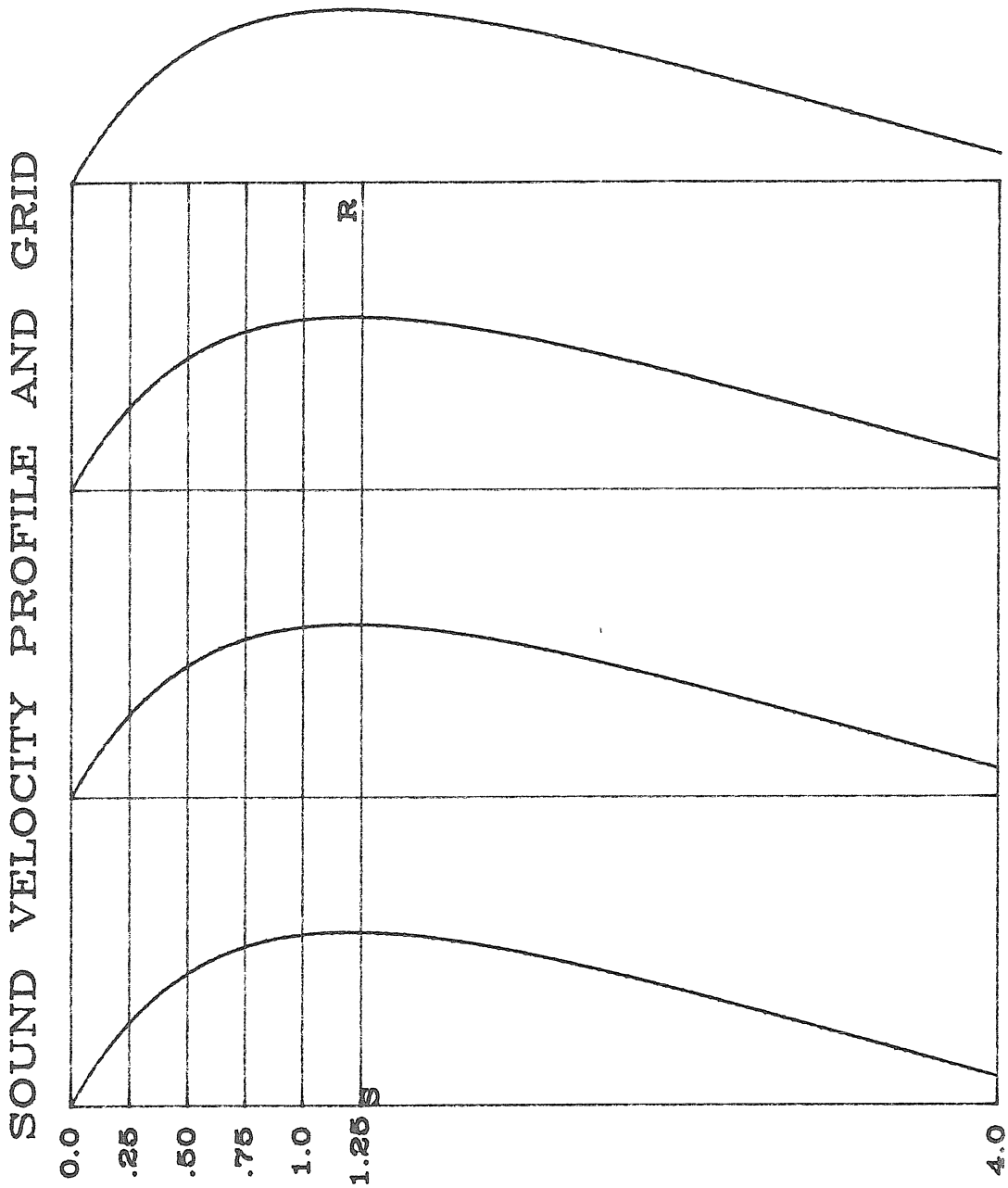

FIGURE 5-1: LINEARITY TEST CASE 1

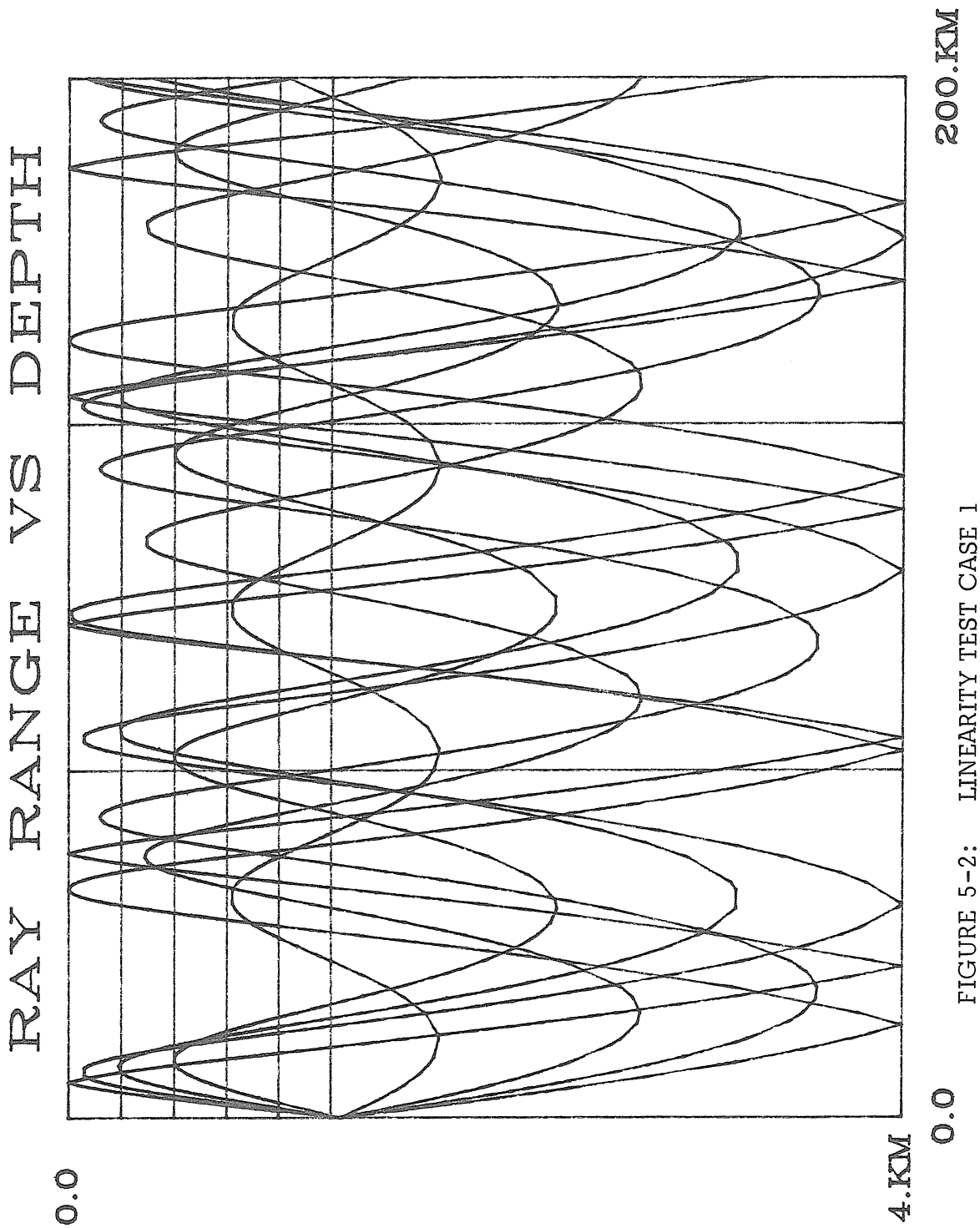

FIGURE 5-2: LINEARITY TEST CASE 1

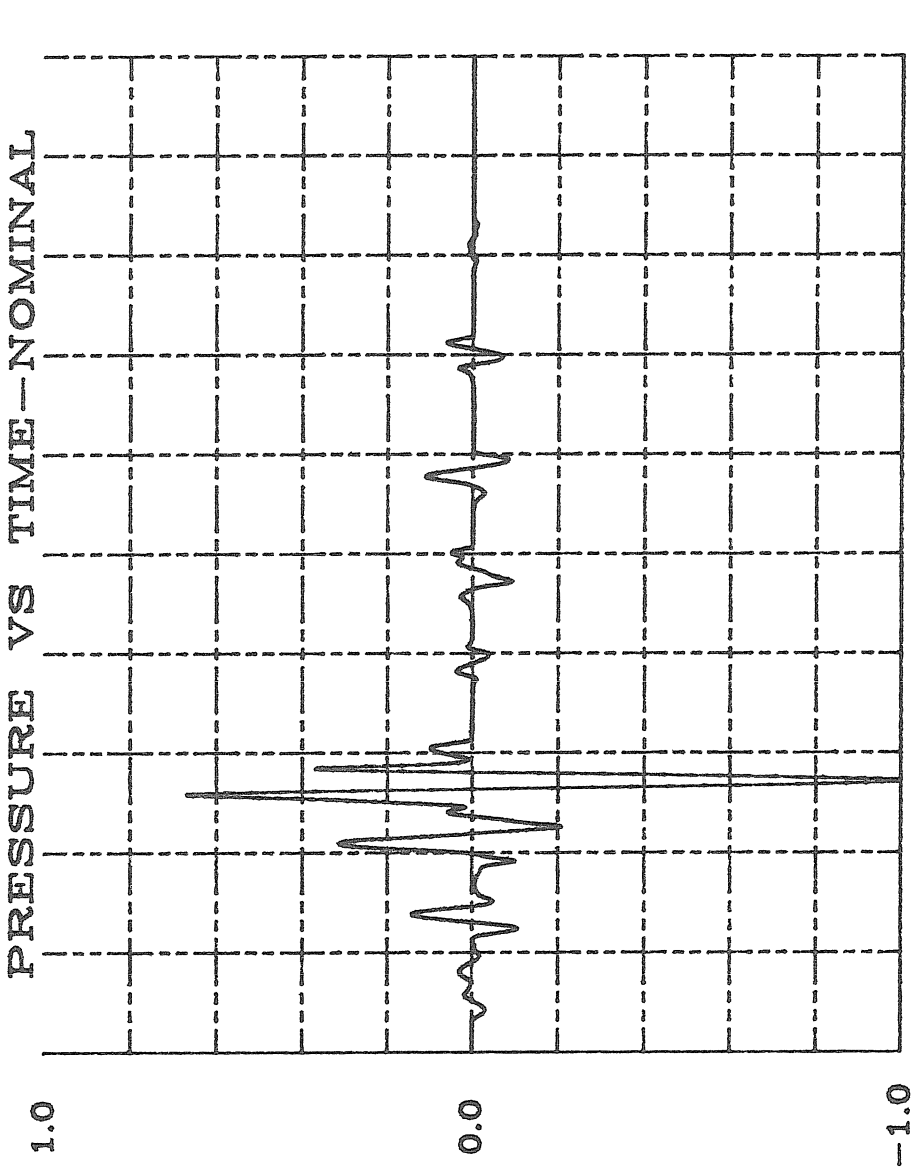

FIGURE 5-3: LINEARITY TEST CASE 1

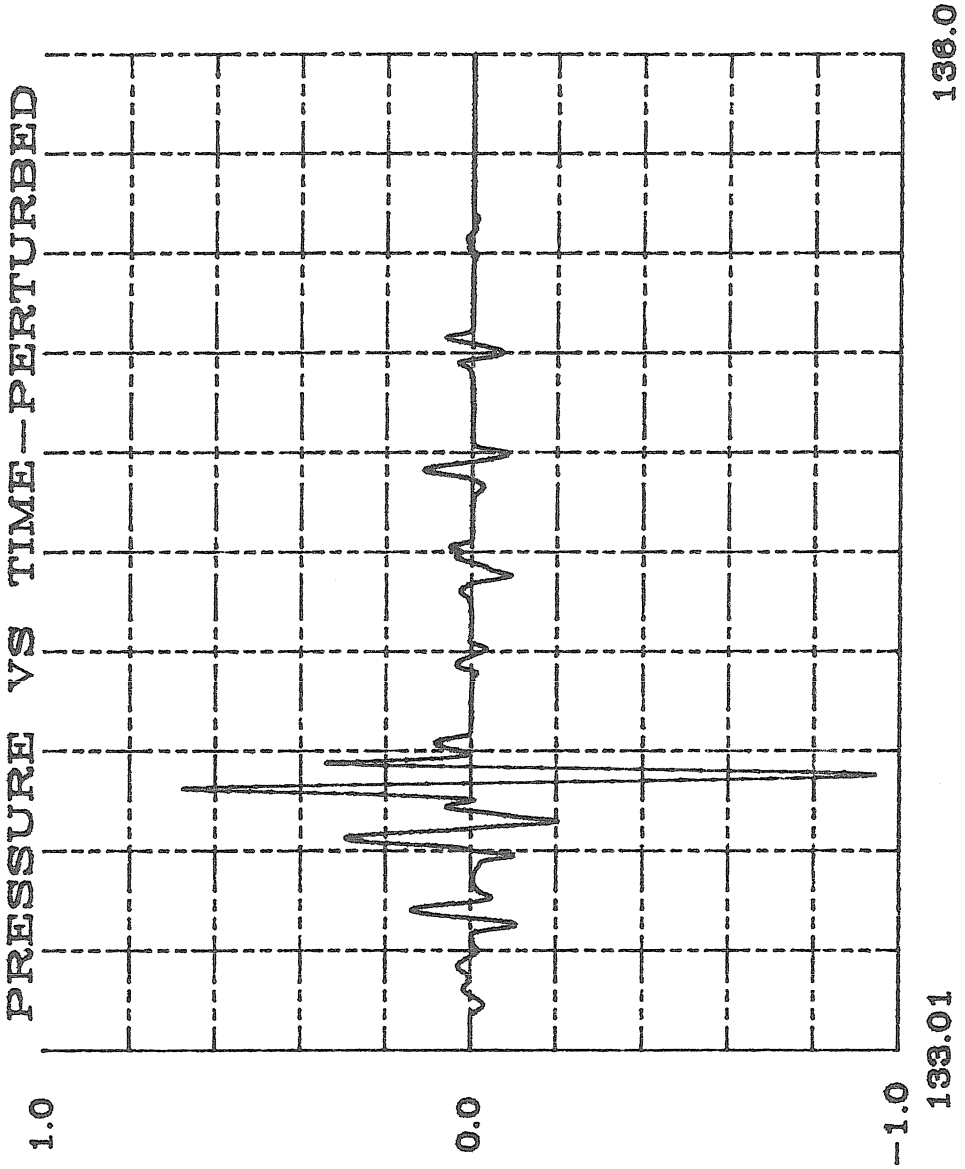

FIGURE 5-4: LINEARITY TEST CASE 1

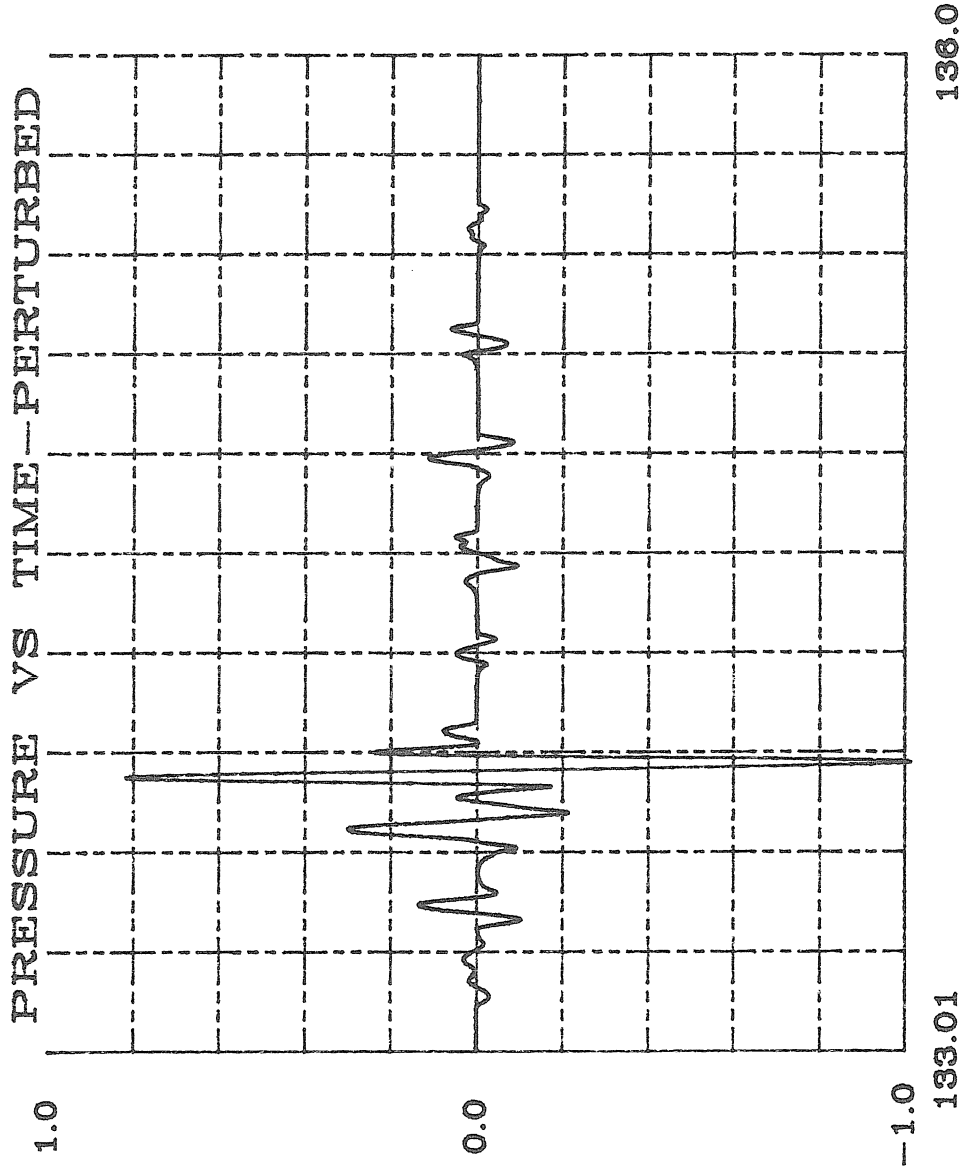

FIGURE 5-5: LINEARITY TEST CASE 2

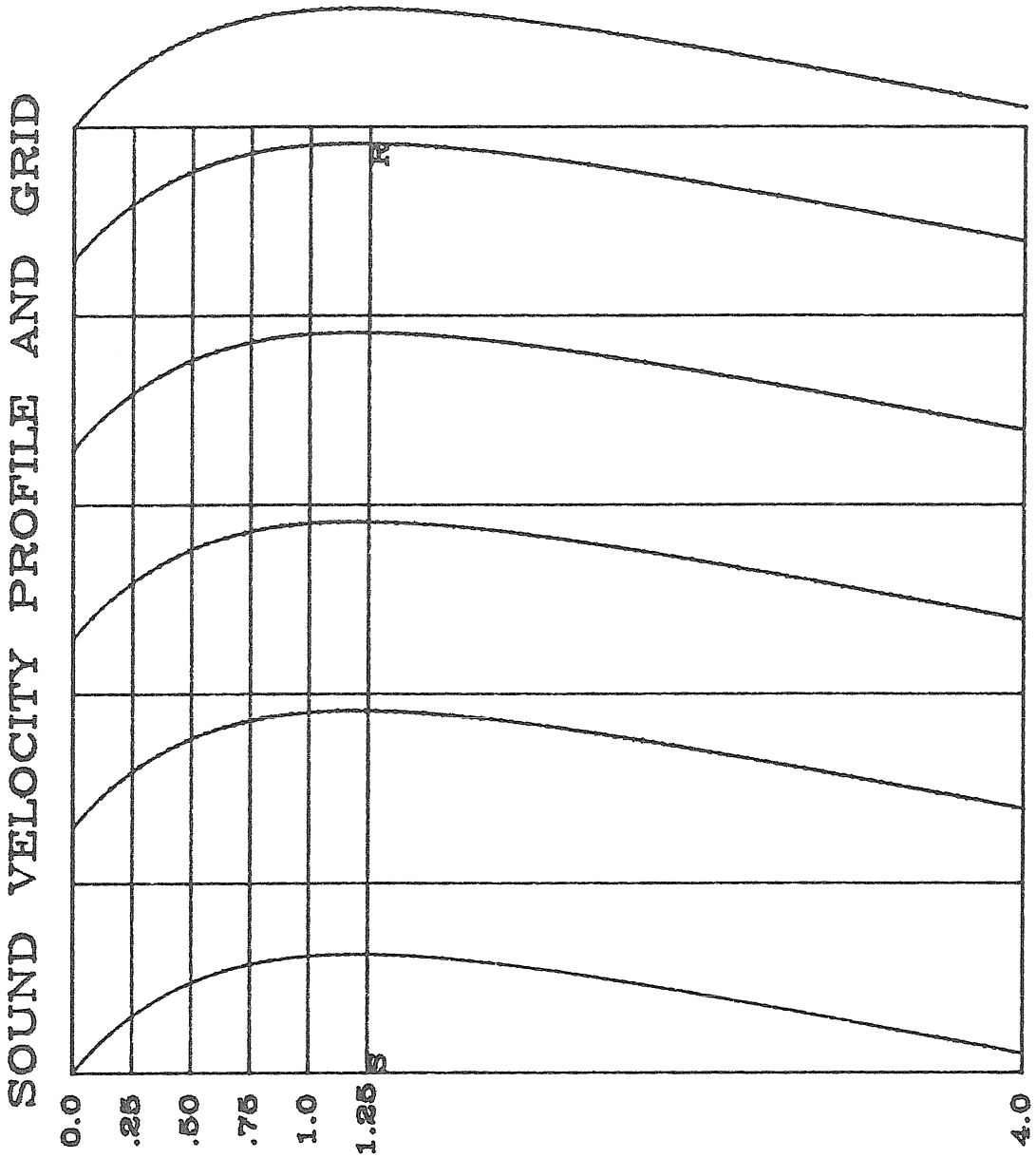

FIGURE 5-6: LINEARITY TEST CASE 3

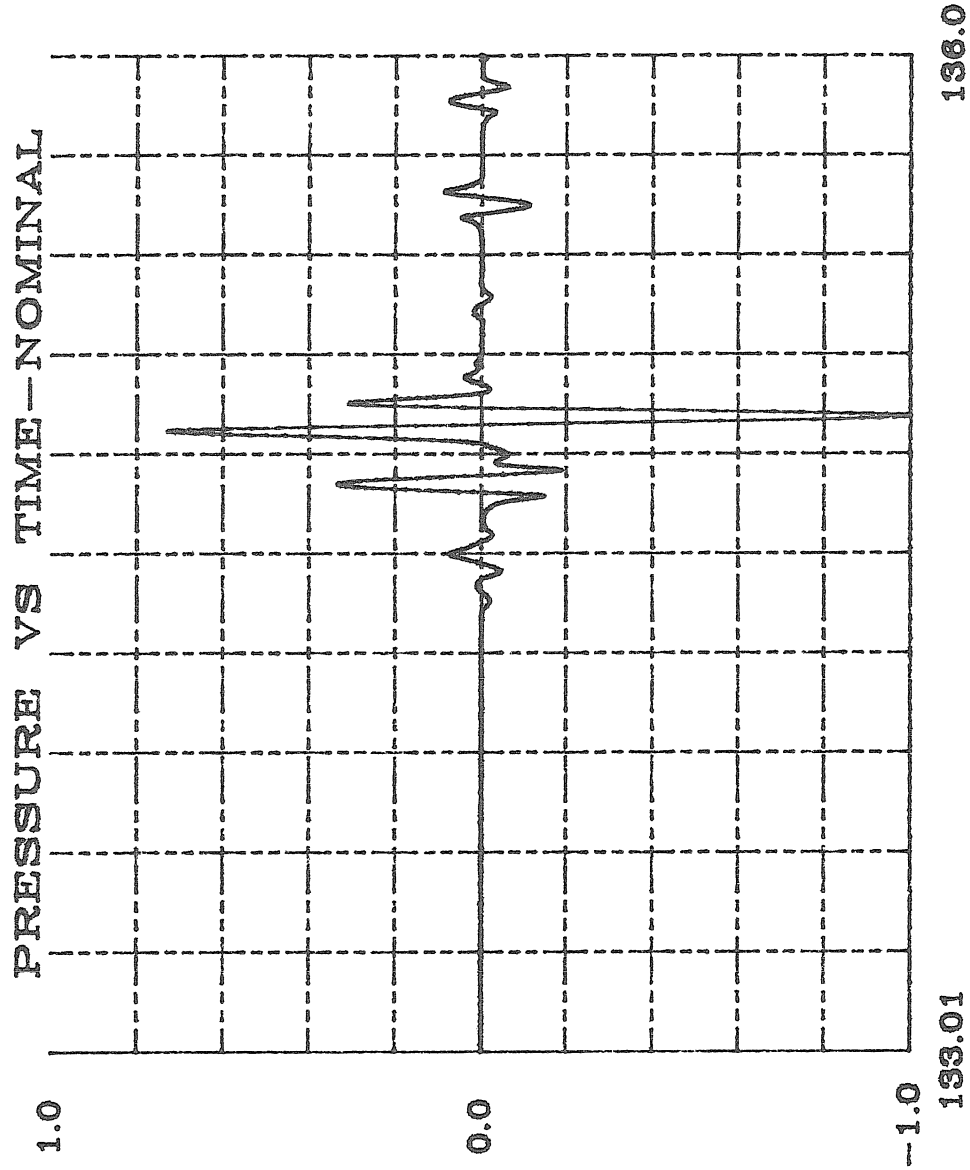

FIGURE 5-7: LINEARITY TEST CASES 3, 4, AND 5

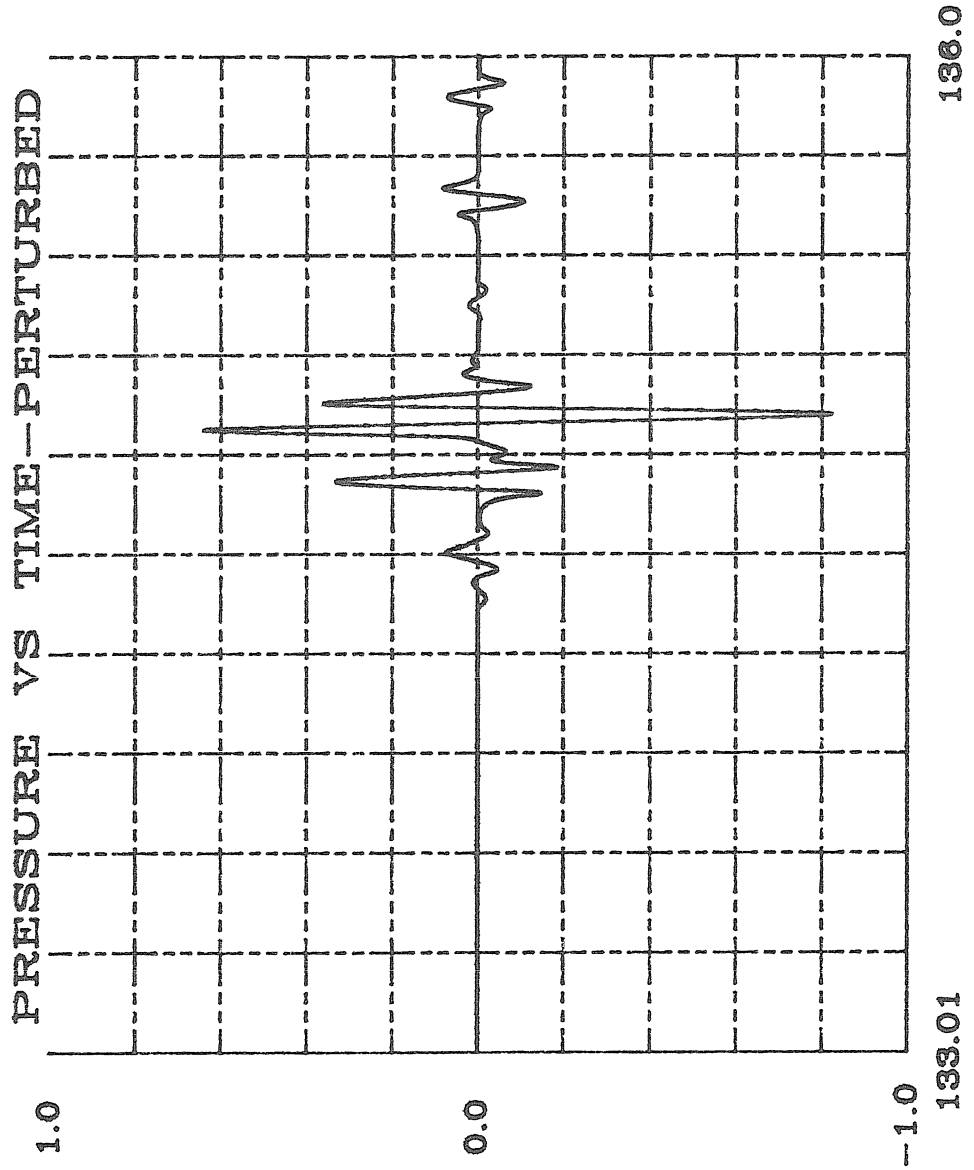

FIGURE 5-8: LINEARITY TEST CASE 3

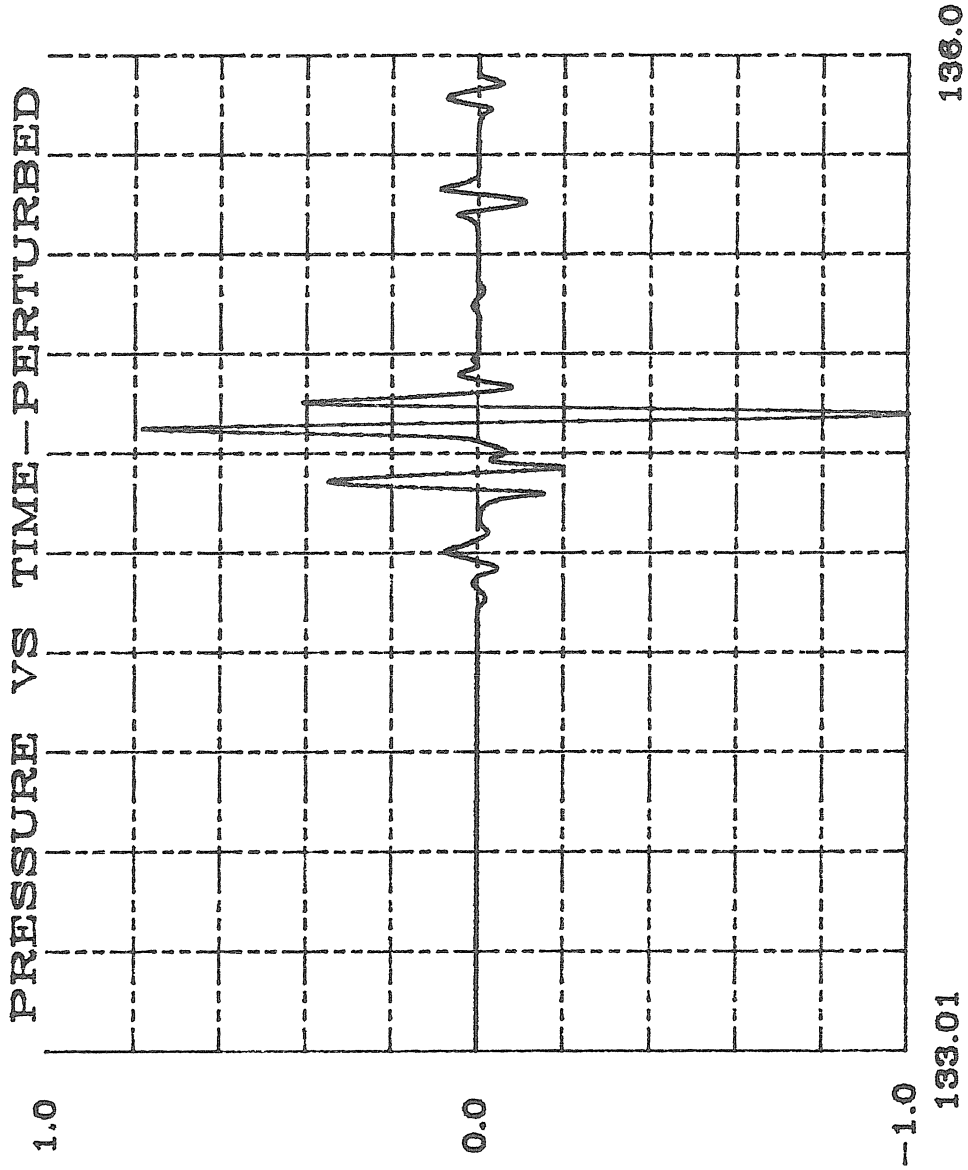

FIGURE 5-9: LINEARITY TEST CASE 4

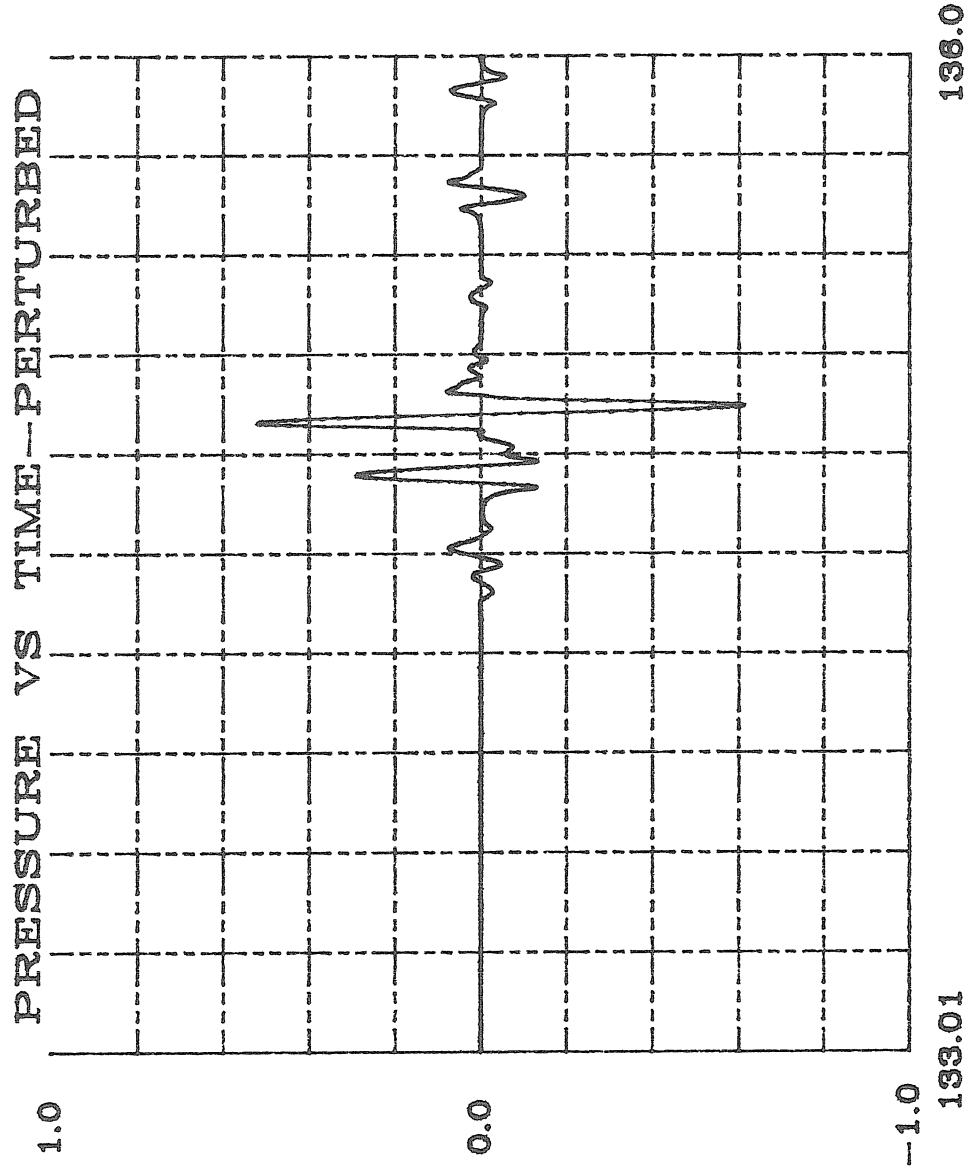

FIGURE 5-10: LINEARITY TEST CASE 5

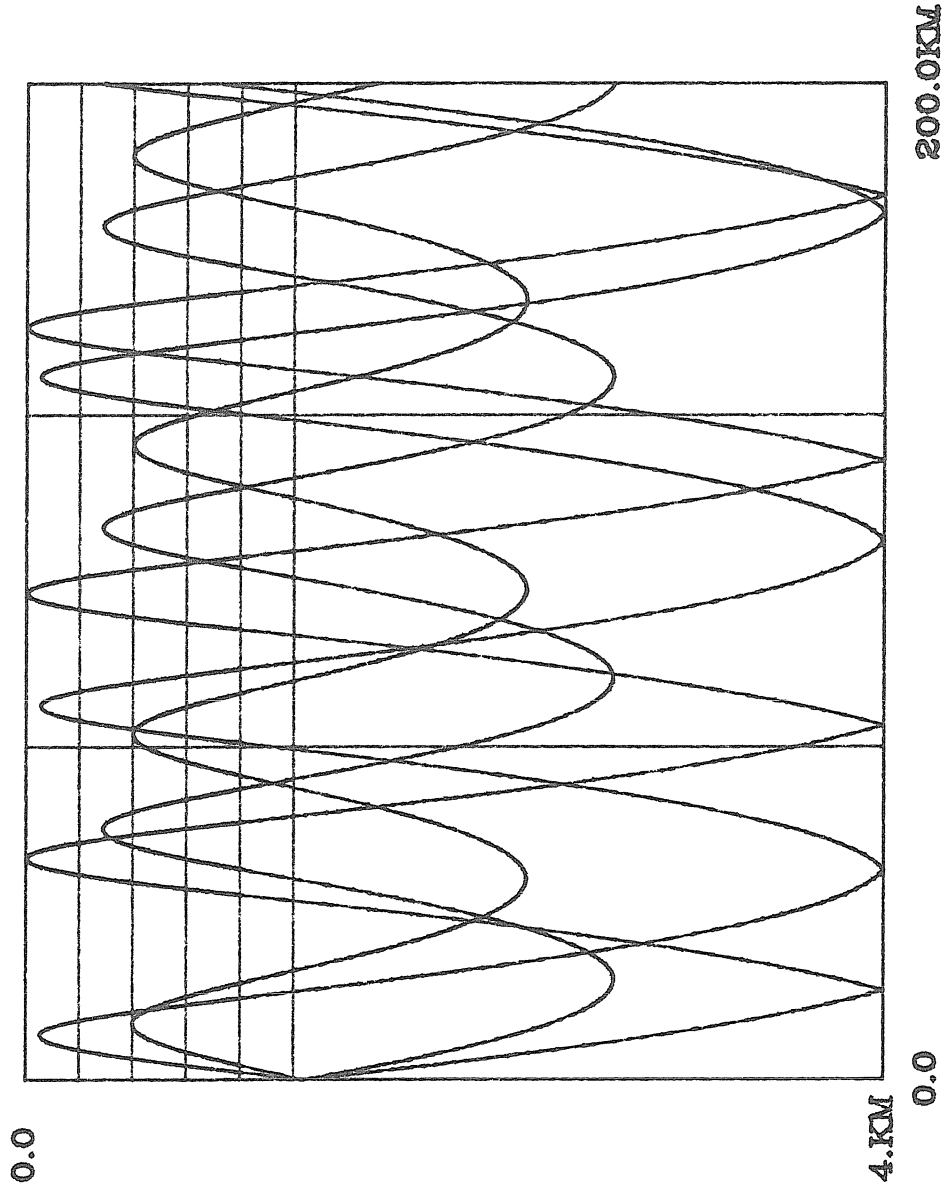

FIGURE 5-11: SAMPLE TOMOGRAPHY EXERCISE

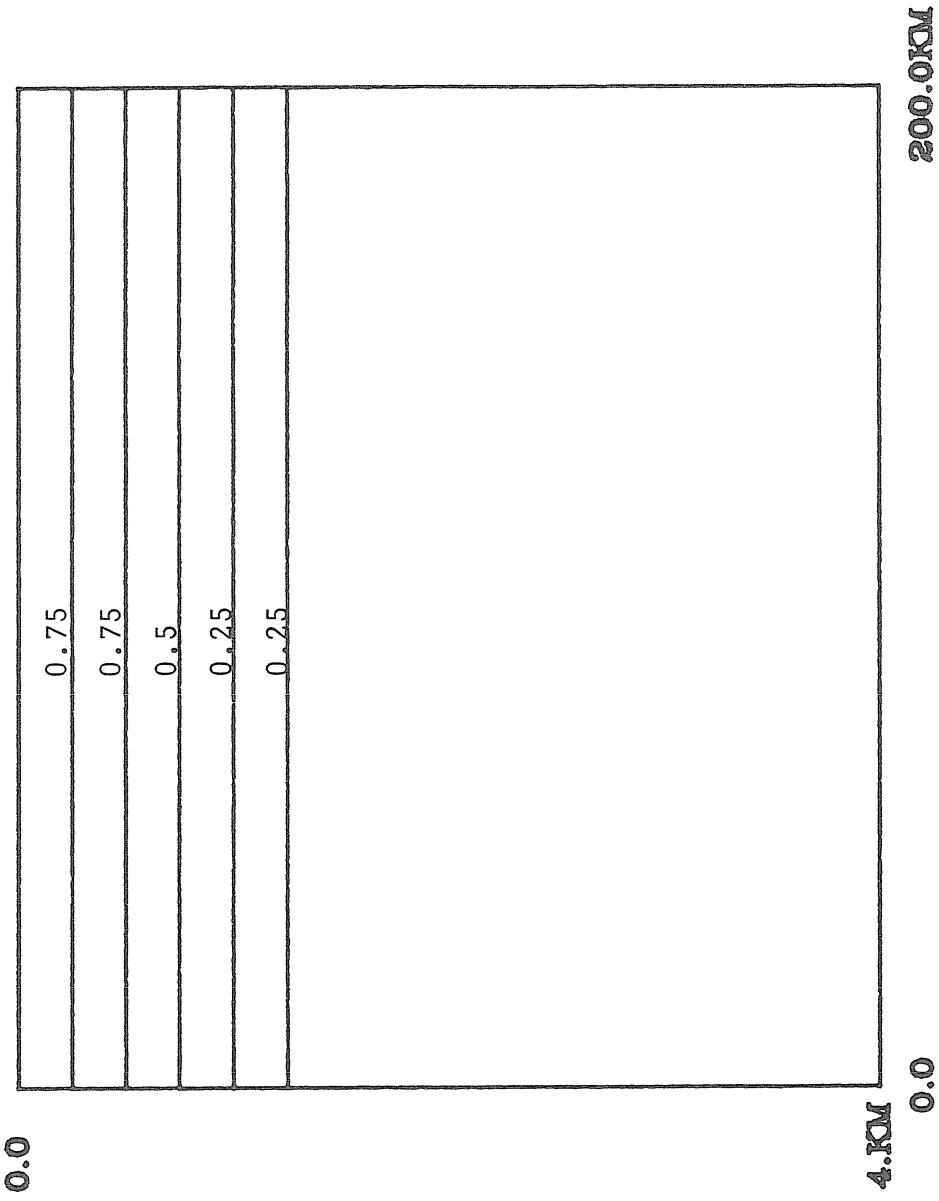

FIGURE 5-12: FIVE BLOCK TRUE DISTURBANCE

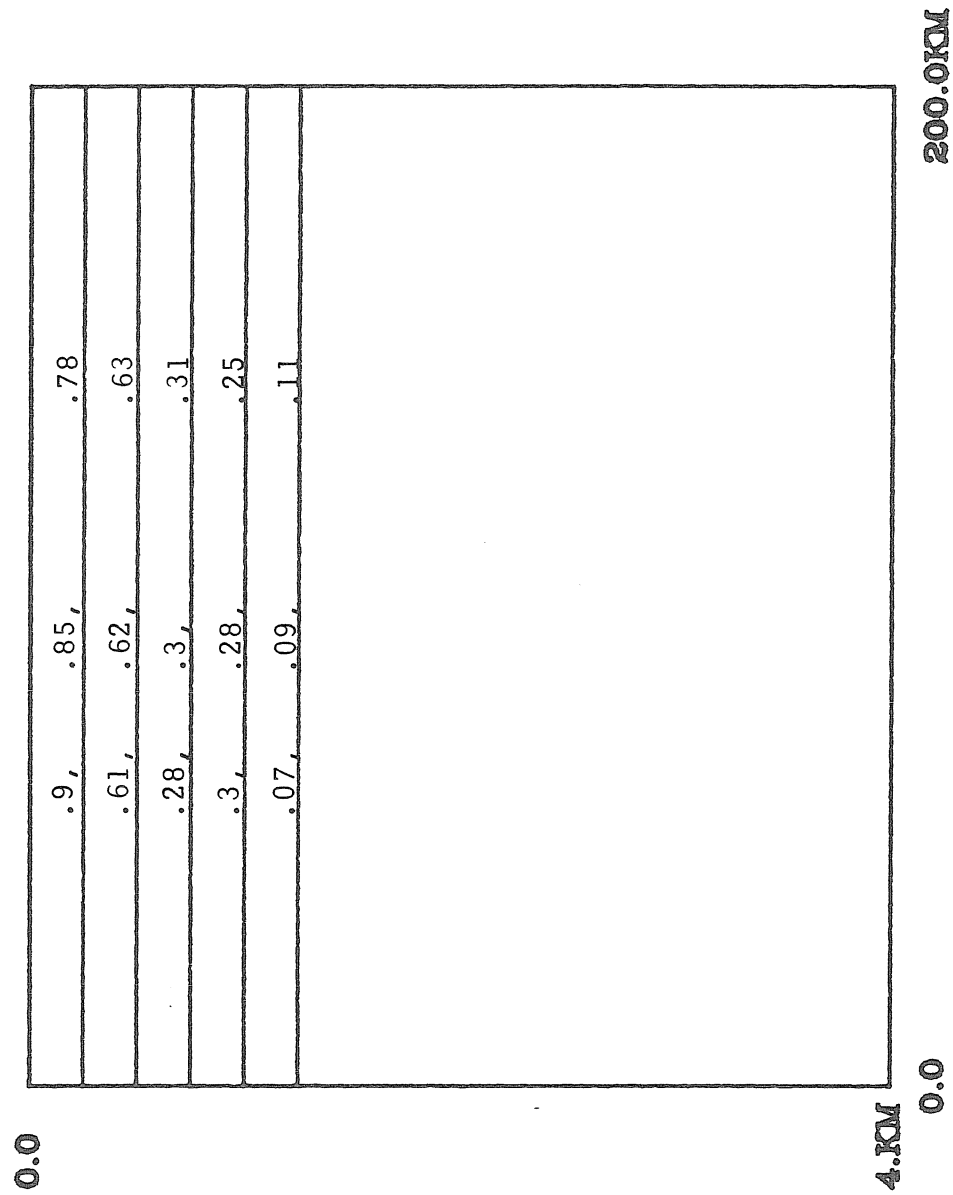

FIGURE 5-13: H1 RESULTS

FOR 10%, 20%, AND 30% NOISE STANDARD DEVIATION

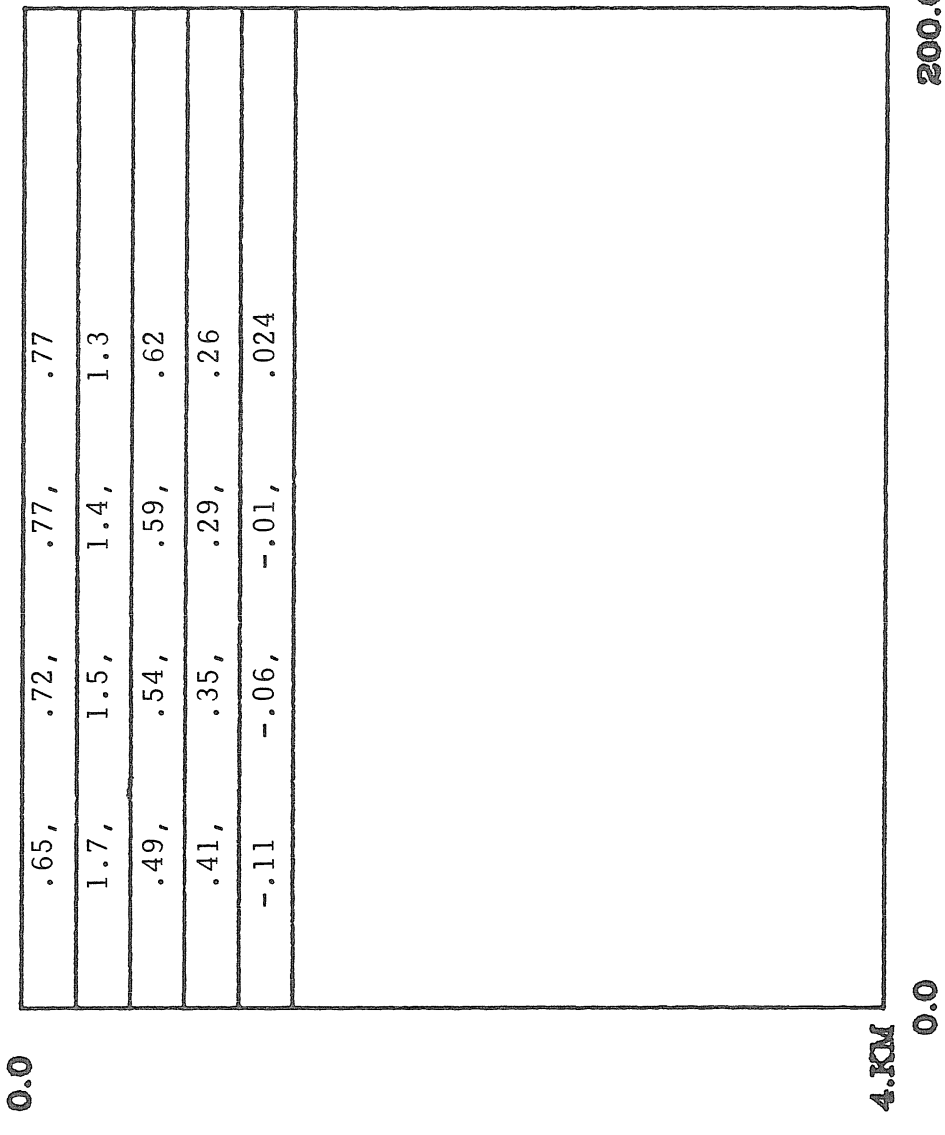

FIGURE 5-14: G1 RESULTS

FOR 10%, 20%, 30%, and 40% NOISE

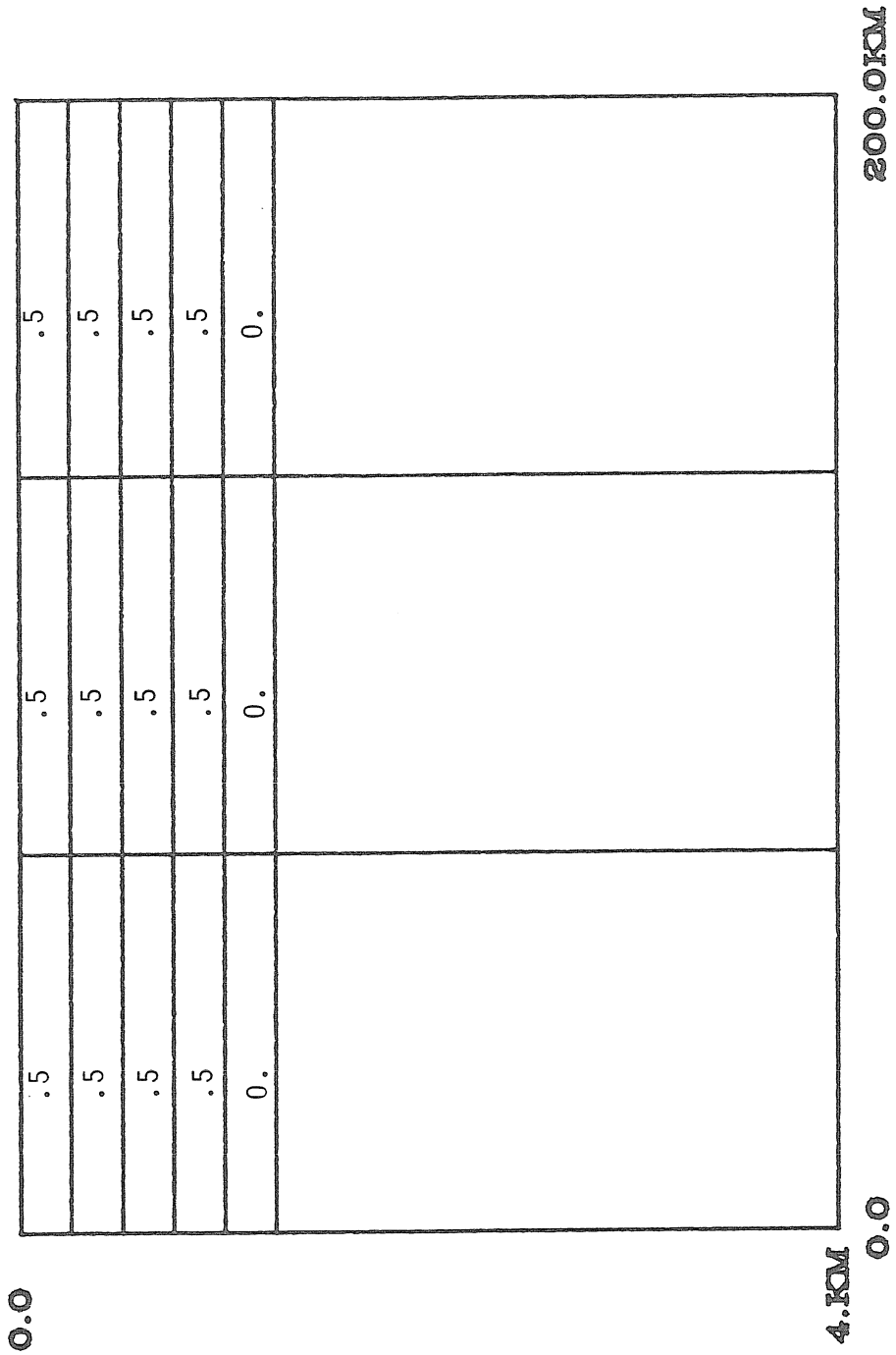

FIGURE 5-15: 15 BLOCK DISTURBANCE FOR RUNS K3 AND P3

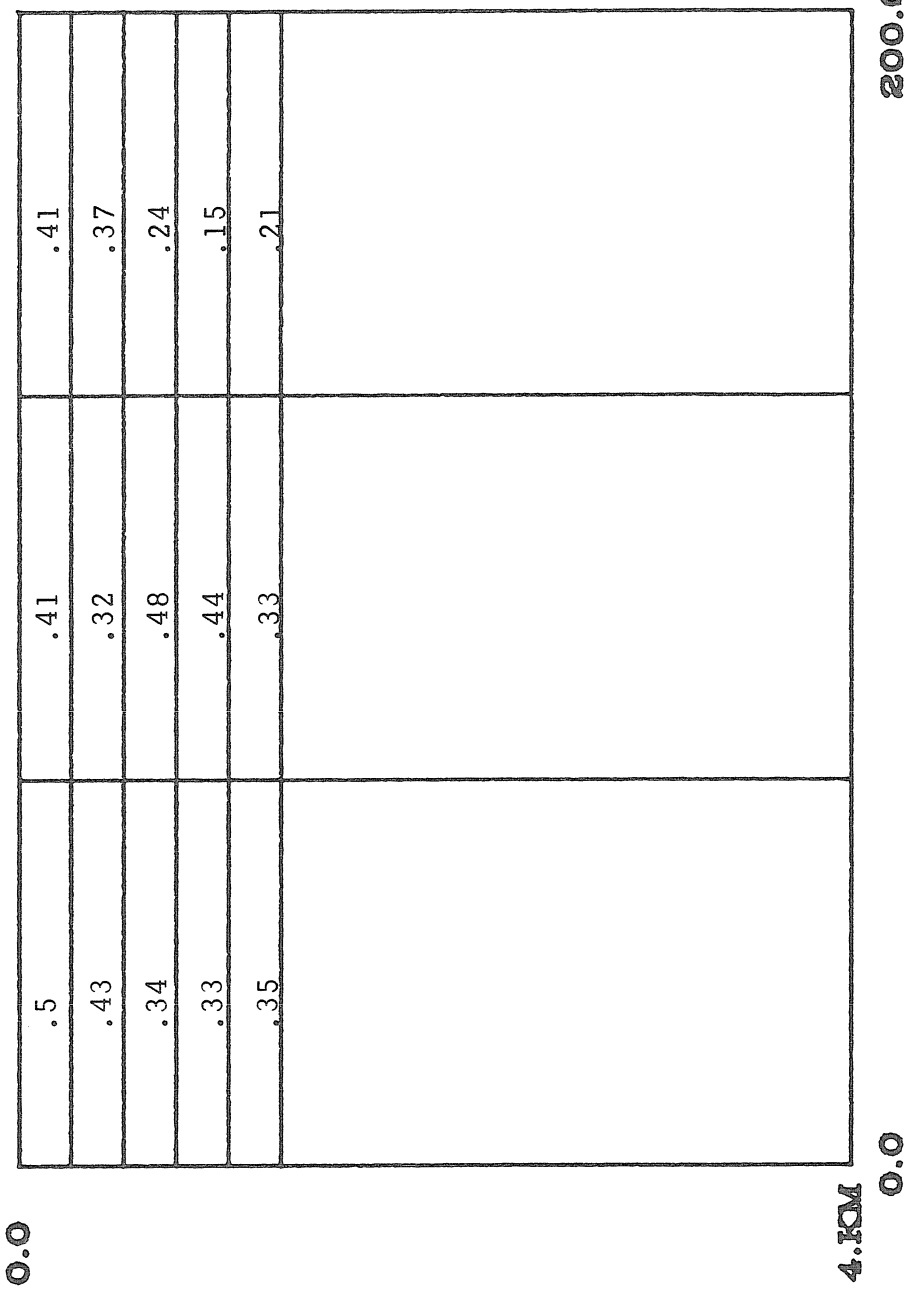

FIGURE 5-16: INVERSION FROM RUN K3-1, 15% NOISE

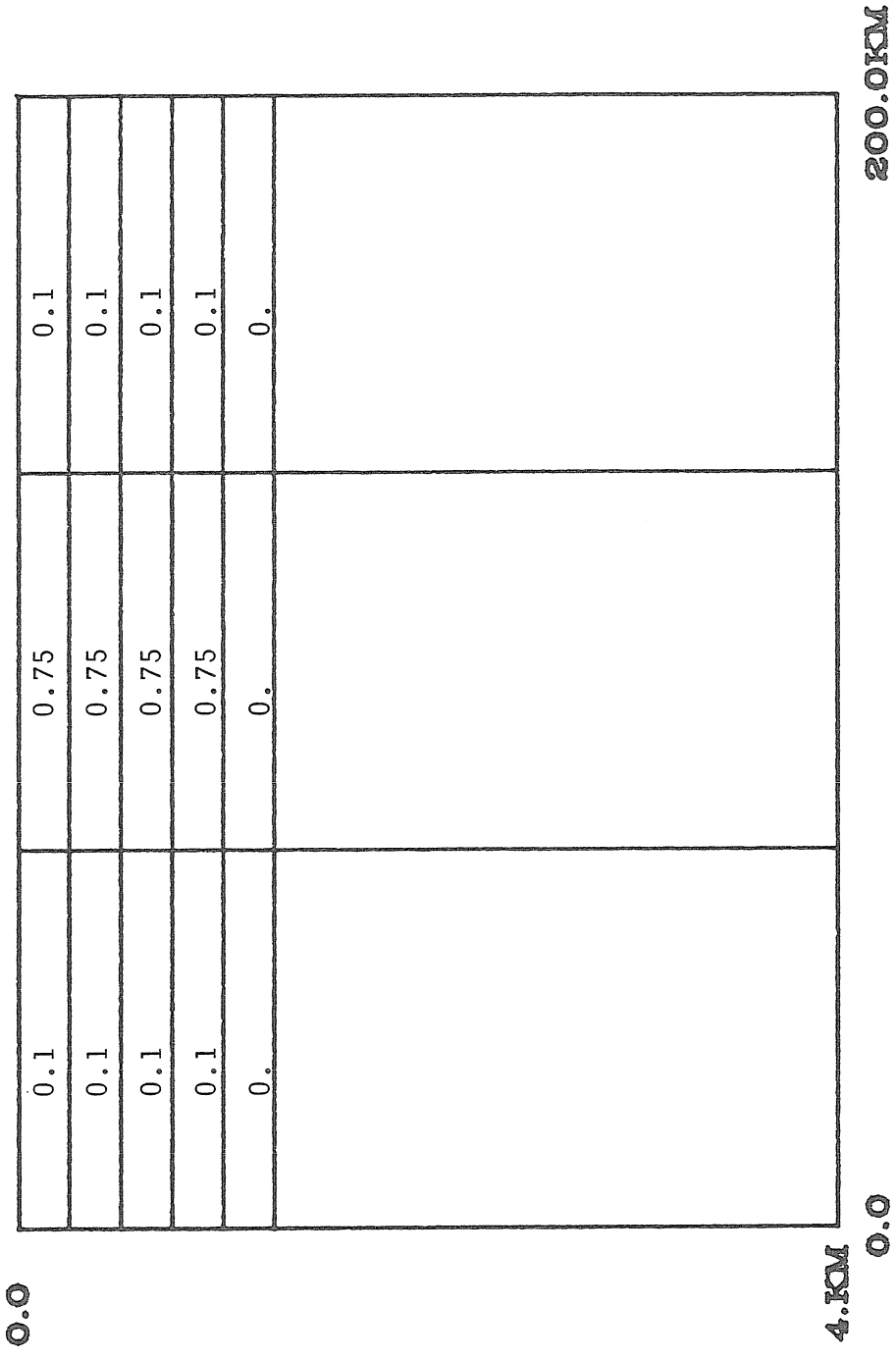

FIGURE 5-17: 15 BLOCK DISTURBANCE FOR RUN I

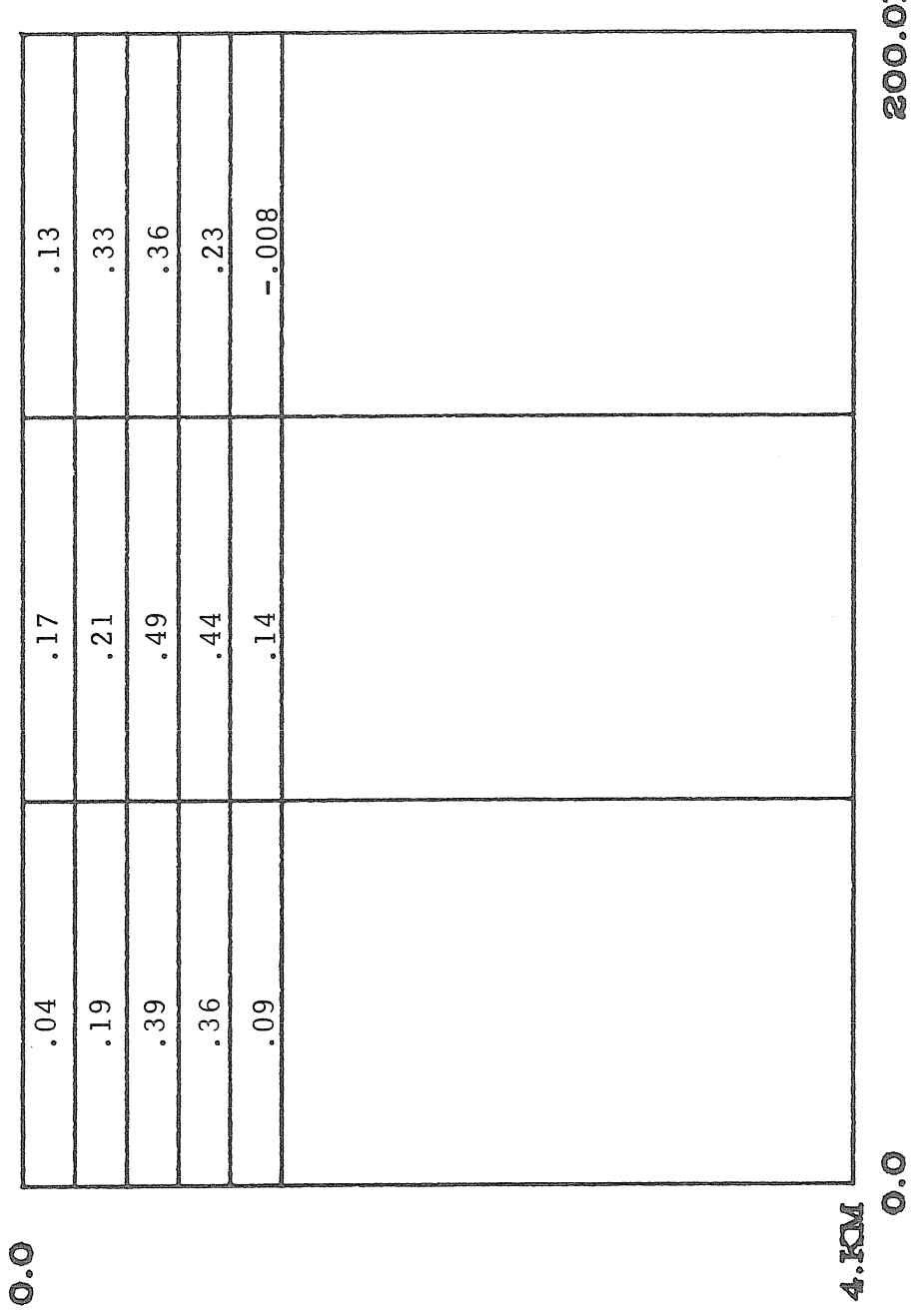

FIGURE 5-18: INVERSION FROM RUN I3-1, 20% NOISE

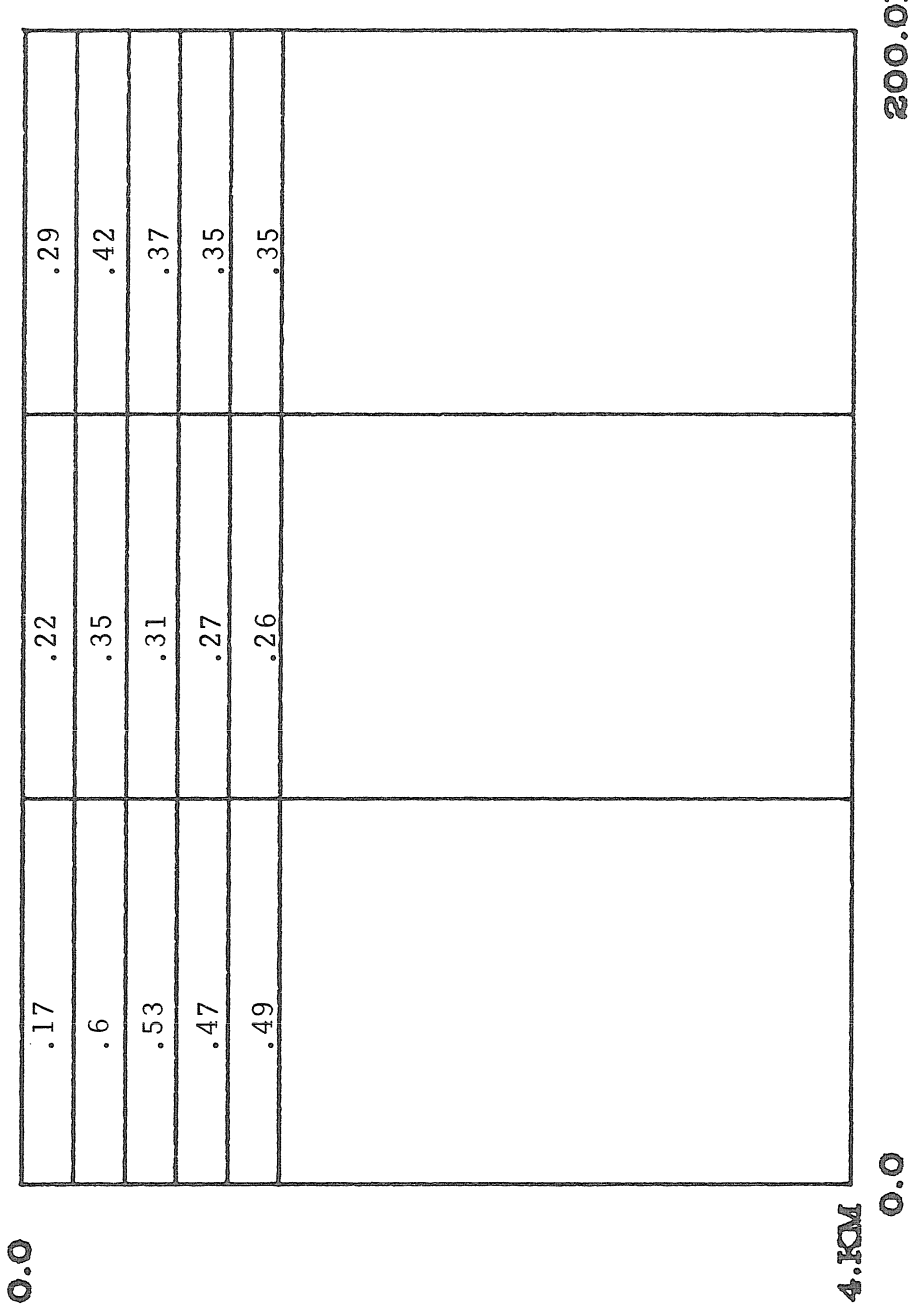

FIGURE 5-19: INVERSION FROM RUN P3, 20% NOISE

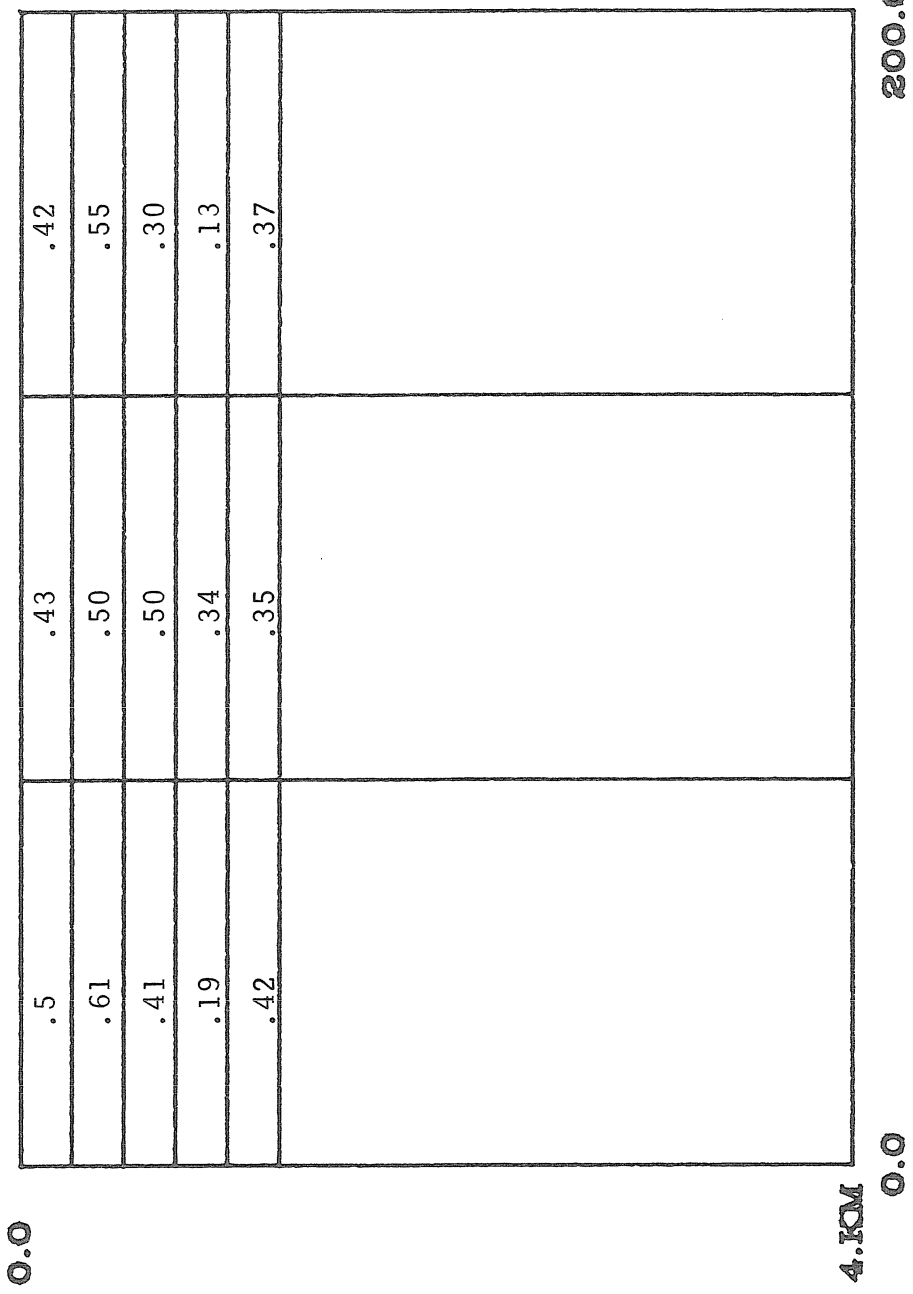

FIGURE 5-20: INVERSION FROM RUN K3 + H3, 20% NOISE

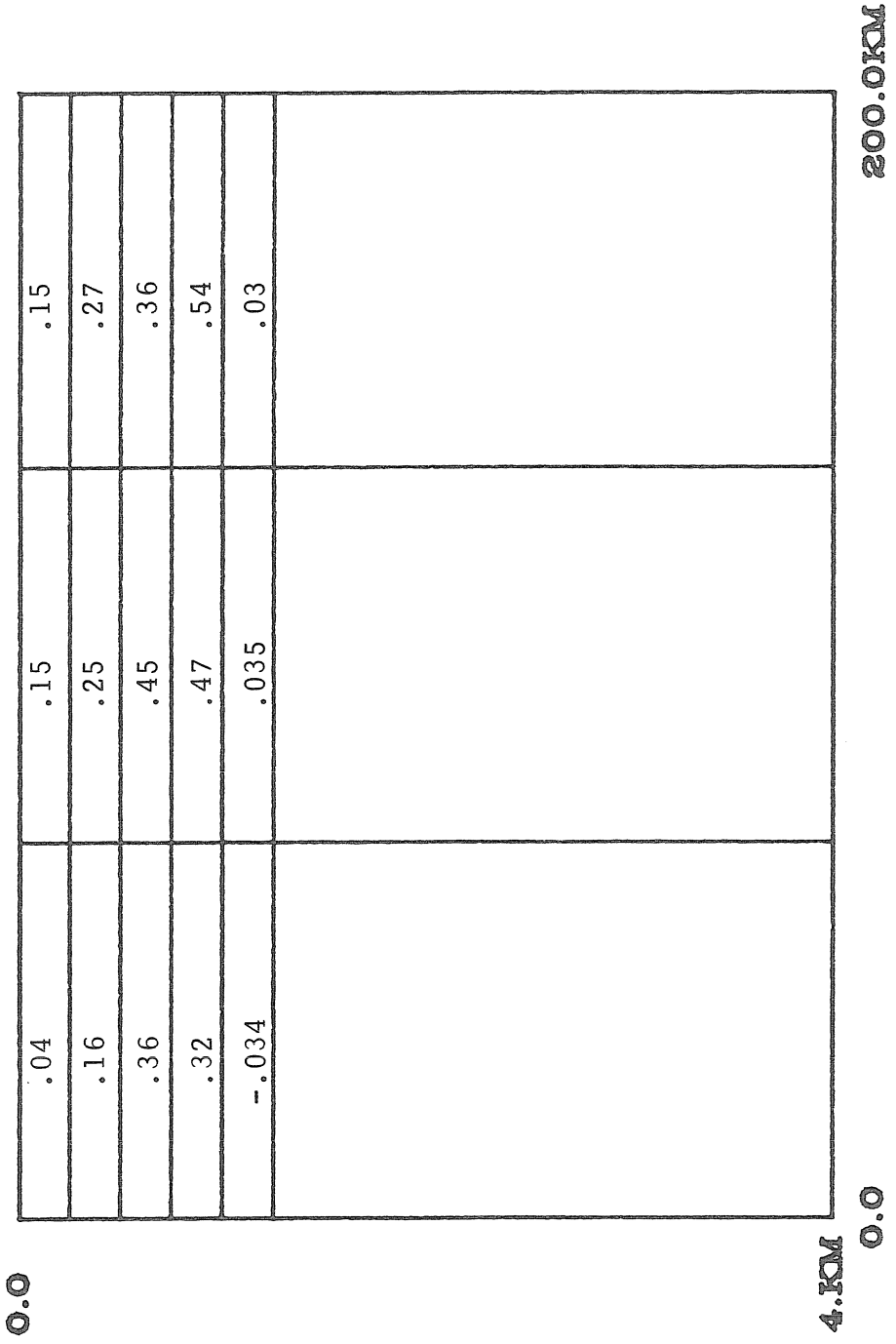

FIGURE 5-21: INVERSION FROM I3 + L3 RUN, 20% NOISE

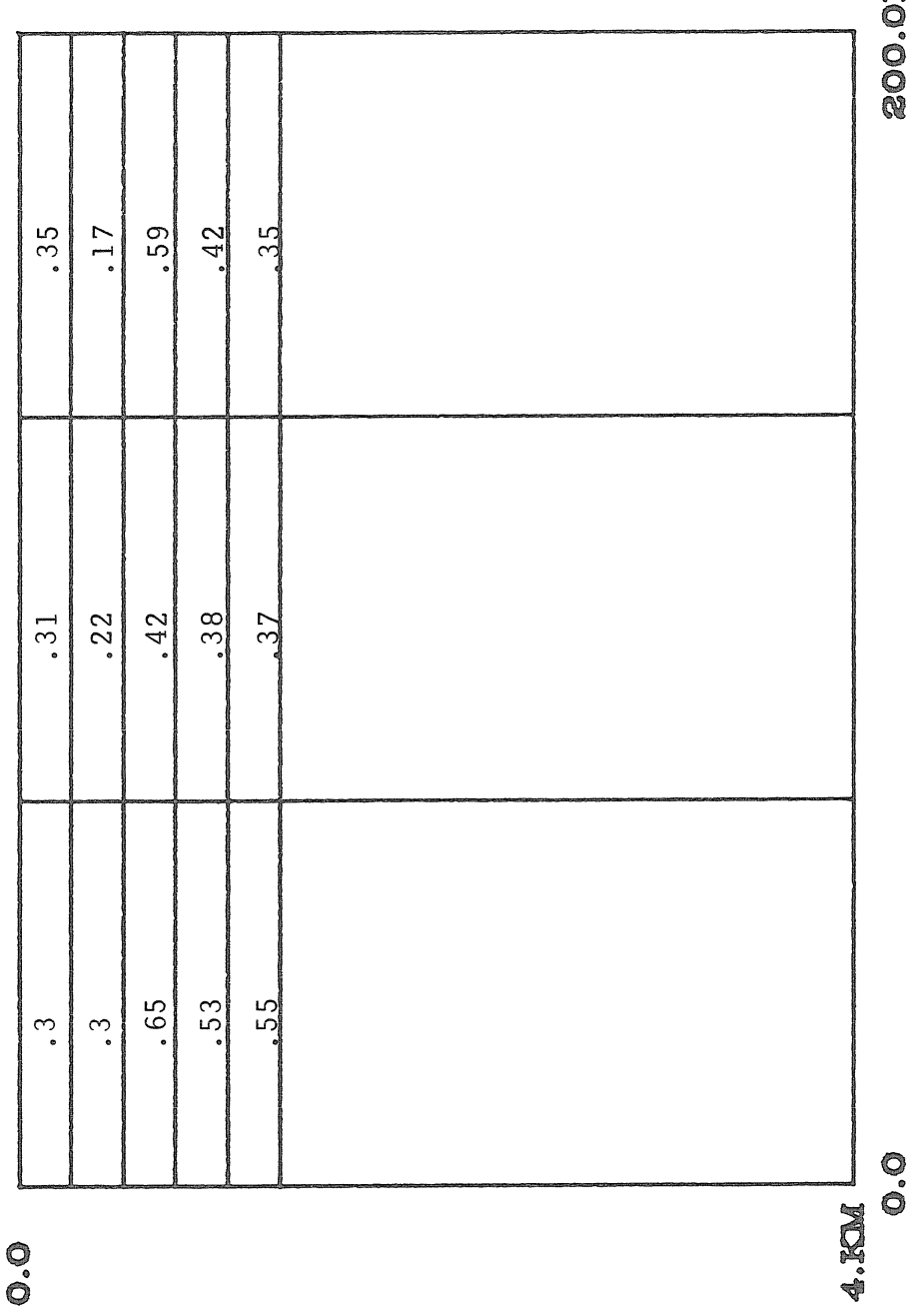

FIGURE 5-22: INVERSION FROM P3 + Q3 RUN, 20% NOISE

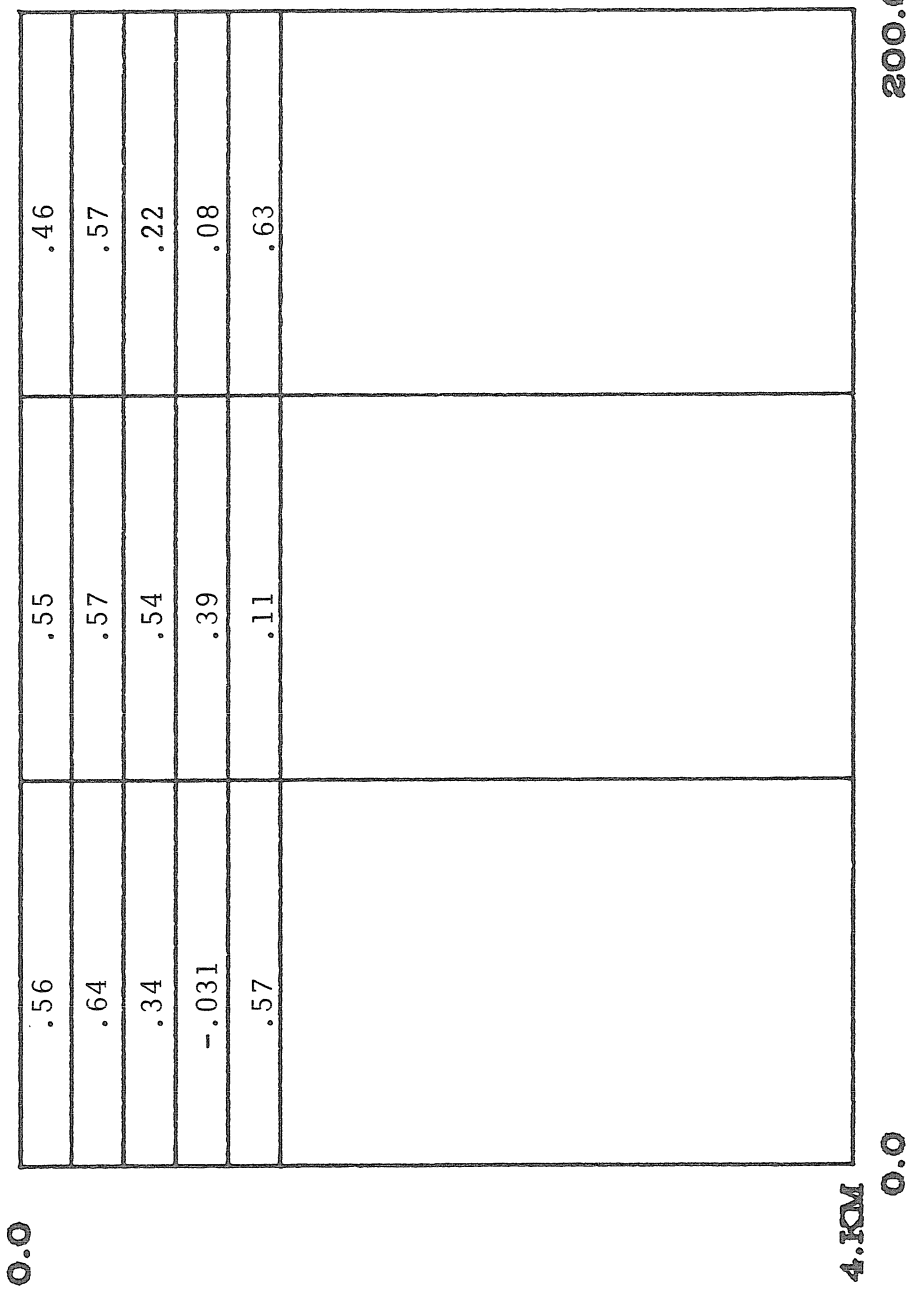

FIGURE 5-23: INVERSION FROM K3 + H3 + N3, 25% NOISE

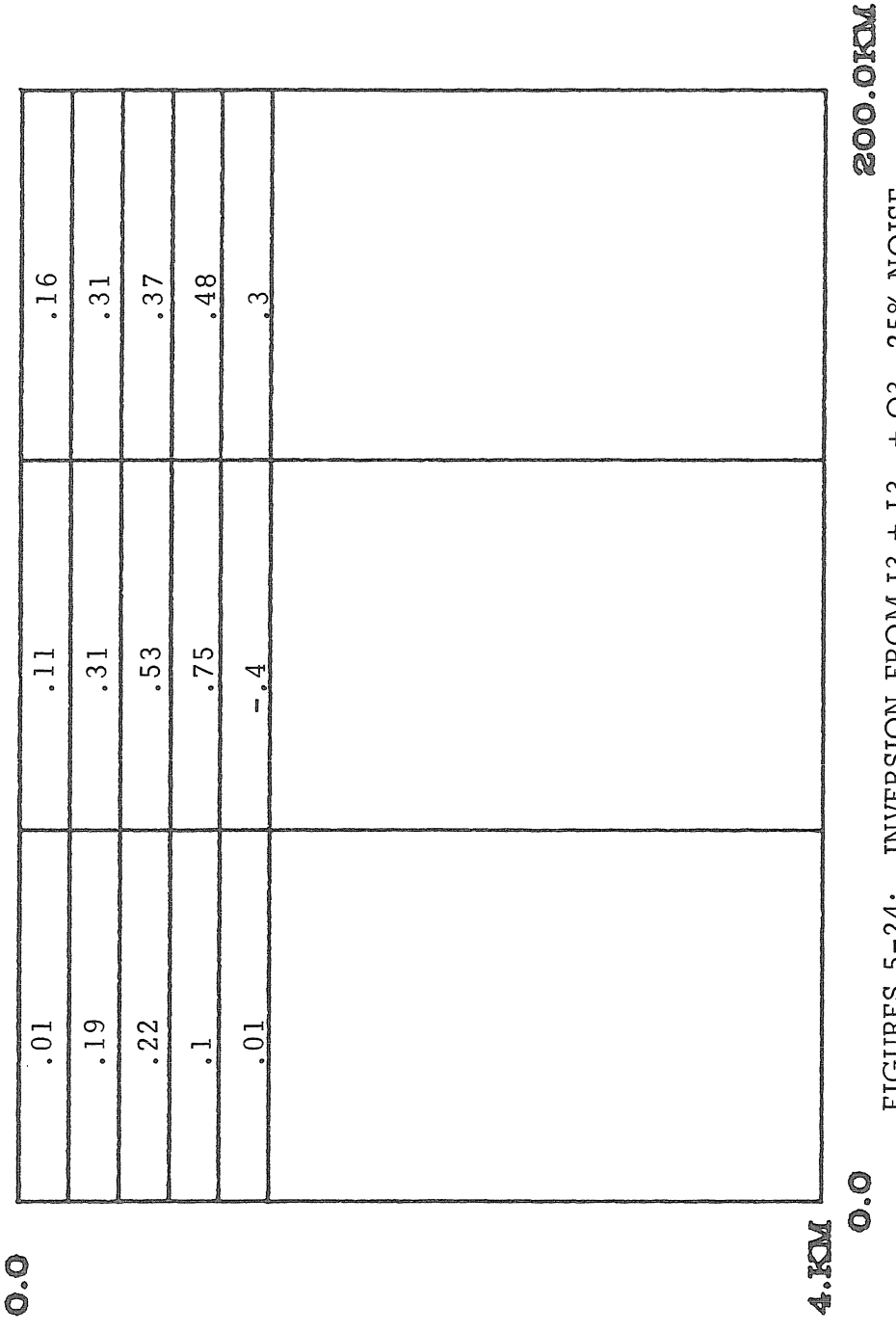

FIGURES 5-24: INVERSION FROM I3 + L3 + O3, 25% NOISE

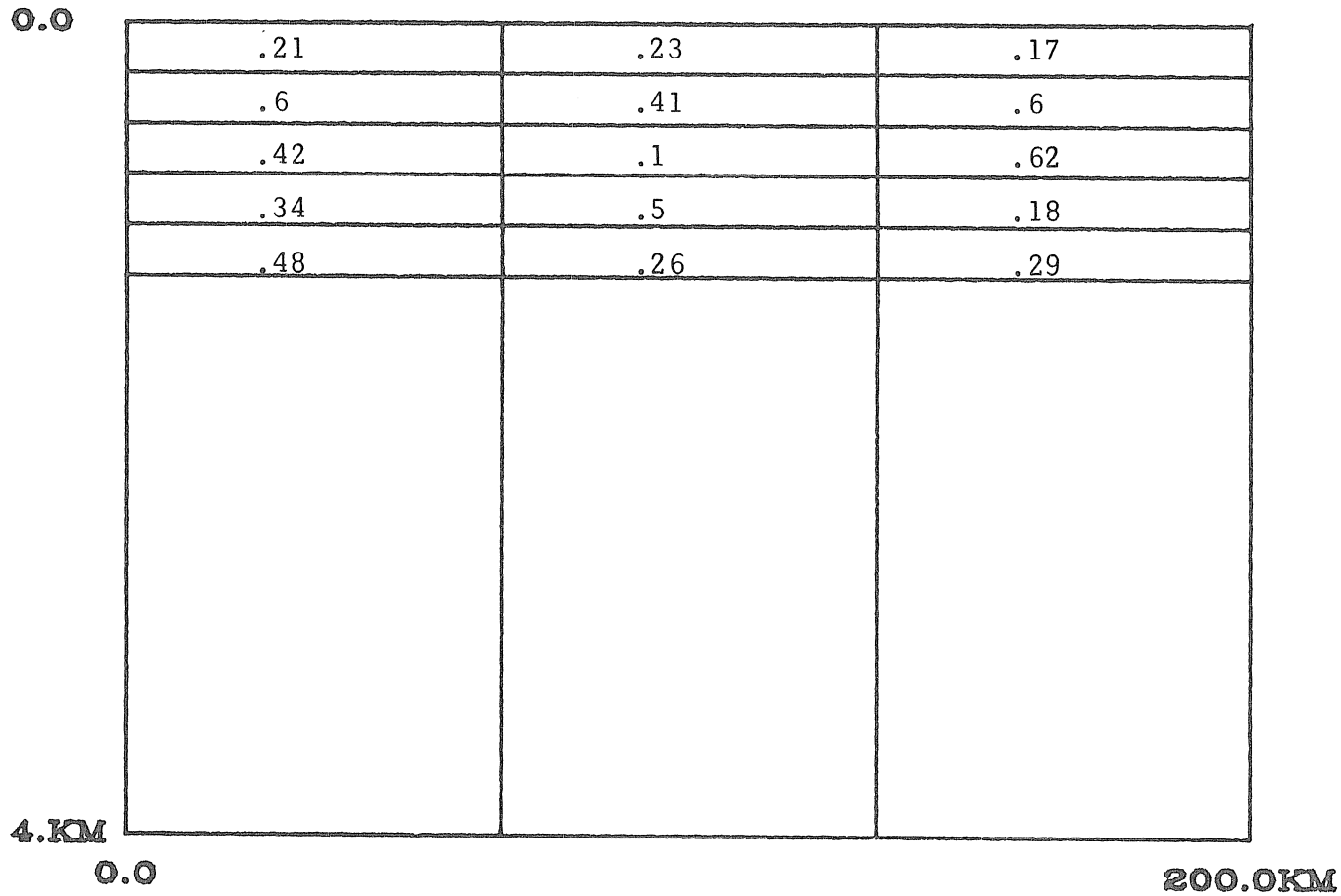

FIGURE 5-25: INVERSION FROM P3 + Q3 + R3, 25% NOISE

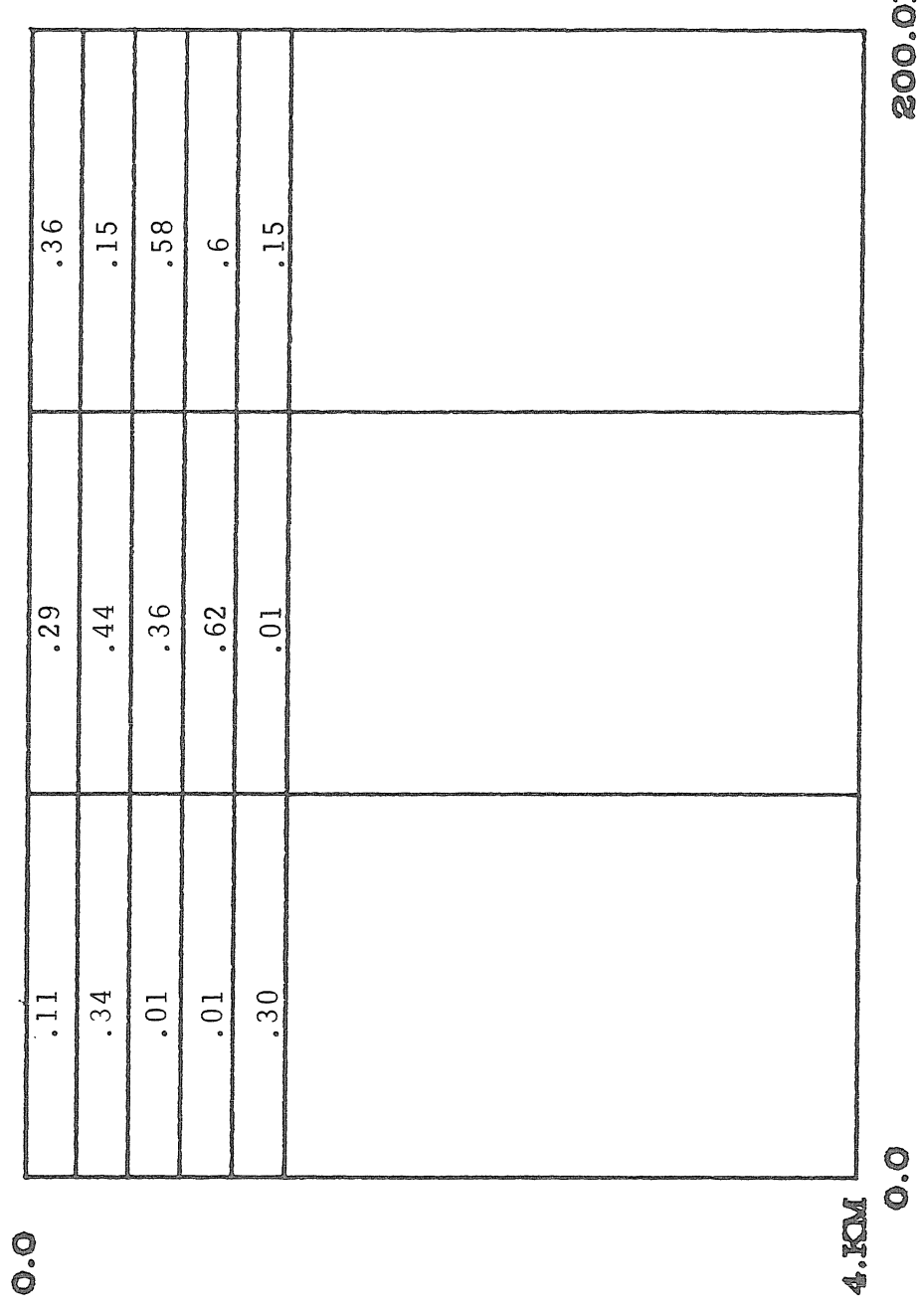

FIGURE 5-26: MAXIMUM ENTROPY INVERSION FROM I3 + L3 + O3, 2.5% NOISE

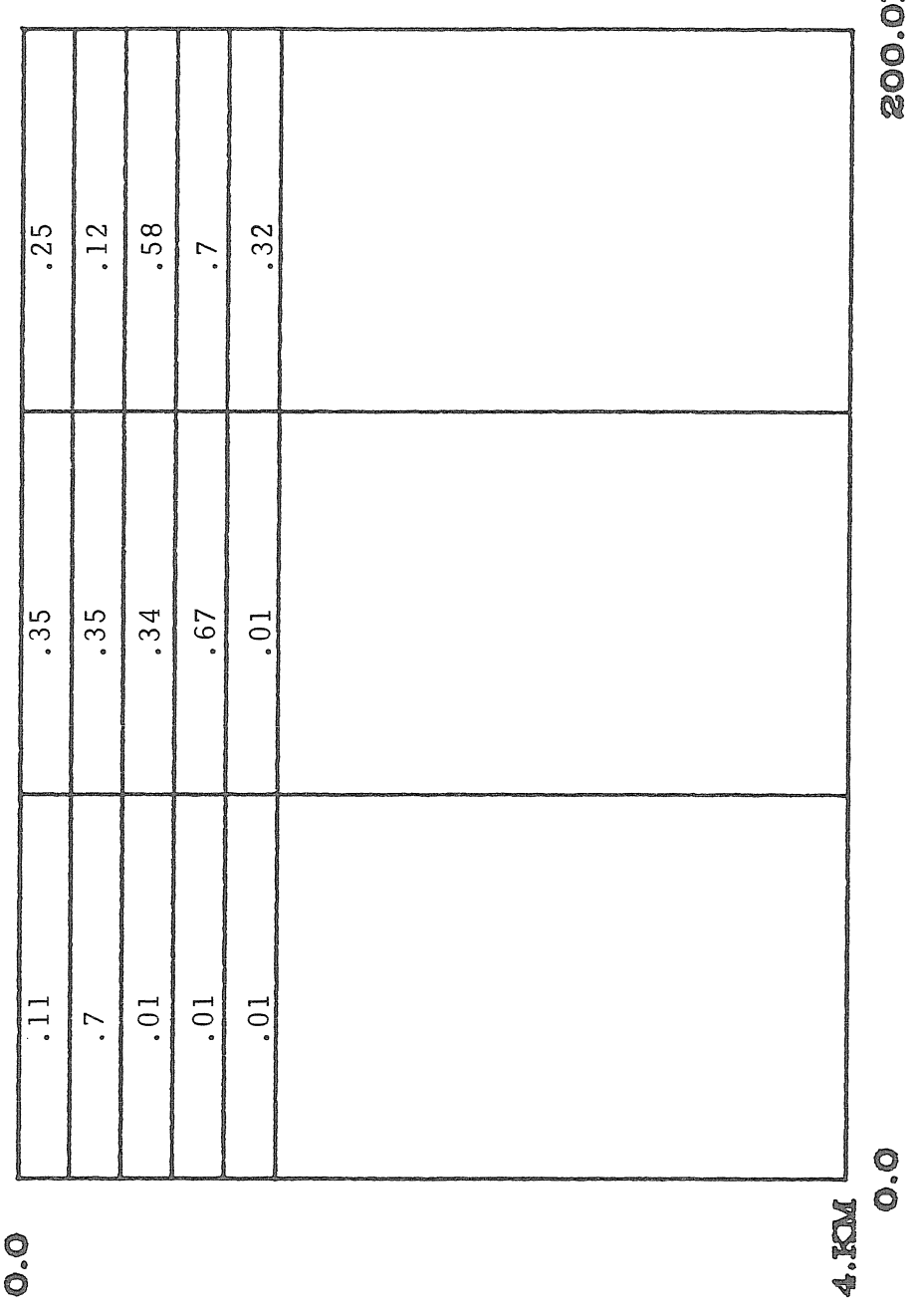

FIGURE 5-27: MAXIMUM ENTROPY INVERSION FROM I3 + L3 + O3, 5% NOISE

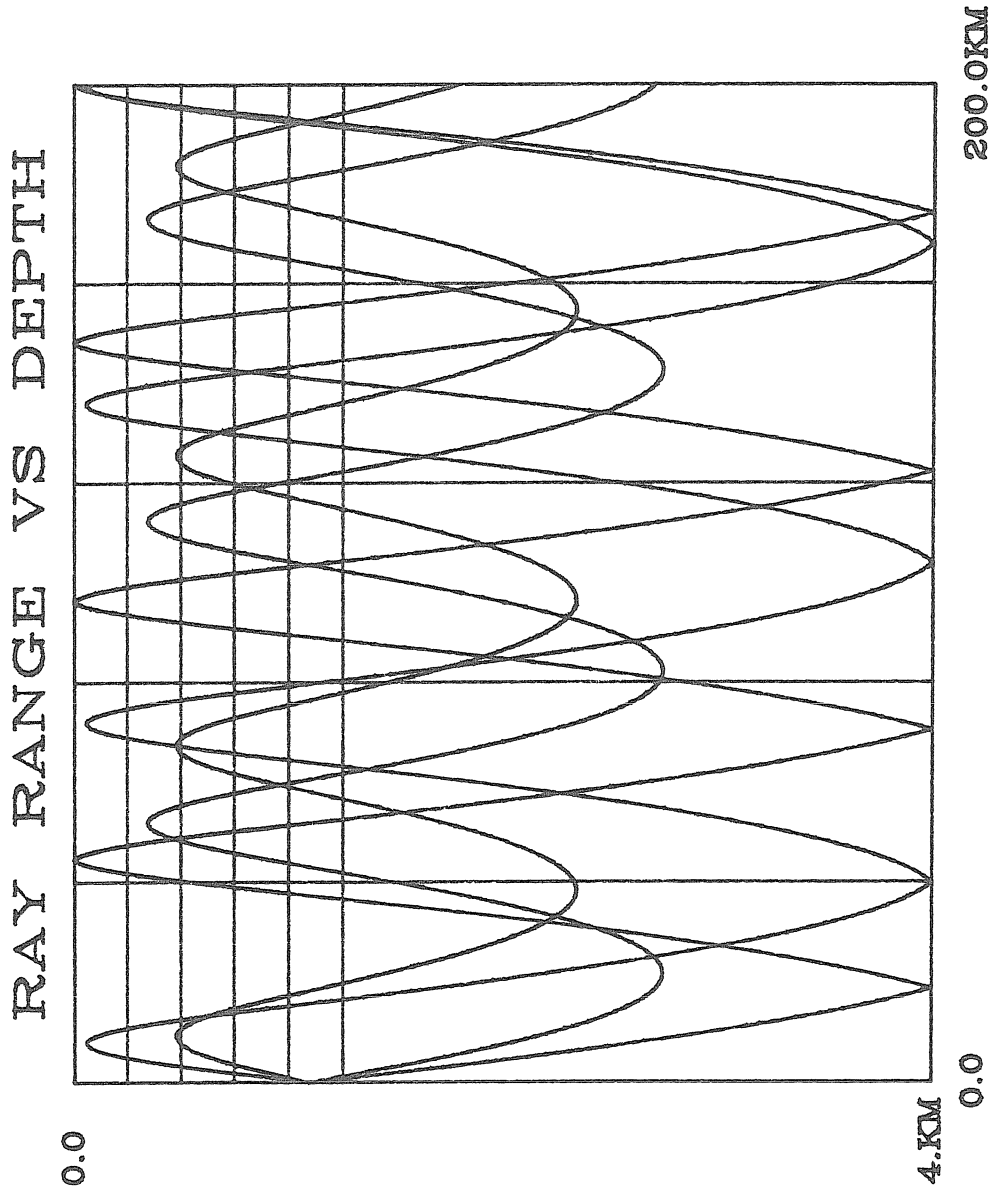

FIGURE 5-28: SAMPLE TOMOGRAPHY EXERCISE

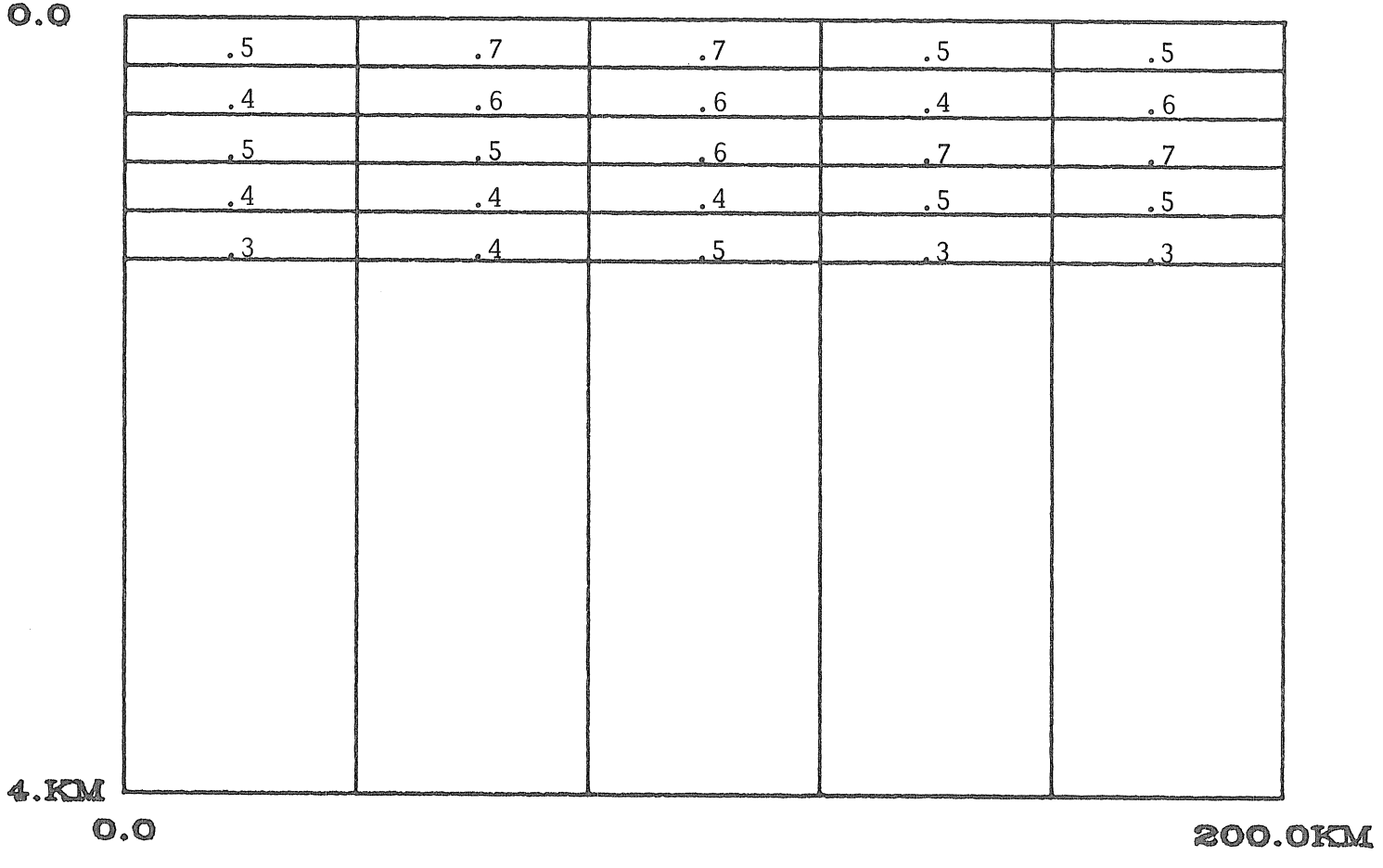

FIGURE 5-29: RESOLUTION MATRIX DIAGONALS

2.5% NOISE, ONE SOURCE

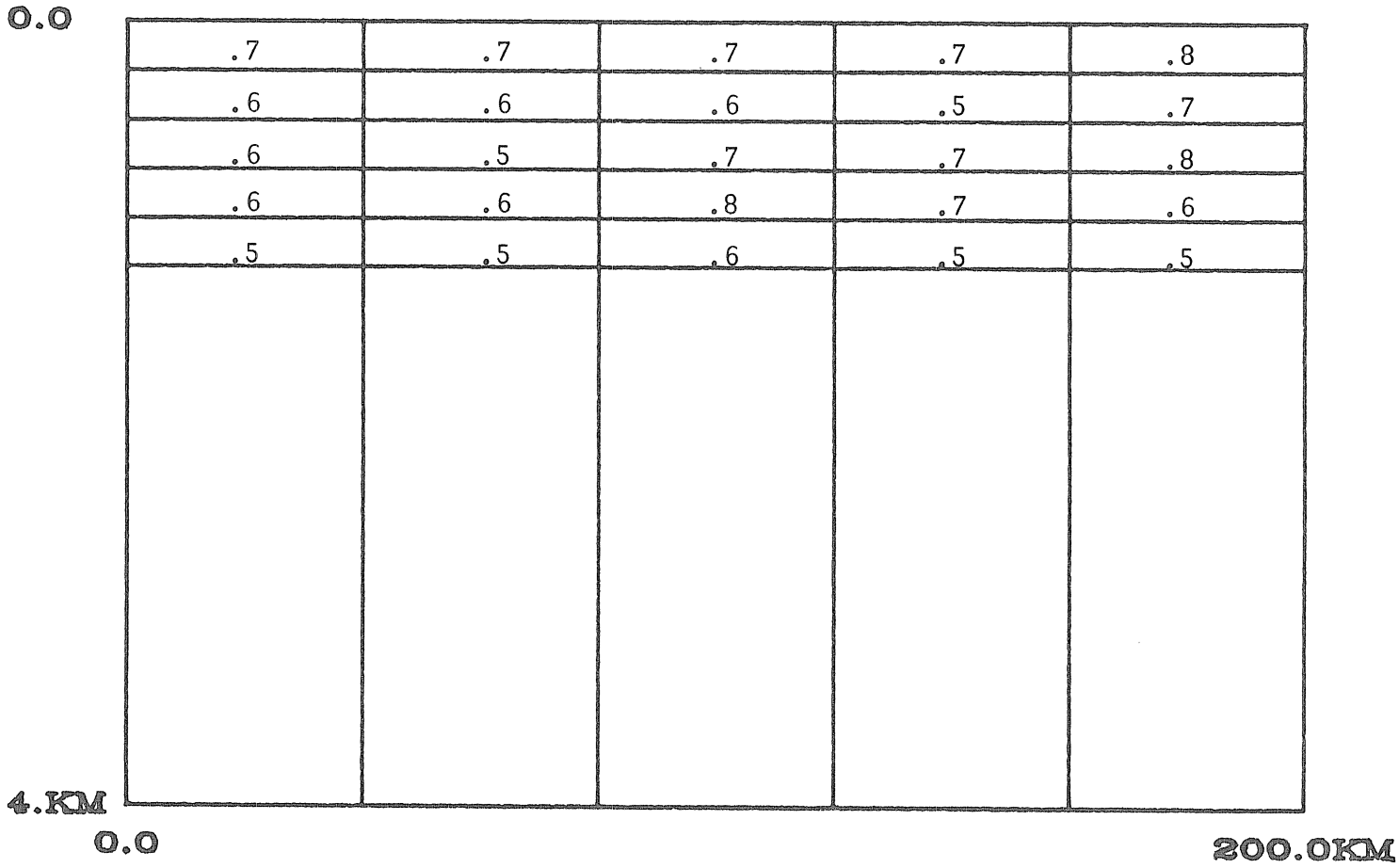

FIGURE 5-30: RESOLUTION MATRIX DIAGONALS

2.5% NOISE, TWO SOURCES

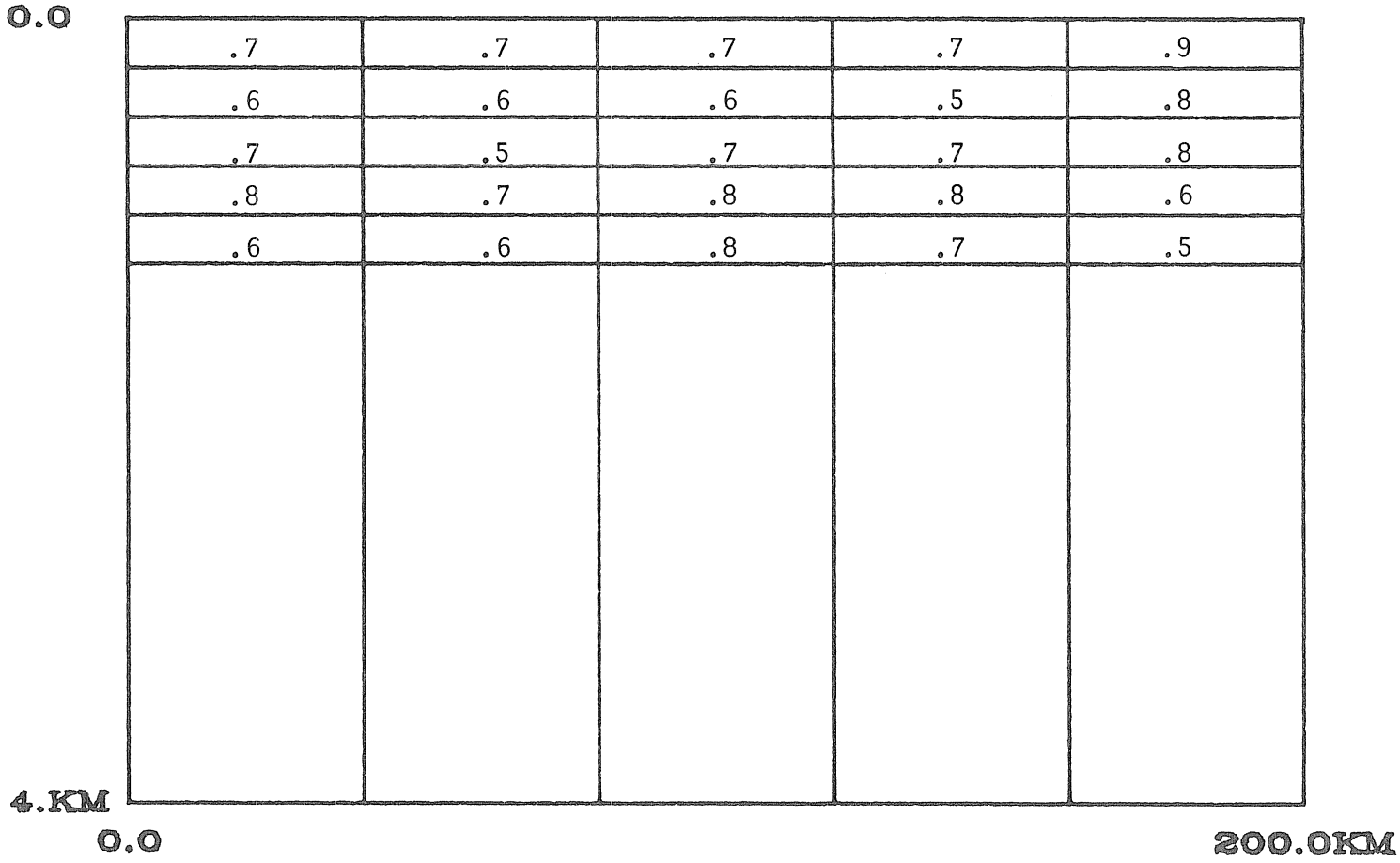

FIGURE 5-31: RESOLUTION MATRIX DIAGONALS

2.5% NOISE, THREE SOURCES

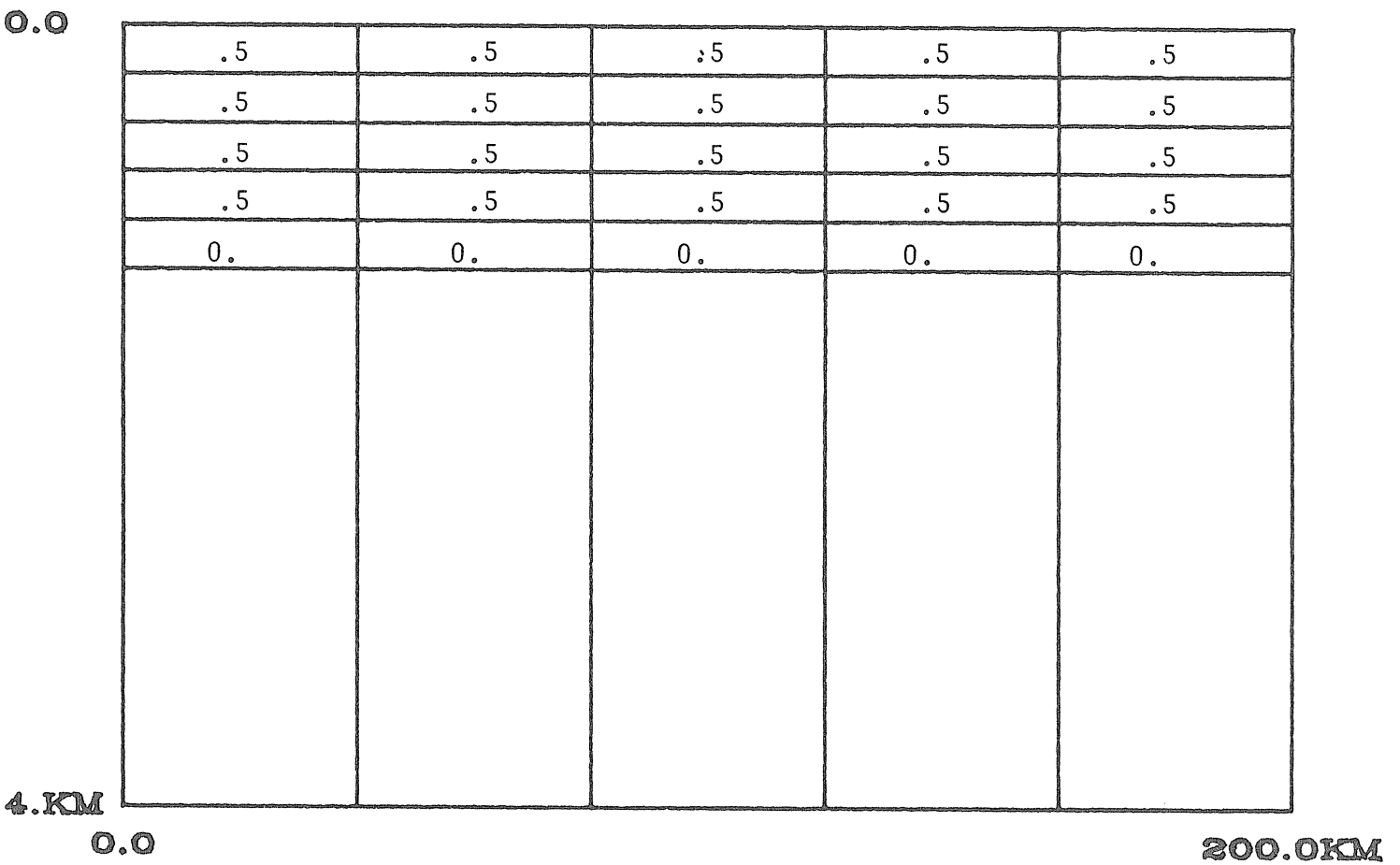

FIGURE 5-32: CASE 1 PERTURBATION

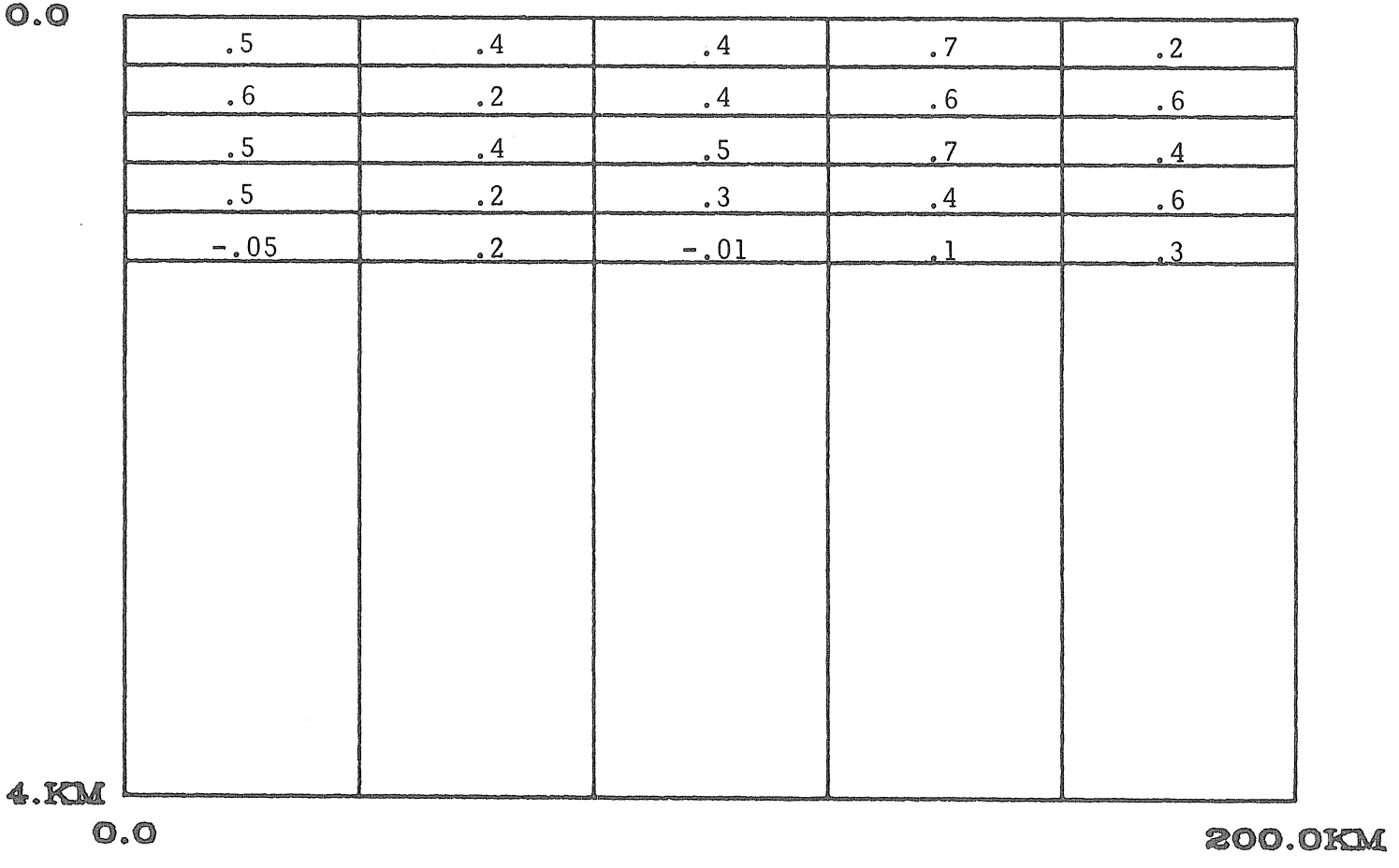

FIGURE 5-33: GINV - CASE 1

2.5% NOISE, ONE SOURCE - AV. DIFF. = .11

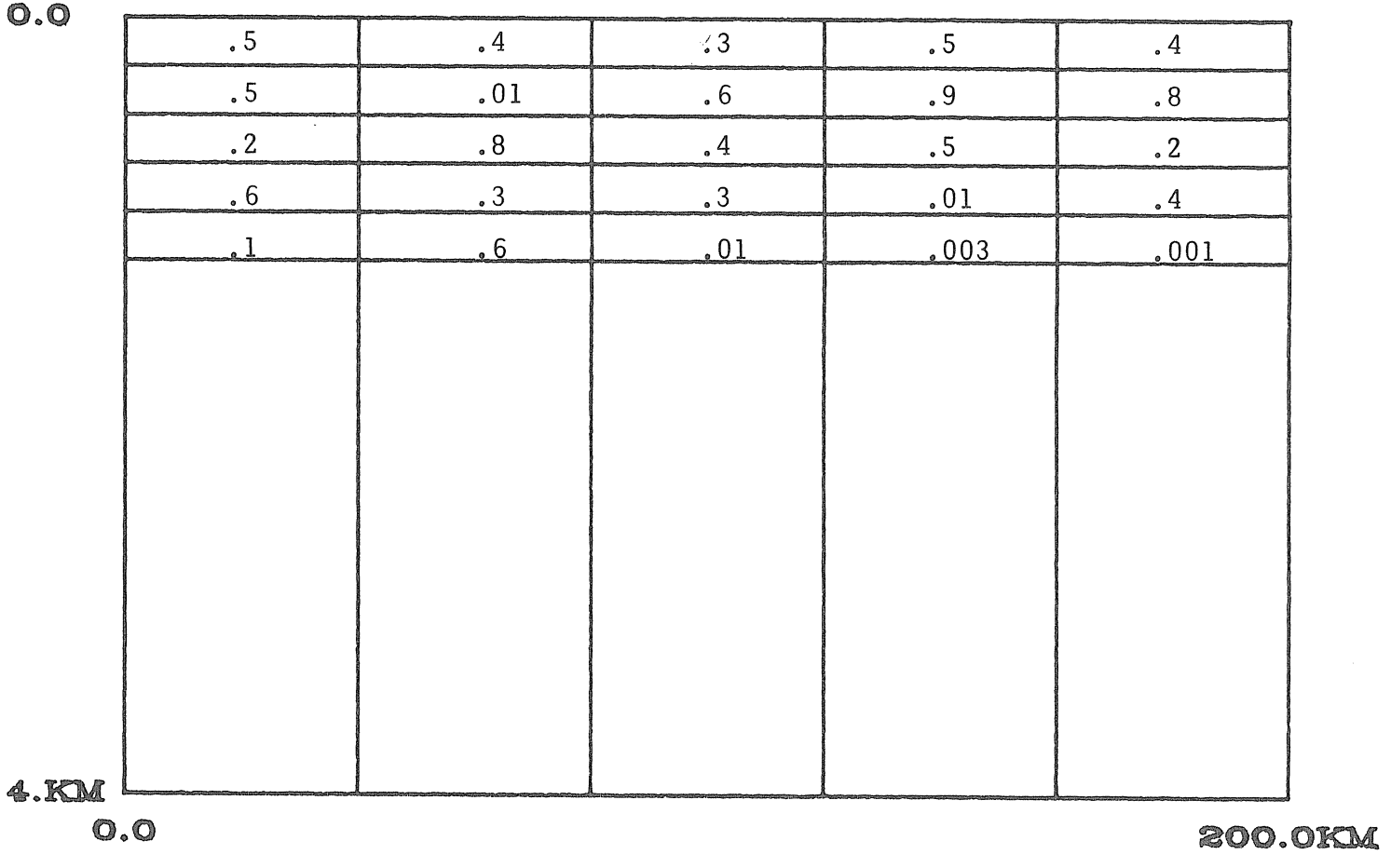

FIGURE 5-34: GMAX - CASE 1

2.5% NOISE, ONE SOURCE - AV. DIFF. = .15

0.0

.5	.5	.3	.5	.4
.4	.6	.4	.4	.4
.5	.5	.3	.5	.5
.3	.5	.4	.4	.4
.001	.2	.05	.2	.09

4.KM

0.0 FIGURE 5-35: GINV - CASE 1 200.0KM

2.5% NOISE, TWO SOURCES - AV. DIFF. = .07

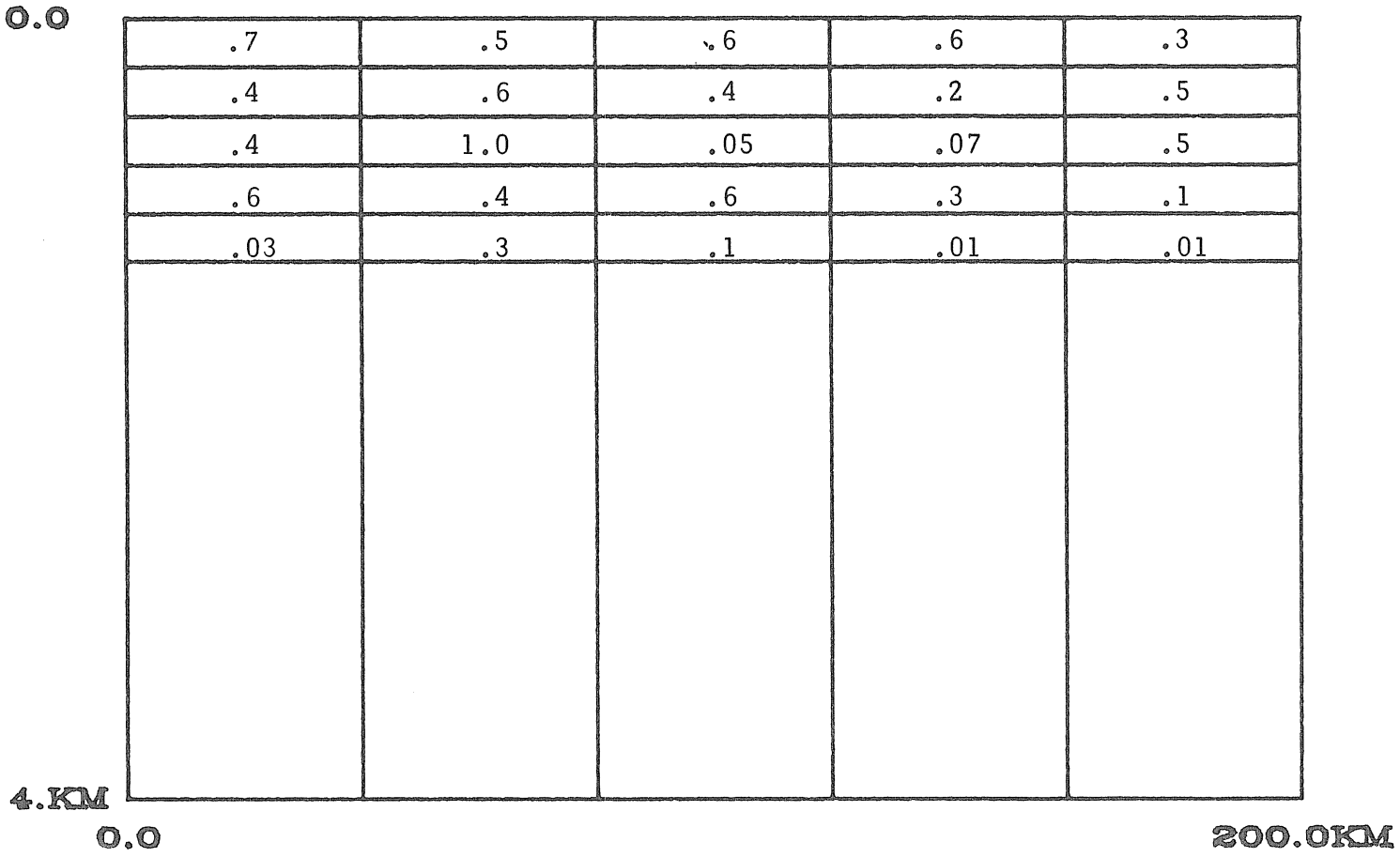

FIGURE 5-36: GMAX - CASE 1

2.5% NOISE, TWO SOURCES, AV. DIFF = .13

0.0

.5	.6	.045	.3	.5
.6	.4	.62	.6	.2
.4	.15	.5	.7	.7
.4	.4	.4	.5	.6
.1	.5	.06	-.1	-.4

4.KM

0.0 200.0KM

FIGURE 5-37: GINV - CASE 1

2.5% NOISE, THREE SOURCES, AV. DIFF. = .13

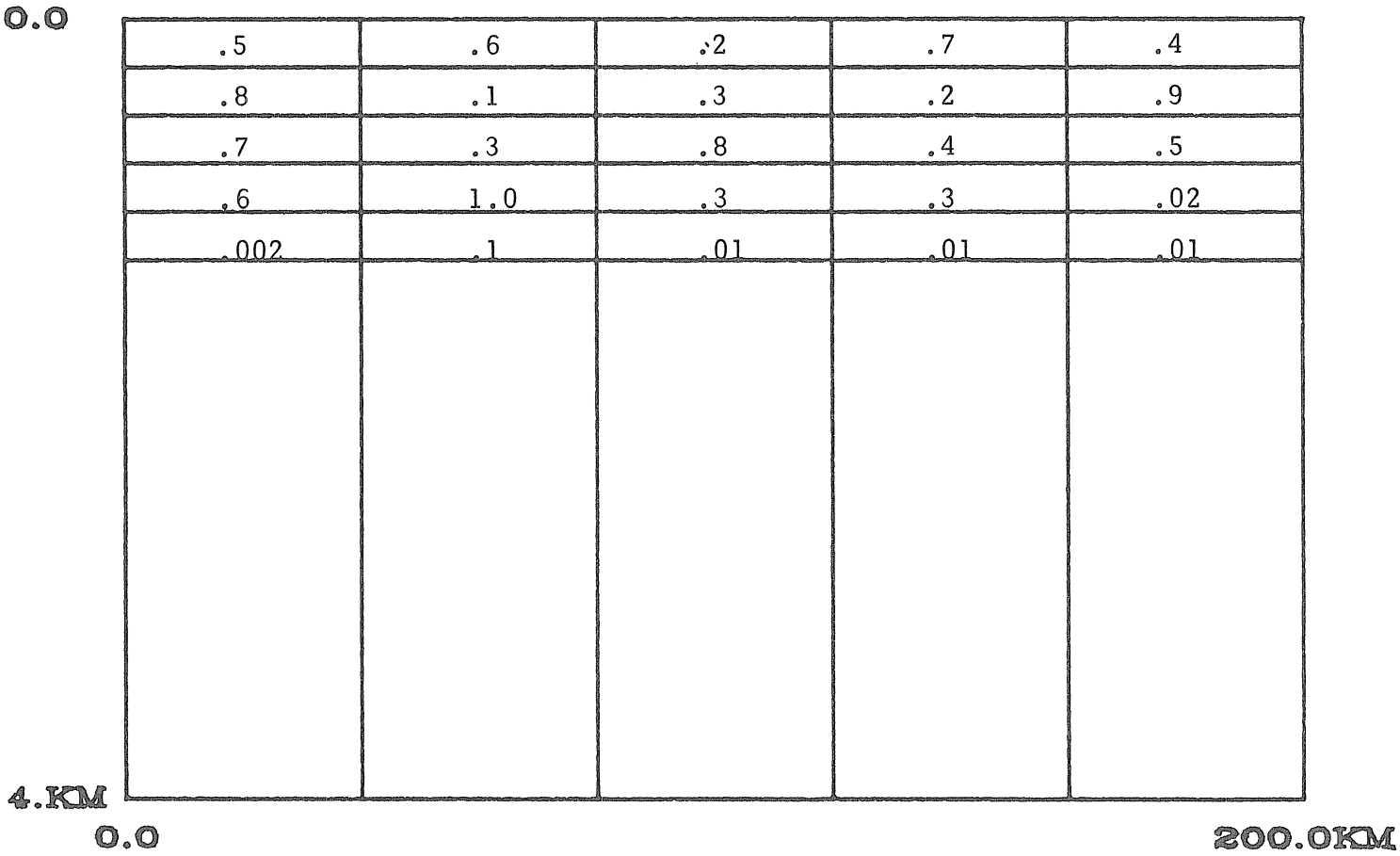

FIGURE 5-38: GMAX - CASE 1

2.5% NOISE, THREE SOURCES, AV. DIFF. = .15

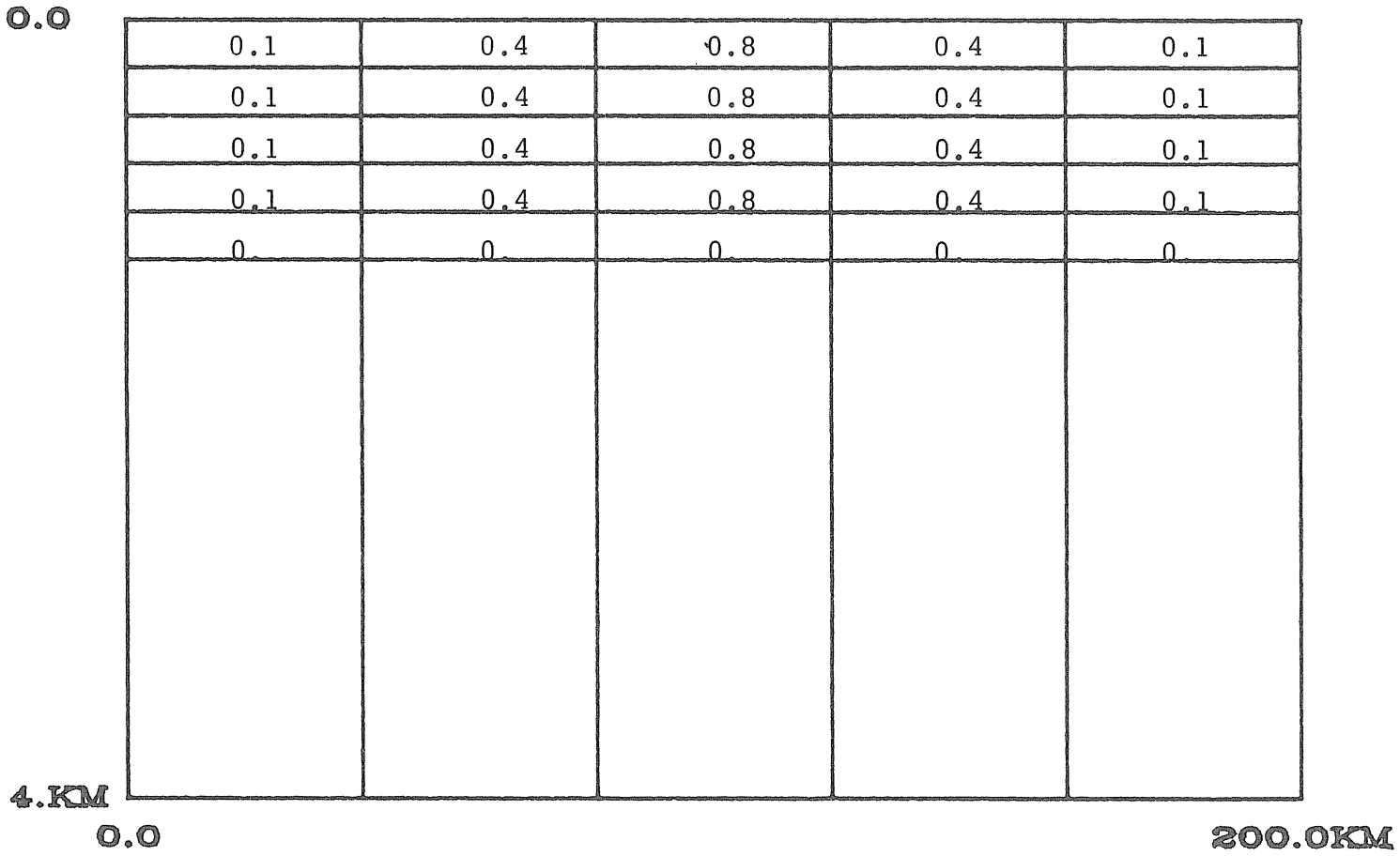

FIGURE 5-39: CASE 2 PERTURBATION

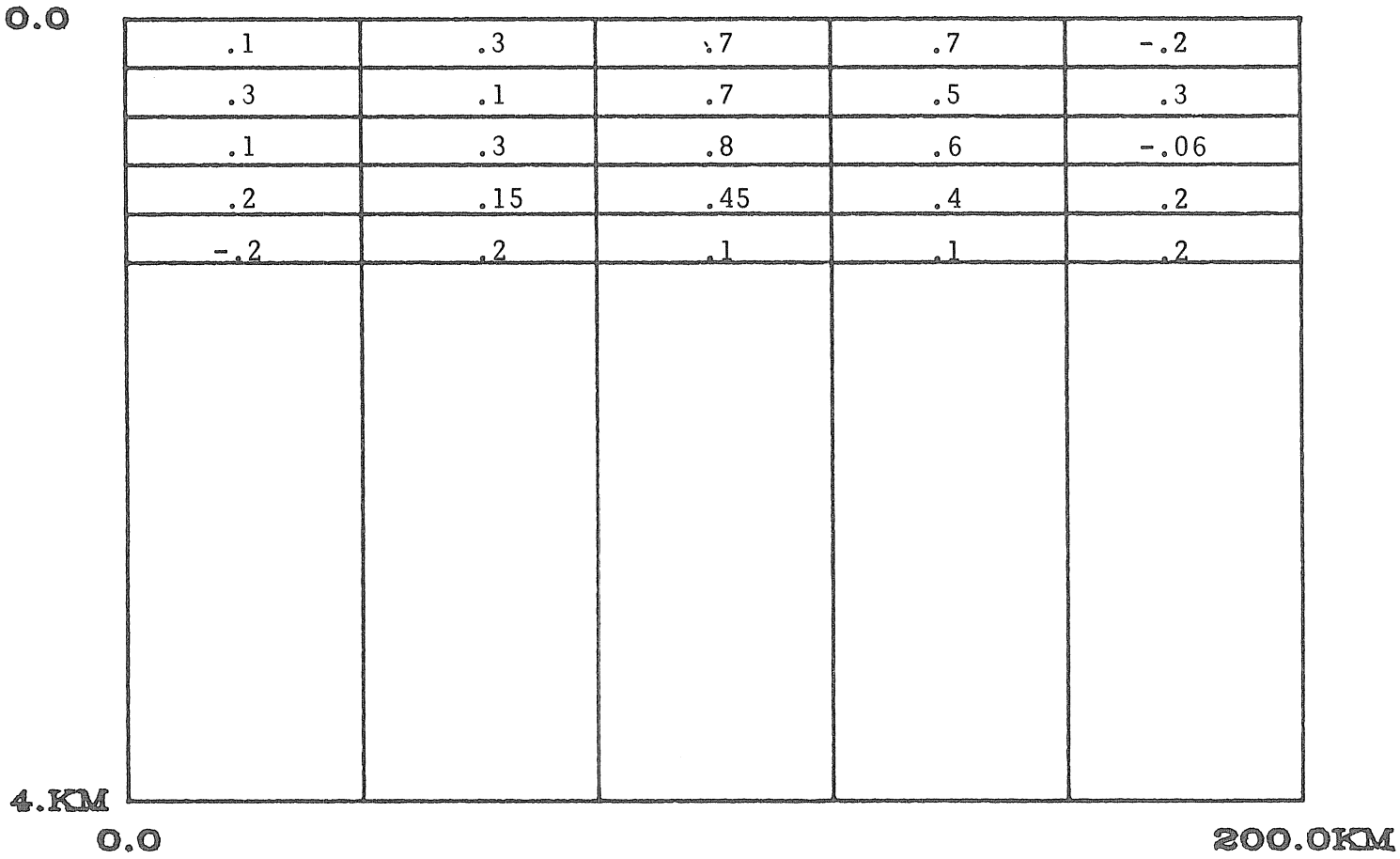

FIGURE 5-40: CASE 2 GINV

2.5% NOISE, ONE SOURCE, AV. DIFF. = .13

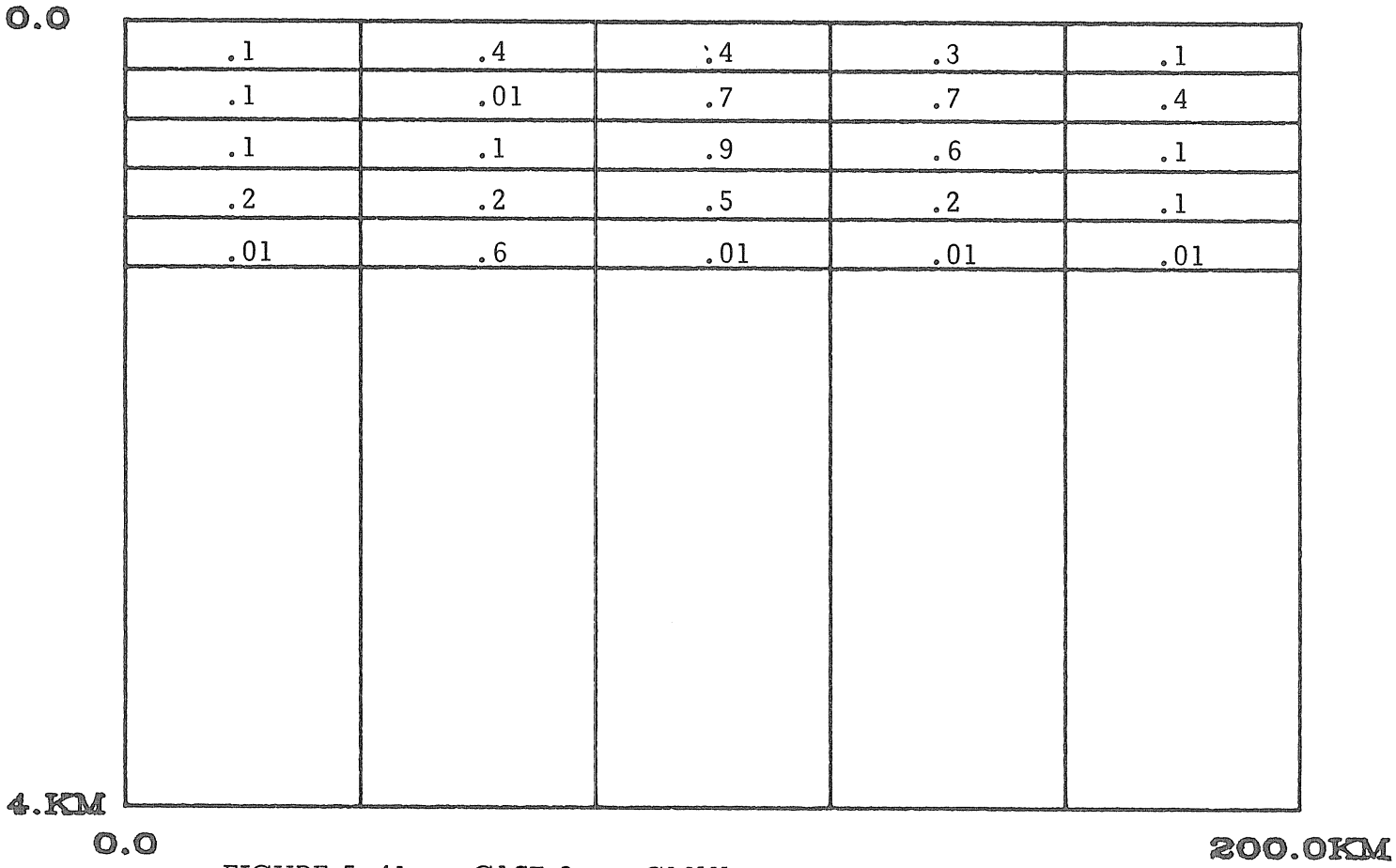

FIGURE 5-41: CASE 2 GMAX

2.5% NOISE, ONE SOURCE, AV. DIFF. = .13

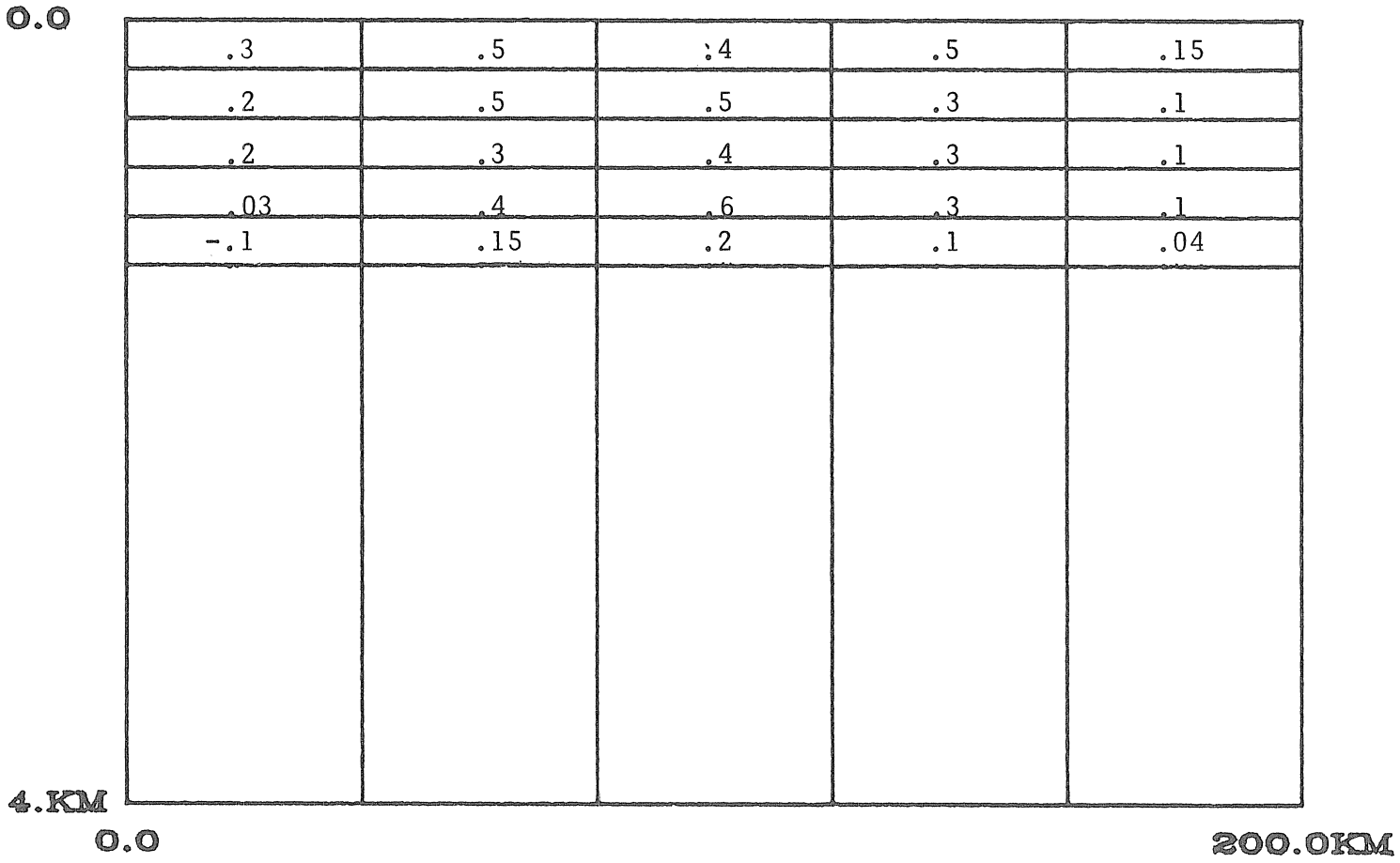

FIGURE 5-42: CASE 2 GINV

TWO SOURCES, AV. DIFF. = .10

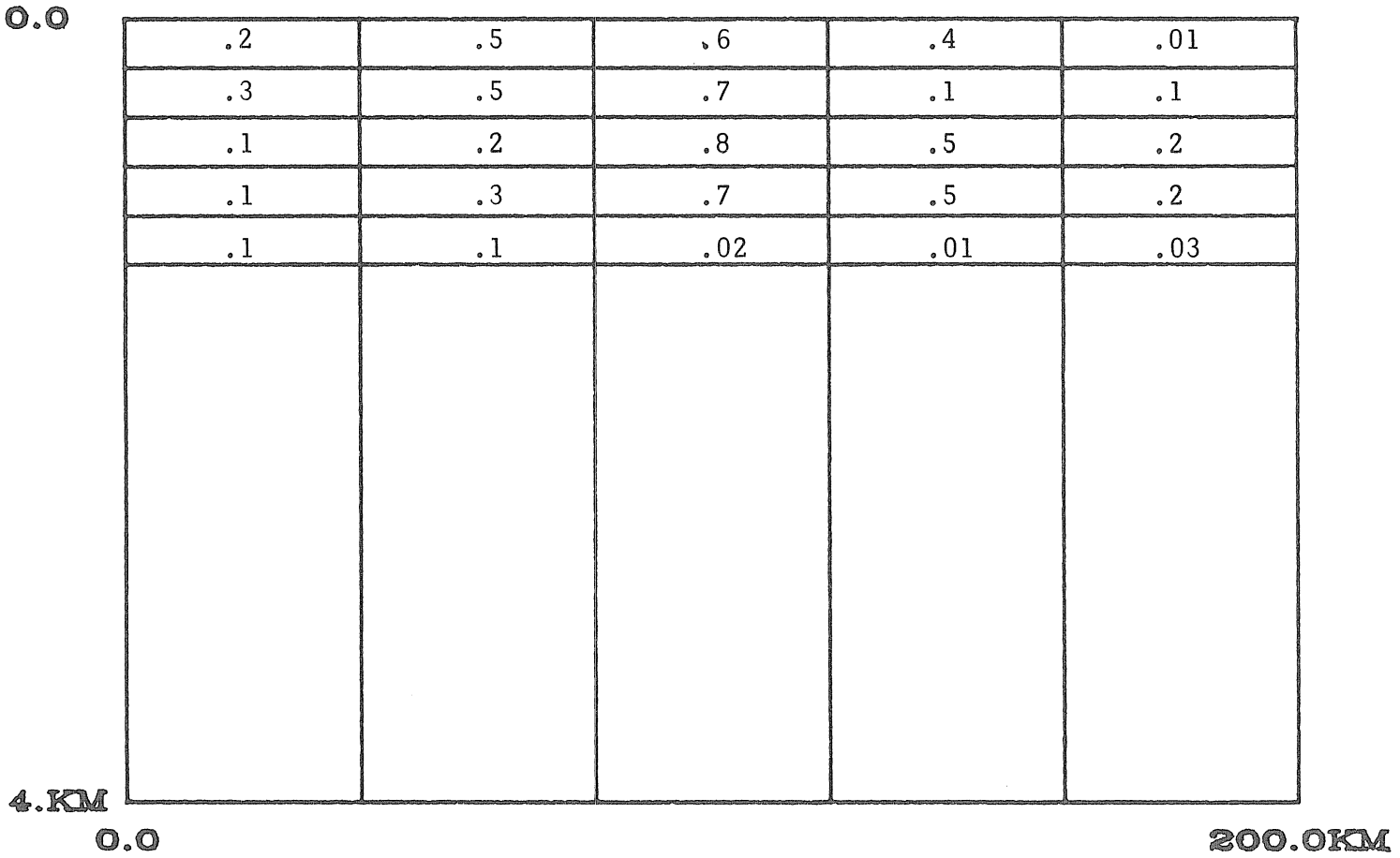

FIGURE 5-43: CASE 2 GMAX

TWO SOURCES, AV. DIFF. = .08

0.0

.3	.5	:1	.25	.3
.4	.2	.7	.5	-.05
.1	-.02	.6	.5	.4
.01	.4	.6	.4	.3
.04	.4	.2	-.2	-.43

4.KM

0.0 200.0KM

FIGURE 5-44: CASE 2 GINV

THREE SOURCES, AV. DIFF. = .16

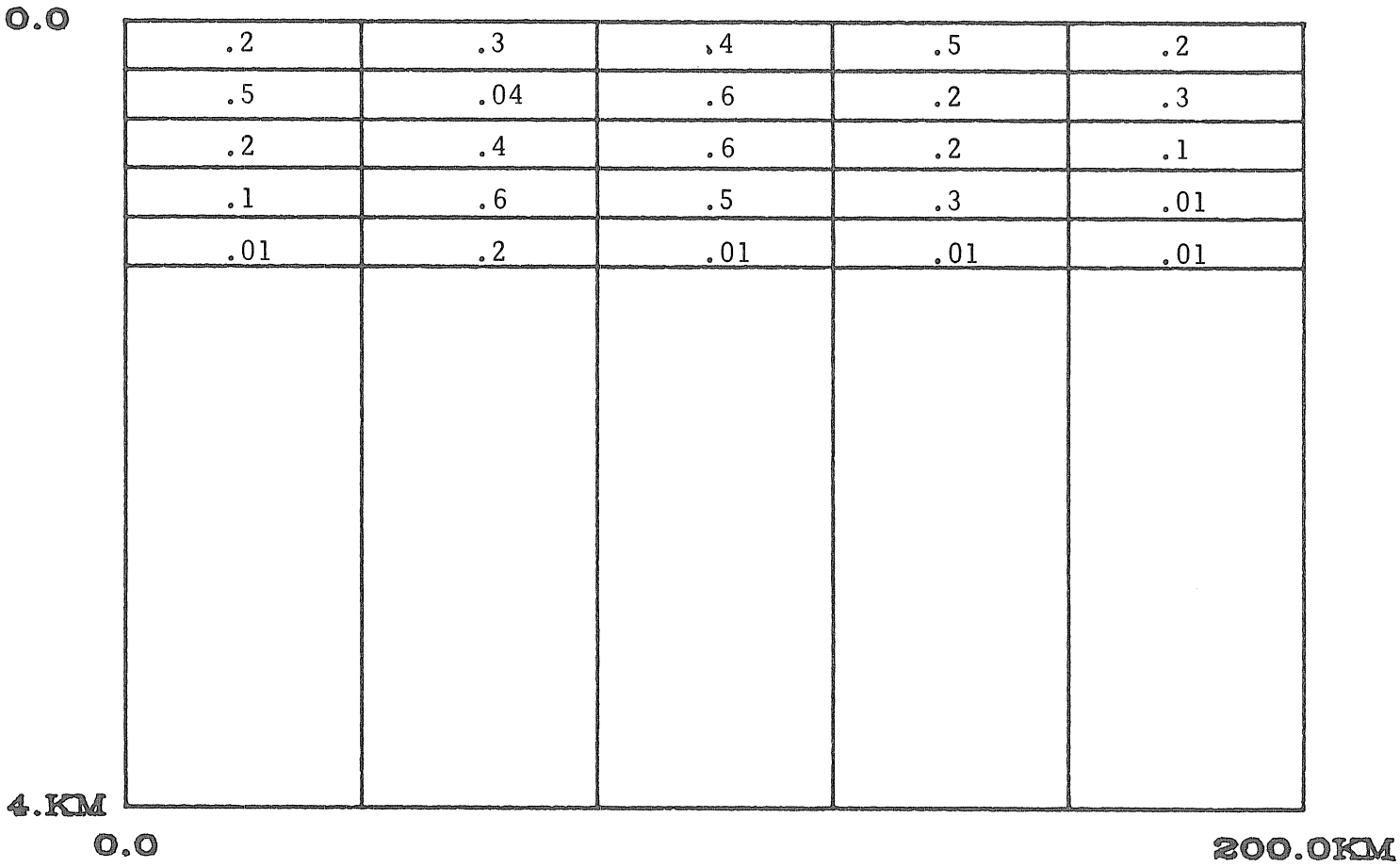

FIGURE 5-45: CASE 2 GMAX

THREE SOURCES, AV. DIFF. = .12

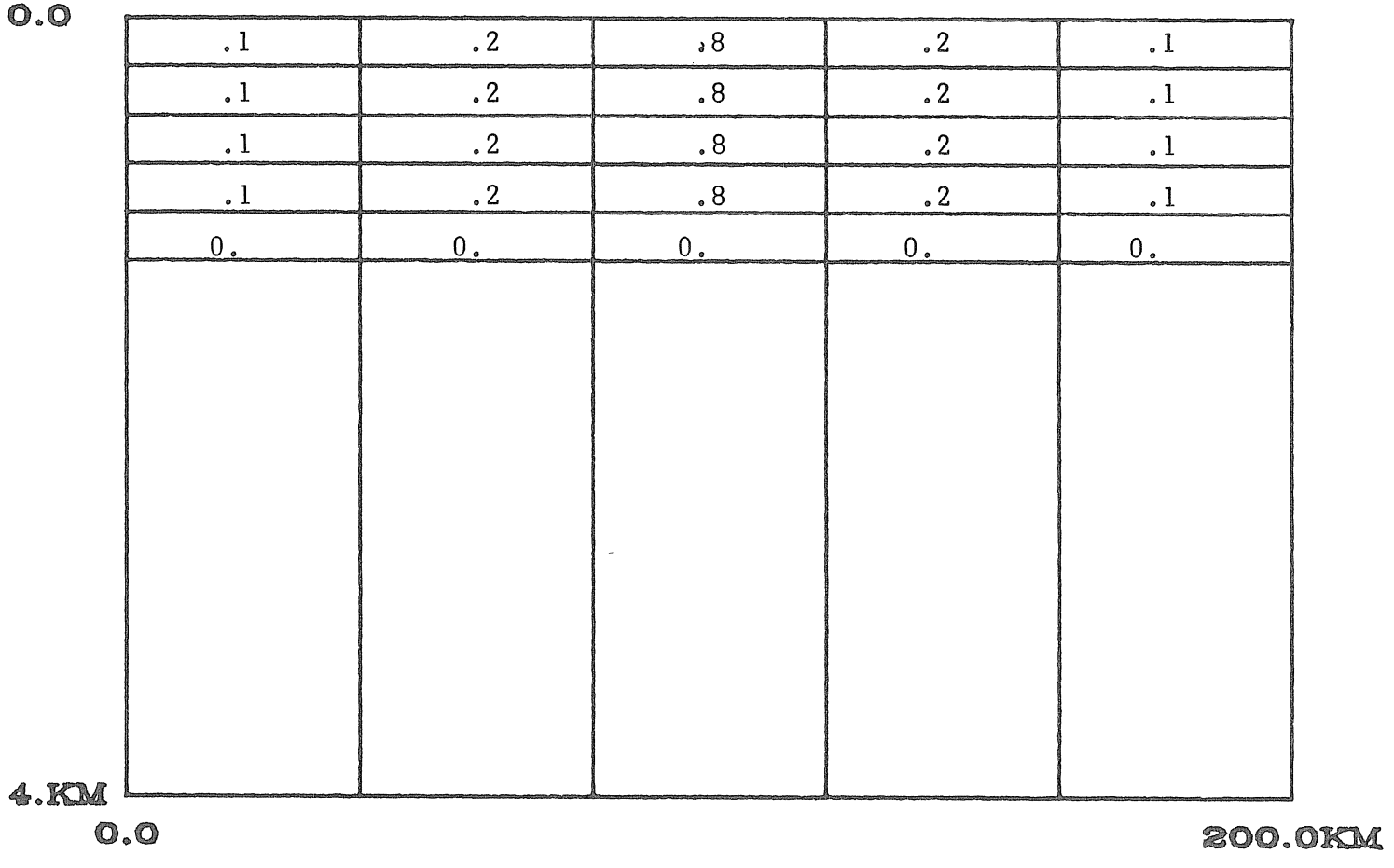

FIGURE 5-46: CASE 3 PERTURBATION

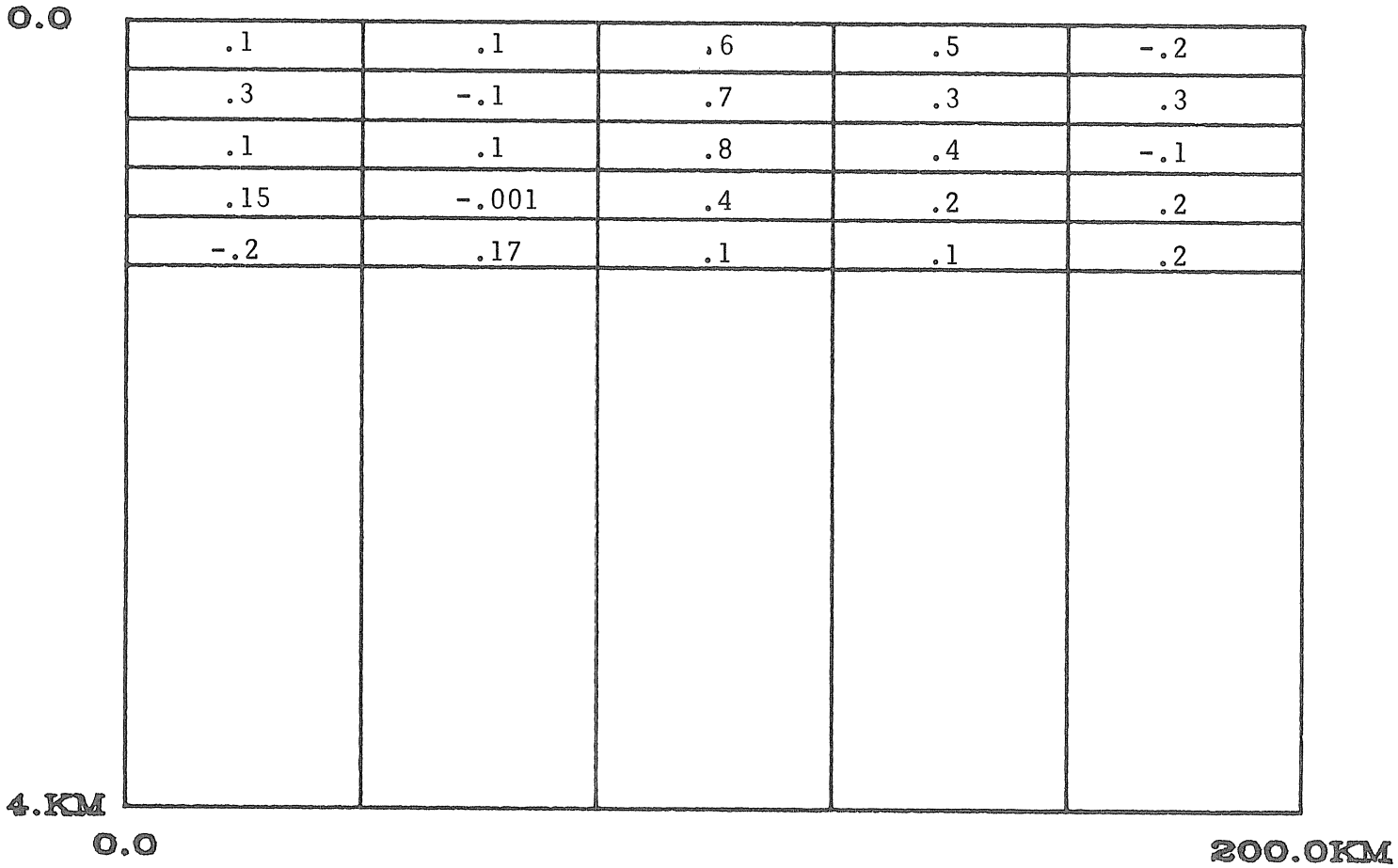

FIGURE 5-47: CASE 3 GINV

ONE SOURCE, AV. DIFF. = .12

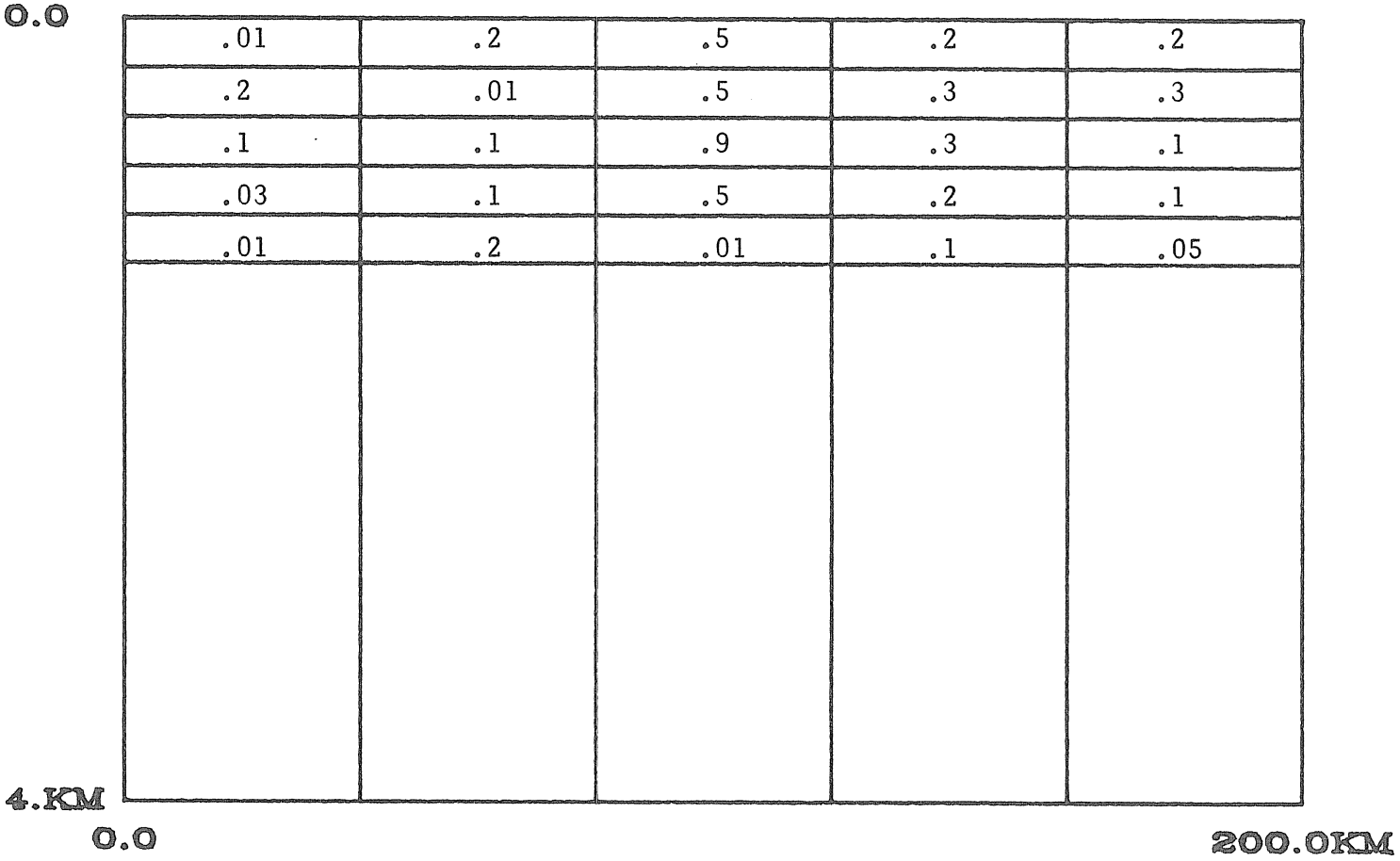

FIGURE 5-48: CASE 3 GMAX

ONE SOURCE, AV. DIFF. = .093

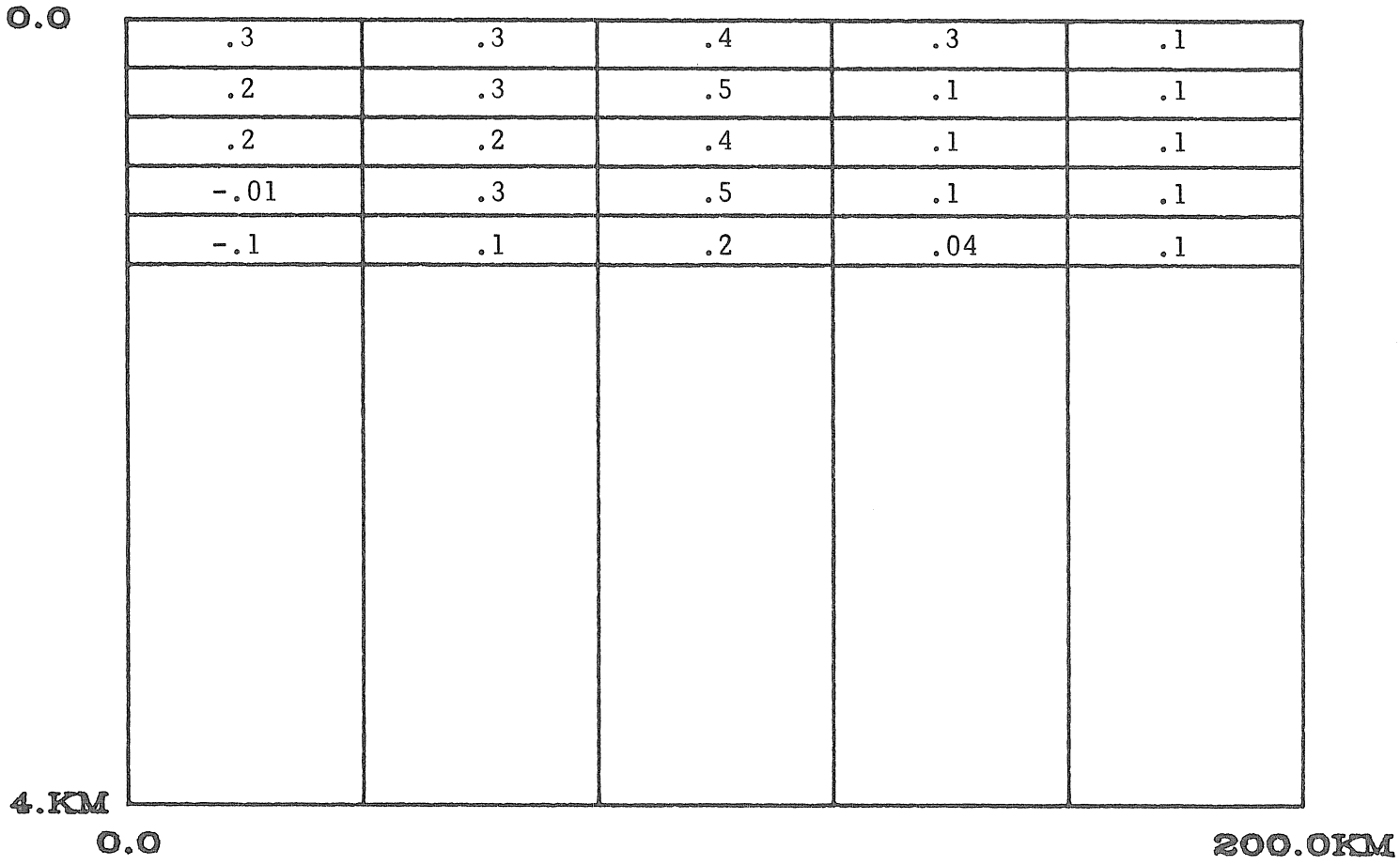

FIGURE 5-49: CASE 3 GINV

TWO SOURCES, AV. DIFF. = .10

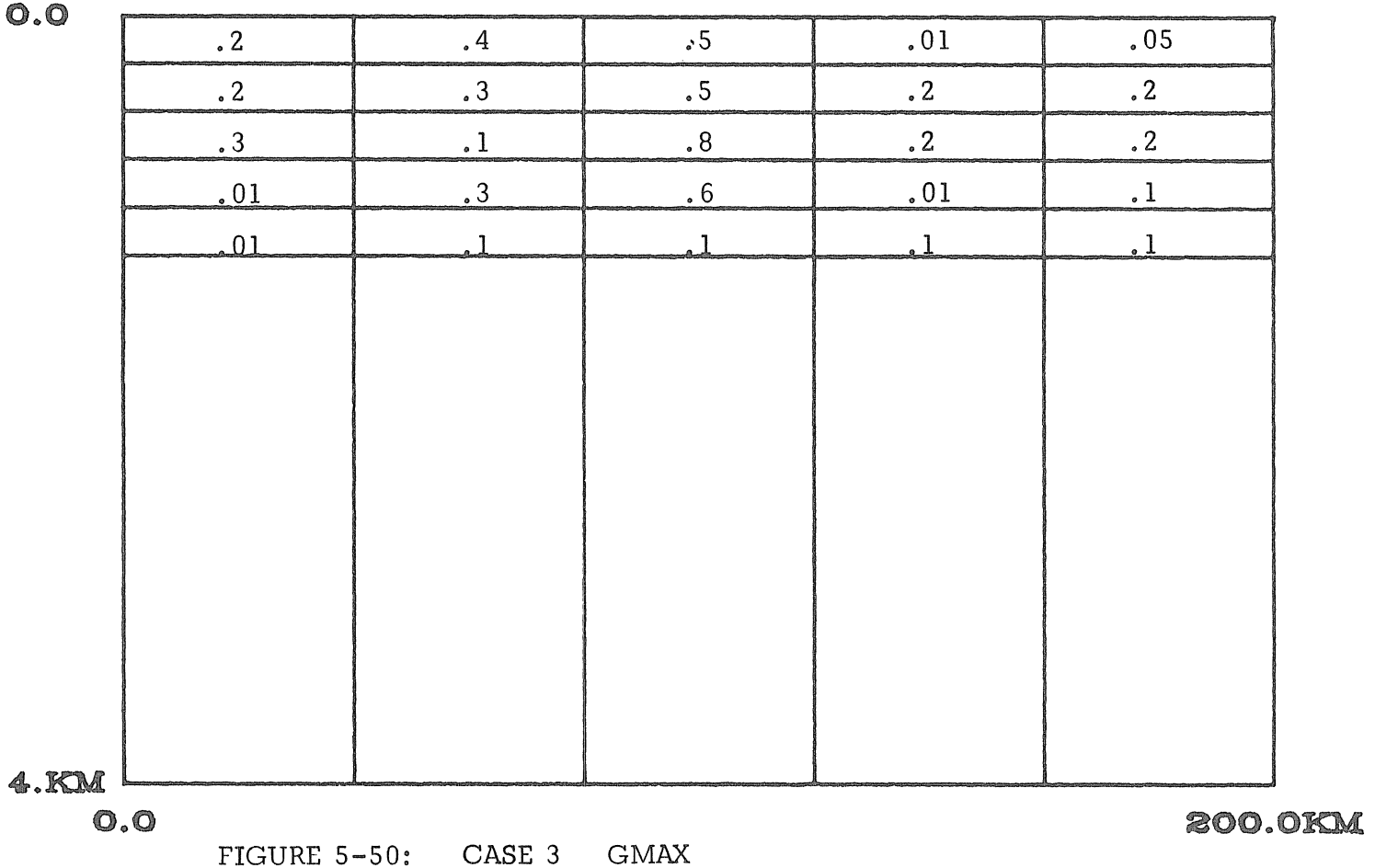

FIGURE 5-50: CASE 3 GMAX

TWO SOURCES, AV. DIFF. = .094

0.0

.3	.3	.1	.08	.3
.3	.02	.7	.3	-.1
.03	-.2	.6	.4	.4
-.02	.3	.6	.2	.3
.04	.4	.2	-.2	-.4

4.KM

0.0 200.0KM

FIGURE 5-51: CASE 3 GINV
THREE SOURCES, AV. DIFF. = .16

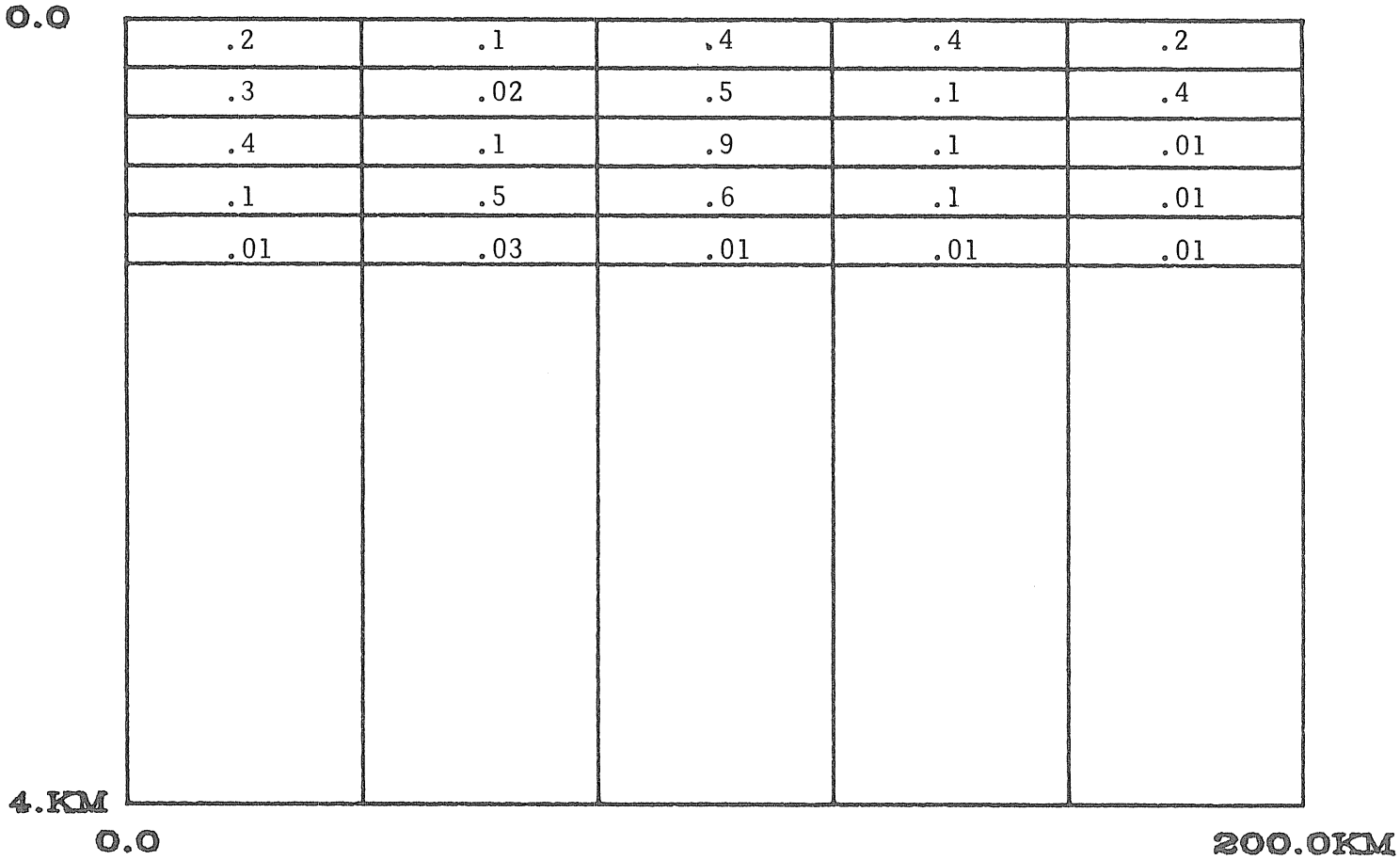

FIGURE 5-52: CASE 3 GMAX

THREE SOURCES, AV. DIFF. = .12

TABLE 5-1: RATIOS FOR LINEARITY TEST CASE 1

PERFECT DERIVATIVES	ESTIMATED DERIVATIVES	NOMINAL ONLY
0.8927912	0.5840421	0.7839633
0.9033380	-0.7246869	0.7182676
0.9194558	0.9206566	0.6596429
0.9386899	0.9403496	0.6032097
0.9573548	0.9603574	0.5418117
0.9704947	0.9763642	0.4642514
0.9742877	0.9853376	0.3540094
0.9702371	0.9984448	0.1867938
0.9637307	0.8805872	-8.7320626E-02
0.9581830	0.9301703	-0.6176642
0.9527138	0.9202213	-2.123486
0.8669935	0.4864224	-49.21580
0.9616508	0.9827201	4.469344
0.9573879	0.9658377	2.636691
0.9555629	0.9603204	2.046106
0.9546821	0.9578626	1.751392
0.9544875	0.9569330	1.573009
0.9547112	0.9567854	1.451783
0.9550250	0.9569066	1.362410
0.9551544	0.9569632	1.292397
0.9550098	0.9568396	1.235017
0.9548105	0.9567639	1.186563
0.9549189	0.9570259	1.144758
0.9553525	0.9575507	1.107807
0.9557955	0.9581060	1.074285
0.9561112	0.9586042	1.043068
0.9563506	0.9589807	1.013170
0.9564338	0.9591371	0.9837955
0.9562459	0.9590184	0.9543018
0.9558977	0.9586849	0.9241929
0.9005725	0.9412662	0.2106719
0.9096664	0.7374171	-6.0813200E-02
0.9450934	0.8893700	-0.5288153
1.042758	0.9762965	-1.689193
1.973565	1.703633	-12.92109

TABLE 5-1: RATIOS FOR LINEARITY TEST CASE 1 (Continued)

PERFECT DERIVATIVES	ESTIMATED DERIVATIVES	NOMINAL ONLY
0.5179011	0.5780003	4.636967
0.7001143	0.7218726	2.388741
0.7496987	0.7616380	1.722186
0.7717840	0.7792892	1.377922
0.7819034	0.7854076	1.146164
0.7824591	0.7771502	0.9555801
0.7811927	0.7611379	0.7889469
0.7939939	0.7603891	0.6611473
0.8296384	0.7877916	0.5815160
0.8847633	0.8370705	0.5426317
0.9539178	0.9096972	0.5413165
1.022652	0.9947873	0.5722418
0.8915142	0.8937019	0.8770320
0.8969961	0.8999189	0.7988524
0.9087840	0.9130213	0.7302699
0.9258084	0.9319463	0.6682086
0.9449471	0.9535668	0.6060999
0.9476331	0.9506390	1.039438
0.9475799	0.9504791	1.007911
0.9477648	0.9506004	0.9773752
0.9481661	0.9510121	0.9474962
0.9486969	0.9514363	0.9176950
0.8906716	0.8937917	-7.8079417E-02
0.9158949	0.9198607	-0.5417690
0.9822043	0.9859998	-1.648852
1.459831	1.465153	-9.647625
0.5575901	0.5580142	5.355191
0.7210617	0.7222651	2.564044
0.7621742	0.7635221	1.808208
0.7800578	0.7812599	1.428751
0.7874819	0.7870193	1.176605
0.7864675	0.7788082	0.9727750
0.7856132	0.7650750	0.7992323
0.8019881	0.7712362	0.6713380
0.8445888	0.8119425	0.5980287

TABLE 5-1: RATIOS FOR LINEARITY TEST CASE 1 (Continued)

PERFECT DERIVATIVES	ESTIMATED DERIVATIVES	NOMINAL ONLY
0.9068565	0.8750331	0.5667341
0.9760095	0.9442171	0.5613061
1.036379	1.010423	0.5729623
0.9432026	0.9479436	1.182662
0.9423434	0.9469209	1.105178
0.9420463	0.9465536	1.034713
0.9422910	0.9468894	0.9677560
0.9427860	0.9478875	0.9010591
0.9435964	0.9495018	0.8312634
0.9458734	0.9523301	0.7561641
0.9523872	0.9597490	0.6764717
0.9652312	0.9783247	0.5908397
0.9794454	1.012397	0.4791290
0.9807985	1.091204	0.2815140
0.9524323	0.7097449	-0.1581578
0.8550262	0.7538983	-1.645324
1.867972	2.220806	17.20002
1.092220	1.131398	3.087594
1.039497	1.057697	2.111268
1.021698	1.032085	1.741405
1.013234	1.020089	1.540889
1.008569	1.013679	1.412100
1.005639	1.009781	1.320024
1.003577	1.007097	1.248903
1.002051	1.005115	1.190773
1.000841	1.003577	1.141196
0.9997860	1.002282	1.097435
0.9988921	1.001115	1.057888
0.9985597	1.000403	1.022391
0.9994268	1.000949	0.9920600
1.002511	1.004720	0.9262857
1.000049	1.002713	0.9043444
0.9966339	0.9995777	0.8793204
0.9931444	0.9962471	0.8504632
0.9896480	0.9929976	0.8169279
0.9858347	0.9896386	0.7772724

TABLE 5-2: LINEARITY TEST RESULTS

LINEARITY TEST CASE	C PERTURBATION	AVERAGE DISCREPANCY PERFECT	AVERAGE DISCREPANCY ESTIMATED	AVERAGE DISCREPANCY NOMINAL ONLY	AVG. DISCREPANCY WITH FILTERING - ESTIMATED APPROACH
1 - range indpt. SVP	0.5 top four layers all ranges	0.51	0.60	2.7	0.21
2 - range indpt. SVP	2.0 top four layers all ranges	2.5	2.3	4.1	1.2
3 - range dpt. SVP	0.5 top four layers all ranges	1.0	1.05	2.1	0.39
4 - range dpt. SVP	0.25 top four layers first & last ranges, 0.5 in middle range	0.62	0.78	1.3	0.32
5 - range dpt. SVP	1.0 top four layers first & last ranges, 2.0 in middle range	1.6	1.6	3.2	0.70

TABLE 5-3

RUN TYPES USED IN INVERSIONS

RUN	SOURCE DEPTH	RECEIVER DEPTH	SVP
G	1195	1190	I
H, I	1195	1190	II
K, L	1295	1190	II
N, O	1095	1190	II
P	405	905	III
Q	605	905	III
R	805	905	III
U	1295	1290	IV

TABLE 5-4

SOUND VELOCITY PROFILES
USED IN INVERSIONS

I. Outer Ranges: minimum C = 1495, axis depth = 1200
scale depth = 1200, coefficient = .005

Inner Ranges: minimum C = 1485

II. Min. C = 1495, axis depth = 1200
scale depth = 1200, coefficient = .005

III. Minimum C = 1495, axis depth = 1000
scale depth = 1000, coefficient = .005

IV. Outer Ranges: minimum C = 1495, axis depth = 1200
scale depth = 1200, coefficient = .005

Inner Ranges: minimum C = 1480

TABLE 5-5

5 BLOCK INVERSIONS

Case	dC	Average Discrepancy	% Noise Std. Deviation	Min., Max. Resolution	Total dC Ratio	Average Difference
H1	.75, .5,	.32	10	.95, .99	.86	.12
	.25		20	.92, .97	.86	.1
			30	.87, .93	.83	.08
G1	.75, .5,	1.2	10	.85, .97	1.26	.26
	.25		20	.8, .94	1.24	.25
			30	.66, .89	1.22	.18
			40	.41, .74	1.19	.15

TABLE 5-6

15 BLOCK, ONE SOURCE INVERSIONS

Case	dC	Average Discrepancy	% Noise Std. Deviation	Min., Max. Resolution	Total dC Ratio	Average Difference
K3-1	.5	.19	10	.24, .54	.96	.16
			15	.19, .47	.88	.14
K3-5	.5	.15	10	.18, .52	.90	.15
			15	.1, .46	.81	.17
I3-1	.1, .75,	.71	10	.28, .63	.96	.18
	.1		20	.19, .46	.94	.17
I3-5	.1, .75,	.41	10	.27, .51	.95	.19
	.1		20	.19, .43	.94	.18

TABLE 5-6 (Continued)

15 BLOCK, ONE SOURCE INVERSIONS

CASE	dC	Average Discrepancy	% Noise Std. Deviation	Min., Max. Resolution	Total dC Ratio	Average Difference
P3	.5	.42	10	.06, .42	.99	.19
			20	.04, .25	.91	.17
U3	2.0	.70	10	.14, .81	.57	1.8
			20	.06, .71	.61	1.5

TABLE 5-7

15 BLOCK, TWO SOURCE INVERSIONS

Case	dC	Average Discrepancy	% Noise Std. Deviation	Min., Max. Resolution	Total dC Ratio	Average Difference
K3 + H3	.5	.19	10	.25, .59	1.11	.21
			20	.17, .46	1.00	.14
I3 + L3	.1, .75, .1	.50	10	.3, .65	.98	.21
			20	.23, .49	.94	.18
P3 + Q3	.5	.43	10	.1, .6	1.07	.22
			20	.08, .48	.98	.18

TABLE 5-8

15 BLOCK, THREE SOURCE INVERSIONS

Case	dC	Average Discrepancy	% Noise Std. Deviation	Min., Max. Resolution	Total dC Ratio	Average Difference
K3 + H3 + N3	0.5	.26	10	.31, .74	1.13	.39
			20	.2, .55	1.08	.20
			25	.18, .49	1.03	.18
I3 + L3 + O3	.1, .75, .1	.50	10	.35, .77	.95	.27
			20	.26, .59	.92	.2
			25	.23, .53	.91	.18
P3 + Q3 + R3	0.5	.37	10	.17, .74	1.01	.36
			20	.13, .59	.93	.2
			25	.12, .54	.9	.18

TABLE 5-9

25 BLOCK INVERSIONS

Case	dC	Average Discrepancy	% Noise Std. Deviation	Min., Max. Resolution	Total dC Ratio	Average Difference
H5	.5	.23	10	.17, .47	1.1	.2
			20	.1, .36	.96	.17
H5 + K5	.5	.5	10	.26, .51	1.08	.27
			20	.11, .36	.93	.22
H5 + K5 + N5	.5	.53	10	.27, .62	1.06	.35
			20	.13, .5	.94	.27
			25	.1, .44	.89	.26

TABLE 5-10: COMPENSATED DATA RESULTS, 2.5% NOISE

	CASE	NUMBER OF SOURCES	MATRIX SIZE	AV. DIFF.
GINV	1	1	397	.11
		2	608	.07
		3	800	.13
	2	1	397	.13
		2	608	.10
		3	800	.16
	3	1	397	.12
		2	608	.10
		3	800	.16
GMAX	1	1	26	.15
		2	26	.13
		3	26	.15
	2	1	26	.13
		2	26	.08
		3	26	.12
	3	1	26	.093
		2	26	.094
		3	26	.12

CHAPTER 5 NOTATION

A_g	geometric arrival amplitude term
$C(\underline{x})$	sound velocity
$\underline{d}$	data vector
$d\mathscr{s}$	incremental ray path length
E	derivative matrix
G	amplitude term for geometric arrivals that depend on $C(\underline{x})$
$\mathscr{I}(\underline{x},t)$	acoustic intensity
$\mathscr{I}_m$	imaginary part
$M(t)$	source function
$M'(t)$	time derivative of the source function
n_i	noise term on compensated amplitude data
$P(\underline{x},t)$	acoustic pressure
P_i	perturbed acoustic pressure at time t_i
P_{o_i}	nominal pressure at time t_i
p	horizontal wave slowness
q	vertical wave slowness
T_i	geometric arrival time at time t_i
W	amplitude term for transform arrivals
w_a, w_t	weighting factors

$\underline{\delta C}$	sound velocity model vector
δC_j	portion of $C(\underline{x})$ perturbation in block j
Γ_i	ray path i
Γ_{ij}	ray path i portion in block j
$\frac{\partial P_i}{\partial C_j}$	derivative of pressure at time t_i with respect to $C(\underline{x})$ in block j
$\left(\partial P_i / \partial C_j\right)_o$	nominal derivative
$\partial T_i / \partial C_j$	derivative of arrival time T_i
$\partial W_i / \partial C_j$	derivative of transform amplitude

6.0 SUMMARY AND CONCLUSIONS

The major results of this investigation are reiterated here. This work considered three separate topics:

1. Simulated range dependent underwater acoustic signals by Maslov asymptotic theory,
2. Maximum entropy inversions,
3. Range dependent acoustic amplitude inversions,

and a synopsis of the conclusions for each of these issues follows.

Maslov asymptotic theory is a viable alternative to the parabolic approximation for simulating underwater acoustic signals in range dependent environments. It has the following features:

1. It provides an innovative, informative way to deal with range dependent problems.
2. It may be faster than the PE approach for some cases.
3. The method provides insight into caustics and the mixed parameter space.

The numerical algorithm for computing Maslov asymptotic theory signals needs more work, including:

1. An investigation of sound velocity profile and source and receiver depth effects.

2. Define ray and sound velocity resolution requirements.
3. Study the transition between ART and WKBJ solutions.
4. Compare Maslov asymptotic theory solutions with those from the parabolic approximation.

The maximum entropy inverse can be faster and more accurate than the generalized inverse for generic tomography problems and underwater acoustic inversions, and the following observations came out of this work:

1. Bryan and Skilling's χ statistic approach for maximum entropy inversions of noisy data is stable and converges for all cases. An improved numerical algorithm is given in this thesis.
2. Maximum entropy computations are proportional to the square of the number of unknowns, while the generalized inverse inverts a matrix of the size of the number of known data points, squared. Typical amplitude tomography exercises have 100 unknowns and 500 to 1000 signal points, so the maximum entropy inverse is calculated in 25 to 100 times less time.
3. Maximum entropy inverses are more accurate for cases with structure. They perform best for low noise cases, but high

noise cases can also be handled. The minimum norm generalized inverse is not designed for cases with identifiable structure.

4. The generalized inverse and maximum entropy inverse need to be compared for ocean tomography exercises where vertical mode or orthogonal function structure in the ocean can be assumed. Such structure is often found, and it is not known at this time whether it is more compatible with the generalized or maximum entropy approach.

Due to linearity and resolution problems, no accurate simulated amplitude tomography inversions were performed. More effort is required, including:

1. Additional amplitude derivatives may improve the linearity over that for the travel time derivative alone.
2. Other source and receiver configurations should be investigated to get better resolution.

7.0 COMPUTER PROGRAMS

Synthetic signals and inversions were executed on a VAX 11/750, and listings of some of the computer programs are provided here. Highlights of the Maslov asymptotic theory programs and the maximum entropy inverse routines are discussed.

7.1 MASLOV ASYMPTOTIC THEORY PROGRAMS

A list of the Maslov asymptotic theory programs is provided in Table 7-1, and the programs are split into four groups. GRADWKBJ is the main program, and it calls all the other routines. RAYTRI shoots all the rays through the ocean from the source to the receiver, and the ocean is divided into triangles for the linear sound velocity model. Intersection points are calculated so the point where the ray leaves a triangle is identified, and the transmission matrix for the p and x derivatives is calculated. Both the ART and the WKBJ amplitudes are computed, caustic conditions are identified, and a smooth transition between the two solutions is derived when it is required.

A listing of RAYTRI follows, and the routines CIRDEF, TRIDEF and TRIINT, with functions defined in Table 7-1 are called from RAYTRI. A listing of CIRDEF is also provided.

In Table 7-1, the third group of programs consists of GMRAY, RTHETC and RTHETW. GMRAY finds geometric arrivals by checking for sign changes in the theta table while RTHETC and RTHETW look for WKBJ arrivals with theta between t plus or minus Δt. The signals versus time and the dC_j derivatives are compiled within these routines, and they are all called by GRADWKBJ. Interpolation between rays of the same type is performed for the WKBJ arrivals.

The last two programs in Table 7-1 are CCSQRT and DCONSRC, and the impulse response is convolved with the $\Lambda(t)$ function (Equation 3-30) and the source function. The bandwidth of the source is determined by the ratio of the number of cycles to the carrier frequency. The CCSQRT routine, written by C. H. Chapman, uses a $\Lambda(t)$ function that has been smoothed with a third order boxcar and is approximated by a rational function.

7.2 MAXIMUM ENTROPY INVERSE PROGRAMS

The maximum entropy inverse programs are tabulated in Table 7-2. GMAXENT is the main program, and it calls MENVRT that iterates to solve the linear equations for dC and the Lagrangian multipliers. Either the variance, variance and mean, or $\mathcal{E}$ statistic approaches presented in Section 4.3 can be utilized, and Marquardt's method (26) is used to assure convergence.

DMEPAR, called by MENVRT, calculates terms used in the linear equations, and MINV is a general purpose matrix inversion program. CHISQ and XNORM carry out probability density computations.

Listings of MENVRT and DMEPAR are provided at the end of this chapter.

TABLE 7-1

MASLOV ASYMPTOTIC THEORY PROGRAMS

1. GRADWKBJ - main program

2. RAYTRI - trace rays through triangles
   a. CIRDEF - define circular ray paths
   b. TRIDEF - identify triangle
   c. TRIINT - integrate travel time and derivative

3. GMRAY, RTHETC, RTHETW - select and compile signals for geometric and WKBJ arrivals

4. CCSQRT, DCONSRC - convolve impulse response with $\Lambda(t)$ and source functions

RAYTRI LISTING

```
C
C
C       NEW VERSION OF RAYTRI-TYPED IN 2/2/84
C
C       REVISED JUNE 12,1984 TO NOT PLOT--SEE RAYTRI0.PLT FOR PLOTS
C
C       PROGRAM TO TRACE RAYS THRU A RANGE DEPENDENT OCEAN WITH OCEAN
C       DIVIDED INTO TRIANGLES AND LINEAR INTERPOLATION USED BETWEEN THE
C       VERTICES. METHOD OF CHAPMAN BULL.OF SEIS SOC OF AMERICA,
C       V.72,#6,P.S277,DEC,1982. THE RAYS ARE SECTIONS OF CIRCLES.
C       FOLLOW CHAPMAN'S NOTATION, KEY IS TO TAKE COORD FRAME WHERE
C        P=CONST.
C       DEFINITIONS:*****************************
C       XS,XR1,DX-SRC AND REC RANGE
C       CPT(IR,JL)-SOUND VELOCITY AR XRNG(IR),ZP(JL)
C       X0,Z0,RC-X,Z COORDS OF CENTER OF CIRCLE,RADIUS OF CIRCLE
C       X,Z,PHI-PRESENT VALUE OF X,Z AND PHI-ANGLE TO HORIZONTAL
C       TRANS(I1),THETA(I1)-TRANSMISSION ANGLE,THETA=DELAY TIME-P*
C              RANGE
C       DPDC(1,IR,JL)-DERIVATIVE OF TRAVEL TIME W.R.T.DC VALUES
C       DPDC(2,IR,JL)-DERIVATIVE OF DPDP0 W.R.T. DC VALUES, FOUND THAT
C              DPDP0 CAN CHANGE BY 100% FOR SOME DC VALUES
C       AX,BZ,C0- VALUES FOR LINEAR INTERPOLATION OF C,SOUND VELOCITY
C       ISDXDP-SIGN OF DXDP AT END POINT,USED IN EXPONENT OF WKBJ SOLN
C       DPDP0- DERIVATIVE OF P W.R.T. INITIAL P VALUE, P FOR HORIZ.
C              SLOWNESS
C       DXDP0-DERIVATIVE OF X W.R.T. INITIAL P VALUE
C       QFIN,PFIN-FINAL VALUES OF P AND Q, Q FOR VERTICAL SLOWNESS
C       CBJ-PRODUCT OF REFLECTION AND REFRACTION COEFFS.
C       GAMPL,WAMPL-TRANS ANGLE GEOM AND WKBJ AMPLITUDE
C       ALSO DEFINE VECTORS AND TRANSMISSION MATRICES IN CHAPMANS'
C       NOTATION:*****************************
C       VNJ,VMJ-RAY PATH VECTOR AND PERPENDICULAR
C       VMB,VM1-M VECTOR AT BREAK OUT POINT AND M AT FIRST TRIANGLE
C       VIJ,VKJ-LOCAL HORIZ AND VERTICAL VECTORS
C       VLJ-VECTOR AT BOUNDARY OF TRIANGLE
C       TMAT,QMAT,RMAT,SMAT,BMAT,DMAT-TRANSMISSION MATRICES
C
C       METHOD:*****************************************
C
C       1. START AT SOURCE DEPTH,STEP THRU TRIANGLES, IDENTIFY
C       TRIANGLES AND CIRCLES.
C       2. FIND FIRST BREAK OUT POINT, AT TRIANGLE DIAGONAL, HORIZ OR
C       VERTICAL BOUNDARY.
C       3. CALCULATE TRANSMISSION MATRICES FOR DPDP0,DXDP0,ETC.
C       4. TO STOP,(X,Z) IS SUCH THAT X>XR AND IF Z CROSSED ZR DEPTH
C       THEN WATCH THETA AND DPDC CALCULATIONS. USE TRIINT FOR
C       INTEGRALS.
C       5. DERIV1 HOLDS GEOM ARRIVAL DERIVATIVES W.R.T. DC AND DERIV3
C              HOLDS DPDP0 DERIVATIVES
C       6. NEED TO KEEP TRACK OF RAY TYPES SO YOU DON'T INTERPOLATE
C       BEYOND THEM. ITYPE STORES FIRST ANGLE INDEX FOR EACH NEW RAY
C       TYPE
C
C
C
C
      SUBROUTINE RAYTRI(TRANS,THETA,NTRANS,GAMPL,WAMPL)
      COMMON /SVPVAL/CPT,DCVAL
      COMMON /ENDPT/XFIN,PHIFIN,ITFIN
      COMMON /SOURCE/XS,ZS,XR1,ZR,C1S,C1R
      COMMON /DER/DPDC,THNO,DNO,ISTOP,ICROSS
      COMMON /ANGTER/PFIN,WGT,PHIMIN,XRAY,ITYPE,NTYP
      COMMON /TRICOF/AX,BZ,C0
```

```
      COMMON /GRID/ XR,ZP,ZL,DX,DZ,NX,NZP,NXL,NZL,ZMAX,NBLOCK
      PARAMETER N5=2000
      DIMENSION CPT(201,51),AX(20000),BZ(20000),XR(201),ZL(11),
     1 C0(20000),TRANS(N5),THETA(N5),DPDC(2,10,10),DNO(2,10,10),
     2 GAMPL(N5),WAMPL(2,N5),XPLT(15000),ZPLT(15000),PPLT(15000),
     3 PFIN(N5),WGT(N5),XRAY(2000),ITYPE(200),ZP(100)
      COMPLEX CBJ
      DOUBLE PRECISION TMAT(2,2),QMAT(2,2),RMAT(2,2),SMAT(2,2),BMAT(2,2),ZD,
     1 DPDC,DNO
      DOUBLE PRECISION DMAT(2,2),DTEMP(2,2),X0D,Z0D,RCD,F1D,GD,BETAD,XMAX,
     1 SSTART,XTST1A,XTST1B,XTST2A,XTST2B,XTST1,XTST2,XTST3,XTST2T,XLP,
     2 PHID,XBRKD,VMJ1,VMJ3,VMBJ1,VMBJ3,VNJ1,VNJ3,VNBJ1,VNBJ3,DWON,DZER,
     3 VMJ11,VMJ13,VM11,VM13,VMB11,VMB13,VMDVI,VMBDVI,DTWO,VMBJ11,VMBJ13,
     4 VIJ1,VIJ3,VLJ1,VLJ3,VLJ11,VLJ13,VKJ1,VKJ3,VKJ11,VKJ13,VIJ11,VIJ13,
     5 VI11,VI13,F2D,F3D,SEND,PHILP,VMLP1,VMLP3,PHIOUT,VLPDVI,VLDVM,VLDVB1,
     6 VI1DVB,VIDVB,XD,THETA,THNO,TEXTRA,XFIN,PHIFIN,CPFIN,SPFIN,XRAY,ZBRKD,
     7 SXN,SXM
      PI=3.14159
      NPLT9=80
      TYPE *,' MINIMUM VALUE FOR CAUSTIC CONDITION=?
     1 ENTER 4,5, OR 6 FOR 5.0E-05,1.0E-05 OR 2.0E-06'
      ACCEPT *,NCAUS
      NCAUS=5
      IF(NCAUS.EQ.4)CAUS=5.0E-05
      IF(NCAUS.EQ.5)CAUS=1.0E-05
      IF(NCAUS.EQ.6)CAUS=2.0E-06
      TYPE *,' IS THE SOURCE BEAM GAUSSIAN?(0=NO)'
      ACCEPT *,NGAUSS
      IF(NGAUSS.EQ.0)GO TO 95
      TYPE *,' INPUT MEAN ANGLE,STANDARD DEVIATION='
      ACCEPT *,PMEAN,PSIG
C
C     FIND COEFFS FOR TRIANGLES, NUMBER COUNTER
C     CLOCKWISE
C
95    DO 10 I=1,50
10    ITYPE(I)=0
      DO 100 IX=1,NX-1
      DO 100 JZ=1,NZP-1
      DZ=ZP(JZ+1)-ZP(JZ)
      C1=CPT(IX,JZ)
      C2=CPT(IX,JZ+1)
      C3=CPT(IX+1,JZ+1)
      C4=CPT(IX+1,JZ)
      IT=2*(NZP-1)*(IX-1)-2*(JZ-1)
      AX(IT+1)=(C4-C1)/DX
      AX(IT+2)=(C3-C2)/DX
      BZ(IT+1)=(C2-C1)/DZ
      BZ(IT+2)=(C3-C4)/DZ
      C0(IT+1)=C1-AX(IT+1)*XR(IX)-BZ(IT-1)*ZP(JZ)
      C0(IT+2)=C3-AX(IT+2)*XR(IX-1)-BZ(IT-2)*ZP(JZ-1)
100   CONTINUE
      DZER=DBLE(0.0)
      DWON=DBLE(1.0)
      TMAT(2,1)=DZER
      TMAT(2,2)=DWON
      SMAT(1,2)=DZER
      SMAT(2,1)=DZER
      SMAT(2,2)=DWON
      QMAT(1,1)=DWON
      QMAT(1,2)=DZER
      RMAT(1,1)=DWON
      RMAT(1,2)=DZER
```

```
      XSIZE=7.0
      YSIZE=9.0
      JBOT0=0
      JTOP0=0
      JTURN0=0
      DXLAY=XR1/FLOAT(NXL-1)
      NB2=NBLOCK*2
      OPEN(UNIT=3,NAME='DERIV1.DAT',FORM='UNFORMATTED',TYPE='NEW',
     1 ACCESS='DIRECT',RECORDSIZE=NB2)
      OPEN(UNIT=2,NAME='DERIV3.DAT',FORM='UNFORMATTED',TYPE='NEW',
     1 ACCESS='DIRECT',RECORDSIZE=NB2)
      OPEN(UNIT=1,NAME='RAYPLT.PLT',TYPE='NEW',FORM='UNFORMATTED')
      NRAY9=NTRANS/NPLT9
      WRITE(1)NRAY9
      DO 8000 I1=1,NTRANS
      GAMPL(I1)=0.0
      WAMPL(1,I1)=0.0
      WAMPL(2,I1)=0.0
      WRITE(3'I1)((0.0,J3=1,NZL-1),I3=1,NXL-1)
      WRITE(2'I1)((0.0,J3=1,NZL-1),I3=1,NXL-1)
      NP1=0
      X=XS+0.001
      VLJ1=1.0
      XD=DBLE(XS+0.001)
      Z=ZS
      ZD=DBLE(ZS)
      PHI=TRANS(I1)
      GBEAM=1.0
      IF(NGAUSS.EQ.0)GO TO 6
      GBEAM=EXP(-((PHI-PMEAN)/PSIG)**2)
6     XFIN=DBLE(0.0)
      XRAY(I1)=XFIN
      PHID=DBLE(TRANS(I1))
      THETA(I1)=DZER
      DO 200 I=1,NXL-1
      DO 200 J=1,NZL-1
      DO 200 K=1,2
      DNO(K,I,J)=DBLE(0.0)
200   DPDC(K,I,J)=DBLE(0.0)
      JTRIAN=1
      ISTOP=1
      JTURN=0
      JTURN1=0
      JTOP=0
      JTOP1=0
      JBOT=0
      JBOT1=0
      THNO=DZER
      IFLAG=0
      ICROSS=1
C
C     RETURN HERE FOR EACH NEW POINT IN A TRIANGLE
C
      NI1STP=1
300   CONTINUE
      ITRI0=ITRI
      IXT0=IXT
      JZT0=JZT
      CALL TRIDEF(XD,ZD,IXT,JZT,ITRI,XI,ZT,ZB)
      ICROSS0=ICROSS
      ICROSS=1
      DTWO=DZER
      FACT=AX(ITRI)**2-BZ(ITRI)**2
```

```
      IF(ABS(FACT).LE.1.0E-10)GO TO 302
      FACT=SQRT(FACT)
      VKJ1=DBLE(-AX(ITRI)/FACT)
      VKJ3=DBLE(-BZ(ITRI)/FACT)
      GO TO 303
302   VKJ1=DZER
      VKJ3=DWON
303   VIJ1=VKJ3
      VIJ3=-VKJ1
      XTRI=X
      ZTRI=Z
      CVAL=AX(ITRI)*X+BZ(ITRI)*Z-C0(ITRI)
      FLAGDC=0.0
      IF(VLJ1.NE.0.0)GO TO 310
      FLAGDC=1.0
      CPHIFL=COS(PHI)
      SPHIFL=SIN(PHI)
      CVALFL=CVAL
310   VNJ1=DCOS(PHID)
      VNJ3=DSIN(PHID)
      VMJ1=VNJ3
      VMJ3=-VNJ1
      PHITRI=PHI
      PVAL=1.0/CVAL*SNGL(VNJ1*VIJ1+VNJ3*VIJ3)
      PNOW=1.0/CVAL*SNGL(VNJ1)
      PS=SIGN(1.0,PVAL)
      IF(X.NE.XS+0.001)GO TO 325
      IXS=IXT
      JZS=JZT
      VM11=VMJ1
      VM13=VMJ3
      VI11=VIJ1
      VI13=VIJ3
      TEXTRA=DZER
      PFIN(I1)=1.0
      QFIN=1.0E-06
      DXDP0=1.0E28
      DPDP0=1.0
      PSTART=1.0/CVAL*COS(PHI)
      QSTART=1.0/CVAL*SIN(PHI)
325   X01=X0
      NI1STP=NI1STP-1
C
C     IF THERE IS NO GRADIENT IN THE TRIANGLE, USE STRAIGHT LINE RAYS
C
      CVALN=C0(ITRI)+AX(ITRI)*X+BZ(ITRI)*Z
      PHIN=PHI
      IF(ABS(FACT).LE.1.0E-05)GO TO 2100
      CALL CIRDEF(X,Z,PHID,ITRI,X0D,Z0D,RCD)
      X0=SNGL(X0D)
      Z0=SNGL(Z0D)
      RC=SNGL(RCD)
      IF(Z0.NE.Z)PHIN=ATAN((X-X0)/(Z0-Z))
326   NP1=NP1+1
      IF(NP1.GT.14999)NP1=14999
      XPLT(NP1)=X
      ZPLT(NP1)=Z
      PPLT(NP1)=ABS(1.0/CVALN*COS(PHIN))
      IF(X.EQ.XTRI)SSTART=DBLE(SIGN(1.0,(XTRI-X0)))
      IF(Z.EQ.ZS)X01=X0
500   CONTINUE
C
C     FIND BREAKOUT POINT, HIT DIAG.,HORIZ OR VERT BOUNDARY
```

```
C
1000    CONTINUE
        ZLP=Z0
        XLP=XE+DX*2.0
C
C       DIAGONAL?
C
        DZ=ZB-ZT
        RMU=DZ/DX
        RMU2=RMU*RMU
        FZ=ZT-Z0+RMU*XE
        BETAD=X0D+DBLE(RMU*FZ)
        GD=X0D**2-RCD**2+DBLE(FZ**2)
        F1D=BETAD**2-DBLE((1.0-RMU2))*GD
        XTST1=DZER
        IF(F1D)1200,1120,1130
1120    XTST1=BETAD/DBLE((1.0-RMU2))
        ZTST1=RMU*(XE-SNGL(XTST1))+ZT
        GO TO 1200
1130    XTST1A=(BETAD+DSQRT(F1D))/DBLE((1.0-RMU2))
        XTST1B=(BETAD-DSQRT(F1D))/DBLE((1.0-RMU2))
        BTST=SNGL(BETAD)/(1.0-RMU2)
        ZTST1A=RMU*(XE-SNGL(XTST1A))+ZT
        ZTST1B=RMU*(XE-SNGL(XTST1B))+ZT
        IF(IFLAG.EQ.1.AND.X.LT.BTST)XTST1B=DZER
        IF(IFLAG.EQ.1.AND.X.GT.BTST)XTST1A=DZER
        IF(XTST1B.GT.XLP.OR.XTST1B.LT.DBLE(X))GO TO 1150
        XTST1=XTST1B
        ZTST1=ZTST1B
        GO TO 1200
1150    IF(XTST1A.GE.XLP.OR.XTST1A.LT.DBLE(X))GO TO 1200
        XTST1=XTST1A
        ZTST1=ZTST1A
C
C       HIT DEPTH LIMITS?
C
1200    CONTINUE
        XTST2=DZER
        Z2=ZT
        GO TO 1210
1205    CONTINUE
        XTST2=DZER
        Z2=ZB
1210    F1D=RCD**2-(DBLE(Z2)-Z0D)**2
        IF(F1D.LT.DZER)GO TO 1290
        IF(F1D.NE.DZER)F1D=DSQRT(F1D)
        XTST2A=X0D-F1D
        XTST2B=X0D-F1D
        IF(IFLAG.EQ.2.AND.X.LT.X0)XTST2B=DZER
        IF(IFLAG.EQ.2.AND.X.GT.X0)XTST2A=DZER
        IF(XTST2B.GE.XLP.OR.XTST2B.LT.DBLE(X))GO TO 1220
        XTST2=XTST2B
        GO TO 1290
1220    IF(XTST2A.GE.XLP.OR.XTST2A.LT.DBLE(X))GO TO 1290
        XTST2=XTST2A
1290    CONTINUE
        IF(Z2.EQ.ZT)GO TO 1295
        IF(XTST2T.EQ.DZER)GO TO 1300
        IF(XTST2T.LT.XTST2.OR.XTST2.EQ.DZER)XTST2=XTST2T
        IF(XTST2.EQ.XTST2T)Z2=ZT
        GO TO 1300
1295    XTST2T=XTST2
        GO TO 1205
```

```
C
C       HIT RANGE LIMIT?
C
1300    XTST3=DZER
        IF(XLP.LT.DBLE(XE))GO TO 1500
        XTST3=DBLE(XE)
        F1D=RCD**2-(X0D-XTST3)**2
        IF(F1D.LT.DZER)F1D=DZER
        IF(F1D.NE.DZER)F1D=DSQRT(F1D)
        ZTST3=SNGL(Z0D-F1D)
        IF(Z0.LT.Z)ZTST3=SNGL(Z0D+F1D)
1500    CONTINUE
        XMAX=XLP
        IF(XTST1.LT.XMAX.AND.XTST1.GT.DZER)XMAX=XTST1
        IF(XTST2.LT.XMAX.AND.XTST2.GT.DZER)XMAX=XTST2
        IF(XTST3.LT.XMAX.AND.XTST3.GT.DZER)XMAX=XTST3
        IFLAG=0
1510    IF(XMAX.EQ.XLP)TYPE *,' XLP REACHED ',I1,XLP,ZLP
        IF(XMAX.EQ.XLP)GO TO 8000
        VLJ1=DWON
        VLJ3=DZER
        ZMAX2=Z2
        IFLAG=2
        IF(XMAX.EQ.XTST1)GO TO 1520
        IF(XMAX.EQ.XTST3)GO TO 1540
        GO TO 1550
1520    CONTINUE
        SCALE=SQRT(DX**2+DZ**2)
        VLJ1=DBLE(DX/SCALE)
        VLJ3=DBLE(-DZ/SCALE)
        ZMAX2=ZTST1
        IFLAG=1
        GO TO 1550
1540    VLJ1=DZER
        VLJ3=DWON
        ZMAX2=ZTST3
        IFLAG=0
C
C       ADD SOME INCREMENT TO AVOID BEING STUCK
C
1550    EPS=0.001
1560    XBRKD=XMAX
        IF(XMAX.EQ.XTST3)XBRKD=XMAX-DBLE(EPS)
        XBRK=SNGL(XBRKD)
C
C       ALLOW FOR ERROR IN RAY
C
        IF(ZMAX2.LT.(ZT-1.0).AND.ZT.GT.0.0)GO TO 6999
        IF(ZMAX2.GT.(ZB-1.0).AND.ZB.LT.ZMAX)GO TO 6999
        ZBRKD=DBLE(ZMAX2)
        ZBRK=SNGL(ZBRKD)
        IF(ZBRK.NE.Z0)PTEMP=(X0-XBRK)/(ZBRK-Z0)
        PTEMP=SIGN(1.0,PTEMP)
        IF(XMAX.EQ.XTST3)GO TO 1660
        IF(ZMAX2.GT.Z.AND.ZMAX2.LT.ZMAX)ZBRKD=DBLE(ZMAX2-EPS)
        IF(ZMAX2.LT.Z.AND.ZMAX2.GT.0.0)ZBRKD=DBLE(ZMAX2-EPS)
        XMARK=1.0
        IF(XBRK.NE.X0)XMARK=(X-X0)/(XBRK-X0)
        IF(XMARK.GT.0.0)GO TO 1660
        IF(ZMAX2.GT.0.0.ANB.PTEMP.LT.0.0)ZBRKD=DBLE(ZMAX2-EPS)
        IF(ZMAX2.LT.ZMAX.AND.PTEMP.GT.0.0)ZBRKD=DBLE(ZMAX2-EPS)
1660    IF(ZBRKD.LE.0.0)GO TO 2020
        IF(ZBRKD.GE.ZMAX)GO TO 2030
```

```
      REFLEC=1.0
      GO TO 2050
2020  JTOP1=JTOP1-1
      ZBRKD=0.001
      GO TO 2040
2030  JBOT1=JBOT1-1
      ZBRKD=ZMAX-0.001
2040  REFLEC=-1.0
      F1D=RCD**2-(Z0D-ZBRKD)**2
      IF(F1D.LT.DZER)F1D=DZER
      IF(F1D.NE.DZER)F1D=DSQRT(F1D)
      XBRKD=X0D-F1D
      IF(XBRKD.LT.XD)XBRKD=X0D-F1D
      XBRK=SNGL(XBRKD)
      ZBRK=SNGL(ZBRKD)
C
C     INTEGRATE FOR TAU,THETA AND DERIVATIVES
C
2050  IF(DABS(XD-XBRKD).LE.0.0001)GO TO 6999
      IF(NI1STP.GT.25000)GO TO 6999
      CALL TRIINT(XD,ZD,XBRKD,ZBRKD,ITRI,I1,X0D,Z0D,RCD,THETA)
      SXM=DSIGN(DWON,X0D-XD)
      SXN=DSIGN(DWON,X0D-XBRKD)
      IF(SXM.NE.SXN)JTURN1=JTURN1+1
      IF(Z0D.NE.ZBRKD)PHID=DATAN((XBRKD-X0D)/(Z0D-ZBRKD))
      IF(Z0.EQ.ZBRK)PHID=1.5707963
      PHIOUT=PHID
      PHID=DBLE(REFLEC)*PHID
      PHI=SNGL(PHID)
2054  CVAL0=C0(ITRI)+AX(ITRI)*XBRK+BZ(ITRI)*ZBRK
      GO TO 2500
C
C     EQUATIONS FOR INTERSECTIONS,TRAVEL TIME, DERIVATIVE AND PLOTS FOR
C     STRAIGHT LINE RAYS
C
2100  CONTINUE
      NP1=NP1+1
      IF(NP1.GT.14999)NP1=14999
      XPLT(NP1)=X
      ZPLT(NP1)=Z
      PPLT(NP1)=ABS(1.0/CVALN*COS(PHIN))
2110  DZ=ZB-ZT
      RMU=DZ/DX
      SCALE=SQRT(DX**2+DZ**2)
      BETAD=1.0/DTAN(PHID)
C     FIND THREE POSSIBLE INTERSECTION POINTS
      XTST1=XD+((-XD+DBLE(XE-DX-ZB/RMU)-ZD*BETAD)/(DBLE(1.0/RMU)+BETAD)
     1 -ZD)*BETAD
      IF(ABS(XTST1-XD).LE.0.01.OR.XTST1.LT.XD)XTST1=DBLE(1.0E06)
      Z2=ZT
      IF(PHID.GT.DZER)Z2=ZB
      XTST2=XD+(DBLE(Z2)-ZD)*BETAD
      IF(ABS(XTST2-XD).LE.0.01.OR.XTST2.LT.XD)XTST2=DBLE(1.0E06)
      IF(XTST1.GT.XTST2.OR.XTST1.GT.DBLE(XE))GO TO 2120
      XBRKD=XTST1
      VLJ1=DBLE(DX/SCALE)
      VLJ3=DBLE(-DZ/SCALE)
      GO TO 2150
2120  IF(XTST2.GT.DBLE(XE))GO TO 2130
      XBRKD=XTST2
      VLJ1=DWON
      VLJ3=DZER
      GO TO 2150
```

```
2130    XBRKD=DBLE(XE)
        VLJ1=DZER
        VLJ3=DWON
2150    ZBRKD=ZD+(XBRKD-XD)/BETAD
        NSTEP=1
        IF(SNGL(ZBRKD).LT.ZR.AND.SNGL(ZD).GT.ZR)GO TO 2200
        IF(SNGL(ZBRKD).GT.ZR.AND.SNGL(ZD).LT.ZR)GO TO 2200
        IF(SNGL(ZBRKD).EQ.ZR)GO TO 2200
        GO TO 2300
2200    ICROSS=0
        NSTEP=2
        XTST2=XBRKD
        XTST3=ZBRKD
        ZBRKD=DBLE(ZR)
        XBRKD=XD+(ZBRKD-ZD)*BETAD
        GO TO 2300
2250    XD=XBRKD
        ZD=ZBRKD
        XBRKD=XTST2
        ZBRKD=XTST3
        NSTEP=1
2300    F2D=(XD-XBRKD)**2+(ZD-ZBRKD)**2
        IF(F2D.GT.0.0)F2D=DSQRT(F2D)
        THNO=THNO-F2D/C0(ITRI)
        DNO(1,IXT,JZT)=DNO(1,IXT,JZT)-F2D/(C0(ITRI)**2)
        IF(ZD.NE.DBLE(ZR))F3D=ZD
        IF(NSTEP.NE.2)GO TO 2400
        THETA(I1)=THNO
        XFIN=XBRKD
        TYPE *,' STRGT RAY THETA,XFIN=',THETA(I1),XFIN
        PHIFIN=PHID
        ITFIN=ITRI
        DO 2310 I7=1,NXL-1
        DO 2310 J7=1,NZL-1
        DO 2310 K=1,2
2310    DPDC(K,I7,J7)=DNO(K,I7,J7)
2400    PHI=SNGL(PHID)
        XBRK=SNGL(XBRKD)
        X=SNGL(XD)
        ZBRK=SNGL(ZBRKD)
        Z=SNGL(ZD)
2454    IF(NSTEP.EQ.2)GO TO 2250
        CVAL0=C0(ITRI)+AX(ITRI)*XBRK+BZ(ITRI)*ZBRK
C       IF RAY HITS TOP OR BOTTOM OF OCEAN NEED TO REVERSE
        PHIOUT=PHID
        IF(ZBRKD.GT.0.01.AND.ZBRKD.LT.DBLE(ZMAX-0.01))GO TO 2475
        PHID=-PHID
        IF(ZBRKD.LE.0.01)JTOP1=JTOP1-1
        IF(ZBRKD.GE.DBLE(ZMAX-0.01))JBOT1=JBOT1-1
        XD=XBRKD
        IF(ZBRKD.LT.DZER)ZBRKD=DZER
        IF(ZBRKD.GT.DBLE(ZMAX))ZBRKD=DBLE(ZMAX)
        ZD=ZBRKD
        GO TO 2110
2475    ZBRKD=ZBRKD-0.001
        IF(PHID.GE.DZER)ZBRKD=ZBRKD-0.002
        IF(XBRKD.EQ.DBLE(XE))XBRKD=XBRKD-0.001
        IF(XBRKD.GE.DBLE(XR1))ISTOP=0
2500    XD=XBRKD
        X=SNGL(XBRKD)
        Z=SNGL(ZBRKD)
        ZD=ZBRKD
        VNBJ1=DCOS(PHIOUT)
```

```
      VNBJ3=DSIN(PHIOUT)
      CVALB=AX(ITRI)*XBRK+BZ(ITRI)*ZBRK+C0(ITRI)
      IF(XBRK.EQ.SNGL(XLP).AND.ISTOP.EQ.0)GO TO 7000
C
C     CALCULATE TRANSMISSION MATRICES*****USES CHAPMAN'S NOTATION
C
      VMBJ1=VNBJ3
      VMBJ3=-VNBJ1
      VMDVI=VMJ1*VIJ1+VMJ3*VIJ3
      VMBDVI=VMBJ1*VIJ1+VMBJ3*VIJ3
      VLPDVI=VMLP1*VIJ1+VMLP3*VIJ3
      IF(FACT.GT.1.0E-05)GO TO 2565
C     NO GRADIENT, TRANSMISSION MATRIX IS  ALMOST IDENTITY MATRIX
      TMAT(1,1)=DWON
C     THIS IS DERIVATIVE OF RANGE W.R.T. P, FACTOR OF 1/SIN(PHI)
C     IS ADDED ON LATER
      TMAT(1,2)=DBLE(CVAL)*(ZBRKD-F3D)/VMBJ1**2
      IF(JTRIAN.EQ.1)GO TO 3000
      VI1DVB=VIJ11*VMBJ11+VIJ13*VMBJ13
      VLDVM=VLJ11*VMJ1+VLJ13*VMJ3
      VLDVB1=VLJ11*VMBJ11+VLJ13*VMBJ13
      IF(VLDVB1.NE.DZER)BMAT(1,1)=VLDVM/VLDVB1
      BMAT(2,1)=DZER
      BMAT(2,2)=DWON
      IF(VI1DVB.NE.DZER.AND.VLDVM.NE.DZER)BMAT(2,2)=VMDVI/VI1DVB
     1 *VLDVB1/VLDVM
      BMAT(1,2)=DZER
      GO TO 2590
2565  TMAT(1,1)=DWON
      IF(VMDVI.NE.0.0)TMAT(1,1)=VMBDVI/VMDVI
      IF(FACT.NE.0.0)F1D=DBLE(1.0/(PVAL**2*FACT))
2567  TMAT(1,2)=F1D*(TMAT(1,1)-DWON)
      IF(JTRIAN.EQ.1)GO TO 3000
      VLDVM=VLJ11*VMJ1+VLJ13*VMJ3
      VLDVB1=VLJ11*VMBJ11+VLJ13*VMBJ13
      VI1DVB=VIJ11*VMBJ11+VIJ13*VMBJ13
      SMAT(1,1)=DWON
      IF(VLDVB1.NE.0.0)SMAT(1,1)=(VLJ11*VMJ1+VLJ13*VMJ3)/VLDVB1
      RMAT(2,2)=DWON
      IF(VLDVM.NE.0.0)RMAT(2,2)=(VIJ1*VMJ1+VIJ3*VMJ3)/VLDVM
      RMAT(2,1)=DZER
      IF(VLDVM.NE.0.0)RMAT(2,1)=-(VLJ11*VKJ1+VLJ13*VKJ3)**2*DBLE(FACT)/
     1 (VLDVM**2)/DBLE(CVAL**2)
      QMAT(2,2)=DWON
      IF(VI1DVB.NE.0.0)QMAT(2,2)=(VLJ11*VMBJ11+VLJ13*VMBJ13)/VI1DVB
      QMAT(2,1)=DZER
      IF(VLDVB1.NE.0.0.AND.VI1DVB.NE.0.0)QMAT(2,1)=(VLJ11*VKJ11+VLJ13*VKJ13)
     1 **2*DBLE(FACT1)/(VLDVB1*VI1DVB*DBLE(CVALB1**2))
C
C     MULTIPLY R*S*Q TO GET B
C
      BMAT(1,1)=SMAT(1,1)
      BMAT(1,2)=DBLE(0.0)
      BMAT(2,2)=RMAT(2,2)*QMAT(2,2)
      BMAT(2,1)=RMAT(2,1)*SMAT(1,1)+RMAT(2,2)*QMAT(2,1)
      IF(FLAGDC.NE.1.0)GO TO 2590
      NRP=1
      IF(CPHIFL.EQ.0.0.OR.CVALFL.EQ.0.0)GO TO 2585
      DR22=-BZ(ITRI)/FACT*SPHIFL/CVALFL/CPHIFL
      DS11=-SPHIFL**2/(CVALFL*CPHIFL)
      DR21=-2.0*RMAT(2,1)/CVALFL
2585  DSUM=DMAT(1,2)*(SMAT(1,1)*DR21-RMAT(2,1)*DS11+QMAT(2,1)*DR22)-
     1 DMAT(2,2)*QMAT(2,2)*DR22
```

```
      IF(NRP.EQ.0)DNO(2,IXT0,JZT0)=DSUM-DNO(2,IXT0,JZT0)
      IF(NRP.EQ.0)GO TO 2590
      DNO(2,IXT,JZT)=DSUM-DNO(2,IXT,JZT)
      DR22=-DR22
      DS11=-DS11
      DR21=-DR21
      NRP=0
      GO TO 2585
C
C     MULTIPLY T*B*D TO GET NEW D
C
2590  DO 2600 IM=1,2
      DO 2600 JM=1,2
      DTEMP(IM,JM)=0.0
      DO 2600 KM=1,2
2600  DTEMP(IM,JM)=DTEMP(IM,JM)+TMAT(IM,KM)*(BMAT(KM,1)*DMAT(1,JM)-
     1 BMAT(KM,2)*DMAT(2,JM))
      DO 2610 IM=1,2
      DO 2610 JM=1,2
2610  DMAT(IM,JM)=DTEMP(IM,JM)
      GO TO 3050
3000  CONTINUE
      DO 3005 IM=1,2
      DO 3005 JM=1,2
3005  DMAT(IM,JM)=TMAT(IM,JM)
      VMB11=VMBJ1
      VMB13=VMBJ3
3050  CONTINUE
3333  CONTINUE
      IF(ICROSS.NE.0)GO TO 6000
      CPFIN=DCOS(PHIFIN)
      SPFIN=DSIN(PHIFIN)
      XRAY(I1)=XFIN
      CFIN=C0(ITFIN)-BZ(ITFIN)*ZR-AX(ITFIN)*SNGL(XFIN)
      QFIN=SNGL(SPFIN)/CFIN
      PFIN(I1)=SNGL(CPFIN)/CFIN
C
C     CALCULATE EXTRA TRAVEL TIME FOR RAY TO GET FROM RANGE
C     TO RECEIVER
C
      TEXTRA=CPFIN/DBLE(CFIN)*(DBLE(XR1)-XFIN)
      JTURN=JTURN1
      JTOP=JTOP1
      JBOT=JBOT1
C
C     SIGN OF DXDP,NEGATIVE IF TURNING POINT OCCURS
C
      ISDXDP=1
      PHIIN=SIGN(1.0,PHITRI)
      SPHI=SIGN(1.0,SNGL(PHIOUT))
      IF(SPHI.NE.PHIIN)ISDXDP=-1
      VIDVB=VIJ1*VMBJ1-VIJ3*VMBJ3
      F1D=(VM11*VI11-VM13*VI13)/VM11
      IF(VIDVB.EQ.0.0.AND.VMBJ1.EQ.0.0)GO TO 5100
      IF(VIDVB.EQ.0.0)GO TO 5110
      IF(ABS(VMBJ1).LE.CAUS)GO TO 5120
      F2D=VMBJ1/VIDVB
      F3D=VKJ1**2/VMBJ1**2
      DPDP0=SNGL(F1D*F2D*(DMAT(2,2)+DMAT(1,2)*DBLE(FACT/(CVALB**2))*F3D))
      QDPDP0=QFIN*DPDP0
      GO TO 5150
5100  DPDP0=F1D*DMAT(2,2)
      TYPE *,' DPDP0 2'
```

```
      QDPDP0=0.0
      GO TO 5150
5110  DPDP0=1.0E06
      TYPE *,' DPDP0 3'
      QDPDP0=QFIN*DPDP0
      GO TO 5150
5120  DPDP0=1.0E06
      TYPE *,' DPDP0 4'
      QDPDP0=SNGL(F1D/VIDVB*DMAT(1,2)*VKJ1**2)*FACT/CVALB**2
5150  CONTINUE
      IF(ABS(QDPDP0).LT.CAUS.AND.X.GE.(XR1-DX))TYPE *,' Y CAUSTIC '
     1 ,I1,TRANS(I1),X,Z,QFIN,DPDP0
      F1D=(VM11*VI11-VM13*VI13)/VM11
      DXDP0=1.0E28
      IF(VMBJ1.NE.0.0)DXDP0=SNGL(F1D*DMAT(1,2)/VMBJ1)
      QDXDP0=QFIN*DXDP0
      IF(VMBJ1.EQ.0.0)QDXDP0=SNGL(F1D*DMAT(1,2))/CVALB
      IF(ABS(QDXDP0).LE.CAUS.AND.X.GE.(XR1-DX))TYPE *,' X CAUSTIC ',
     1 I1,TRANS(I1),X,Z,QFIN,DXDP0
6000  IF(ISTOP.EQ.0)GO TO 7000
      VMJ11=VMJ1
      VMJ13=VMJ3
      VIJ11=VIJ1
      VIJ13=VIJ3
      VMBJ11=VMBJ1
      VMBJ13=VMBJ3
      VKJ11=VKJ1
      VKJ13=VKJ3
      VLJ11=VLJ1
      VLJ13=VLJ3
      CVALB1=CVALB
      FACT1=FACT
      JTRIAN=JTRIAN-1
C
C     ************************************************************
C     COMPLETED TRANSMISSION MATRIX
C     ************************************************************
C
      GO TO 300
6999  CONTINUE
      TYPE *,' LINE 6999 BAD RAY WITH INDEX AND THETA=',I1,XD,XBRKD
     1 ,THETA(I1-1),NI1STP
C     BAD RAY----PATCH TO PREVIOUS RAY
      IF(I1.EQ.1)GO TO 8000
      THETA(I1)=THETA(I1-1)
      PFIN(I1)=PFIN(I1-1)
      XRAY(I1)=XRAY(I1-1)
      WAMPL(1,I1)=WAMPL(1,(I1-1))
      WAMPL(2,I1)=WAMPL(2,(I1-1))
      GAMPL(I1)=GAMPL(I1-1)
      JTURN=JTURN0
      JBOT=JBOT0
      JTOP=JTOP0
      READ(3'I1-1)((DPDC(1,I2,J2),J2=1,NZL-1),I2=1,NXL-1)
      READ(2'I1-1)((DPDC(2,I2,J2),J2=1,NZL-1),I2=1,NXL-1)
      GO TO 7195
7000  CONTINUE
      NP1=NP1-1
      XPLT(NP1)=X
      ZPLT(NP1)=Z
      PPLT(NP1)=PFIN(I1)
      NFIF=(I1-1)/NPLT9
      RFIF=FLOAT(I1-1)/FLOAT(NPLT9)
```

```
      IF(RFIF.NE.FLOAT(NFIF))GO TO 7150
      WRITE(1)NP1,(XPLT(IO),ZPLT(IO),PPLT(IO),IO=1,NP1)
7150  THETA(I1)=THETA(I1)+TEXTRA
      TYPE *,' I1,THETA,XFIN=',I1,THETA(I1),XFIN
      IF(TRANS(I1).GT.0.0.AND.TRANS(I1-1).LT.0.0)GO TO 7155
      IF(XFIN.EQ.DZER)GO TO 8000
      IF(ABS(XFIN-XR1).LT.2.0*DXLAY)GO TO 7152
C     DON'T INCLUDE ARRIVALS THAT ARE WAY BEYOND RECEIVER BLOCK- SET PFIN TO
C     1.0 SO WEIGHTING FACTORS AREN'T CHANGED
      THETA(I1)=0.0
      XFIN=0.0
      WAMPL(1,I1)=0.0
      WAMPL(2,I1)=0.0
      GAMPL(I1)=0.0
      PFIN(I1)=1.0
      IF(JTURN.NE.JTURN0.OR.JBOT.NE.JBOT0.OR.JTOP.NE.JTOP0)
      1 GO TO 7155
      GO TO 8000
7152  CBJ=((0.0,-1.0))**JTURN*((-1.0,0.0)**JTOP)
     1 *((1.0,0.0)**JBOT)
      BJ1=REAL(CBJ)
      BJ2=AIMAG(CBJ)
      ANG=(1.0-FLOAT(ISDXDP))*PI/4.0
      CANG=COS(ANG)
      SANG=-SIN(ANG)
      BJ1A=BJ1*CANG-BJ2*SANG
      BJ2A=BJ2*CANG+BJ1*SANG
C
C     NAME RAY TYPE- KEEP RAYS OF SAME TYPE TOGETHER
C
      IF(I1.EQ.1)GO TO 7155
      IF(TRANS(I1).GT.0.0.AND.TRANS(I1-1).LT.0.0)GO TO 7155
      IF(JTURN.EQ.JTURN0.AND.JBOT.EQ.JBOT0.AND.JTOP.EQ.JTOP0)
      1 GO TO 7160
7155  NTYP=NTYP+1
      ITYPE(NTYP)=I1
      TYPE *,' NTYP,ITYPE,JTURN,JTOP,JBOT=',NTYP,ITYPE(NTYP),
      1 JTURN,JTOP,JBOT
      JTURN0=JTURN
      JTOP0=JTOP
      JBOT0=JBOT
      IF(XFIN.EQ.DZER)GO TO 8000
7160  IF(ABS(QDPDP0).LE.CAUS)GO TO 7180
C
C     NOTE--WKBJ AMPLITUDE HAS XR1 IN DENOMINATOR RATHER
C     THAN XFIN. THIS IS IN CONTRAST WITH CHAPMAN'S EQN.--
C     2/24/84 REMOVED Q0 FACTOR- USING P IN RTHETAC
C
      WTERM=ABS(COS(TRANS(I1))*SIN(TRANS(I1)))/
      1 ABS((XR1-XS)*QDPDP0)
      WTERM=SQRT(WTERM)*ABS(DPDP0)/4.4429*GBEAM
      WAMPL(1,I1)=BJ1A*WTERM
      WAMPL(2,I1)=BJ2A*WTERM
7180  IF(ABS(QDXDP0).LE.CAUS)GO TO 7190
      GTERM=1.0/ABS((XR1-XS1)*QDXDP0*TAN(TRANS(I1)))
      GAMPL(I1)=BJ1*SQRT(GTERM)*GBEAM
C
C     NEED A SMOOTH TRANSITION BETWEEN SOLUTIONS
C
7190  CONTINUE
7195  CONTINUE
      WRITE(3'I1)((DPDC(1,I,J),J=1,NZL-1),I=1,NXL-1)
      DO 7400 I=1,NXL-1
```

```
      DO 7400 J=1,NZL-1
      IF(DPDP0.NE.0.0)DPDC(2,I,J)=DBLE(0.5*SIGN(1.0,DPDP0)/ABS(DPDP0))
     1 *DPDC(2,I,J)
7400  CONTINUE
      WRITE(2'I1)((DPDC(2,I,J),J=1,NZL-1),I=1,NXL-1)
8000  CONTINUE
      TYPE *,' NTYP,ITYPE=',NTYP,(ITYPE(JK),JK=1,NTYP)
      AC=1.0
      DO 8005 I1=1,NTRANS
      WGT(I1)=0.0
      IF(AC.EQ.0.0)WGT(I1)=0.5
      AC=ABS(WAMPL(1,I1))+ABS(WAMPL(2,I1))
C
C     IF A ZERO ARRIVAL OR AN ARRIVAL BEYOND RECEIVER
C     BLOCK, DON'T CHANGE WEIGHTING
C
      IF(PFIN(I1).EQ.1.0)AC=1.0
      IF(AC.NE.0.0)GO TO 8005
      WGT(I1)=1.0
      IF(WGT(I1-1).EQ.0.0)WGT(I1-1)=0.5
8004  TYPE *,' I1,WAMPL,WGTG,GAMPL OF I1 AND I1-1=',I1,WAMPL(1,I1),
     1 WAMPL(2,I1),WGT(I1),GAMPL(I1),I1-1,WAMPL(1,I1-1),WAMPL(2,I1-1),
     2 WGT(I1-1),GAMPL(I1-1)
8005  CONTINUE
      CLOSE(UNIT=3)
      CLOSE(UNIT=2)
      CLOSE(UNIT=1)
      RETURN
      END
```

CIRDEF LISTING

31-Oct-1984 17:04:0
16-Jul-1984 15:57:3

```
0001    C
0002    C
0003            SUBROUTINE CIRDEF(X,Z,PHID,IT,X0D,Z0D,RCD)
0004    C
0005    C       SUBROUTINE TO DEFINE ORIGIN (X0,Z0) AND RADIUS RC FOR A CIRCLE
0006    C       STARTING AT (X,Z) WITH ANGLE PHI WITHIN TRIANGLE ITRI.
0007    C       MODIFIED 11/9/83 TO USE CHAPMAN'S ALGORITHM, CENTER OF CIRCLE
0008    C       IS WHERE RAY PERPENDICULAR HITS LINE OF C=0. BUT CHAPMAN'S EQN
0009    C       HAS SIGN ERROR---VALID ONLY FOR UPPER LOOP, NEED SIGN CHANGE FOR
0010    C       LOWER.
0011    C
0012            DOUBLE PRECISION X0D,Z0D,RCD,RCOEFF,PHID,CP,SP,DIF,
0013            1 AXD,BZD
0014            COMMON /TRICOF/AX,BZ,C0
0015            COMMON /SOURCE/ XS1,ZS1,XR1,ZR1
0016            DIMENSION AX(20000),BZ(20000),C0(20000)
0017            CVAL=AX(IT)*X-BZ(IT)*Z-C0(IT)
0018            CP=DCOS(PHID)
0019            SP=DSIN(PHID)
0020            AXD=DBLE(AX(IT))
0021            BZD=DBLE(BZ(IT))
0022            DIF=-BZD*CP-AXD*SP
0023            RCD=DBLE(1.0E09)
0024            IF(DIF.NE.0.0)RCD=DABS(DBLE(CVAL)/DIF)
0025            SMK=SIGN(1.0,(-AX(IT)*SNGL(SP)-BZ(IT)*SNGL(CP)))
0026            RCOEFF=RCD*DBLE(SMK)
0027            X0D=DBLE(X)-RCOEFF*SP
0028            Z0D=DBLE(Z)-RCOEFF*CP
0029            RETURN
0030            END
```

TABLE 7-2

MAXIMUM ENTROPY INVERSE PROGRAMS

1. GMAXENT - main program

2. MENVRT - iterates to solve linear equations for dC and Lagrangian multiplier

   a. DMEPAR - calculates terms used in linear equations

   b. MINV - matrix inversion

3. CHISQ, XNORM - probability density calculations

MENVRT LISTING

```
C
      SUBROUTINE MENVRT(NR,NC,JSOLN,DCEST)
C
C     SUBROUTINE TO COMPUTE THE MAXIMUM ENTROPY INVERSE
C     ESTIMATE SOLUTION DCEST TO A TRAVEL TIME INVERSE PROBLEM.
C     NOTATION FOLLOWS BEVENSEE,IEE AP-29,MARCH,1981,P. 271,
C
C
C     MODIFIED 8/19/83 TO USE MARQUARDT'S METHOD
C
C
C     MODIFIED 10/10/83 TO USE GULL - DANNIELL'S NOISY
C     MAXENT INVERSE WITH SET VARIANCE(JSOLN=1), OR SET
C     ZERO MEAN AND VARIANCE(JSOLN=2)
C
C     MODIFIED 3/1/84 FOR RANGE DEPT WKBJ ACOUSTIC SOLNS
C     PHI REPRESENTS NC-2(OR 1) EQNS FOR NC+2(OR 1) UNKNOWNS
C     CAN NOW USE E STATISTIC FOR ORDERED GAUSSIAN SET PER
C     BRYAN AND SKILLING, MON.NOT.R.ASTR.SOC.,1980,P.69-79.
C
C     DEFINE: E-RANGE/C0 MATRIX OR P,I DERIVATIVES
C             DCTRU-TRUE DC FLUCTUATIONS VECTOR
C             G-MATRIX OF DDPHIDDCEST DERIVATIVES
C             DPHI-DIFFERENCE BETWEEN DCEST AND EXP
C                 FCN,OR BETWEEN TERMN,TERVAR AND 0.0,1.0
C             DPEST,DPEST1-ESTIMATED TRAVEL TIME P OR I VECTORS
C             DCEST-ESTIMATE FOR SVP AND LAST TWO SLOTS ARE
C             LAGRANGIAN MULTIPLIERS
C             DPORD-DPTRU-DPEST IN ORDERED SET,NORD KEEPS TRACK OF
C                     INDICES
C
C     USES: DMEPAR,MINV
C
      COMMON /RINIT/ESP0,RLAM0,FACT,BIAS
      COMMON /DERIV/G,FACT2
      COMMON /TRUTH/DPTRU,DPNEW,E,DCTRU,PNSIG,CSQ,VNORM,RNU,ESTAT,DPORD,
      1 NORD
      COMMON /LIMIT/ENTRO,VRATO,IREAL
      COMMON /DCNO/NBR,NOTOT
      PARAMETER NG=2000,NM=50,NM2=52
      DIMENSION E(NG*NM),G(NM2*NM2),DPTRU(NG),DCTRU(NM),DCEST(NM2),
      1 DPHI(NM2),DB(NM2),DPEST(NG),DCEST1(NM2),DPEST1(NG),RNU(NG),
      2 DPORD(NG),NORD(NG),DPORD1(NG),DPNEW(NG),NBR(10)
      ITER=0
      IFLAG=0
      TYPE *,' USE ACTUAL OR PERFECT DATA?(0 FOR ACTUAL)='
      ACCEPT *,NPER
      IF(NPER.EQ.0)GO TO 8
      DO 5 IJ=1,NR
5     DPTRU(IJ)=DPNEW(IJ)
D     TYPE *,' IREAL=',IREAL
8     IF(IREAL.GT.1)GO TO 11
      TYPE *,' MAXENT INVERSE WITH NOISY DATA'
      TYPE *,' USE GAUSSIAN WITH VAR,MEAN CALC
      1 OR E STATISTIC'
      TYPE *,' INPUT DC0,LAMB10,LAMB20 INITIAL DC AND LAGRANGIAN
      1 MULTIPLIERS='
      TYPE *,' RECOMMEND INITIAL LAMB=10. FOR TRAVEL TIME, 0.1 FOR
      1 SIGNAL INVERSION'
      ACCEPT *,DC0,RLAM10,RLAM20
D     TYPE *,' INPUT FINAL RLAM FOR MARQUARDT,FINAL TEST RATIO='
D     ACCEPT *,FRLAM,FTEST
      FRLAM=1000.0
```

```
      FTEST=0.02
11    DPMAX=0.0
      DO 50 I=1,NR
50    IF(ABS(DPTRU(I)).GT.DPMAX)DPMAX=DPTRU(I)
      NC2=NC+1
      IF(JSOLN.EQ.2)NC2=NC+2
      DO 70 I=1,NC
70    DCEST(I)=DC0
      DO 71 IJ=1,NOTOT
      IJ2=NBR(IJ)
71    DCEST(IJ2)=BIAS
      DCEST(NC+1)=RLAM10
      IF(JSOLN.EQ.2)DCEST(NC2)=RLAM20
      V1=0.0
      DO 80 K=1,NR
80    V1=V1+ABS(DPTRU(K))
C     ESTAT IS EXPECTED VALUE
C     NOTE THIS IS SQ OF VALUE USED BY BRYAN & SKILLING
      IF(NR.GT.100)GO TO 95
      ESTAT=0.0
      DO 85 IJ=1,NR/2
      RIJ=FLOAT(IJ)-0.5
85    ESTAT=ESTAT+1.0/(RIJ*LOG(FLOAT(NR)/RIJ))
      GO TO 96
95    ESTAT=LOG(LOG(FLOAT(NR)))
96    FACT2=FACT
      WGT0=1000.0
C
C     CALCULATE DPEST,DCEST
C     WILL RETURN TO THIS SPOT ON EACH ITERATION
C
C
C     ITERATE TO FIND TWO LAGRANGIAN MULTIPLIERS AND DCEST.
C
C     ****************************************************
100   CONTINUE
C     ****************************************************
      ITER=ITER+1
      ENTROP=0.0
      DO 120 J=1,NC
120   ENTROP=-DCEST(J)*LOG(DCEST(J))+ENTROP
D     TYPE *,' ITER,DCEST=',ITER,(DCEST(I),I=1,NC-2)
      DO 140 I=1,NR
      DPEST(I)=0.0
      DO 140 J=1,NC
140   DPEST(I)=FACT*E(NR*(J-1)-I)*DCEST(J)+DPEST(I)
      TERMN=0.0
      TERVAR=0.0
      DO 160 K=1,NR
      DPER=DPTRU(K)-DPEST(K)
      TERMN=TERMN+DPER
160   TERVAR=TERVAR+DPER**2
      TERMN=TERMN/FLOAT(NR)/PNSIG
      TERVAR=TERVAR/FLOAT(NR)/PNSIG**2
      TYPE *,' TERMN,TERVAR,ENTROPY=',TERMN,TERVAR,
     1 ENTROP
      IF(JSOLN.EQ.3)GO TO 170
      V21=ABS(TERMN-VNORM)
      IF(JSOLN.NE.2)V21=0.0
      V22=ABS(TERVAR-CSQ)
      GO TO 210
170   CONTINUE
C
```

```
C       E STATISTIC CALCULATIONS, CASE 3,JSOLN=3
C
        DO 172 IO=1,NR
        NORD(IO)=IO
172     DPORD(IO)=DPTRU(IO)-DPEST(IO)
        DO 175 IO=1,NR-1
        DO 175 JO=IO+1,NR
        IF(DPORD(IO).LT.DPORD(JO))GO TO 175
        B=DPORD(IO)
        KO=NORD(IO)
        DPORD(IO)=DPORD(JO)
        DPORD(JO)=B
        NORD(IO)=NORD(JO)
        NORD(JO)=KO
175     CONTINUE
        SUME=0.0
        DO 180 IJ=1,NR
180     SUME=SUME+(DPORD(IJ)/PNSIG-RNU(IJ))**2
        TYPE *,' PRESENT E STAT,VALID ONE=',SUME,ESTAT
        V21=0.0
        V22=ABS(SUME-ESTAT)
210     IF(ITER.GT.15)TYPE *,' DO YOU WANT TO CONTINUE(0=NO)?'
        IF(ITER.GT.15)ACCEPT *,MCONT
        IF(ITER.GT.15.AND.MCONT.EQ.0)IFLAG=1
        TYPE *,' ITERATION,NORMS=',ITER,V21,V22
D       TYPE *,' V1=',V1
        IF(ITER.GT.1.AND.V1.GT.1.E-36)TEST=ABS(V22/ESTAT)+ABS(V21/V1)
        IF(ABS(TEST).LE.FTEST.AND.ITER.GE.2)GO TO 3000
        DO 300 K=1,NC
        SUM1=0.0
        SUM2=0.0
        DO 250 I=1,NR
        IF(JSOLN.EQ.3)GO TO 240
        SUM1=SUM1+E(NR*(K-1)+I)*(DPTRU(I)-DPEST(I))/PNSIG/FLOAT(NR)
        SUM2=SUM2+E(NR*(K-1)+I)
        GO TO 250
240     SUM1=SUM1+E(NR*(K-1)+NORD(I))*(DPORD(I)/PNSIG-RNU(I))
250     CONTINUE
        SOL2=0.0
        IF(JSOLN.EQ.2)SOL2=DCEST(NC2)/FLOAT(NR)/PNSIG*SUM2
300     DPHI(K)=1.0-(-LOG(DCEST(K))-2.0*DCEST(NC+1)/PNSIG
        1 *SUM1-SOL2)
        DPHI(NC+1)=CSQ-TERVAR
        DPHI(NC+2)=VNORM-TERMN
        IF(JSOLN.EQ.3)DPHI(NC+1)=ESTAT-SUME
D       TYPE *,' DPHI=',(DPHI(I),I=1,NC2)
        RLAM=RLAM0/10.0
        NTRY=0
C
C       REPEAT HERE UNTIL NORM IS REDUCED
C
C       ****************************************************************
350     CONTINUE
C       ****************************************************************
        RLAM=RLAM*10.0
        IF(RLAM.GT.FRLAM)GO TO 3000
        IF(IFLAG.NE.0)GO TO 3000
D       NTRY=NTRY+1
D       DCFACT=1.2
D       IF(NTRY.GT.NC2)DCFACT=1.0/1.2
D       RLAM=RLAM0*100.0
D       IF(NTRY.GT.NC2*2)GO TO 3000
D       IF(NTRY.GT.1.AND.NTRY.LE.NC2)DCEST(NTRY-1)=DCEST(NTRY-1)/DCFACT
```

```
D       IF(NTRY.GT.1.AND.NTRY.GT.NC2)DCEST(NTRY-NC2-1)=DCEST(NTRY-NC2-1)/DCFACT
D       DCEST(NTRY)=DCEST(NTRY)*DCFACT
D       IF(NTRY.GT.NC2)DCEST(NTRY-NC2)=DCEST(NTRY-NC2)*DCFACT
C
C       GET DERIVATIVE MATRIX
C
353     CALL DNOIS(DCEST,DPEST,NR,NC,JSOLN)
D       TYPE *,' G=',(G(IJ),IJ=1,NC2*NC2)
        DO 360 I=1,NC2
        I1=NC2*(I-1)+I
360     G(I1)=G(I1)-RLAM
        CALL MINV(NC2,DETER)
        DO 390 I2=1,NC2
        DB(I2)=0.0
        DO 390 J2=1,NC2
390     DB(I2)=DB(I2)+G(I2+(J2-1)*NC2)*DPHI(J2)
D       TYPE *,' DB=',(DB(JK),JK=1,NC2)
        DIV=1.1
C
C       ADD TO OLD VALUES
C
395     DIV=DIV/1.1
        DO 400 M=1,NC2
        DCEST1(M)=DCEST(M)-DB(M)*DIV
400     IF(M.LE.NC.AND.DCEST1(M).LE.0.0)GO TO 395
D       TYPE *,' DCEST1=',(DCEST1(IJ),IJ=1,NC2)
        DO 401 IJ2=1,NOTOT
        IJ3=NBR(IJ2)
401     DCEST1(IJ3)=BIAS
        ENTRP1=0.0
        DO 420 J=1,NC
420     ENTRP1=ENTRP1-DCEST1(J)*LOG(DCEST1(J))
D       TYPE *,' ENTROPY=',ENTRP1
        DO 450 I=1,NR
        DPEST1(I)=0.0
        DO 440 J=1,NC
440     DPEST1(I)=DPEST1(I)+FACT*E(NR*(J-1)+I)*DCEST1(J)
        V11=V11+(DPTRU(I)-DPEST1(I))
450     V12=V12+(DPTRU(I)-DPEST1(I))**2
        IF(JSOLN.EQ.3)GO TO 500
        V11=ABS(V11/FLOAT(NR)/PNSIG-VNORM)
        IF(JSOLN.NE.2)V11=0.0
        V12=ABS(V12/FLOAT(NR)/PNSIG**2-CSQ)
        GO TO 590
500     CONTINUE
        DO 502 IO=1,NR
502     DPORD1(IO)=DPTRU(IO)-DPEST1(IO)
        DO 575 IO=1,NR-1
        DO 575 JO=IO+1,NR
        IF(DPORD1(IO).LT.DPORD1(JO))GO TO 575
        B=DPORD1(IO)
        DPORD1(IO)=DPORD1(JO)
        DPORD1(JO)=B
575     CONTINUE
        SUME1=0.0
        DO 580 IJ=1,NR
580     SUME1=SUME1+(DPORD1(IJ)/PNSIG-RNU(IJ))**2
        V11=0.0
        V12=ABS(SUME1-ESTAT)
590     CONTINUE
D       TYPE *,' DPEST1=',(DPEST1(IJ),IJ=1,NR)
        TYPE *,' RLAM,V11,V12 NORM=',RLAM,V11,V12
        IF(V11.GT.V21.OR.V12.GT.V22)GO TO 350
```

```
      DO 600 K=1,NC2
600   DCEST(K)=DCEST1(K)
      GO TO 100
3000  CONTINUE
C
C     WRITE OUTPUT
C
      TYPE *,' INITIAL WGT FACT=',RLAM0
      TYPE *,' INITIAL DC,RLAM1,RLAM2='
      TYPE *,DC0,RLAM10,RLAM20
      TYPE *,' FINAL RLAM1,RLAM2=',DCEST(NC-1),DCEST(NC2)
D     PRINT *,' INITIAL WGT FACT=',RLAM0
D     PRINT *,' INITIAL DC,RLAM1,RLAM2='
D     PRINT *,DC0,RLAM10,RLAM20
D     PRINT *,' FINAL RLAM1,RLAM2=',DCEST(NC-1),DCEST(NC2)
D     PRINT *,' FINAL E STAT, VALID ONE=',SUME,ESTAT
      NN=NR
      IF(NC.GT.NR)NN=NC
      DCNORM=0.0
      TYPE *,' DO YOU WANT TO TYPE DT VALUES?(0=NO)'
      ACCEPT *,NPRIN
      IF(NPRIN.EQ.0)GO TO 3111
      TYPE *,' TRUE AND EST DT VALUES=',(DPTRU(I),
     1 DPEST(I),I=1,NR)
3111  CONTINUE
      TYPE *,' TRUE AND EST DC VALUES=',(DCTRU(I),(DCEST(I)-BIAS),I=1,NC)
D     PRINT *,' TRUE AND EST DC VALUES=',(-DCTRU(I),(DCEST(I)-BIAS),I=1,NC)
D     TYPE *,' RATIO OF NORMS OF DT ERROR/DT SUM=',V21/V1,V22/V1
      ENT1=0.0
      ENT2=0.0
      DO 3700 J=1,NC
      X=0.0
      Y=0.0
      IF(DCTRU(J).GT.0.0)X=LOG(DCTRU(J))
      IF(DCEST(J).GT.0.0)Y=LOG(DCEST(J))
      ENT2=ENT2-X*DCTRU(J)
      ENT1=ENT1-Y*DCEST(J)
3700  CONTINUE
D     TYPE *,' CONFIG ENTROPIES OF DCTRUE,DCEST=',ENT2,ENT1
D     TYPE *,' MEAN T ERROR,VAR,SUME=',TERMN*PNSIG,TERVAR*PNSIG**2,
D     1 SUME
      ENTRO=ENT1
      VRATO=V2/V1
      RETURN
      END
```

DMEPAR LISTING

```
C
      SUBROUTINE DNOIS(DCEST,DPEST,NR,NC,JSOLN)
C
C     SUBROUTINE TO CALCULATE DERIVATIVES OF DPHI
C     WITH RESPECT TO TWO LAGRANGIAN MULTIPLIERS AND DC.
C     CALLED BY MENVRT, THE MAX. ENTROPY INVERSION ROUTINE
C     FOR NOISY DATA. PRESENTLY FOR GAUSSIAN WITH VARIANCE AND
C     MEAN,JSOLN=2 OR FOR JUST VARIANCE SPECIFIED,JSOLN=1,
C     OR FOR E STATISTIC,JSOLN=3.
C     NOTATION FOLLOWS BEVENSEE,1981 AND MY NOTES OF 1/27/83 AND 3/2/84.
C
      COMMON /DERIV/G,FACT
      COMMON /TRUTH/DPTRU,DPNEW,E,DCTRU,PNSIG,CSQ,VNORM,RNU,ESTAT,
     1 DPORD,NORD
      PARAMETER NG=2000,NM2=52,NM=50
      DIMENSION E(NG*NM),G(NM2*NM2),DCTRU(NM),DPTRU(NG),DPORD(NG),
     1 NORD(NG),DCEST(NM2),DPEST(NG),RNU(NG),DPNEW(NG)
      NC2=NC-2
      IF(JSOLN.NE.2)NC2=NC-1
      COEF1A=-2.0/FLOAT(NR)/PNSIG**2
      COEF1=COEF1A*DCEST(NC+1)
      IF(JSOLN.EQ.3)COEF1A=-2.0/PNSIG
      IF(JSOLN.EQ.3)COEF1=COEF1A/PNSIG*DCEST(NC-1)
      IF(JSOLN.NE.2)GO TO 5
      COEF2A=-1.0/FLOAT(NR)/PNSIG
      COEF2=COEF2A*DCEST(NC-2)
5     DO 10 K=1,NC2*NC2
10    G(K)=0.0
C
C     G IS DDPHIDDCEST CALCULATED FOR SVP AND ONE OR TWO
C     LAGRANGIAN MULTIPLIERS(JSOLN=1 OR 2).
C     SVP DERIVATIVE CALCULATED FIRST,THEN L.MULTS.
C
      DO 50 J=1,NC
      DO 50 K=1,NC
      SUM=0.0
      DO 40 I=1,NR
40    SUM=SUM-E(I+NR*(J-1))*E(I+NR*(K-1))
      SUM=COEF1*SUM
      IF(J.EQ.K)SUM=-1.0/DCEST(K)-SUM
50    G(J-NC2*(K-1))=SUM
C
C     MORE DERIVATIVE W.R.T. SVP
C
      DO 100 K=1,NC
      SUM1=0.0
      SUM2=0.0
      DO 90 I=1,NR
      IF(JSOLN.EQ.3)GO TO 80
      SUM1=SUM1+E(I+NR*(K-1))*(DPTRU(I)-DPEST(I))
      SUM2=SUM2+E(I+NR*(K-1))
      GO TO 90
80    IO=NORD(I)
      SUM1=SUM1+E(IO+NR*(K-1))*(DPORD(I)/PNSIG-RNU(I))
90    CONTINUE
      G(NC-1+NC2*(K-1))=COEF1A*SUM1
100   IF(JSOLN.EQ.2)G(NC2+NC2*(K-1))=COEF2A*SUM2
C
C     DERIVATIVE W.R.T. 1 OR 2 L.MULTS
C
      DO 200 J=1,NC
      SUM1=0.0
```

```
      SUM2=0.0
      DO 190 I=1,NR
      IF(JSOLN.EQ.3)GO TO 180
      SUM1=SUM1-E(I-NR*(J-1))*(DPTRU(I)-DPEST(I))
      SUM2=SUM2-E(I-NR*(J-1))
      GO TO 190
180   IO=NORD(I)
      SUM1=SUM1-E(IO-NR*(J-1))*(DPORD(I)/PNSIG-RNU(I))
190   CONTINUE
      G(J+NC2*NC)=-COEF1A*SUM1
200   IF(JSOLN.EQ.2)G(J-NC2*(NC-1))=-COEF2A*SUM2
      RETURN
      END
```

REFERENCES

(1) Ables, J. G., "Maximum Entropy Spectral Analysis," Astron. Astrophys. Suppl. Series, Vol. 15, pp. 385 - 393, 1974.

(2) Ahluwalia, D. S., and J. B. Keller, "Exact and Asymptotic Representations of the Sound Field in a Stratified Ocean," in Wave Propagation and Underwater Acoustics, edited by J. B. Keller and J. Papadakis, Lecture Notes in Physics, Vol. 70, Springer, Berlin, pp. 54 - 55, 1977.

(3) Aki, K., and P. G. Richards, Quantitative Seismology, W. H. Freeman, San Francisco, 1980.

(4) Bevensee, R. M., "Solution of Underdetermined Electromagnetic and Seismic Problems by the Maximum Entropy Method," IEEE Trans. on Antennas and Propagation, Vol. AP-29, No. 2, pp. 271 - 274, March, 1981.

(5) Brown, M. G., "Inverting for the Ocean Sound Speed Structure," PhD Dissertation, University of California at San Diego, 1982.

(6) Bryan, R. K., and J. Skilling, "Deconvolution by Maximum Entropy, as Illustrated by Application to the Jet of M87," Mon. Not. R. Astr. Soc., Vol. 191, pp. 69 - 79, 1980.

(7) Burg, J. P., "Maximum Entropy Spectral Analysis," in Proc. of 37th Annual Meeting of Soc. of Exploration Geophysicists, 1967.

(8) Chapman, C. H., "A New Method for Computing Synthetic Seismograms," Geophys. J. R. Astr. Soc., Vol. 54, pp. 481 - 518, 1978.

(9) Chapman, C. H., and S. K. Dey-Sarkar, "A Simple Method for the Computation of Body-Wave Seismograms," Bull. of Seis. Soc. of America, Vol. 68, No. 6, 11. 1577 - 1593, Dec. 1978.

(10) Chapman, C. H., and R. Drummond, "Body-Wave Seismograms in Inhomogeneous Media Using Maslov Asymptotic Theory," Bull. of Seismological Soc. of America, Vol 72, No. 6, pp. S277 - S317, Dec. 1982.

(11) Chapman, C. H., and R. Buland, "The Computation Travel Time Tables," Bull. Seis. Soc. of America, Vol. 73, pp. 1271 - 1302, 1983.

(12) Chapman, C. H., "The Triangularized Velocity Model," Unpublished notes, 1983.

(13) Cohen, J. K., and N. Bleistein, "Inverse Methods for Reflector Mapping and Sound Speed Profiling," in Ocean Acoustics edited by J. A. DeSanto, (Springer, Berlin), Topics in Current Physics, Vol. 8, pp. 225 - 243, 1979.

(14) Cornuelle, B. D., "Acoustic Tomography," IEEE Trans. on Geoscience and Remote Sensing, Vol. GE-20, No. 3, pp. 326 - 332, July, 1982.

(15) Cornuelle, B. D., "Inverse Methods and Results from the 1981 Ocean Acoustic Tomography Experiment," PhD Dissertation, Massachusetts Institute of Technology and Woods Hole Oceanographic Institute, April, 1983.

(16) Flatte, S. M., R. Dashen, W. H. Munk, K. M. Watson, and F. Zachariasen, Sound Transmission through a Fluctuating Ocean, Cambridge U. Press, Cambridge, 1979.

(17) Franklin, J. N., "Well-Posed Stochastic Extensions of Ill-Posed Linear Problem," J. of Math. Analysis Appl., Vol. 31, pp. 682 - 716, 1970.

(18) Goldstein, H., Classical Mechanics, Addison-Wesley, 1957.

(19) Gull, S. F., and G. J. Daniell, "Image Reconstruction from Incomplete and Noisy Data," Nature, Vol. 272, pp. 686 - 690, 20 April 1978.

(20) Gull, S. F., and G. J. Daniell, "Maximum Entropy Algorithm Applied to Image Enhancement," IEE Proc., Vol. 127 Pt. E, No. 5, pp. 170 - 172, September, 1980.

(21) Jaynes, E. T., "Prior Probabilities," IEEE Trans. Syst. Sci. Cybern., Vol. SSC - 4, pp. 227 - 241, September, 1968.

(22) Jaynes, E. T., "On the Rationale of Maximum-Entropy Methods," Proc. IEEE, Vol. 70, No. 9, pp. 939 - 952, September, 1982.

(23) Jensen, F., and H. Krol, "The Use of the Parabolic Equation Method in Sound Propagation Modelling," SACLENT Memorandum SM-72, SACLENT ASW Research Center, La Spezia, Italy, August, 1975.

(24) Kravtsov, Yu. A., "Two New Asymptotic Methods in the Theory of Wave Propagation in Inhomogeneous Media (Review)," Soviet Physics-Acoustics, Vol. 14, pp. 1 - 17, 1968.

(25) Lanczos, C., Linear Differential Operators, Van Nostrand, New York, 1961.

(26) Marquardt, D. W., "An Algorithm for Least-Squares Estimation of Nonlinear Parameters," J. Soc. Indust. Appl. Math., Vol. 11, No. 2, pp. 431 - 441, June, 1963.

(27) Maslov, V. P., Theory of Perturbations and Asymptotic Methods (Russian), Izd. MGV, Moscow, USSR, 1965.

(28) Maslov, V. P., Théorie des Perturbations et Méthodes Asymptotiques, Dunod, Paris, France, 1972.

(29) Mercer, J. A., and J. R. Booker, "Long-Range Propagation of Sound through Oceanic Mesoscale Structures," J. Geophysical Research, Vol. 88, No. C1, pp. 689 - 699, January 20, 1983.

(30) Munk, W., and Wunsch, C., "Ocean Acoustic Tomography: A Scheme for Large Scale Monitoring," Deep Sea Research, Vol. 26A, pp. 123 - 161, 1979.

(31) Parker, R. L., "Understanding Inverse Theory," Ann. Rev. Earth and Planet. Sci., Vol. 5, pp. 35 - 64, 1977.

(32) Roberts, B. G., "Horizontal-Gradient Acoustical Ray-Trace Program TRIMAIN," Naval Research Lab., Report 7827, December, 1974.

(33) Rockmore, A. J., "A Tomographic Approach to Multiarray Ocean Surveillance," IEEE J. Oceanic Engineering, Vol OE - 7, No. 2, pp. 83 - 89, April, 1982.

(34) Ziolkowski, R. W., and G. A. Deschamps, "The Maslov Method and the Asymptotic Fourier Transform: Caustic Analysis," Electromagnetics Laboratory Scientific Report No. 80-9, U. Illinois at Urbana - Champaign, 1980.